Optical Properties and Visual Appearance of Printed Special Effect Colors

Vom Fachbereich Maschinenbau

an der Technischen Universität Darmstadt

zur

Erlangung des Grades eines Doktor-Ingenieurs (Dr.-Ing.)

genehmigte

D i s s e r t a t i o n

von

Dipl.-Ing. Katharina Kehren

aus Hilden

Berichterstatter:	*Prof. Dr.-Ing. Edgar Dörsam*
Erster Mitberichterstatter:	*Prof. Dr.-Ing. habil. Tran Quoc Khanh*
Zweiter Mitberichterstatter:	*PD Dr.-Ing. habil. Peter Bodrogi*
Datum der Einreichung:	30.01.2013
Datum der müdlichen Prüfung:	30.04.2013

Darmstadt 2013

D17

Katharina Kehren

Optical Properties and Visual Appearance of Printed Special Effect Colors

Erklärung

Hiermit erkläre ich, dass ich die vorliegende Arbeit, abgesehen von den in ihr ausdrücklich genannten Hilfen, selbständig verfasst habe.

Abstract

Think of perfume wrappings and chocolate boxes. For such high quality printing products, printing inks with special effect pigments are used more frequently due to the unique optical properties and visual appearance. The shifting color, the pearlescent gloss and the visible texture of printed special effect colors fascinate the observer. A lack of knowledge about the printing of special effect colors and about the description of the optical properties and visual appearance causes problems.

First, special effect printing calls for knowledge about the influence of different printing parameters. Therefore, multiple samples varying in the special effect pigment, paper quality, varnishing state and background color were printed. In screen printing, 22 inks with pigments of *BASF SE* were applied on a white glossy and black uncoated paper. The combination of 22 pigments with two paper grades or background colors results in 44 application cases. In total, 224 application cases were realized in flexo printing with 28 pigments of *MERCK KGaA*, two paper qualities, two background colors and two varnishing states. A white glossy and matt coated paper was partially primed with a black light-absorbing ink and partly finished with a clear gloss varnish.

Furthermore, some knowledge about the bidirectional reflectance and texture distribution is required to specify the optical properties. A database was thus generated basing on spectral and imaging measurements in multiple geometric configurations. The determined reflectance spectra, color coordinates and texture parameters are filed in a hierarchical structure. Using the freely available bidirectional reflectance and texture data (*www.idd.tu-darmstadt.de*, *office@idd.tu-darmstadt.de*), the influence of the varied printing parameters on perception-related parameters was investigated. A medium and very high hue difference sum is caused by interference effect and multi-color pigments, respectively. For the comparably large sparkle pigments, the sparkle parameters are particularly high. Perceptually, the lightness difference sum and the relative luminance difference do not satisfactorily represent the lightness shift and the contrast gloss or distinctness-of-image gloss. All considered parameters are significantly lower for the white paper than the black printed background.

Finally, the essential visual appearance attributes should be known for the description of the visual appearance. Their number and nature was determined by means of visual experiments and statistical evaluations. In a color matching light both and a multi-angle test bench, 14 rolled screen and 20 planar flexo printing samples were presented, respectively. Visual differences and twelve attributes were rated in relative and absolute category scaling experiments, respectively. They were evaluated in classical multidimensional scaling, in two correlation analyses, a principal component analysis and in an exploratory factor analysis. According to the *STRESS* values, cumulated variances and the eigenvalues, at most six attributes are essential. Significantly positive correlation coefficients between the two and three tested gloss and texture attributes, respectively, suggest their joint consideration. The composition and factor loadings indicate that the six essential attributes are the four color attributes hue, chroma, lightness and hue shift as well as the two combined attributes for gloss and texture.

Kurzfassung

Man denke an Parfümverpackungen und Pralinenschachteln. Für solche hochqualitativen Druckprodukte werden aufgrund ihrer besonderen optischen Eigenschaften und visuellen Wirkung immer häufiger Druckfarben mit Spezialeffektpigmenten eingesetzt. Die wechselnde Farbe, der perlenartige Glanz und die sichtbare Textur faszinieren den Betrachter. Mangelndes Wissen über das Drucken mit Spezialeffektfarben sowie die Beschreibung der optischen Eigenschaften und visuellen Wirkung rufen Probleme hervor.

Zunächst einmal erfordert das Spezialeffektdrucken Wissen über die Einflüsse der Druckparameter. Deshalb wurden Proben gedruckt, die sich im Spezialeffektpigment, der Papiersorte, dem Lackierungszustand und der Untergrundfarbe unterscheiden. Im Siebdruckverfahren wurden 22 Druckfarben mit Pigmenten der *BASF SE* auf ein weißes, glänzend und ein schwarzes, ungestrichenes Papier aufgetragen. Die Kombination aus 22 Pigmenten mit zwei Papiersorten bzw. Untergrundfarben ergibt 44 Anwendungsfälle. Insgesamt 224 Anwendungsfälle wurden im Flexodruck mit 28 Pigmenten der *MERCK KGaA*, zwei Papiersorten, zwei Untergrundfarben und zwei Lackierungszuständen realisiert. Ein weißes, glänzend und matt gestrichenes Papier wurde zur Hälfte mit schwarzer Absorptionsfarbe grundiert und zum Teil mit glänzendem Klarlack veredelt.

Weiterhin ist Wissen über die bidirektionale Reflexions- und Texturverteilung erforderlich, um die optischen Eigenschaften zu beschreiben. Auf Basis von spektralen und bildgebenden Messungen an den hergestellten Druckproben wurde deshalb eine Datenbank aufgebaut. Die ermittelten Reflexionsspektren, Farbkoordinaten und Texturkennwerte wurden in einer hierarchischen Struktur gespeichert. Unter Verwendung der bidirektionalen Reflexions- und Texturdaten (*www.idd.tu-darmstadt.de*, *office@idd.tu-darmstadt.de*) wurden die Einflüsse der variierten Druckparameter auf empfindungsverwandte Kennwerte untersucht. Eine mittel- bzw. sehr hohe Bunttondifferenzsumme wird von Interferenzeffekt- und Mehrfarbenpigmenten hervorgerufen. Für die vergleichbar großen Glitzerpigmente sind die Glitzerintensität und der Glitzergrad besonders hoch. Die Helligkeitsdifferenzsumme und die relative Leuchtdichtedifferenz repräsentieren den Helligkeitswechsel bzw. den Kontrastglanz und die Glanzabbildungsschärfe empfindungsgemäß nicht zufriedenstellend. Alle betrachteten Kennwerte sind für den weißen Papieruntergrund deutlich niedriger als für den schwarz bedruckten Untergrund.

Schließlich erfordert die Beschreibung der visuellen Wirkung Wissen über die wesentlichen visuellen Wahrnehmungsattribute. Also wurden ihre Anzahl und Art in visuellen Experimenten und statistischen Auswertungen ermittelt. In einer Lichtkabine und einem Mehrwinkelprüfstand wurden 14 gerollte Sieb- bzw. 20 ebene Flexodruckproben präsentiert. Ihre visuellen Unterschiede und zwölf Attribute wurden in relativen bzw. absoluten kategorischen Skalierungsexperimenten bewertet. Sie wurden durch klassische multidimensionale Skalierung, in zwei Korrelationsanalysen, in einer Hauptkomponentenanalyse und in einer exploratorischen Faktoranalyse ausgewertet. Gemäß den *STRESS*-Werten, kumulierten Varianzen und Eigenwerten sind höchstens sechs Attribute von Bedeutung. Signifikant positive Korrelationskoeffizienten zwischen den zwei bzw. drei getesteten Glanz- und Texturattributen erlauben ihre gemeinsame Betrachtung. Die Komponenten- und Faktorladungen geben an, dass es sich bei den sechs wesentlichen Attributen um die vier Farbattribute Buntton, Buntheit, Helligkeit und Bunttonverschiebung sowie die zwei kombinierten Attribute für Glanz und Textur handelt.

Danksagung

Die vorliegende Arbeit ist im Zuge meiner wissenschaftlichen Tätigkeit am *Institut für Druckmaschinen und Druckverfahren* der *Technischen Universität Darmstadt* entstanden. Mein besonderer Dank gilt Herrn *Prof. Dr.-Ing. Edgar Dörsam* für die Freiheiten in meiner Themenfindung und Zielsetzung sowie das Vertrauen in meine Vorgehensweise und Selbstorganisation. In dieser interessanten und lehrreichen Zeit konnte ich mich sowohl fachlich als auch persönlich weiterentwickeln.

Weiterhin danke ich Herrn *Prof. Dr.-Ing. habil. Tran Quoc Khanh* vom *Fachgebiet Lichttechnik* der *Technischen Universität Darmstadt* für die Übernahme der Mitberichterstattung. Herrn *PD Dr.-Ing. habil. Peter Bodrogi* auch vom *Fachgebiet Lichttechnik* danke ich nicht nur für die Mitberichterstattung, sondern auch für die fachliche Beratung zu und bereitwillige Teilnahme an meinen visuellen Experimenten.

Herrn *Dr. Philipp Urban*, dem Gruppenleiter der Forschungsgruppe Farbe am *Institut für Druckmaschinen und Druckverfahren* der *Technischen Universität Darmstadt*, danke ich für die Begleitung meiner Arbeitsschritte und die Hilfestellung bei Veröffentlichungen. Bei Herrn *Prof. Dr. Augustin Kelava* vom *Institut für Psychologie* der *Technischen Universität Darmstadt* bedanke ich mich für die fachliche Diskussion zu meinen visuellen Experimenten und statistischen Auswertungen. Frau *Prof. Galina Paramei* vom *Department of Psychology* der *Liverpool Hope University* danke ich für die konstruktiven Anmerkungen zu meiner schriftlichen Darstellung der visuellen Experimente und statistischen Auswertungen. Bei Herrn *Dr. rer. nat. Andreas Höpe* und Herrn *Kai-Olaf Hauer* von der *Physikalisch-Technischen Bundesanstalt Braunschweig* bedanke ich mich für das Interesse an meinem Arbeitsthema und die Vermessung meiner Druckproben. Herrn *Dr.-Ing. Hans Helmut Jühe* und auch Herrn *Dr. rer. nat. Paul-Heinz Dähling* vom *Stora Enso Research Center Mönchengladbach* gilt großer Dank für die Freiheiten in meinem beruflichen Werdegang, das Vertrauen in eine erfolgreiche Entwicklung und natürlich für die Papierrollen für meine Druckversuche.

Herrn *Dr. Thomas Frey*, Herrn *Christian Fabian* und Frau *Ruth Bauer* von der *BASF SE* sowie Herrn *Andreas Becker* von der *MERCK KGaA* danke ich für die fachliche Information über Spezialeffektpigmente und die großzügige Versorgung mit Druckfarben. Herrn *Dr. Martin Schmitt-Lewen* von der *Heidelberger Druckmaschinen AG* gilt mein Dank für die technische Beratung zu meinen Druckversuchen und die bereitgestellte Laufzeit der Druckmaschine. Bei Herrn *Uwe Schröder* von *Farbmesstechnik Schröder* bedanke ich mich für die technischen Informationen über Mehrwinkelmessungen und das flexible Verleihen der Mehrwinkelspektralfotometer.

Bei *Frank Sperber* bedanke ich mich für seine Studienarbeit zur Entwicklung des Mehrwinkelprüfstands. *Manuel Becher*, *Sabrina Hornig*, *Tobias Roos* und *Carolin Wildner* danke ich für ihr Advanced Design Project zur Evaluierung des Mehrwinkelprüfstands anhand visueller Experimente. *Tobias Schwind* danke ich für seine Hilfe bei den Druckversuchen und der Probenvermessung. *Eric Schunda* gebührt großer Dank für die Konstruktion, den Zusammenbau und die Programmierung des Mehrwinkelprüfstands.

Bei meinen Kollegen bedanke ich mich für die bereitwillige Teilnahme an meinen visuellen Experimenten. *Karsten Rettig* und *Timo Stelzer* danke ich für die Werkstattarbeiten am Mehrwinkelprüfstand. *Thorsten Euler*, *Evgeny Kurmakaev* und *Stephanie Hafner* gilt großer Dank für die Druckversuche. Bei *Nils Bornemann*, *Dr. Hans Martin Sauer*, *Constanze Ranfeld*, *Jens Preiss*, *Dieter Spiehl*, *Maria Haas*, *Alexandra Theopold* und anderen bedanke ich mich für das Korrekturlesen. Bei dem Mitarbeitern vom *Institut für Papierfabrikation und Mechanische Verfahrenstechnik* bedanke ich mich für die freundliche Aufnahme und die angenehme Atmosphäre. Insbesondere Herrn *Prof. Dr.-Ing. Samuel Schabel* danke ich für die Bereitstellung eines ruhigen Arbeitsplatzes zum Zusammenschreiben der Arbeit. Den Mitarbeitern vom *Fachgebiet Lichttechnik* danke ich für die Einladung zu euren visuellen Experimenten und die Beratung zu meinen visuellen Experimenten.

Meinem Partner *Henri Kröling* danke ich nicht nur für das geduldige Zuhören, die fachlichen Diskussionen und das kritische Korrekturlesen, sondern auch für die nötige regelmäßige Ablenkung, die liebevolle mentale Unterstützung sowie die besonders in der Endphase fast täglich erforderliche

Motivation.

Bei meinen Eltern *Monika* und *Dietmar Kehren* bedanke ich mich für die Begleitung meines Lebensweges und die Unterstützung meiner Ausbildung sowie für ihr immer währendes Vertrauen und die vielen aufmunternden Worte.

Abschließend danke ich allen Freunden und Bekannten dafür, dass sie mich bei gemeinsamen Aktivitäten auf andere Gedanken gebracht haben.

Contents

Notations

0.1 Abbreviations

ACS	absolute category scaling
AG	Aktiengesellschaft
AHDS	angular hue difference sum
al.	alia, aliae, alii
an	greenness
ap	redness
ARGon^3	three-dimensional appearance robot-based gonioreflectometer
ASTM	American Society for Testing and Materials
B	blue
BBRRDF	bispectral bidirectional reflectance and reradiation distribution function
BDP	Berufsverband Deutscher Psychologinnen und Psychologen
bn	blueness
BO	*BlackOlive*
bp	yellowness
BPB	black paper background
BPB	black printed background
BRDF	bidirectional reflectance distribution function
BRTD	bidirectional reflectance and texture database
BTF	bidirectional texture function
BUCP	black uncoated paper
C	*Colorstream*
C	chroma
CA	correlation analysis
CCD	charge-coupled device
CCT	correlated color temperature
CDS	chroma difference sum
CFA	confirmatory factor analysis
CG	contrast gloss
CIE	International Commission on Illumination
CIELAB	International Commission on Illumination L^*, a^*, b^*
CIELCH	International Commission on Illumination L^*, C^*_{ab}, h°_{ab}
CMDS	classical multidimensional scaling
CMOS	complementary metal-oxide-semiconductor
Co.	Compagnie
comp.	composition
conc.	concentration
conf.	configuration

$D50$	daylight 5000 K
$D65$	daylight 6500 K
$DGPs$	Deutsche Gesellschaft für Psychologie
DIN	Deutsches Institut für Normung
$DOIG$	distinctness-of-image gloss
$Dr.$	Doctor
DU	drying unit
dH	hue shift
$diss.$	dissimilarity
dL	lightness shift
$dLCG$	lightness shift and contrast gloss
DR	dimension reduction
EFA	exploratory factor analysis
$e.\ V.$	eingetragener Verein
F	*Firemist*
FA	factor analysis
FFG	far-from-gloss
G	*Glacier*
G	gloss
G	gold
G	graininess
G	green
GC	graininess and coarseness
$GmbH$	Gesellschaft mit beschränkter Haftung
$GMDS$	generalized multidimensional scaling
GVS	glossy varnished surface
$habil.$	habilitus
HDR	high dynamic range
HDS	hue difference sum
I	*Iriodin*
IDD	Institut für Druckmaschinen und Druckverfahren
IE	interference effect
$Inc.$	Incorporated
$Ing.$	Ingenieur
IO	iron oxide
IR	infra-red
ISO	International Organization for Standardization
KG	Kommanditgesellschaft
L	lightness
L	*Lumina*
LDR	low dynamic range
LDS	lightness difference sum
LED	light emitting diode
$Ltd.$	Limited

M	*Miraval*
MC	multi-color
MDS	multidimensional scaling
$MMDS$	metric multidimensional scaling
NAG	near-at-gloss
nat.	nature
nat.	naturalium
$NIST$	National Institute of Standards and Technology
$NMMDS$	non-metric multidimensional scaling
num.	number
OR	orthogonal rotation
param.	parameter
PCA	principal component analysis
PD	Privatdozent
PPS	Parker Print Surf
Prof.	Professor
PU	printing unit
PTB	Physikalisch-Technische Bundesanstalt
$PTFE$	polytetrafluorethylen
rat.	rating
R	red
RCS	relative category scaling
rer.	rerum
$RGon$	robot-based gonioreflectometer
$RMDS$	replicatedmultidimensional scaling
RYD	relative luminance difference
S	sparkle
SF	*SantaFe*
SG	sparkle and glint
$STARR$	spectral tri-function automated reference reflectometer
$STARR\ II$	second spectral tri-function automated reference reflectometer
$STRESS$	standardized residual sum of squares
$SVBRDF$	spatially varying bidirectional reflectance distribution function
SW	silver white
$TAPPI$	Technical Association of the Pulp and Paper Industry
TC	Technical Committee
TC	texture contrast
$TVBRDF$	temporally varying bidirectional reflectance distribution function
UV	ultra-violet
UVS	unvarnished surface
VAA	visual appearance attributes
VAD	visual appearance difference
VIS	visible
$WGCP$	white glossy coated paper
$WMCP$	white matte coated paper
$WMDS$	weighted multidimensional scaling
WPB	white paper background

0.2 Mathematical Symbols

A	arithmetic mean in the unit of the variable
A	arbitrary square matrix in an arbitrary unit
A	unit element, dimensionless
a	model parameter in an arbitrary unit
a^*	greenness-redness value, dimensionless
a_i^*	greenness-redness value number i, dimensionless
a_j^*	greenness-redness value number j, dimensionless
α	incidence angle in degree °
b^*	blueness-yellowness value, dimensionless
b_i^*	blueness-yellowness value number i, dimensionless
b_j^*	blueness-yellowness value number j, dimensionless
β	reflection angle in degree °
$\boldsymbol{C}$	color matrix, dimensionless
C	covariance in the unit of the variable
C_{ab}^*	chroma, dimensionless
$C_{ab,i}^*$	chroma number i, dimensionless
$C_{ab,j}^*$	chroma number j, dimensionless
d	viewing distance in meter m
$\Delta a_{i,j}^*$	greenness-redness difference, dimensionless
$\Delta b_{i,j}^*$	blueness-yellowness difference, dimensionless
$\Delta C_{ab,i,i+1}^*$	geometry-induced chroma difference, dimensionless
$\Delta C_{ab,i,j}^*$	chroma difference, dimensionless
$\Delta C_{ab,1,N}^*$	chroma difference sum, dimensionless
$\Delta E_{ab,i,i+1}^*$	geometry-induced color difference, dimensionless
$\Delta E_{ab,i,j}^*$	color difference, dimensionless
$\Delta E_{ab,1,N}^*$	color difference sum, dimensionless
$\Delta H_{ab,i,i+1}^*$	geometry-induced hue difference, dimensionless
$\Delta H_{ab,i,j}^*$	hue difference, dimensionless
$\Delta H_{ab,1,N}^*$	hue difference sum, dimensionless
$\Delta h_{ab,i,i+1}^\circ$	geometry-induced angular hue difference in degree °
$\Delta h_{ab,i,j}^\circ$	angular hue difference in degree °
$\Delta h_{ab,1,N}^\circ$	angular hue difference sum in degree °
$\Delta L_{i,i+1}^*$	geometry-induced lightness difference, dimensionless
$\Delta L_{i,j}^*$	lightness difference, dimensionless
$\Delta L_{1,N}^*$	lightness difference sum, dimensionless
$\Delta Y_{r,FFG,NAG}$	relative luminance difference, dimensionless
$\Delta \phi_r$	reflection azimuth angle resolution in degree °
$\boldsymbol{E}$	unit matrix, dimensionless
E_e	irradiance in Watt W per square meter m^2
E_i	incident irradiance in Watt W per square meter m^2

f	case distinction function, dimensionless
f	model function in an arbitrary unit
f_r	bidirectional reflectance distribution function in one per steradian sr
G	graininess, dimensionless
H^*_{ab}	hue, dimensionless
h°_{ab}	hue angle in degree $^\circ$
$h^\circ_{ab,i}$	hue angle number i in degree $^\circ$
$h^\circ_{ab,j}$	hue angle number j in degree $^\circ$
I	incident light ray, dimensionless
I_e	radiant intensity in Watt W per steradian sr
J_e	radiosity in Watt W per square meter m^2
$\boldsymbol{K}$	correlation matrix, dimensionless
L	lower boundary, dimensionless
L^*	lightness, dimensionless
L^*_i	lightness number i, dimensionless
L^*_j	lightness number j, dimensionless
$\boldsymbol{LAMBDA}$	wavelength matrix in nanometer nm
L_e	radiance in Watt W per steradian sr and per square meter m^2
λ	wavelength in nanometer nm
λ	eigenvalue, dimensionless
λ_i	eigenvalue number i, dimensionless
λ_i	incidence wavelength in nanometer nm
λ_r	reflection wavelength in nanometer nm
M_e	radiant exitance in Watt W per square meter m^2
m	number for samples, dimensionless
m_C	number of geometric configurations in color matrix $\boldsymbol{C}$, dimensionless
m_{OMEGA}	number of geometric configurations in geometry matrix $\boldsymbol{OMEGA}$, dimensionless
m_R	number of geometric configurations in reflectance matrix $\boldsymbol{R}$, dimensionless
n	number for eigenvalue λ, dimensionless
n	number for variable X, dimensionless
n	order, dimensionless
n	refraction index, dimensionless
n_{LAMBDA}	number of spectral measuring points in wavelength matrix $\boldsymbol{LAMBDA}$, dimensionless
n_{OMEGA}	number of specified angles in geometry matrix $\boldsymbol{OMEGA}$, dimensionless
n_R	number of spectral measuring points in reflectance matrix $\boldsymbol{R}$, dimensionless
$\boldsymbol{OMEGA}$	geometry matrix in degree $^\circ$
Ω	solid angle in steradian sr
$\boldsymbol{\omega}$	direction in meter m or degree $^\circ$
$\boldsymbol{\omega}_i$	incidence direction in meter m or degree $^\circ$
$\boldsymbol{\omega}_r$	reflection direction in meter m or degree $^\circ$

P_{CG}	contrast gloss parameter, dimensionless
P_{DOIG}	distinctness-of-image gloss parameter, dimensionless
$\boldsymbol{p}$	location in meter m
$\boldsymbol{p}_i$	incidence location in meter m
$\boldsymbol{p}_r$	reflection location in meter m
Φ_e	radiant flux in Watt W
ϕ	azimuth angle in degree °
ϕ_{az}	at-specular aspect angle in degree °
ϕ_i	incidence azimuth angle in degree °
ϕ_r	reflection azimuth angle in degree °
Q	radiant energy in Joule J
q	quotient of tristimulus value X and X_n, Y and Y_n, Z and Z_n
R	correlation coefficient, dimensionless
$\boldsymbol{R}$	correlation matrix, dimensionless
$\boldsymbol{R}$	reflectance matrix, dimensionless
R	reflected light ray, dimensionless
r	radius in meter m
$\boldsymbol{r}$	rotation matrix, dimensionless
$\boldsymbol{S}$	covariance matrix in the unit of the variables
S	sparkle matrix, dimensionless
S_A	sparkle area, dimensionless
S_G	sparkle grade, dimensionless
S_I	sparkle intensity, dimensionless
S	standard deviation in the square root of the unit of the variable
S	stress value, dimensionless
s	object size in meter m
$\boldsymbol{s}$	scaling matrix, dimensionless
T	transmitted light ray, dimensionless
$\boldsymbol{t}$	translation matrix in the unit of the target, reference and transformed matrix
t	time in second s
t	unit time in second s
t_i	incidence time in second s
t_r	reflection time in second s
θ	polar angle in degree °
θ	visual angle in degree °
θ_{as}	in-plane aspect angle in degree °
θ_i	incidence polar angle in degree °
θ_r	reflection polar angle in degree °

U	upper boundary, dimensionless
V	variance in the unit of the variable
V_c	cumulated variance in the unit of the variable
V_e	explained variance in the unit of the variable
X	independent variable in an arbitrary unit
X	tristimulus value, dimensionless
$\boldsymbol{X}$	target matrix in an arbitrary unit
X_i	random variable number i in an arbitrary unit
X_n	tristimulus value of reference for normalization, dimensionless
x	coordinate in meter m
$\boldsymbol{x}$	eigenvector, dimensionless
$\boldsymbol{x}_i$	eigenvector number i, dimensionless
x_i	incidence coordinate in meter m
$x_{i,k}$	sampled number in the unit of the variable X_i
X_j	random variable number j in an arbitrary unit
$x_{j,k}$	sampled number in the unit of the variable X_j
x_r	reflection coordinate, dimensionless
Y	dependent variable in an arbitrary unit
Y	luminance, dimensionless
$\boldsymbol{Y}$	reference matrix in an arbitrary unit
Y	tristimulus value, dimensionless
Y_{FFG}	far-from-gloss luminance, dimensionless
Y_G	gloss luminance, dimensionless
Y_n	tristimulus value of reference for normalization, dimensionless
Y_{NAG}	near-at-gloss luminance, dimensionless
y	coordinate in meter m
y_i	incidence coordinate in meter m
y_r	reflection coordinate in meter m
$\boldsymbol{Z}$	transformed matrix in an arbitrary unit
Z	tristimulus value, dimensionless
Z_n	tristimulus value of reference for normalization, dimensionless
z	coordinate in meter m
z_i	incidence coordinate in meter m
z_r	reflection coordinate in meter m
$z_{i,k}$	standard score in the square root of the unit of the variable

0.3 Indices

A	area in sparkle area S_A
a	greenness-redness value a^* in color coordinates
b	blueness-yellowness b^* in color coordinates
as	aspect in in-plane aspect angle θ_{as}
az	azimuth in at-specular aspect angle ϕ_{az}
c	cumulated in cumulated variance V_c
CG	contrast gloss in contrast gloss parameter P_{CG}
$DOIG$	distinctness-of-image gloss in distinctness-of-image gloss parameter P_{CG}
e	energy in radiometric dimensions
e	explained in explained variance V_e
FFG	far-from-gloss in far-from-gloss luminance Y_{FFG} and relative luminance difference $\Delta Y_{r,FFG,NAG}$
G	gloss in gloss luminance Y_G
G	grade in sparkle grade S_G
I	intensity in sparkle intensity S_I
i	incidence in incidence dimensions
i	number in color coordinates
i	number in eigenvalue λ_i
i	number in random variable X_i
j	number in color coordinates
j	number in random variable X_j
k	number in sampled number $x_{i,k}$, $x_{j,k}$
N	number in color coordinates
n	normalization in normalized tristimulus values X_n, Y_n, Z_n
n	number in random variable X_n
NAG	near-at-gloss in near-at-gloss luminance Y_{NAG} and relative luminance difference $\Delta Y_{r,FFG,NAG}$
r	reflectance in bidirectional reflectance distribution function f_r
r	reflection in reflection dimensions
r	relative in relative luminance difference $\Delta Y_{r,FFG,NAG}$
C	color in number of geometric configurations m_C
$LAMBDA$	wavelength in number of spectral measuring points n_{LAMBDA}
$OMEGA$	direction in number of geometric configurations m_{OMEGA}
$OMEGA$	direction in number of specified angles n_{OMEGA}
R	reflectance in number of geometric configurations m_R

0.4 Chemical Formula

Al_2O_3	aluminum oxide
$BaSO_4$	barium sulfate
Cr_2O_3	chromium(III) oxide
FeO	iron(II) oxide
Fe_2O_3	iron(III) oxide
Fe_3O_4	iron(II, III) oxide
SiO_2	silicon dioxide
SnO_2	tin dioxide
TiO_2	titanium dioxide

Chapter 1

Problem and Approach

In your daily life, you get in touch with an incredibly wide variety of printed products. The following invented description of your daily routine just names a small fraction of them.

You start your day with a hot off the press newspaper at the breakfast table. On the kitchen table, there are also milk in a printed composite packaging as well as cereals in a printed cardboard box. Many more examples for printed packaging materials, you can find during your short visit to the supermarket on the way to work. Think of your soft drink in a printed metal can and of your candy bar in a printed plastic foil. When arriving in the office, you first take a look in your calendar for your today's events. On the way home after work, you get in touch with price tags and bank notes in the shopping center.

In your mind, you can expand this story about your daily contact with printed products. But, do not forget the most important thing at the end of the day. Every evening, you read in your favorite book. The book is about printing such as the book of *Kipphan* [148, 149].

The so-called letterpress printing was invented by Johannes Gutenberg in the 15^{th} century. Movable types made of metal or wood were composed to words, phrases, paragraphs and pages. The elevated areas of the letters were inked with printing inks containing light-absorbing pigments. By the use of a printing press, the inked printing plate is pressed on the printing substrate.

Apart from the invention of the printing technology, your book tells you about the important technological developments and actual trends. The trends of the last years go towards more finishing measures like varnishing or embossing and towards higher color standards. The actual trend towards higher color standards is expressed in the increased application of chromatic light-absorbing inks and the market introduction of special effect inks. Printing inks containing special effect pigments are used more frequently for high quality printing products [209, 218, 220]. For example, these are admission tickets, bank notes, price tags, jewelry casings, perfume wrappings, chocolate boxes, cigarette packets, wine labels, wall papers and decor papers.

Printed special effect colors fascinate due to their special object characteristics causing unique optical properties and a fascinating visual appearance. Printing parameters such as the special effect pigment, the paper quality, the varnishing state and the background color, have an influence on the optical properties and visual appearance. The bidirectional reflectance and texture distribution describes the dependence of the optical properties on the geometric configuration of light source and detection system relative to the sample. The visual appearance of color, gloss and texture is described by visual appearance attributes such as hue, chroma, lightness, color shift, hue shift, contrast gloss, distinctness-of-image gloss, metal gloss, pearl gloss, texture contrast, graininess, coarseness, sparkle, glint or others. This study focuses on the description of the optical properties and of the visual appearance of printed special effect colors produced with varied printing parameters. This chapter is an introduction to the underlying *problem* (section 1.1) and gives an idea about the respective *approach* (section 1.2).

1.1 Problem

The main problem consists of three individual but interrelated partial problems. These are the *poorly researched special effect printing* (section 1.1.1), the *complex bidirectional optical properties* (section 1.1.2) as well as the *incomplete perception-based characterization* (section 1.1.3).

1.1.1 Poorly Researched Special Effect Printing

The application of special effect inks in printing increases due to the particular optical properties resulting in a unique visual appearance. The optical properties and thus the visual appearance are influenced by multiple printing parameters as pointed out in the study of *Haas* [93, 94], the books of *Glausch et al.* [86] and *Pfaff et al.* [204, 205] and in the color cards of the *MERCK KGaA* for offset [185], gravure [184], flexo [182] and screen [183] printing. These printing parameters are material, design and process parameters.

Material parameters are for example the type of the special effect pigment and their concentration in the printing ink as well as the roughness and porosity of the substrate. An optional priming with a light-absorbing ink, the tonal value of the special effect print and an optional finishing with a clear gloss varnish are examples for design parameters. Examples for process parameters are the machine speed or the ink supply. The ink supply is a directly adjustable machine parameter as well as an indirectly adaptable equipment parameter. This is the mesh width of the fabric in screen printing or the dispersion volume of the anilox roll in flexo printing. All these printing parameters also influence the process stability and reliability.

The influences on process stability and reliability are known to a large extent for light-absorbing inks and to a wide extend for special effect inks. For printed light-absorbing colors, the influence on the optical properties and thus the visual appearance are known to some degree [197, 198]. In contrast to this, the influence on the optical properties and thus the visual appearance of printed special effect colors was rarely considered in research. *Haas* [93, 94] used optical and visual data to optimize printing parameters with regard to a maximum optical and visual effect. In contrast, the printing parameters can be varied to produce optically and visually different samples for further investigations concerning the optical properties and visual appearance. Thus, the *poorly researched influence* of the *printing parameters* on the *optical properties* and *visual appearance* of printed special effect colors is the first partial problem.

1.1.2 Unavailable Bidirectional Optical Data

The interest on computer simulations grows in various fields. Think of computer games, architectural visualizations or product design. For a realistic representation of any material, computer graphical rendering requires measured or modeled bidirectional reflectance and texture distributions. This is illustrated in the books of *Ward Larson* and *Shakespeare* [244] and of *Pharr* and *Humphreys* [207].

Precise measurements of bidirectional reflectance and texture distributions are expensive. Measured bidirectional reflectance and texture data are not particularly representative and difficult to process in graphical rendering. Modeling of bidirectional reflectance and texture distributions allows their representation in a simple model equation with a few model parameters. Variations in the model parameters admit variations in the bidirectional reflectance and texture distributions.

For several materials such as metal, plastic, fabric and rocks, databases with measured bidirectional reflectance and texture distributions are available. It was achieved to model bidirectional reflectance and texture distributions of these rather simple materials. For example, the measuring and modeling of bidirectional reflectance and texture data is described by *Dana et al.* [52, 53, 51, 54], *Matusik et al.* [175, 178, 177], *Berns* [22, 23] and others [196, 36, 11]. For the rather complex special effect colors, measured and modeled bidirectional reflectance and texture distributions are both very rarely available. Due to their high complexity, the second partial problem is thus the *availability* of *measured* or *modeled bidirectional reflectance* and *texture distributions* of special effect colors.

1.1.3 Incomplete Perception-Based Characterization

Increasing quality demands result in enhanced measures for process control. A stable, reliable printing process is essential for reproducible high printing qualities as considered by *Hupp* [112, 113], *Hupp* and *Dörsam* [115] and *Kehren et al.* [144]. The printing quality is monitored by means of perception-based tolerances of the associated parameters.

The perception-based parameters are visual appearance attributes for color, gloss and texture. These visual appearance attributes are determined on the basis of measurable optical parameters [211]. The visual appearance attributes are connected with the measurable optical parameters by the so-called psychophysical equation. The psychophysical functions as well as the number and nature of the essential visual appearance attributes are determined in visual experiments followed by statistical evaluations. Among others [167, 92], *Rao* and *Lohse* [212] determined the number and nature of essential texture attributes. The number and nature of the essential gloss attributes as well as their psychophysical function was determined by *Pellacini et al.* [200] and *Ferwerda et al.* [80] and continued by *Phillips et al.* [208].

As described by *Young* [255], *Maxwell* [179], *Hering* [99] and *Judd* [135, 136, 137, 138, 139, 140], the number and nature of the essential visual appearance attributes as well as their psychophysical function are widely known for light-absorbing colors . These are the three color attributes hue, chroma and lightness. Gloss and texture attributes are not that significant for a printed light-absorbing color as solid area without subsequent varnishing. Printed special effect colors show a geometry-dependent color, a metal to pearlescent gloss and clearly visible texture. The number and nature of essential color, gloss and texture attributes as well as the psychophysical functions are widely unknown in case of printed special effect colors as pointed out by *Kehren et al.* [146]. The *incomplete knowledge* about the *essential visual appearance attributes* for the *perception-based characterization* of special effect colors is the third partial problem.

1.2 Approach

The three partial problems introduced in section 1.1 each call for an approach. The approaches for the three partial problems suggest a somehow three-part structure of the main part in this document. Figure 1.1 shows the complete structure of the thesis including the problem and approach at the beginning (chapter 1) as well as the summary and outlook at the end (chapter 8).

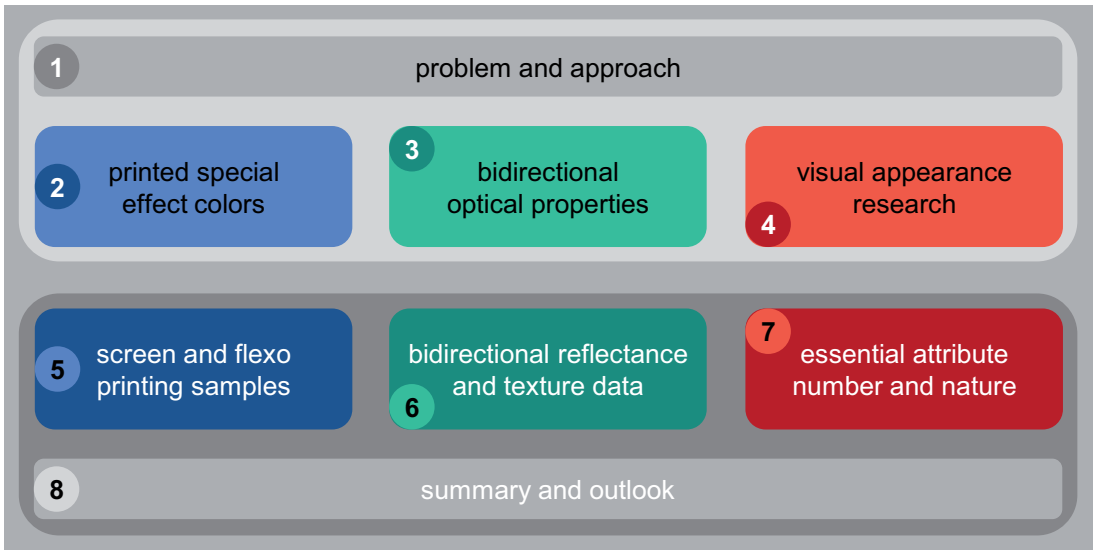

Figure 1.1: Structure of the thesis.

Apart from chapter 1 and chapter 8, the main part of this thesis consists of two times three chapters. The first three main chapters are intended to induce a better understanding of the just presented problems (section 1.1). According to the three introduced problems, chapter 2, chapter 3 and chapter 4 give a review about *printed special effect colors*, *bidirectional optical properties* and *visual appearance research*, respectively. The expressions *screen and flexo printing samples*, *bidirectional reflectance and texture database* as well as *number and nature of essential attributes* are the headlines of chapter 5, chapter 6 and chapter 7. These last three main chapters describe the approach followed in this study. The *production of special effect samples* (section 1.2.1), the *collection of bidirectional optical data* (section 1.2.2) and the *identification of the essential visual appearance attributes* (section 1.2.3) are the three approaches derived in the following.

1.2.1 Production of Special Effect Samples

For the derivation of the first approach, remember the first partial problem (section 1.1.1). There is a lack of knowledge about the influence of the printing parameters on the optical properties and visual appearance of printed special effect colors.

Any examination on the influence of printing parameters requires a set of printed samples. The samples of printed special effect colors should vary in at least one of the most important printing parameters. The study of *Haas* [93, 94] gives an overview about possible variations in the printing parameters. The application cases ought to differ in the roughness or porosity of the substrate, the color of the background, the varnishing of the surface and in the type or occupancy of the special effect pigment.

Fine and specific variations in multiple printing parameters would allow to collect detailed optical data in bidirectional measurements and meaningful perceptual data in visual experiments. With the measured optical data, the bidirectional reflectance and texture distribution could be modeled. The model parameters would give information about the influence of the printing parameters on the optical properties. The determined perceptual data could be used to determine

the psychophysical functions of the essential visual appearance attributes. The psychophysical functions would give information about the influence of the printing parameters on the visual appearance.

This approach is too extensive for a first study on the optical properties and the visual appearance of printed special effect colors. The achievement of fine and specific variations in multiple printing parameters is difficult and requires several preliminary studies.

Therefore, gross variations in a few printing parameters are intended to be realized in this first approach. The variations in the most important printing parameters are chosen fine enough to collect representative optical data and sufficient perceptual data. The measured optical data allow for the calculation of perception-related parameters (section 1.2.2). These are an indication for the influences of the printing parameters on the visually perceived characteristics. The determined perceptual data allow to identify the number and nature of the essential visual appearance attributes (section 1.2.3). The number and nature of the essential visual appearance attributes should be known before the determination of the psychophysical function makes sense.

In summary, the approach for the first partial problem is the *production* of *special effect samples* in several representative application cases with varying printing parameters. The printing samples varying in the special effect pigment, the paper quality, the varnishing state and in the background color will be sufficient to be used in the second and third approach (section 1.2.2, section 1.2.3).

1.2.2 Collecting of Bidirectional Optical Data

The second approach is a result of the second partial problem (section 1.1.2). Due to the high complexity, neither measured nor modeled bidirectional reflectance and texture distributions of special effect colors are available.

Before any steps towards the modeling of the bidirectional reflectance and texture distribution are taken, reflectance and texture data need to be collected in bidirectional measurements on samples of printed special effect colors. The measured reflectance and texture data should be filed in a freely available database such as those of *Dana et al.* [52, 53, 54], *Matusik et al.* [175, 178, 177], *Berns* [22, 23] and others [196, 36, 11].

Due to the free availability, the bidirectional reflectance and texture database can be used in any studies on printed special effect colors. The data might be useful to model the bidirectional reflectance and texture distribution or to determine the psychophysical functions of the essential visual appearance attributes. A bidirectional reflectance and texture model represents the complex bidirectional reflectance and texture distribution in a comparably simple model equation with several physically plausible model parameters. The model equation with arbitrarily varying model parameters allows to simulate printed special effect colors by computer graphics rendering. The rendered computer graphics can be used to collect complex perceptual data allowing the determination of the psychophysical functions of visual appearance attributes. The psychophysical functions give information about the influences of the model parameters.

The just explained approach is beyond the scope of a first study about the optical properties and the visual appearance of printed special effect colors. The reproduction of the measured bidirectional reflectance and texture distribution in a model requires an extensive knowledge in this domain.

In the present case, the bidirectional measurements are intended to be conducted on the previously printed special effect samples (section 1.2.1). A freely available bidirectional reflectance and texture database will be generated on the basis of the measured reflectance spectra, calculated color coordinates and determined texture parameters. The bidirectional reflectance and texture data are intended to be used to calculate perception-related parameters. As mentioned above, the perception-related parameters give information about the influences of the printing parameters on the perceived properties of printed special effect colors.

As result, the approach of the second partial problem intends to *collect bidirectional reflectance* and *texture data* for the special effect samples printed during the approach of the first partial problem (section 1.2.1). The measured reflectance spectra, the calculated color coordinates and

the determined texture parameters will be used to calculate perception-related parameters giving information about the influences of the varied printing parameters.

1.2.3 Identification of Essential Visual Appearance Attributes

The third partial approach is based on the third partial problem explained in section 1.1.3. Until now, there is not enough knowledge to completely characterize the unique visual appearance of printed special effect colors.

Prior to the determination of any psychophysical function, the number and nature of the essential visual appearance attributes should be known. The number and nature can be determined by means of visual experiments followed by statistical evaluations as realized by *Pellacini et al.* [200], *Ferwerda et al.* [80], *Rao* and *Lohse* [212] and others [208, 245, 167, 92].

For the determination of the psychophysical function of any visual appearance attribute, stimuli with fine and specific variations in the considered visual appearance attribute are required. In the present case, the stimuli could be printed samples or rendered images. For all stimuli, physically-based parameters describing the optical properties and perceptual data collected in visual experiments should be available. Their linking in an equation results in the psychophysical function of the considered visual appearance attribute.

In this first study, neither printed samples nor rendered images with fine and specific variations in multiple printing or model parameters, respectively, are available. Furthermore, the number and nature of the essential visual appearance attributes is not known.

In contrast to that, the previously printed samples (section 1.2.1) roughly varying in the most important printing parameters are available. In spite of the rather gross variations, these samples allow for the identification of the essential visual appearance attributes. For this purpose, relative and absolute category scaling experiments on visual appearance differences and visual appearance attributes are planned. The collected dissimilarity and rating data will be evaluated by the use of different statistical methods such as classical multidimensional scaling, a correlation analysis, a principal component analysis and an exploratory factor analysis.

In conclusion, the approach of the third partial problem focuses on the *identification* of the *essential visual appearance attributes*. Their number and nature will be identified in statistical evaluations of visual experiments on the samples of printed special effect colors produced during the first approach (section 1.2.1).

Chapter 2

Printed Special Effect Colors

Due to the poorly researched influence of the printing parameters on the optical properties and visual appearance, printing of special effect colors causes problems (section 1.1.1). A better understanding of this first partial problem is provided in this chapter.

Furthermore, it illustrates the need of the respective approach. It is intended to produce special effect samples varying in the most important printing parameters (section 1.2.1, chapter 5).

Thus, section 2.1 gives an introduction to *special effect pigments*. Their application in *special effect printing* is considered in section 2.2.

2.1 Special Effect Pigments

In the following, the fundamental features of special effect pigments are itemized. At first, the *pigment structure* (section 2.1.1) is explained. Based on these explanations, the underlying *optical effects* (section 2.1.2) are pointed out. The special effect pigments are then assigned to different *pigment classes* (section 2.1.3). Finally, typical *pigment applications* (section 2.1.4) are listed.

2.1.1 Pigment Structure

In their shape and size, special effect pigments considerably differ from conventional light-absorbing pigments. Conventional light-absorbing pigments are spherical particles with diameters below 1 μm [20]. In contrast to that, special effect pigments are shaped like thin flakes with diameters of up to 200 μm [204, 205].

According to their particle size, special effect pigments are assigned to one of five classes distinguished by *Glausch et al.* [86] and by *Pfaff et al.* [206, 202, 201, 204, 205]. These five particle size classes range from 1 μm to 15 μm, 5 μm to 20 μm, 10 μm to 50 μm, 10 μm to 130 μm and from 40 μm to 200 μm (table A.2, table A.6). The particle size of an arbitrary special effect pigment is also specified in the data sheets of the pigment producers.

The particle size has an influence on the visual perception of gloss and texture. In contrast to this, the perceived color mainly depends on the structure of a special effect pigment. The pigment structure is described by *Pfaff et al.* [206, 202, 201, 203, 204, 205] and others [14, 86, 171, 172, 221]. Special effect pigments are composed of a flaky substrate covered with one or more thin coating layers as shown in figure 2.1.

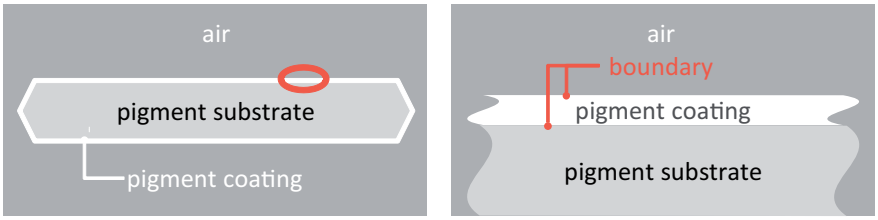

(a) General view. (b) Detailed view.

Figure 2.1: Structure of a special effect pigment.

This two-component structure fulfills all demands on mechanical strength and optical specialty. The mechanically stable substrate serves as supporting basis for the optically active coating inducing the intended effect. The materials used for *substrate* and *coating* are described in the following.

Pigment Substrate

According to *Pfaff et al.* [206, 202, 201, 203, 204, 205] and others [14, 86, 171, 172, 221], the transparent substrate consists of natural mica or synthetic materials. The synthetic materials are namely aluminum oxide (Al_2O_3), silicon dioxide (SiO_2) or borosilicate (table A.3, table A.7).

In contrast to natural mica, the synthetic materials are larger in particle size, more even in surface structure and free of coloring impurities. Due to the minimized scattering on the substrate surface and the eliminated optical absorption of coloring impurities, the printed result is clearer in color, gloss and texture.

Pigment Coating

As described by *Pfaff et al.* [206, 202, 201, 203, 204, 205] and others [14, 86, 171, 172, 221], the pigment coating is formed of one or more thin layers of a high-refractive metal oxide. Titanium

dioxide (TiO_2), iron(III) oxide (Fe_2O_3), tin dioxide (SnO_2) and chromium(III) oxide (Cr_2O_3) are the most common ones (table A.4, table A.8) .

Compared to the substrate materials, the refractive index of the coating materials is high. While mica has an index of refraction between 1.5 and 1.6, the refractive indexes of all enlisted metal oxides are above 2.5. The elevated refractive index of the thin coating layer induces a more or less pronounced light interference effect. The same optical effect is responsible for the well-known Newton's rings, a circular interference pattern. In case of special effect pigments, the effect of interference on thin layers results in a geometry-dependent color impression.

The rutile form of titanium dioxide (TiO_2) with a refractive index of approximately 2.7 is favored over its anatase form with a refractive index of approximately 2.5. The same holds for the iron oxide forms hematite and magnetite with refractive indexes of approximately 2.9 and 2.4, respectively. The iron(III) oxide (Fe_2O_3) is called hematite. Magnetite is used for iron(II, III) oxide (Fe_3O_4) a mixture of iron(II) oxide (FeO) and iron(III) oxide (Fe_2O_3). Sometimes, an intermediate layer of low-refractive silicon dioxide (SiO_2) with a refractive index of approximately 1.5 is applied to increase the interference effect.

In contrast to the geometry-dependent interference effect, optical absorption causes only a color impression independent of the geometric configuration. The optical properties of many other metal oxides are dominated by absorption characteristics [39]. All high-absorptive metal oxides are not adequate to induce an interference effect, but useful to accentuate the geometry-independent coloring. Iron(III) oxide (Fe_2O_3) is the only adequate metal oxide for special effect pigments with absorption characteristics being in balance with the interference effect.

2.1.2 Optical Effects

Considering a single special effect pigment, multiple optical effects take place. All individual optical effects occurring in this multi-layer system are introduced below. The most important combined effect of interference on thin layers is explained in detail.

Isolated Optical Effects

In the following, the fundamental optical effects named *absorption*, *scattering*, *reflection*, *refraction* and *transmission* are explained in general. Furthermore, each of the enlisted optical effects is deeply considered on the example of special effect pigments.

For a better understanding, small spots of the whole special effect pigment are zoomed in. The diameter of the zoomed spots lies in the visible wavelength range. Thus, the differentiation of geometric optics and physical optics is not clearly set. The predominantly geometric approach is expanded by some details originating from physical optics.

Absorption of Iron Oxide and Coloring Impurities In the physical sense, absorption describes the reception of an agent, a particle or a wave. More precisely, the absorption of light is defined as the total or partial, wavelength-dependent transfer of electromagnetic energy to matter. Thus, absorption comes along with a conversion into another form of energy like heat. Further information on absorption is given in the books of *Kortüm* [157] and *Pedrotti et al.* [199] as well as in the technical report *CIE TC*1-65 [120].

Black materials like carbon pigments are almost ideal absorbers. The electromagnetic energy of an incident ray of white light is transformed to heat in the whole visible wavelength range. Other materials are selective absorbers. The absorption of incident white light is limited to electromagnetic energy of specific wavelengths or wavelength regions. The electromagnetic energy of the remaining wavelengths or wavelength regions is reflected or transmitted as colored light.

For a single special effect pigment, absorption is achieved by an iron oxide (Fe_2O_3) coating or by coloring impurities in the natural mica substrate. The other metal oxides used as coating materials are colorless. Substrate materials produced synthetically are free from coloring impurities. Figure 2.2a highlights the mentioned spots of absorption.

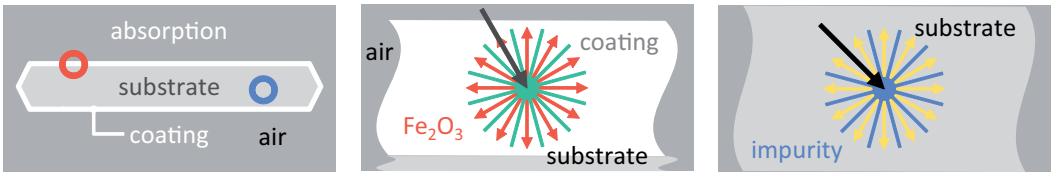

(a) Spot at pigment. (b) Zoom in coating. (c) Zoom in substrate.

Figure 2.2: Absorption of a special effect pigment.

The iron oxide (Fe_2O_3) in the coating absorbs electromagnetic energy in the wavelength range of green light. The absorption of green light comes along with the scattering of red light as shown in figure 2.2b. The resulting rusty, reddish brown color is independent from the geometric configuration of the light source and observer relative to the sample.

In contrast to the welcome reddish iron oxide color, the yellowish tint of the substrate is not desired in commercial applications like graphical printing. Yellowish colors give the impression of being dirty. As shown in figure 2.2c, the scattered yellow light results from blue absorbing impurities in natural mica. Commonly, such coloring impurities absorbing blue light are not incorporated in synthetic substrates.

Internal Scattering in Coating and Substrate In general, scattering describes the deflection of radiation from the straight propagation direction due to irregularities in the crossed medium as defined in the technical report *CIE TC*1-65 [120]. For example, rays of light are deflected on dust or particles in the air.

For comparably large particles with diameters above the visible wavelength range, light is considered as a ray. The scattering of light rays obeys the geometric laws of refraction at a sphere. Apart from this so-called geometric scattering, the Mie scattering with the special case of Rayleigh scattering are known and described by *Kortüm* [157] and *Pedrotti et al.* [199]. Mie scattering occurs at spherical particles with diameters in the visible wavelength range. For very small particles with diameters below the wavelength range of light, the Rayleigh scattering model for waves is applicable.

Depending on the considered medium, the deflection of light rays is induced by either internal or external irregularities. External surface scattering on the boundaries of the considered medium is explained later. The now treated internal scattering is induced by non-uniformities like bubbles or droplets inside of the considered medium.

Internal scattering occurs in the coating as well as in the substrate of a special effect pigment. These centers of internal scattering are highlighted in figure 2.3a.

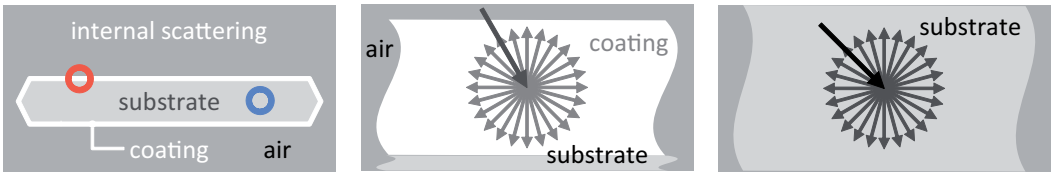

(a) Spot at pigment. (b) Zoom in coating. (c) Zoom in substrate.

Figure 2.3: Internal scattering of a special effect pigment.

Figure 2.3b and figure 2.3c show the internal scattering in the coating and the substrate. For both media, the most frequent irregularities are entrapped air and lattice defects.

External Scattering or Diffuse Reflection on Boundaries As mentioned above, the deflection of radiation from its straight trajectory due to irregularities is called scattering [120]. Scattering is explained in the paper of *Bäumer* [15] and the book of *Kortüm* [157]. The specification as external surface scattering indicates the irregularity to be located at the boundary between

two media. For example, the surface roughness induces multiple misaligned specular reflections overall called diffuse reflection. Therefore, external scattering and diffuse reflection describe the same optical effect.

In the present context, external scattering is caused by irregularities, such as bumps and grooves, at the boundaries between air, coating and substrate. The highlights in figure 2.4a indicate spots of external scattering.

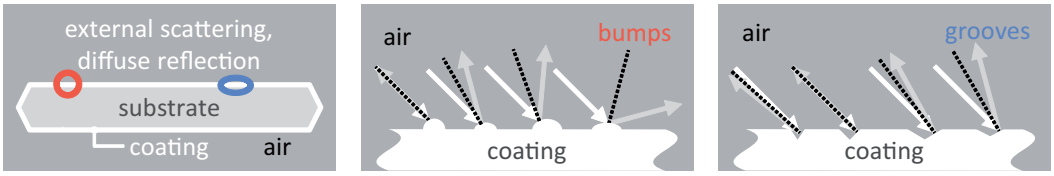

(a) Spot at pigment. (b) Zoom in bumps. (c) Zoom in grooves.

Figure 2.4: External scattering or diffuse reflection of a special effect pigment.

Figure 2.4b shows an uneven pigment surface with several protruding bumps. Parallel rays of incident light are reflected in specular direction with respect to the local surface normal. Due to the misalignment of the individual surface normals, the overall reflection is diffuse. The same explanation holds for the scattering on the notched grooves shown in figure 2.4c.

Specular Reflection on Boundaries Previously, the meaning of reflection in general and specular reflection in particular was used in an intuitive sense. *Jackson* [129], *Kortüm* [157], *Pedrotti et al.* [199] describe the specular reflection in detail. At this point, reflection is remembered to be the change in the propagation direction of a wave at a boundary between two media with different indices of refraction [120] . Figure 2.5 shows the specular reflection on an ideally even boundary.

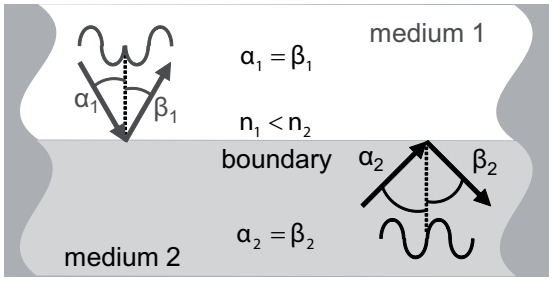

Figure 2.5: Specular reflection on the boundary between two arbitrary media.

The propagation direction of a reflected wave is given by the law of specular reflection [15]. As given in equation 2.1, the reflection law [15, 129, 157, 199] postulates an equality of incidence angle α and reflection angle β with respect to the surface normal.

$$\alpha = \beta \tag{2.1}$$

However, equation 2.1 gives no statement about the phase inversion. A 180° phase shift is affected during the reflection at the surface to an optically denser medium. In the contrary case of a reflection at the surface of a lower refraction index, a 180° phase shift does not occur. The occurrence and absence of the phase inversion is shown in figure 2.5 by means of a disturbed wave and regular wave, respectively.

In case of a special effect pigment, specular reflection takes place at the boundaries between air and coating as well as between coating and substrate. These spots of specular reflection are highlighted in figure 2.6a.

The specular reflection from the ideally even boundary between air and coating is shown in figure 2.6b. Figure 2.6c shows the specular reflection from the boundary between coating and

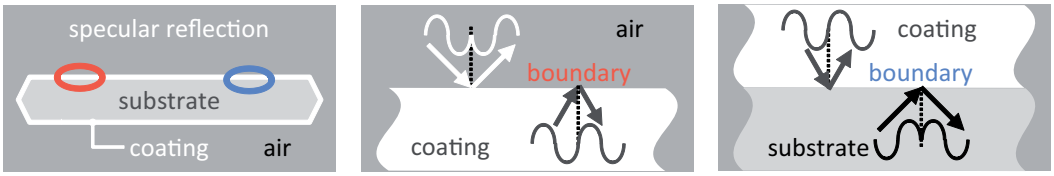

(a) Spot at pigment.

(b) Zoom on air-coating boundary.

(c) Zoom on coating-substrate boundary.

Figure 2.6: Specular reflection from a special effect pigment.

substrate assumed to be ideally flat. The disturbed wave and the regular wave of an arbitrary wavelength again show the occurrence and absence of a phase inversion, respectively.

Refraction at Boundaries The refraction of an arbitrary wave is defined as the change in its propagation direction induced by a change of the index of refraction. Refraction is explained in the paper of *Bäumer* [15], the books of *Jackson* [129], *Kortüm* [157] and *Pedrotti et al.* [199]. In contrast to reflection, the wave passes the boundary between the two media and propagates into the other medium. Figure 2.7 shows the refraction at the boundary between two media with different refraction indices.

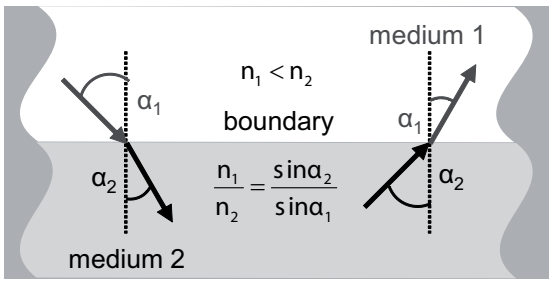

Figure 2.7: Refraction at the boundary between two arbitrary media.

Please note that the index of refraction is wavelength-dependent. In two media with refraction indexes n_1 and n_2, a wave propagates in a direction indicated by angles α_1 and α_2 with respect to the normal direction to the boundary. The interrelation of refraction indexes and propagation angles is given by means of *Snell*'s law [15, 129, 157, 199] of refraction in equation 2.2.

$$\frac{n_1}{n_2} = \frac{\sin\alpha_2}{\sin\alpha_1} \tag{2.2}$$

In the present case of special effect pigments, refraction occurs at the boundary between air and coating as well as between coating and substrate. In figure 2.8a, the spots of refraction are highlighted.

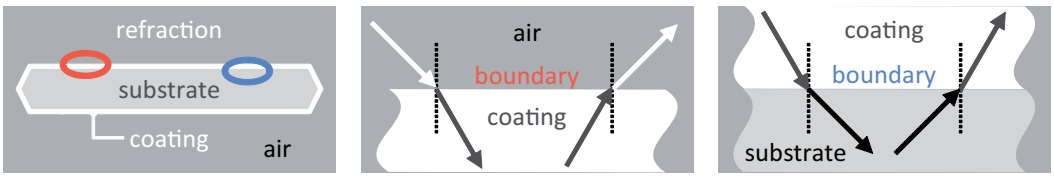

(a) Spot at pigment.

(b) Zoom on air-coating boundary.

(c) Zoom on coating-substrate boundary.

Figure 2.8: Refraction at a special effect pigment.

For both spots, the optical effect of refraction is shown in figure 2.8b and figure 2.8c. The angle of the light ray to the perpendicular on the boundary changes in both cases, but in the opposite way.

Figure 2.8b shows the transition from the air with a low refraction index to the coating with a higher optical density. According to *Snell*'s law, the light ray is refracted in a direction closer to the perpendicular on the boundary. In contrast to this, the angle between the perpendicular and the propagation direction increases for a decreasing refraction index. The transition from the high-refracting coating to the low-refracting substrate is shown in figure 2.8c.

Transmission through Coating and Substrate From the physical point of view, the term transmission describes the more or less disturbed propagation of a wave like sound or light through the bulk of an arbitrary medium. Transmission is treated in the books of *Kortüm* [157], *Jackson* [129] and *Pedrotti et al.* [199] as well as in the technical report *CIE TC*1-65 [120].

Considering a special effect pigment, light is transmitted through the coating as well as through the substrate. The spots of transmission are highlighted in figure 2.9a.

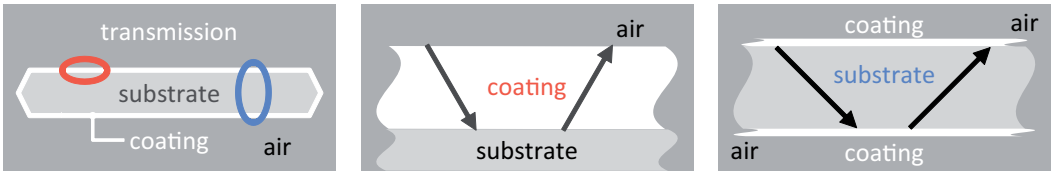

(a) Spot at pigment. (b) Zoom in coating. (c) Zoom in substrate.

Figure 2.9: Transmission of a special effect pigment.

Figure 2.9b shows the downward and upward transmission of a light ray through the coating. The downward and upward transmission through the substrate of the special effect pigment is shown in figure 2.9c.

Combined Optical Effect of Interference from Thin Coating Layers

Basing on the concepts of absorption, scattering, reflection, refraction and transmission, the interference effect on thin layers is the next topic. The books of *Glausch et al.* [86], *Kortüm* [157], *Maisch* and *Weigand* [172], *Pedrotti et al.* [199] and of *Pfaff et al.* [202, 204, 205] and other literature [15, 28, 101, 112, 113] give an introduction to thin layer interference. It is a combined optical effect of more or less specular reflection with refraction and transmission. The complex effect of interference from a thin layer is shown in figure 2.10.

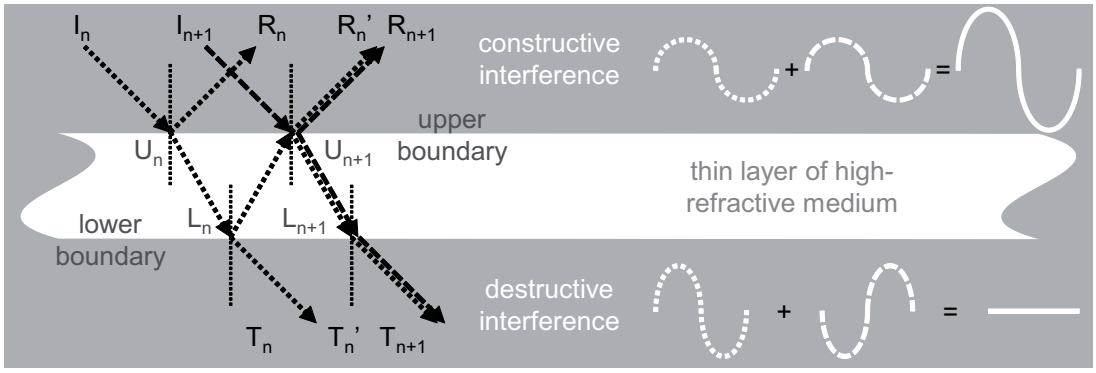

Figure 2.10: Interference from a thin layer.

Figure 2.10 is used to explain the thin layer interference in more detail. Consider a ray of white light incident on a thin layer with a comparably high refraction index. The considered ray can be

regarded as a beam of an infinite number of partial rays with the same incident angle. For two of these parallel partial rays with equal wavelength, the mechanisms of mutual optical interference is explained subsequently.

Both partial rays called I_n and I_{n+1} hit the upper boundary of the thin layer at the locations U_n and U_{n+1}. One part of both partial rays is reflected at the upper boundary of the thin layer. The reflected partial rays are named R_n and R_{n+1}. The remaining part is each refracted at the upper boundary and transmitted through the bulk. The transmitted partial rays hit the lower boundary of the thin layer at the locations L_n and L_{n+1}. A partial refraction at the lower boundary of the thin layer results in the overall transmitted partial rays T_n and T_{n+1}.

So far, no special optical effect occurs to the overall reflected partial rays R_n and R_{n+1} as well as the overall transmitted partial rays T_n and T_{n+1} of the first order. The reflected partial rays and the transmitted partial rays of the second order have to be taken into account. Therefore, the further propagation of the remaining part of the nth partial ray is tracked.

The part of the nth partial ray not refracted before is now reflected at the lower boundary at location L_n. It transmits through the bulk and hits the upper boundary at the location U_{n+1}. Here, one part is refracted resulting in an overall reflected partial ray R'_n of the second order. The other part is again reflected at the upper boundary and transmitted through the bulk to location L_{n+1} at the lower boundary. The result of a final refraction is an overall transmitted partial ray T'_n of the second order.

Now consider the phase relations of the nth second-order and $(n+1)$th first-order reflected partial rays R'_n and R_{n+1} as well as the nth second-order and $(n+1)$th first-order transmitted partial rays T'_n and T_{n+1}. Due to phase shifts and geometric differences, the optical path traversed by both partial rays is not equal in length. A superposition of both reflected and transmitted waves of equal wavelength results in an amplification or an attenuation of the amplitude. An example of an ideally constructive and destructive superposition is shown in figure 2.10.

The corresponding formulas of constructive and destructive interference for reflection and transmission are available in literature [15, 86, 172]. For a given incidence angle, light of specific wavelengths is amplified or attenuated depending on the thickness of the thin layer and the refractive indexes of the involved materials [204, 205].

Special effect pigments are often terminated with an additional color attribute. The termination with the hue specifies the interference effect color of the light reflected in specular direction. For a red special effect pigment, the effect of thin layer interference occurs at the high-refracting coating as shown in figure 2.11a [145].

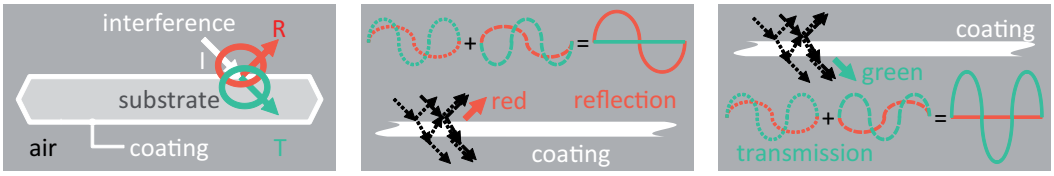

(a) Spot at pigment. (b) Zoom in reflected light. (c) Zoom in transmitted light.

Figure 2.11: Interference from a special effect pigment [145].

Figure 2.11b shows the origination of the red interference effect color of the reflected light in detail. For reddish light with long wavelengths, the superposition of two reflected waves is constructive. Destructive interference occurs in reflected waves with medium wavelengths of greenish light. Therefore, the resulting reflected light has an intense red color.

In contrast thereto, the transmitted light is colored in an intense green. The origination of the green interference effect color of the transmitted light is shown in figure 2.11c. In superposition, two transmitted greenish light waves with medium wavelengths are amplified ideally. A total degradation takes place for long wavelengths of reddish light. Thus, the transmitted light has the complementary color of the reflected light.

2.1.3 Pigment Classes

Differences in the particle sizes and material compositions allow the classification of special effect pigments as described by *Pfaff et al.* [204, 205] and others [16, 172]. Six common classes are those of *silver white* (*SW*), *gold* (*G*), *iron oxide* (*IO*), *interference effect* (*IE*), *multi-color* (*MC*) and *sparkle* (*S*) pigments (table A.1, table A.5).

Silver White Pigments

Pfaff et al. [206, 204, 205] and others [16, 102, 172] mention silver white (*SW*) pigments. Silver white pigments (table A.1, table A.5) are composed of natural mica as substrate (table A.3, table A.7) with a thin layer (table A.4, table A.8) of titanium dioxide (TiO_2). With 40 *nm* to 60 *nm*, the titanium dioxide coating layer is very thin causing a silver white interference effect color.

The arising visual impression of gloss and texture depends on the particle size (table A.2, Table A.6) of the silver white pigments. A wide range of particle sized is covered. Particle sizes between 5 μm to 25 μm and 45 μm to 500 μm are available.

Gold Pigments

Gold (*G*) pigments are known by *Maisch* [172] and *Pfaff et al.* [206, 202, 201, 204, 205]. Usually, gold pigments (table A.1, table A.5) consist of a natural mica substrate (table A.3, table A.7) coated with two thin coating layers (table A.4, table A.8). A layer of titanium dioxide (TiO_2) is combined with a layer of iron oxide (Fe_2O_3). Titanium dioxide and iron oxide are either stacked upon another in two separate layers or mixed together in one single layer. The combination of titanium dioxide and iron oxide induces a golden yellow color.

The induced impression of gloss and texture is influenced by the particle size (table A.2, Table A.6). The size of gold pigments varies from low values between 5 μm and 25 μm up to high values between 45 μm and 500 μm.

Iron Oxide Pigments

Pfaff et al. [206, 204, 205] and others [28, 49, 102, 172, 221] use the term iron oxide (*IO*) pigments. Typical iron oxide pigments (table A.1, table A.5) are made of a substrate (table A.3, table A.7) of natural mica with iron oxide (Fe_2O_3) as thin coating layer (table A.4, table A.8). The coating of iron oxide causes a rusty reddish brown color impression.

Iron oxide pigments are available in different fractions of particle sizes (table A.2, Table A.6). The gloss and texture of small particles with diameters between 5 μm and 25 μm differs from the visual appearance of bigger particles with 10 μm to 125 μm in diameter.

Interference Effect Pigments

With respect to the above presented silver white pigments, gold pigments and iron oxide pigments as well as the below presented sparkle pigments, the so-called interference effect (*IE*) pigments (table A.1, table A.5) are featured by the pronounced interference effect on a single thin layer. The strong thin-layer interference results in a considerable change in the perceived color due to a change in the geometric configuration. The geometry-induced color change is called color shift or color flop [204, 205].

Interference effect pigments are referred to as such by *Pfaff et al.* [206, 202, 201, 204, 205], *Hupp* and *Dörsam* [114, 115], *Hupp* [112, 113], *Cramer* and *Gabel* [46], *Cramer* [42, 44] as well as others [16, 28, 102, 172]. They are made of a natural mica substrate (table A.3, table A.7) plus one thin titanium dioxide (TiO_2) coating layer (table A.4, table A.8). Compared to the silver white pigments described above, the coating layer is significantly thicker.

Titanium dioxide layers of 60 *nm* to 80 *nm* reflect a yellow interference effect color. A red interference effect color is reflected for layers of 80 *nm* to 100 *nm*. Between 100 *nm* and 140 *nm*,

the reflected interference effect color is blue. The reflected interference effect color is green for layers with a thickness between 120 nm and 160 nm. As noted above, the transmitted light has the complementary color of the reflected light. Thus, the transmitted interference effect colors are blue, green, yellow and red for the layer thicknesses listed above [204, 205].

For a specified incidence direction, the enlisted interference effect colors are only present in and near the directions of specular reflection and direct transmission, respectively. The intense interference effect color shifts towards an achromatic gray color with an increasing aspect angle. The aspect angle corresponds to the angular difference between specular direction and viewing direction.

Typical particle sizes of interference effect pigments are 5 μm to 25 μm and 10 μm to 60 μm (table A.2, Table A.6). Despite only a minor difference in size, the visual impression of gloss and texture is significantly different.

Multi-Color Pigments

An upgraded version of the previously introduced interference effect pigments are the so-called multi-color (MC) pigments (table A.1, table A.5). Due to the combination of multiple coating layers (table A.4, table A.8) alternating in refraction power, the color shift is more pronounced than for special effect pigments with one coating layer. While the color of an interference effect pigment shifts from an achromatic gray to a specific chromatic color, the color of a multi-color pigment shifts between two specific chromatic colors.

Cramer and *Gabel* [46] as well as *Cramer* [42, 44] use the specification as multi-color pigments. They are composed of an arbitrary substrate (table A.3, table A.7) with more than one high-refractive coating layer (table A.4, table A.8). An intermediate low-refractive silicon dioxide (SiO_2) layer is always located between two high-refractive coating layers [172, 204, 205].

The intense color shift of the multi-color pigments is visually more interesting than the gloss and texture appearance. The perceived gloss and texture are influenced by the particle size (table A.2, Table A.6). The diameter of multi-color pigments ranges from between 5 μm and 50 μm up to between 20 μm and 200 μm.

Sparkle Pigments

The so-called sparkle (S) pigments are named by *Cramer* [44], *Maisch et al.* [172] and *Pfaff et al.* [204, 205]. Sparkle pigments (table A.1, table A.5) are made of a synthetic substrate (table A.3, table A.7) with a coating layer (table A.4, table A.8). As for all types of the above listed special effect pigments, the coating layer generates a characteristic color. But for sparkle pigments, the color shift is the visually less pronounced effect.

As expected from their nomination, sparkle pigments stand out from other types of special effect pigments due to their intense sparkling effect. The visually interesting impression of locally high gloss and visually coarse texture is induced by the comparably big particles (table A.2, table A.6). The particle size of sparkle pigments lies between 10 μm and 100 μm or between 20 μm and 200 μm.

2.1.4 Pigment Applications

Due to the unique optical properties and visual appearance, special effect pigments are applied in multiple products. Typical application fields of special effect pigments are those of *cosmetics*, *plastics*, *industrial varnishes* and *printing inks* as described by *Bäumer* [17], *Maisch et al.* [172] and *Pfaff et al.* [203, 204, 205].

Cosmetics

Some important examples for the application of special effect pigments in cosmetics are nail polishes and eye shadows. Lipsticks, body lotions, shower gels and hair shampoos are further

cosmetic products containing special effect pigments to improve the visual appearance of the skin [17, 172, 204, 205].

Plastics

The application of special effect pigments in plastics provides a wide spectrum of products like computer mice or keyboards, mobile phone housing and eyeglass frames. In addition to the enlisted general plastic products, packaging materials like bottles for washing agents and cloth softeners or paddings in chocolate boxes and biscuit packs are popular application areas for special effect pigments in plastic materials [17, 130, 172, 204, 205].

Industrial Varnishes

Apart from conventional absorption varnishes with organic pigments, automobiles are coated with metal effect varnishes [17, 49, 141]. Metal effect varnishes contain aluminum flakes [172, 206, 204, 205]. Since their introduction to the market, automobiles are coated with special effect varnishes more frequently.

Motorbikes and bicycles are related products covered with special effect coatings. Further application examples of special effect pigments in varnishes are kitchenware like domestic refrigerators or coffee machines and furniture like bed-frames or lampshades.

Printing Inks

In addition to the above described applications on three-dimensional objects of skin, metal or plastics, special effect pigments are applied on even materials like paper or synthetic films [17, 172, 204, 205]. Special effect inks are printed due to safety-related or aesthetic reasons [209, 218].

Common examples for products in the field of safety are banknotes and tickets. In the area of design, jewelry casings, perfume wrappings, chocolate boxes, cigarette packets and wine labels are typical examples for packaging applications. Further examples are printing of wall papers, decor papers and textiles.

2.2 Special Effect Printing

Special effect pigments are used in printing high-quality products as listed in section 2.1.4. In the following, section 2.2.1 explains the most important *printing technologies* in general and points out the *process limitations* for special effect inks. Furthermore, the possible *printing scenarios* are enlisted and the respective *induced variations* are described in section 2.2.2.

2.2.1 Printing Techniques and Process Limitations

As mentioned in section 2.1.1, the shape and size of special effect pigments considerably differs from those of light-absorbing pigments traditionally used in conventional and non-impact printing technologies [148, 149]. In spite of the large diameter of the flaky pigments, special effect inks can be printed by the use of all conventional printing technologies as described in the books of *Glausch et al.* [86] and *Pfaff et al.* [204, 205] as well as in the papers of *Böhm et al.* [28], *Hall-Goulle et al.* [95], *Loy* [168] and *Ullmann* [233]. In addition to *offset* [185], *gravure* [184] and *flexo* [182] printing, the *screen* [183] printing is applicable. The enlisted printing techniques are presented in the following including some information on process limitations.

Offset Printing

The offset printing technology is an indirect plano-graphic printing technology [148, 149]. The printing ink is indirectly transferred from the printing plate on the printing substrate. The transfer is realized by means of the so-called rubber blanket. Furthermore, the printing plate is plane without any elevated or recessed areas. The separation of non-printing and printing areas is based on local differences in the wettability. Figure 2.12 shows the offset printing schematically.

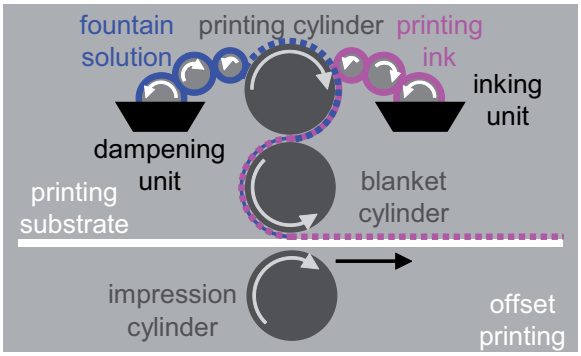

Figure 2.12: Offset printing.

The fountain solution wets the non-printing areas of the printing plate. The remaining printing areas are wetted by printing ink [148, 149]. The printing ink is transferred from the printing plate mounted on the printing cylinder to the rubber blanket mounted on the blanket cylinder. The substrate is transported through the nip between the blanket cylinder and an impression cylinder. At the same time, the fountain solution and the printing ink are transferred on the printing substrate.

The offset process is usually used for the printing of books, newspapers and packaging materials with paper and board as printing substrates. In the case of printing special effect inks, typical applications are labels for wine bottles and clothes or the packing of cosmetics and sweets.

Due to the characteristics of the process, offset printing is restricted to comparably small pigments with 5 μm to 25 μm in diameter. For such small particles, the pigment concentration in the printing ink can be up to 35 % by weight. These process limitations are given in the offset printing color card of *MERCK* [185] as well as in the books of *Glausch et al.* [86] and *Pfaff et al.* [204, 205].

Gravure Printing

The term gravure printing bases on the underlying method of generating the printing areas on the printing plate [148, 149]. The printing areas were originally engraved in the printing plate. The engraved cells are filled with printing ink. From here, the printing ink is directly transferred to the substrate. An exemplary setup of gravure printing is shown in figure 2.13.

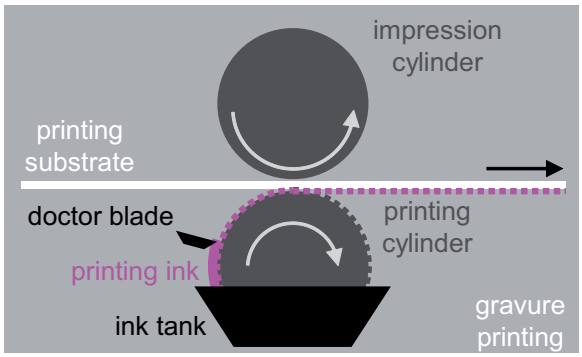

Figure 2.13: Gravure printing.

The printing cylinder rotates in the ink reservoir and picks up a surplus of printing ink on its engraved surface [148, 149]. A doctor blade removes the excess amount of printing ink. The remaining ink in the cells of the printing form is transferred to the substrate in the nip between the inelastic printing cylinder and the elastic impression cylinder.

Besides labeling and packing applications, important products of gravure printing with conventional light-absorbing or special effect inks are wall and decor papers. Paper, board, plastic foils and also textiles can be printed with water-based, solvent-based or UV-curing inks.

In the case of special effect inks, the printing inks are charged with special effect pigments of up to 30 % or 25 % by weight. The feasible percentage depends on the average particle size of the flaky pigments. The higher maximal concentration of 30 % holds for small particle sizes between 5 μm and 25 μm. For bigger particles in the range of 10 μm to 125 μm in diameter, the concentration is usually less than 25 % for gravure printing. In the pravure printing color card of $MERCK$ [184] and in the books of *Glausch et al.* [86] and $Pfaff$ *et al.* [204, 205] these information are given.

In addition to the recommended pigment concentration, reference points for adequate cell sizes of the printing plate are specified. The screen width should be chosen between 40 $lines/cm$ and 70 $lines/cm$, inversely proportional to the particle size. In contrast to pigment concentration and cell size, the recommendations for the cell angle and the cell deepness are independent of the particle size.

Flexo Printing

The flexo or flexographic printing technology originates from letterpress printing [112, 113, 148, 149]. Elevated areas on the printing plate serve for the direct transfer of the printing ink on the substrate. The flexo printing technology is described by means of figure 2.14.

The printing ink is dosed onto the anilox roll by means of a fountain roller including a doctor blade [148, 149]. The anilox roll inks the elevated areas of the flexible polymer printing plate mounted on the printing cylinder. Under pressure between printing cylinder and impression cylinder, the printing ink is transferred onto the substrate.

Besides paper and board, plastic foils, metal foils and textiles can be utilized as printing substrate. Products processed by flexo printing are often used for food packaging with large areas of solid colors. For example, these are egg cartons with low quality standards for color reproduction and image registration. Other products include bags for noodles, rice, bread, biscuits, chips and candies with increasing quality requirements.

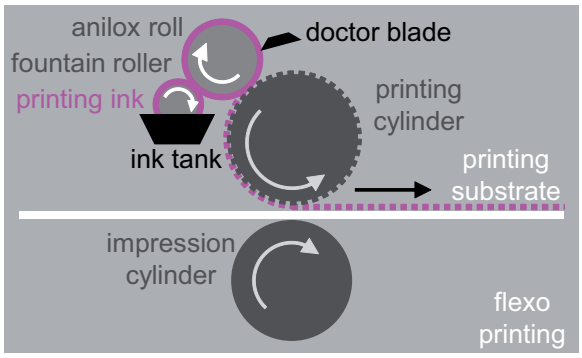

Figure 2.14: Flexo printing.

For high-quality products, special effect pigments with particle sizes up to 200 μm are printed in water-based, solvent-based or UV-curing ink systems. Such large special effect pigments account for 5 % to 15 % of the printing ink by weight. Between 10 % and 25 % special effect pigments by weight are recommended for medium-sized particles of 10 μm to 100 μm. Small special effect pigments with particle sizes between 5 μm and 25 μm can be applied in concentrations of up to 30 % by weight. These specifications are given in the flexo printing color card of *MERCK* [182] and in the books of *Glausch et al.* [86] and *Pfaff et al.* [204, 205].

In addition to the pigment concentration, the screen width and the pick-up volume of the anilox roll have to be adapted to the particle size of the special effect pigments. The screen width should be chosen inversely proportional to the particle size in the range of 40 $lines/cm$ and 120 $lines/cm$. The pick-up volume of the anilox roll is recommended to range from 6 cm^3/m^2 to 25 cm^3/m^2 proportional to the particle sizes.

Screen Printing

The screen printing technology described by *Kipphan* [148, 149] is a form of stencil printing. By means of a squeegee, the printing ink is pressed through the open stencil areas onto the printing substrate. The screen consists of a wire fabric for mechanical support and a stencil material for picture generation. The continuous, rotation-based process operates like the four-stage, flat-bed process shown in figure 2.15.

In the first process stage shown in figure 2.15a, the frame is set down on the printing table. The fabric fixed in the frame does not touch the substrate positioned on the printing desk. A stiff squeegee is scraped over the screen in the second process stage shown in figure 2.15b. The stiff squeegee distributes the printing ink on the fabric. By means of a flexible squeegee, the printing ink is pressed through the open stencil areas and the fabric meshes. The ink transfer happens in the third process stage shown in figure 2.15c. As shown in figure 2.15d, the frame is moved away from the printed substrate in the last process stage. With a new, unprinted substrate, the same process sequence starts again from the beginning.

Besides graphic and packaging applications on paper and plastic foils, textiles for clothing, bags or curtains are processed by means of the screen printing process. Furthermore, it is possible to print on substrates like wood, metal, glass and ceramics. Typical screen printing products are wallpapers, compact discs and traffic signs [148, 149]. Just like conventional absorption pigments, special effect pigments can be printed using water-based, solvent-based or UV-curing ink systems.

In the screen printing color card of *MERCK* [183] and the books of *Glausch et al.* [86] and *Pfaff et al.* [204, 205], pigment concentrations between 8 % and 15 % are referred to be most suitable and common. The higher concentration is valid for smaller particles of less than 60 μm in diameter. For lager particles of up to 200 μm, the lower concentration is adequate. The limiting factor is the mesh opening of the fabric. Mesh widths of 1.5 times to 2.5 times the maximal particle size are recommended. Based on the recommended mesh widths, the thread counts and

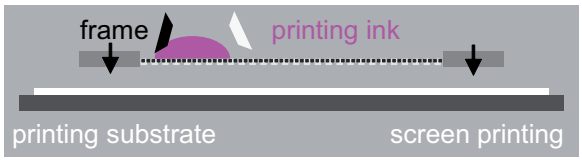

(a) Deposition.

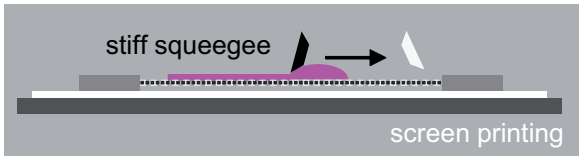

(b) Inking.

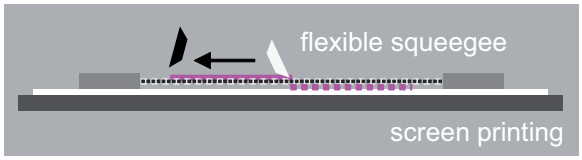

(c) Transfer.

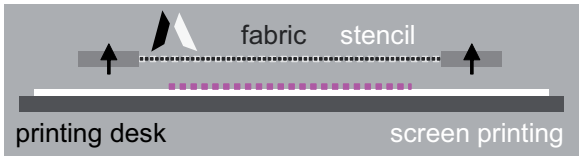

(d) Withdrawal.

Figure 2.15: Screen printing.

the thread thickness of the fabric can be specified.

2.2.2 Printing Scenarios and Induced Variations

Besides the special effect pigments properties, the appearance of printed special effect colors can be influenced by the *substrate roughness*, the *substrate porosity*, the *background color*, the *pigment occupancy* and the *varnishing state*. The resulting variations in color, gloss and texture are described in the following. This detailed description is based on information given in the corresponding literature and on experiences achieved in previous studies and preliminary tests. The books of *Glausch et al.* [86] and of *Pfaff et al.* [204, 205] give an overview. At the *Institute of Printing Science and Technology* (*IDD*), *Hupp* [115, 112, 113], *Kehren* [144, 145] and *Haas* [93, 94] conducted studies on the influence of the pigment occupancy and other printing parameters.

Substrate Roughness

As found by *Haas* [93, 94], the printing substrate has an influence on the optical properties and visual appearance of printed special effect colors. An important property of the printing substrate is the roughness of its surface. The surface roughness of the printing substrate influences the orientation of the flaky pigments. The pigment orientation is considered in the books of *Glausch et al.* [86] and *Pfaff et al.* [204, 205] as well as in papers [32, 171]. The influence on the the visual appearance of color, gloss and texture is explained by means of figure 2.16.

On a glossy coated paper with an even surface (figure 2.16a), the flaky special effect pigments are arranged parallel to each other. For interference effect and multi-color pigments designed to show an intense color shift, the geometry-induced color transition is assumed to be sharp. The parallel alignment induces an intense, sharp highlight in specular direction. The gloss is perceived to be high. In figure 2.16a, the colored and intense specular highlight is symbolized by a single red arrow. There are no small highlights due to misaligned pigments. The resulting texture is regular

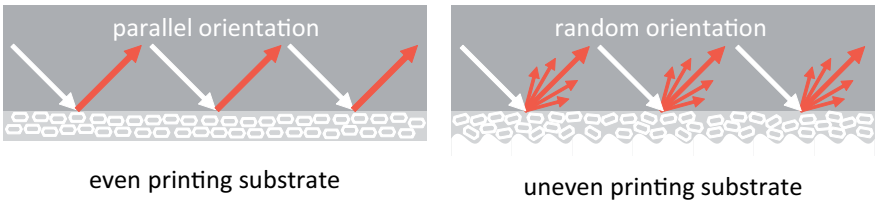

(a) Even substrate. (b) Uneven substrate.

Figure 2.16: Influence of substrate roughness.

in structure and low in contrast. The term contrast describes the perceived lightness difference between dark and light areas.

The pigments are less oriented on a rough surface (figure 2.16b) like that of a matt coated paper or actually an uncoated paper. Thus, the color shift of interference effect pigments and multi-color pigments is expected to be more blurry. The highlight in specular direction is weaker and wider. The perceived gloss is not that high. The fanned red arrows in figure 2.16b symbolize the broad distribution of colored light. Misaligned pigments induce small highlights called sparkles or glints. The texture is less regular with a higher contrast.

Substrate Porosity

As mentioned above, *Haas* [93, 94] found that the optical properties and visual appearance of printed special effect colors is influenced by the printing substrate. Besides the roughness, printing substrates vary in their porosity. The influence of substrate porosity on the optical properties and the visual appearance is shown in figure 2.17 and subsequently explained.

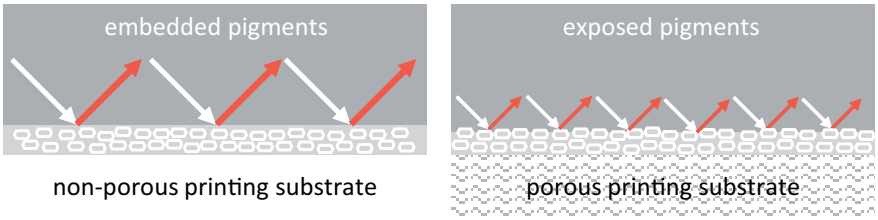

(a) Non-porous substrate. (b) Porous substrate.

Figure 2.17: Influence of substrate porosity.

An example for a nonporous printing substrate is a plastic film. Surface finishing on paper like coating and calendaring also results in a somehow nonporous surface. The binder of the printing ink cannot penetrate into the substrate and forms a compact ink layer on top of the substrate surface (figure 2.17a). The pigments are completely embedded in the binder matrix. The color shift is less distinct, the gloss highlight sharp and the texture blurry. In figure 2.17a, the intense gloss highlight in specular direction is symbolized by the large arrows.

Porous substrates like uncoated papers absorb the binder to some extent. The special effect pigments stay on the surface of the substrate. Due to the partial penetration of the binder in the substrate, the remaining binder is too sparse to embed the special effect pigments completely (figure 2.17b). The special effect pigments are exposed on the surface. The exposure of the special effect pigments results in a sharp color transition, a blurry gloss highlight and a clear texture. The small arrows in figure 2.17b symbolize the intense flashes of light perceived as sparkle or glint.

Background Color

Baba [13] and *Böhm et al.* [28] investigated special effect samples differing in the color of the background. The influence of the background color on the perceived color, gloss and texture is

explained for a black background compared to a white background. For the manipulation of color appearance, the ink layer and the arbitrary colored background are considered separately as shown in figure 2.18 [145].

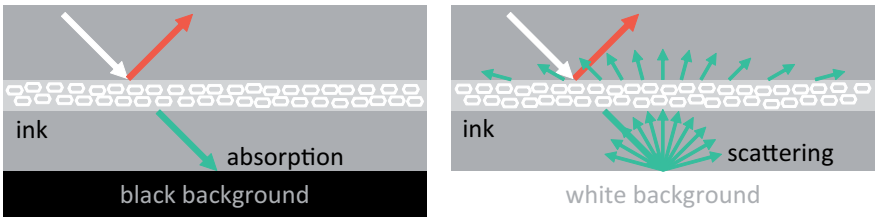

(a) Black background. (b) White background.

Figure 2.18: Influence of background color [145].

In the ink layer, the effect of thin layer interference amplifies and degrades incident light symbolized by a white arrow at specific wavelengths. In specular direction, the reflected light has a specific interference effect color symbolized by a red arrow. The transmitted light is tinted in the complementary color symbolized by a green arrow. The complementary-colored light transmitted through the ink layer hits the background.

In the case of a black background shown in figure 2.18a, the transmitted light is mostly absorbed. Thus, the complementary color (green arrow) has no more influence on the resulting color impression. The perceived color is equal to the interference effect color of the reflected light (red arrow).

In contrast to this, a white background scatters the transmitted light as shown in figure 2.18b. The intense interference effect color (red arrow) in specular direction is superposed with a pale complementary color (green arrows) in the whole half space above the sample.

For gloss and texture, the manipulation concerns the appearance of contrast. The gloss of an arbitrary light surface is a locally bright light reflex. The perceived gloss correlates with the lightness difference of the bright reflex relative to the surrounding. The texture of a surface is based on a pattern of differently colored areas. The color difference of the brightly shining pigments on the somehow natured underground decides about the perceived texture. Thus, gloss and texture are perceived stronger for the black printed underground.

Pigment Occupancy

The pigment occupancy specifies the number or mass of special effect pigments per surface area. As shown in figure 2.19, a specified occupancy (figure 2.19a) can be varied by means of the ink supply (figure 2.19b), the pigment concentration (figure 2.19c) or the tonal value (figure 2.19d).

The ink supply (figure 2.19b) is a controllable process variable. It sets the thickness of the applied ink film. The realized range of ink film thicknesses depends on the printing process. In offset printing, comparably thin ink films are applied on the substrate. The ink films are somehow higher in gravure printing, followed by flexo printing. Screen printing provides the highest ink film thicknesses. The influence of the ink layer thickness was investigated by *Hupp* and *Dörsam* [115], *Hupp* [112, 113], *Kehren* and *Dörsam* [144] and *Haas* [93, 94]. The ink layer thickness linearly correlates with a perception-related parameter called lightness difference. It is equal to the difference of the lightness of the unprinted paper and the printed sample. The lightness difference was introduced by *Hupp* and *Dörsam* [117, 116].

In general, the maximum possible pigment concentration decreases with an increasing particle size as mentioned above. The possible concentration (figure 2.19c) of the special effect pigments in the printing ink depends on the particle size and on the printing technology. Detailed information and multiple recommendations are given in the books of *Glausch et al.* [86] and *Pfaff et al.* [204, 205] as well as in the color cards of *MERCK* for offset [185], gravure [184], flexo [182] and screen [183] printing. The study of *Haas* [93, 94] showed that an increasing pigment concentration results in an increased color shift but a decreased gloss intensity.

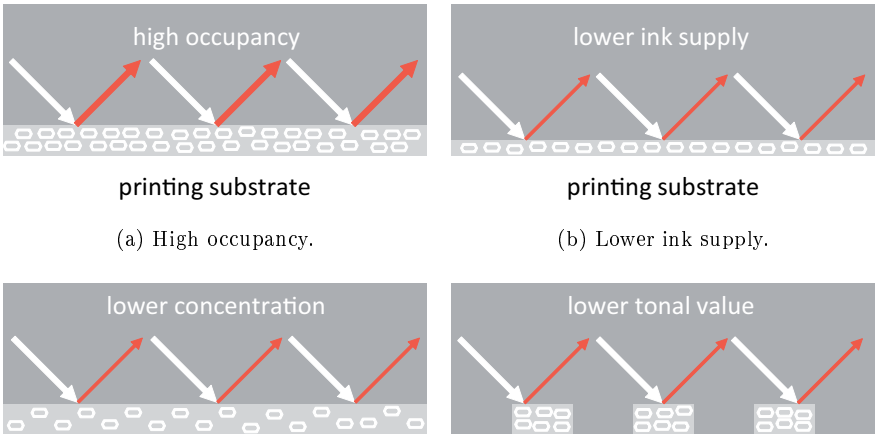

(a) High occupancy.

(b) Lower ink supply.

(c) Lower concentration.

(d) Lower tonal value.

Figure 2.19: Influence of pigment occupancy.

Considering the feasible ranges of ink supply and pigment concentration, the tonal value (figure 2.19d) is the remaining parameter to adjust the pigment occupancy. With the intention to reach maximum optical and visual effects, special effect pigments are commonly printed in solid areas. However, *Haas* [93, 94] investigated the influence of the tonal value in the range from 50 % to 100 %. An increasing tonal value slightly increases the perceived color shift and gloss intensity.

Varnishing State

The surface of a printed ink layer might be more or less rough and thus more or less matte. A clear gloss varnish can be used to smooth the printed surface as shown in figure 2.20.

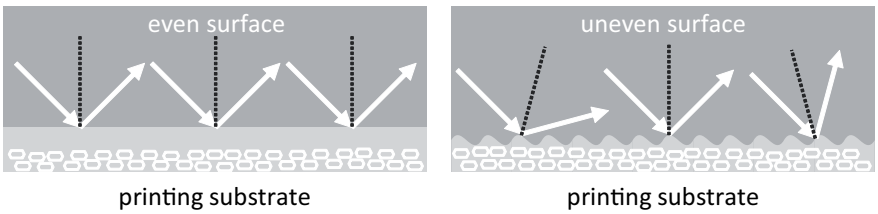

(a) Unvarnished surface.

(b) Varnished surface.

Figure 2.20: Influence of glossy varnishing.

In the case of an ideally even surface shown in figure 2.20a, parallel incident light rays are all reflected in the same direction (parallel arrows). The specular reflection induces an intense gloss impression like a mirror. The highlight in specular direction is sharply framed and rich in contrast.

Independent of the roughness of the printed surface, the law of specular reflection is locally maintained. At each individual surface element, the angle of reflection is equal to the angle of incidence counted to the perpendicular of the respective surface element called micro facet.

For an uneven surface with tilted micro facets, the corresponding perpendiculars are misaligned as shown in in figure 2.20b. The resulting diffuse reflection (nonparallel arrows) has no intense and sharp specular highlight. Thus, an uneven surface is perceived to have a low gloss.

Chapter 3

Bidirectional Optical Properties

For special effect colors, the limited availability of measured and modeled bidirectional reflectance and texture distributions comes along with problems in the description of their complex bidirectional optical properties (section 1.1.2). This chapter provides a deeper insight to this second partial problem.

For the associated approach, the dire necessity is clarified. A freely available bidirectional reflectance and texture database is intended to be generated (section 1.2.2, chapter 6).

The chapter starts with an introduction to the *bidirectional optical description* (section 3.1). Thereafter, the focal point lies on *bidirectional optical measurements* (section 3.2).

3.1 Bidirectional Optical Description

In case of special effect colors, the optical properties depend on the geometric configuration of light source and detector or observer relative to the sample. The optical properties of a material are described by radiometric quantities. Geometry-dependent radiometric quantities are called bidirectional distributions. Subsequent to *coordinate systems* (section 3.1.1) and *radiometric quantities* (section 3.1.2), important information about *bidirectional distribution functions* (section 3.1.3) is given.

3.1.1 Coordinate Systems

Bidirectional distribution functions considered in this chapter are connected with three-dimensional coordinates. Therefore, the *cubical* and *spherical coordinate system* is subsequently introduced.

Cubical Coordinate System

In a cubical coordinate system, the unit body has the shape of a cube. As shown in figure 3.1a, the edges of the unit cube are one unit long.

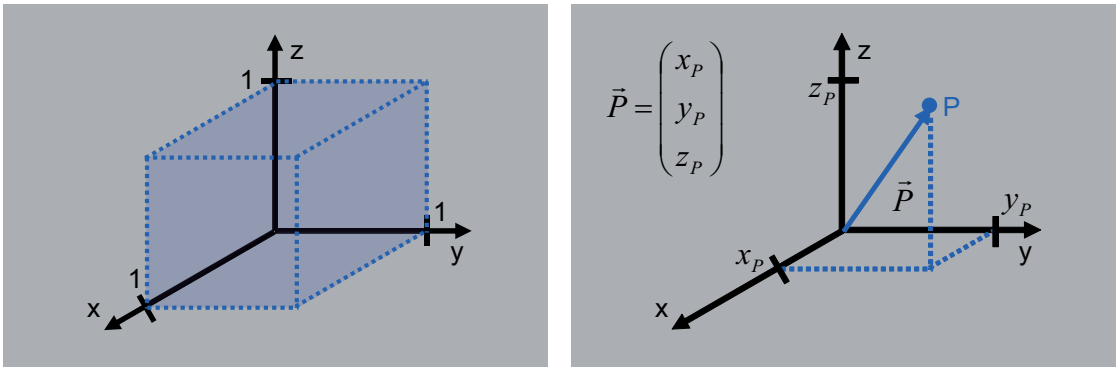

(a) Unit cube.

(b) Vector from origin to point $\boldsymbol{P}$.

Figure 3.1: Cubical coordinate system.

The three axes of the cubical coordinate system are oriented orthogonally to each other. The coordinate axes called x, y and z form a counter-clockwise system as shown in figure 3.1b. The position of a point $\boldsymbol{P}$ is specified by means of a vector with the elements x_P, y_P and z_P. These elements are equal to the distance from the origin in the respective direction.

Spherical Coordinate System

As indicated by the term spherical coordinate system, the unit body is shaped like a sphere. The unit sphere shown in figure 3.2a has a radius of one unit.

The radius r is the first coordinate in the spherical coordinate system. The second and the third coordinate are angles called polar angle θ and azimuth angle ϕ. Polar angle and azimuth angle are counted as shown in figure 3.2b. Thus, the vector elements r_P, θ_P and ϕ_P specify the position of a point $\boldsymbol{P}$ relative to the origin.

3.1.2 Radiometric Quantities

Radiometry deals with the measurement of electromagnetic radiation [85, 98, 199]. By means of radiometric measurements, the power distribution of the electromagnetic radiation in space is determined. Electromagnetic radiation in the visible range from about 380 nm to about 780 nm is called light. The interaction of light with the human eye is handled in photometry. Photometric

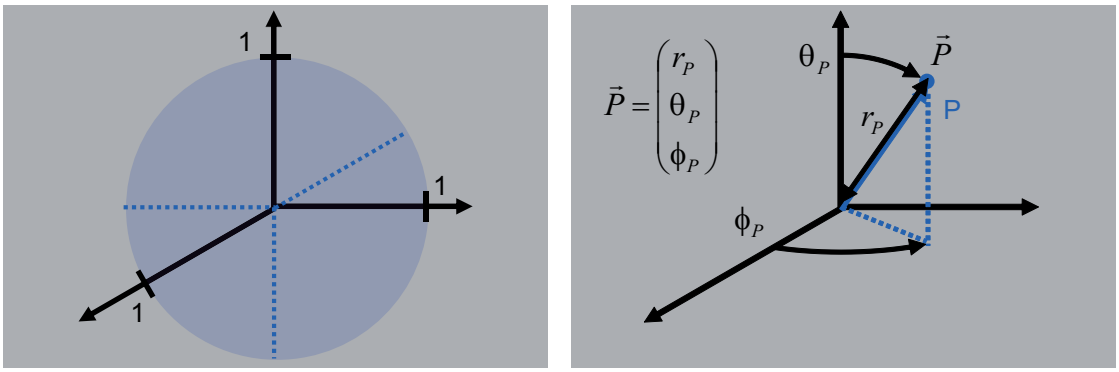

(a) Unit sphere. (b) Vector from origin to point $\boldsymbol{P}$.

Figure 3.2: Spherical coordinate system.

dimensions are indexed with a letter v for visual. The letter e for energy is used as index for radiometric dimensions. In radiometry, one often deals with spectral dimensions. Therefore, spectro-radiometric dimensions are sometimes indexed with the additional Greek letter λ for the wavelength. The most important radiometric dimensions are given by *Nicodemus et al.* [191] and *Pedrotti et al.* [199]. The *radiant flux*, the *radiant intensity*, the *irradiance*, the *radiant exitance*, the *radiosity* and the *radiance* are listed in the following.

Radiant Flux

The radiant energy Q per unit time t is called radiant flux [191, 199]. Mathematically, the radiant flux Φ_e is specified in equation 3.1.

$$\Phi_e = \frac{dQ}{dt} \qquad [W] \tag{3.1}$$

The radiant flux Φ_e is given in Watt (W).

Radiant Intensity

The radiant intensity I_e is equal to the radiant flux Φ_e per solid angle Ω. Equation 3.2 specifies the mathematical relation [191, 199].

$$I_e = \frac{d\Phi_e}{d\Omega} \qquad \left[\frac{W}{sr}\right] \tag{3.2}$$

The unit of radiant intensity I_e is Watt (W) per steradian (sr).

Irradiance

The incident radiant flux Φ_e per surface unit element A is called irradiance [85, 191, 199]. The mathematical expression of irradiance E_e is given in equation 3.3.

$$E_e = \frac{d\Phi_e}{dA} \qquad \left[\frac{W}{m^2}\right] \tag{3.3}$$

Watt (W) per square meter (m^2) is the unit of irradiance E_e.

Radiant Exitance

The radiant exitance M_e is the radiant flux Φ_e emitted from a surface unit element A. In equation 3.4, the radiant exitance M_e is defined mathematically [191, 199].

$$M_e = \frac{d\Phi_e}{dA} \qquad \left[\frac{W}{m^2}\right] \tag{3.4}$$

The unit of the radiant exitance M_e is Watt (W) per square meter (m^2).

Radiosity

The radiant flux Φ_e leaving a surface due to emission and reflection is called radiosity J_e. The mathematical description of radiosity J_e is given in equation 3.5.

$$J_e = \frac{d\Phi_e}{dA} \qquad \left[\frac{W}{m^2}\right] \tag{3.5}$$

The radiosity J_e has the unit Watt (W) per square meter (m^2).

Radiance

Radiance L_e is the emitted radiant flux Φ_e per unit solid angle Ω and per unit projected area $A \cdot \cos\theta$. With the cosine of the polar angle θ for the projection, equation 3.6 is the mathematical expression [85, 191, 199] of the radiance L_e.

$$L_e = \frac{d\Phi_e^2}{d\Omega \cdot dA \cdot \cos\theta} \qquad \left[\frac{W}{sr \cdot m^2}\right] \tag{3.6}$$

Watt (W) per steradian (sr) and per square meter (m^2) is the unit of radiance L_e.

3.1.3 Bidirectional Distribution Functions

Gebhardt [85], *Martonchik et al.* [173] and *Nicodemus et al.* [191] give a definition of the bidirectional distribution function. In a general manner, a bidirectional distribution function f specifies an optical property of an arbitrary object depending on two directions. The direction of incoming light $\boldsymbol{\omega}_i$ and the direction of outgoing light $\boldsymbol{\omega}_o$ describe the geometric arrangement of light source and detector or observer relative to the object. The specified geometry-dependent optical property is mostly the reflectance of a surface and rarely the transmittance of a layer. In the present context, the bidirectional reflectance distribution function f_r specifies the reflectance of a surface depending on the incidence direction $\boldsymbol{\omega}_i$ and the reflection direction $\boldsymbol{\omega}_r$. In other words, the amount of light reflected in direction $\boldsymbol{\omega}_r$ is set in relation to the amount of light incident from direction $\boldsymbol{\omega}_i$. The mathematical definition of the bidirectional reflectance distribution function $(BRDF)$ is given in equation 3.7.

$$f_r(\omega_i, \omega_r) = \frac{dL_r(\omega_r)}{dE_i(\omega_i)} \qquad \left[\frac{1}{sr}\right] \tag{3.7}$$

The radiance L_r is equal to the emitted radiant flux Φ_e per unit solid angle Ω and per unit projected area $A \cdot \cos\theta$ (equation 3.6). The irradiance E_i is the incident radiant flux Φ_e per surface unit element A (equation 3.3). With these definitions in mind, equation 3.7 can be converted to equation 3.8.

$$f_r(\omega_i, \omega_r) = \frac{dL_r(\omega_r)}{L_i(\omega_i) \cdot \cos(\theta_i) \cdot d\omega_i} \qquad \left[\frac{1}{sr}\right] \tag{3.8}$$

The incidence polar angle θ_i is included in the incidence direction $\boldsymbol{\omega}_i$. The dependence on the incidence direction $\boldsymbol{\omega}_i$ and the reflection direction $\boldsymbol{\omega}_r$ is a rather simple form of a $BRDF$. In

addition to this geometric dependence, a $BRDF$ can express the dependence of the reflectance properties on other dimensions. These *dimensions* and the *requirements* are enlisted in the following.

Dimensions

The type and term of a $BRDF$ depends on the number and nature of represented dimensions. In the following descriptions about the dependence on the *direction*, *location*, *wavelength* and *time*, the most important $BRDFs$ are mentioned.

Directions As just mentioned, a $BRDF$ describes the dependence of the reflectance on two directions. These two directions are the incidence direction $\boldsymbol{\omega}_i$ and the reflection direction $\boldsymbol{\omega}_r$.

The incidence direction $\boldsymbol{\omega}_i$ is given by the incidence polar angle θ_i and the incidence azimuth angle ϕ_i. By definition, the incidence polar angle is measured with respect to the normal on the surface. As the surface normal vector, the incidence direction vector is directed away from the surface.

The reflection direction vector is also directed away from the surface. The normal on the surface is the reference for counting the reflection polar angle. The combination of the reflection polar angle θ_r and the reflection azimuth angle ϕ_r specifies the reflection direction $\boldsymbol{\omega}_r$.

Location The $BRDF$ of a textured surface can be described by means of the so-called bidirectional texture function (BTF). *Dana et al.* [52, 53, 51, 54, 50] and *Matusik et al.* [175, 178, 177] determined and investigated $BTFs$. The BTF is also called spatially-varying $BRDF$ ($SVBRDF$) by *Matusik et al.* [176] and *Schnös* [222]. It additionally considers the dependence on the location $\boldsymbol{p}$. The location vector includes the coordinates x, y and z. By definition, the x-axis and y-axis lie in one plane with the surface of the object. The normal on the surface of the object corresponds to the z-axis.

In case of significant internal scattering, the incidence location $\boldsymbol{p}_i$ and reflection location $\boldsymbol{p}_r$ should be distinguished. The incidence location $\boldsymbol{p}_i$ is specified by means of the coordinates x_i, y_i and z_i. The coordinates x_r, y_r and z_r specify the reflection location $\boldsymbol{p}_r$.

Wavelength Even if not explicitly indicated, every $BRDF$ depends on the wavelength λ. The general spectral dependence can be specified individually for incidence and reflection. The distinction of incidence wavelength λ_i and reflection wavelength λ_r is only necessary for fluorescent or phosphorescent materials such as paper [142, 143]. Fluorescence and phosphorescence are based on the absorption and emission of photons.

The process of absorption and emission of photons is also called reradiation. The $BRDF$ describing the absorption-emission process is therefore the so-called bispectral bidirectional reflectance and reradiation distribution function ($BBRRDF$). Bispectral is used in the style of bidirectional. The reflectance distribution shows a double spectral dependence in addition to the dependence on two directions.

Time Besides direction, location and wavelength, a reflectance distribution can depend on time t. A temporally-varying $BRDF$ ($TVBRDF$) describes the burning of wood, toasting of bread, drying of fabric, decaying of fruits or the rusting of metal [88], for example. In the enlisted examples and for the most other materials, the incidence time t_i is equal to the reflection time t_r. Exceptions with considerably different times of incidence and reflection are the above mentioned phosphorescent materials. In contrast to fluorescence, minutes to hours pass from the absorption until the emission of photons in case of fluorescence.

Requirements

To be physically plausible, any *BRDF* should fulfill four requirements given by *Gebhardt* [85] and *Edwards et al.* [69]. These are the *Helmholtz reciprocity*, the *energy conservation*, the *non-negativity* and the *superposition ability*.

***Helmholtz* Reciprocity** In the context of *BRDFs*, the so-called Helmholtz reciprocity describes the reversibility of the direction of the radiant flux [85, 69]. Thus, the incidence direction $\boldsymbol{\omega}_i$ and the reflection direction $\boldsymbol{\omega}_r$ are interchangeable.

Energy Conservation The law on the conservation of energy holds in all energetic systems. The total irradiance of reflected light is equal to or smaller than the total irradiance of the incident light [85, 69].

Non-Negativity Negative radiances or irradiances are physically impossible. Thus, the *BRDF* solely takes values equal to zero or higher than zero.

Linear Additivity or Superposition Ability According to *Jackson* [129], two or more light beams striking each other do not influence each other. They form a linearly additive system. The superposition of light beams is applicable on *BRDFs* described by *Gebhardt* [85].

3.2 Bidirectional Optical Measurements

Apart from densitometers described in the books of *Kipphan* [148, 149] and *Schläpfer* [219], spectrophotometers are the most common optical instruments in the printing industry. The spectral reflectance and thus the color coordinates determined with a spectrophotometer are just valid for the currently used measuring geometry [21]. Instead of a diffuse geometry, the bidirectional geometry with an incidence angle of 45° and a reflection angle of 0° are common in printing industry.

Color coordinates determined with a spectrophotometer in the 45°/0° geometry are sufficient to control the printing process of light absorbing colors. The color appearance of printed light-absorbing inks does not considerably depend on the geometric configuration of light source and detection system relative to the sample surface. In contrast to that, the geometric configuration has considerable influence on the color appearance of printed special effect colors as shown by *Höpe et al.* [106]. For the optical characterization of special effect colors, bidirectional optical measurements in multiple geometric configurations are necessary. According to the technical report *CIE TC*1-65 [120], the optical instruments used for this kind of bidirectional measurements are called multi-angle spectrophotometers and gonioreflectometers.

These bidirectional instruments are considered in the following sections. Section 3.2.1 describes the *instrumental setup*. The common *geometry notation* is introduced in section 3.2.2. Section 3.2.3 gives some examples for such *optical instruments*.

3.2.1 Instrument Setup

All optical instruments for the measurement of object colors consist of the same essential components. According to *Berns* [21], these components are the light source, the sample holder, the detection system and the processing unit. The most important information about common *light sources* and *detection systems* are given by *Pedrotti et al.* [199].

Light Source

As widely known, any visual perception of color as well as gloss and texture is based on the presence of light. The presence of light is guaranteed for self-luminous objects. In case of non-self-luminous objects, light should be provided to perceive color, gloss or texture. As for human perception, the presence of light is also necessary for instrumental measurements. Therefore, optical instruments for measurements on non-self-luminous objects are equipped with a light source.

The task of the light source is the generation of electromagnetic radiation in the visible range. Typical light sources used for optical measurements are mostly incandescent lamps and xenon flash lamps or sometimes stabilized halogen lamps.

Incandescent Lamps Incandescent lamps are often used in optical instruments designed for color measurements in the printing industry. As halogen lamps, incandescent lamps are thermal radiators [199]. A thermal radiator generates light on the basis of heating. The heat-induced vibration of the atoms results in the emission of visible electromagnetic radiation. The emitted light has a continuous spectral power distribution. By definition, the spectral power distribution of the light emitted by an incandescent lamp is equal to that of standard illuminant A (section 4.3.1).

Xenon Flash Lamps Optical instruments with xenon flash lamps are common in other industries, such as paper, textile and automobile industry. In contrast to incandescent and halogen lamps, xenon lamps are luminescence radiators [199]. Luminescence radiators accumulate fed energy as potential energy of electrons in atoms. The accumulated potential energy is released as light energy. Due to the discrete differences between the energy levels, the spectral power distribution is a band or line spectrum. For a xenon lamp, the spectral power distribution of the emitted light nearly corresponds to that of the standard illuminant $D65$ (section 4.3.1).

Optical Detector

The task of the optical detection system is the spectral decomposition and quantitative capture of the reflected light. The spectral decomposition is realized with a dispersing unit. A photosensitive element is responsible for the quantitative capture. Different types of dispersing units and photosensitive elements are available. Their selection and combination depends on or decides about the type of the optical detector. Optical detectors are either spectral or imaging detectors described in the following.

Spectral Detector As mentioned above, a spectral detector as well as an imaging detector consists of a dispersing unit and a photosensitive element. Typically, the following dispersing units and photosensitive elements are used.

In a dispersing unit, light is decomposed spectrally by means of prisms, narrow-band interference filters or diffraction gratings [21]. The spectral dispersion using a prism is based on the dependence of the refraction index on the wavelength. When entering and leaving the prism, light of different wavelengths is refracted in different directions. The technique to use a set of narrow-band interference filters bases on their different spectral properties. The known spectral properties of the filters enable the calculation of the spectral reflectance. The today mostly used diffraction gratings are glasses with hundreds of spaced ruled lines per millimeter. These lines cause the wavelength-dependent diffraction.

Each photosensitive element transforms electromagnetic radiation in an electrical signal. In other words, a photon flux is measured in form of an electrical current. The originally widely distributed photo-multipliers were successively replaced by photo-diodes [199]. The operation of a photo-multiplier is based on the external photo-electric effect occurring in a photo-emissive layer. The main component of a photo-diode is a photo-conductive layer inducing an internal photo-electric effect. Depending on the mode of operation, the combination of multiple photo-diodes in one photosensitive element is called charge-coupled device (CCD) sensor or complementary metal-oxide-semiconductor ($CMOS$) sensor. In spectrophotometers or scanners, one-dimensional line sensors are used. Two-dimensional array sensors are used in imaging systems like cameras.

Imaging Detector As a spectral detector, an imaging detector consists of a dispersing unit and a photosensitive element. The dispersing unit and the photosensitive element of an imaging detection system additionally provide the spatial resolution while the spectral decomposition is limited to three regions. The three regions are those for long-, medium- and short-wave light. The amount of red, green and blue light is each detected by means of photosensitive elements [199]. A photosensitive element for the spatially resolved detection is realized as a two-dimensional array sensor.

The spectral trisection and spatial resolution is realized by means of beam splitters, a filter pattern or a filter wheel in combination with photosensitive arrays. The beam splitter method requires two prisms with a dichroic coating on one surface. Three photosensitive arrays independently detect the amount of separated red, green and blue light. In case of the filter pattern method, the photosensitive element is vaporized with thin color filters in a defined checkered pattern. The amount of the transmitted red, green and blue light is detected by the individual elements of the photosensitive array. In the filter wheel method, three color filters are mounted on a rotatable disc positioned in front of a photosensitive array. The photosensitive array successively detects the amount of transmitted red, green and blue light.

3.2.2 Geometry Notation

In practice, different notations of the geometric configuration are used by *Cramer* [40, 41, 43, 42, 45], *Cramer* and *Gabel* [46, 47, 48], *Gabel et al.* [84, 83], *Hofmeister et al.* [101, 103, 104, 102], *Hupp* [114, 115, 112, 113] and others [18, 144, 217, 215, 216]. The technical report *CIE TC*1-65 [120] and the standard practice *ASTM E* 2175-01 [6] give some general information on the

multi-angle geometry specification. The standard practices *ASTM E* 2194-03 [7] and *DIN* 6175-2 : 2001-03 [64] enlist some preferred geometric configurations.

All used geometry notations contain information about the location of light source and detection system relative to the sample surface. The declaration of the *incidence* or *illumination angle* and the *reflection* or *detection angle* seems to be obvious. Instead of the reflection angle, the most common notations use the so-called *aspecular* or *aspect angle* counted to the so-called specular direction. By then, these are the essential angles for in-plane geometries. Light source, sample normal and detection system lie in the same plane. For out-of-plane geometries, the *azimuth angle* is different from zero and therefore additionally given. The individual angles are explained in the standard practice *ASTM E* 284-03*a* [9], the technical report *CIE TC*1-65 [120] and in the following sections.

Incidence Angle or Illumination Angle

In the case of optical instruments, the incidence angle is also called illumination angle. The illumination angle specifies the location of the light source relative to the sample surface. This specification is used by *Cramer* and *Gabel* [46, 47], *Hupp* [114, 115, 112, 113] and others [104, 191, 217, 215, 216]. As shown in figure 3.3a, the illumination angle is counted from the normal vector to the incidence vector.

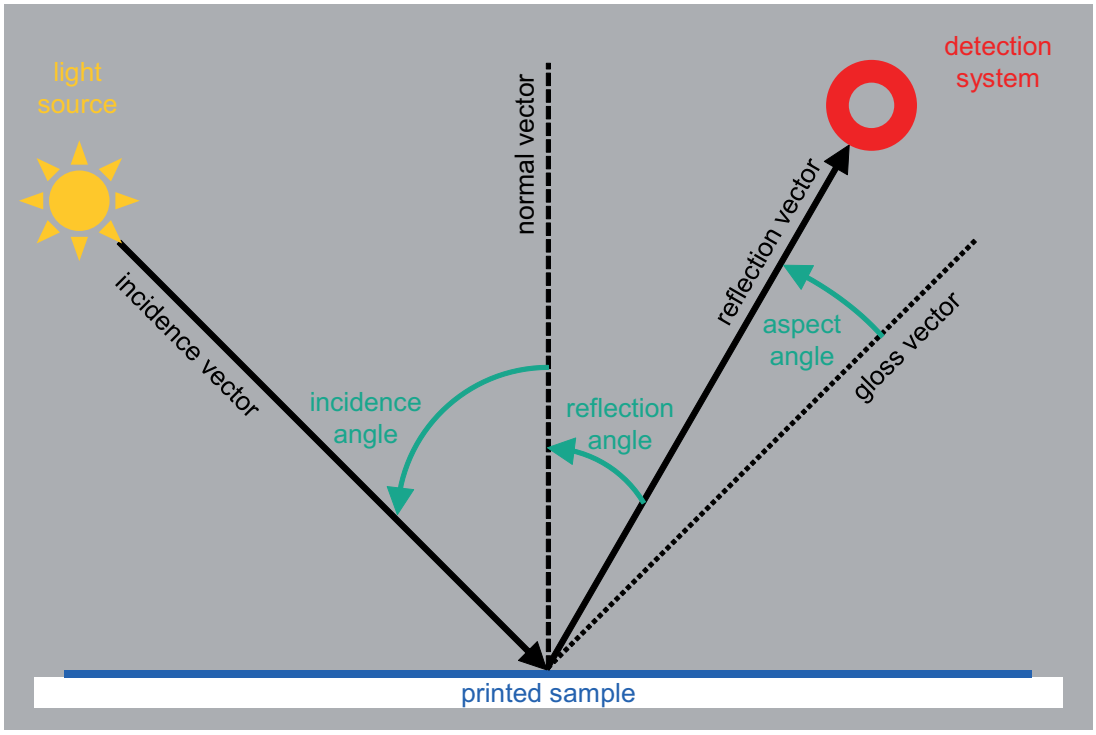

Figure 3.3: Incidence, reflection and aspect angle.

The algebraic sign of the incidence angle is always positive. This does not necessarily hold for the reflection angle.

Reflection Angle or Detection Angle

The reflection angle is counted from the normal vector to the reflection vector with a negative algebraic sign as shown in figure 3.3b. On this way, the location of the detection system relative to the sample surface is specified. *Cramer* and *Gabel* [46, 47], *Hupp* [114, 115, 112, 113] and others

[104, 191, 215, 216, 217] use this specification. The reflection angle is also named detection angle in the case of optical instruments.

Aspecular Angle or Aspect Angle

The other possibility to specify the location of the detection system uses the so-called aspecular or aspect angle. This specification is used by *Cramer* and *Gabel* [46, 47], *Hupp* [114, 115, 112, 113] and others [104, 217, 215, 216]. According to the technical report *CIE TC*1-65 [120], the aspecular angle is defined as the angular difference between the reflection vector and the gloss vector. Figure 3.3a shows a geometric configuration with a positive aspect angle. Such geometries with a positive aspect angle are named cis geometry. In so-called trans geometries, the aspect angle is negative.

Azimuth Angle

In contrast to in-plane geometries, out-of-plane geometries demand for the specification of a further angle called azimuth angle [191]. As shown in figure 3.4b, the azimuth angle specifies the rotation angle of the detection system around the aspect vector.

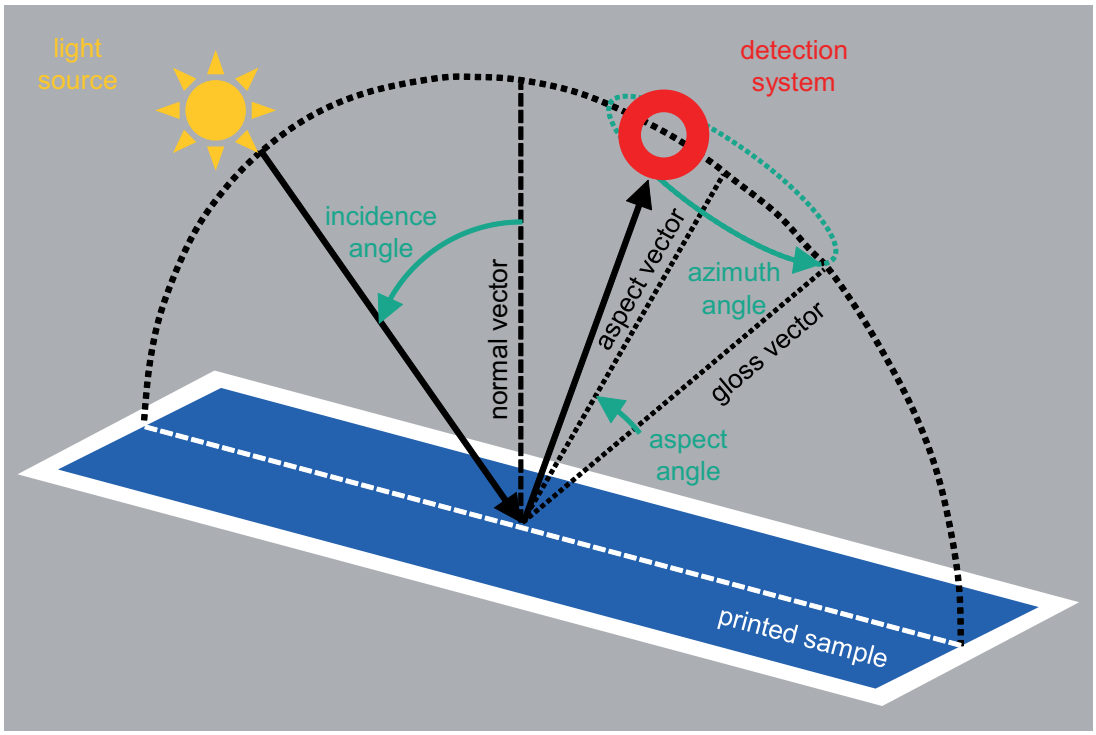

Figure 3.4: Azimuth angle.

3.2.3 Optical Instruments

Based on the introductions to the setup and the geometries, this section itemizes several optical instruments for bidirectional measurements. In doing so, *commercial multi-angle instruments* are distinguished from *exploratory goniometric instruments*.

Commercial Multi-Angle Instruments

Most of the commercial instruments are designed for applications in process control and quality assurance. Besides an adequate performance including repeatability, reproducibility and accuracy [147], the requirements on commercial instruments concern their convenient handling. This includes unlimited mobility, closed traceability, quick measurements and automatic evaluation. Therefore, commercial instruments are mainly portable systems including a software package. They perform relative measurements using a white standard for calibration.

The variation of the geometric configuration is realized by means of variations in the introduced angles in discrete steps. In addition to the incidence angle, the variation of the reflection or aspect angle, respectively, became accepted in the community of instrument suppliers and users. This becomes clear in the geometric configurations realized in the commercial multi-angle instruments.

The multi-angle spectrophotometers *Multi FX*10 and *MA*68*II* were investigated in their reproducibility by *Chorro et al.* [37]. The result of the study is that both instruments determine significantly different data. The inter-instrument reproducibility is missing.

Apart from the reproducibility, the performance includes the repeatability and accuracy. The terms repeatability, reproducibility and accuracy are explained in the standard practice *ASTM E* 2214 [10], the book of *Berns* [21] and in the papers of *Wyble* and *Rich* [249, 250].

The three multi-angle spectrophotometers *Multi FX*10, *MA*98 and *BYK-mac* were investigated in their performance by *Kehren et al.* [147] at the *Institute of Printing Science and Technology* (*IDD*). It was found that the short-term repeatability is better than medium-term repeatability. The reproducibility and accuracy are less good for geometric configurations with detection near the specular direction. These three *multi-angle spectrophotometers Multi FX*10, *MA*98 and *BYK-mac* are presented in the following.

Multi-Angle Spectrophotometer *Multi FX*10 The multi-angle spectrophotometer *Multi FX*10 was formerly developed and originally distributed by the *Datacolor AG* [82]. The most important information about this instrument are given in the book of *Pfaff et al.* [204, 205]. One of these instruments is available at the *Institute of Printing Science and Technology* (*IDD*). It was used by *Hupp* [114, 115, 112, 113], *Haas* [93, 94] and *Kehren* [144, 147] in studies on the influence of printing parameters and on the performance of the considered instrument. Its reproducibility was investigated by *Chorro et al.* [37].

The multi-angle spectrophotometer *Multi FX*10 is a bench-top device with a rectangular aperture of 22 *mm* by 69 *mm*. The sample is positioned in front of the aperture. Behind the aperture, ten geometric combinations of illumination and detection optics are moved consecutively. By means of fiber-optic light guides, each of the ten illumination optics is coupled with a tungsten halogen lamp. In the same way, all ten detection optics are coupled with the monochromator. The sensor detects the reflected light in a wavelength range from 400 *nm* to 780 *nm* in wavelength intervals of 10 *nm*.

The ten pairs of an illumination optic and a detection optic are arranged on a half-pipe. The movement of the half-pipe to change geometric arrangement takes much time. One series of measurements in all ten geometric configurations takes up to 2 *min*. A photo of the multi-angle spectrophotometer *Multi FX*10 is shown in figure 3.5a.

The other illustrations of figure 3.5 show the realized geometric arrangements of light source and detection system relative to the sample. Figure 3.5b shows the geometric configurations with medium illumination from an angle of 45° counted to the perpendicular. These are the geometries 45*as*-15, 45*as*15, 45*as*25, 45*as*45, 45*as*75 and 45*as*110. The steep illumination from an angle of 15° for the geometries 15*as*-15 and 15*as*15 is shown in figure 3.5c. In figure 3.5d, the geometries 65*as*-15 and 65*as*15 with flat illumination from an angle of 65° are shown.

Multi-Angle Spectrophotometer *MA*98 Apart from the multi-angle spectrophotometer *MA*68*II* mentioned by *Cramer* and *Gabel* [46, 47] and *Pfaff et al.* [204, 205] and investigated by *Chorro et al.* [37], the *X-Rite GmbH* provides further developed versions of this instrument. The recent instrument in the multi-angle series is the multi-angle spectrophotometer *MA*98. The

(a) Photo of *Multi FX*10.

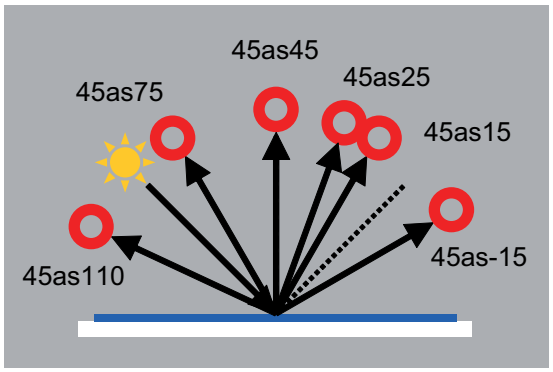

(b) Sketch of medium illumination.

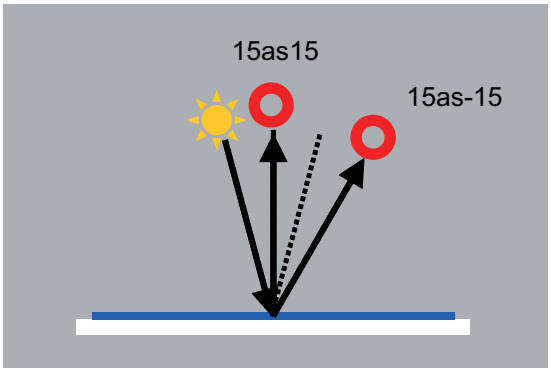

(c) Sketch of steep illumination.

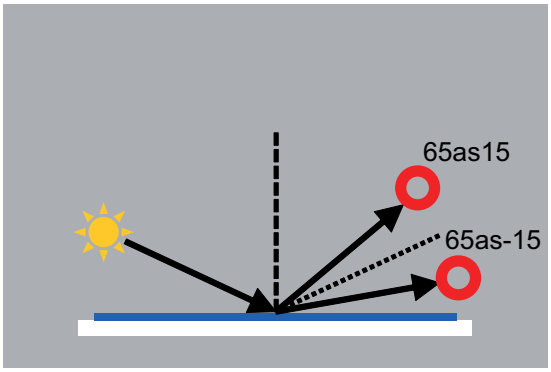

(d) Sketch of flat illumination.

Figure 3.5: Multi-angle spectrophotometer *Multi FX*10.

Institute of Printing Science and Technology (*IDD*) owns such an instrument. Its performance was investigated by *Kehren et al.* [147].

In the multi-angle spectrophotometer *MA*98, tungsten lamps illuminate the sample with a circular aperture of 12 *mm* in diameter. In within 2 *s*, all spectral measurements in the wavelength range from 400 *nm* to 700 *nm* in 10 *nm* wavelength intervals are finished. The multi-angle spectrophotometer *MA*98 is shown in the photo of figure 3.6a.

(a) Photo of *MA*98.

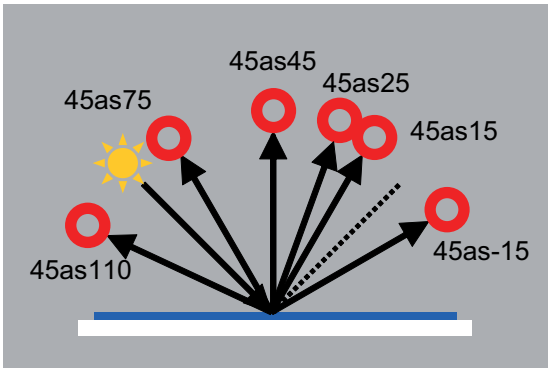

(b) Sketch of medium illumination and in-plane detection.

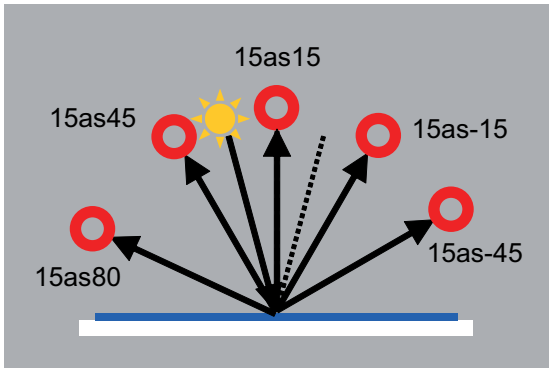

(c) Sketch of steep illumination and in-plane detection.

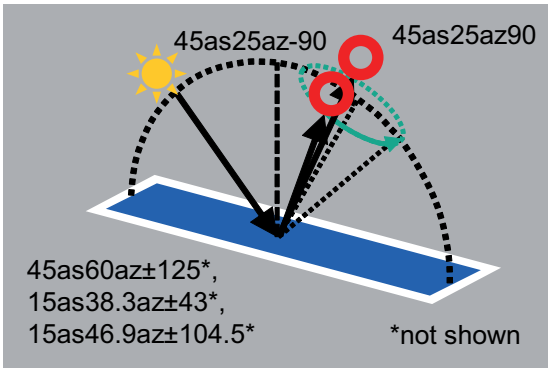

(d) Sketch of medium illumination and out-of-plane detection.

Figure 3.6: Multi-angle spectrophotometer *MA*98.

In total, 19 geometric configurations are realized in this optical instrument. In addition to eleven in-plane geometries, the instrument has eight out-of-plane geometries. Six of the in-plane geometries with an incidence angle of 45° are shown in figure 3.6b. These are namely the geometries 45*as*-15, 45*as*15, 45*as*25, 45*as*45, 45*as*75 and 45*as*110. Figure 3.6c shows the remaining five in-plane geometries with an incidence angle of 15°. Their notation is 15*as*-45, 15*as*-15, 15*as*15, 15*as*45 and 15*as*80.

In figure 3.6d, two of the eight out-of-plane geometries are shown. Besides the illustrated geometries 45*as*25*az*-90 and 45*as*25*az*90, there are the six out-of-plane geometries 45*as*60*az*-125, 45*as*60*az*125, 15*as*38.3*az*-43, 15*as*38.3*az*43, 15*as*46.9*az*-104.5 and 15*as*46.9*az*104.5.

Upgraded Multi-Angle Spectrophotometer *BYK-mac* Another commercial multi-angle spectrophotometer called *BYK-mac* is provided by the *BYK-Gardner GmbH*. *Kehren et al.* [147] investigated its repeatability, reproducibility and accuracy in a performance study.

This instrument has a circular aperture with a diameter of 23 *mm*. Less than 6 *s* are required for all possible measurement methods in all realized geometric configurations. Figure 3.7a shows a photo of the multi-angle spectrophotometer *BYK-mac*.

(a) Photo of *BYK-mac*.

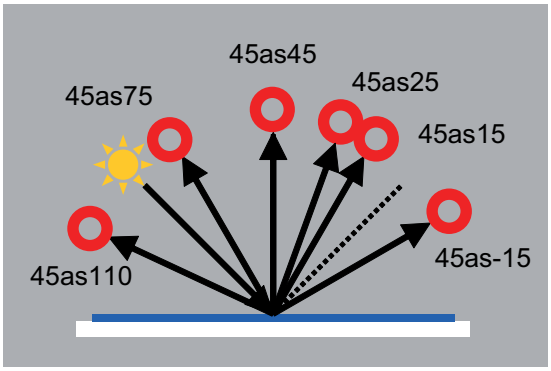

(b) Sketch of directional illumination and spectral detection.

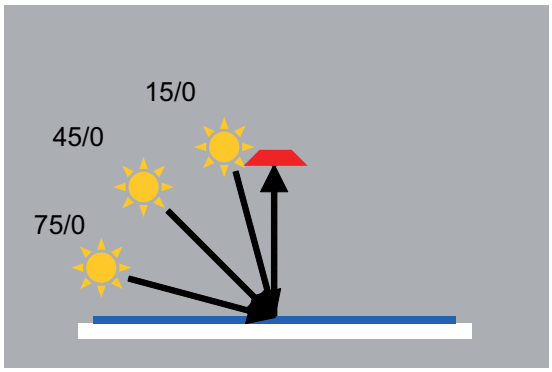

(c) Sketch of directional illumination and spatial detection.

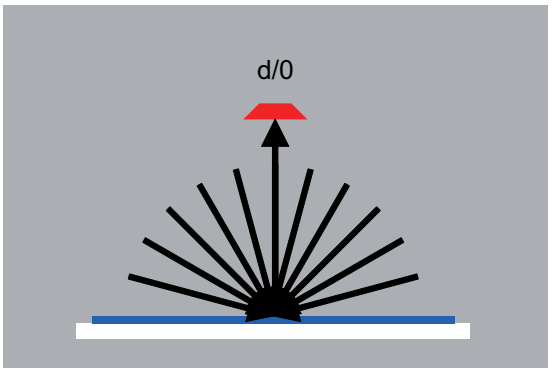

(d) Sketch of diffuse illumination and spatial detection.

Figure 3.7: Upgraded multi-angle spectrophotometer *BYK-mac*.

Spectral measurements are performed in wavelength intervals of 10 nm in the wavelength range from 400 nm to 700 nm in six geometric configurations. These six geometries named $45as$-15, $45as15$, $45as25$, $45sa45$, $45as75$ and $45as110$ are shown in figure 3.7b.

In this thesis, the multi-angle spectrophotometer *BYK-mac* is called an upgraded multi-angle spectrophotometer due to the following reason. In addition to the spectral measurements in the six itemized directional geometries, the multi-angle spectrophotometer *BYK-mac* performs imaging measurements in three directional and a diffuse geometric arrangement. The three directional geometries 15°/0°, 45°/0° and 75°/0° with incidence angles of 15°, 45° and 75° and a reflection angle of 0° are shown in figure 3.7c. Figure 3.7d shows the diffuse geometry $d/0°$ with diffuse illumination and detection at 0°.

In normal direction, a charge-coupled device (CCD) sensor detects the reflected light of a white light emitting diode (LED) as a space-resolved gray-value distribution. The grabbed images are internally used to determine texture parameters. As mentioned in section 4.1.3, these are namely the sparkle area S_A, sparkle intensity S_I and the sparkle grade S_G each for the three bidirectional geometries as well as the graininess G for the diffuse geometry.

Exploratory Goniometric Instruments

The exploratory goniometric instruments introduced in the following are predominantly used at metrological institutes with high demands on the performance for the characterization of materials. White standard materials consisting of ceramic, opal glass, barium sulfate ($BaSO_4$) or polytetrafluorethylen ($PTFE$) [118, 119], are characterized for the calibration of commercial instruments. For research purposes, other materials like printed special effect colors are characterized in their bidirectional optical properties by measurements in the whole hemisphere above the sample.

In contrast to the mentioned commercial multi-angle instruments, measurements with the subsequently introduced exploratory goniometric instruments are not relative to a calibrated standard material. In absolute measurements, the reflected light is determined with respect to the incident light. The measurement of the reflected light as well as the incident light should be considered in the structure of the instrument. Therefore, exploratory goniometric instruments are unique constructions including successor models with potential enhancements. The *robot-based gonioreflectometer RGon* [109, 107, 108, 105, 106] and *three-dimensional appearance robot-based gonioreflectometer ARGon*^{3} [12] are examples for such unique constructions and their enhanced version.

Robot-Based Gonioreflectometer *RGon* Two robot-based gonioreflectometers are owned by the *Physikalisch-Technische Bundesanstalt* (PTB), the German metrology institute. Detailed information about the robot-based gonioreflectometer *RGon* is available in several publications of *Hünerhoff et al.* [109] and *Höpe et al.* [107, 108, 105, 106]. The robot-based gonioreflectometer *RGon* is shown in figure 3.8a.

As all bidirectional optical instruments, the robot-based gonioreflectometer *RGon* is composed of of three main components. These are the light source, the sample holder and the detection system as introduced above.

The light source is a so-called homogeneous sphere radiator. The sphere radiator consists of a small integrating sphere with an inner diameter of 150 mm and a 400 W quartz-halogen lamp. The light source is mounted on a large rotation stage with a diameter of 1500 mm. On this way, the light source can be rotated 360° around the sample holder located in the center of the rotation stage.

On the sample holder, the sample is fixed with adhesive tape or magnetic pads. The sample holder is mounted at a five-axis industrial robot. With the degrees of freedom in the motion of the industrial robot and the rotation stage, measurements of the absolute spectral radiance factor are possible in any desired geometric configuration.

Thereby, the detection system stays stationary in its position outside the rotation stage. The main elements of the detection system are a monochromator and interchangeable photo detectors.

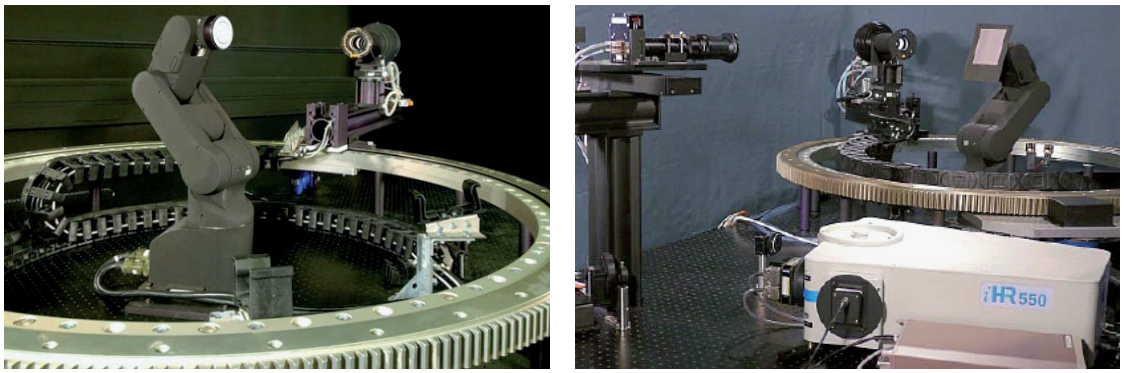

(a) *RGon* [107]. (b) $ARGon^3$.

Figure 3.8: Robot-based gonioreflectometers.

The monochromator spectrally decomposes the reflected light. In narrow wavelength bands, the amount of light is received by photo detectors in the wavelength range from 250 nm to 1700 nm.

The robot-based gonioreflectometer *RGon* was used in several studies [109, 108, 105, 106, 147]. *Hünerhoff et al.* [109] and *Höpe et al.* [108, 105] characterized diffuse standard reflection materials. First experiences about the appearance of printed special effect colors were gained by *Höpe et al.* [106]. *Kehren et al.* [147] used the robot-based gonioreflectometer *RGon* as reference instrument to investigate the accuracy of the previously presented multi-angle spectrophotometers *Multi FX*10, *MA*98 and *BYK-mac*.

Three-Dimensional Appearance Robot-Based Gonioreflectometer $ARGon^3$ Figure 3.8b shows the so-called three-dimensional appearance robot-based gonioreflectometer $ARGon^3$ described in the paper of *Atamas et al.* [12]. Technically, the three-dimensional appearance robot-based gonioreflectometer $ARGon^3$ is composed as the robot-based gonioreflectometer *RGon*. The composition of light source, sample holder and detection system is only slightly different.

In the device designation $ARGon^3$, the exponent 3 denominates three-dimensional. The letter A is for appearance. This add-on specification signifies the capability to measure the three-dimensional appearance. In addition to a detection system for spectral measurements, the reflected radiation can be resolved spatially by means of a camera.

For spectral measurements, the detection system comprises a monochromator and a line-scan charge-coupled device (CCD) camera. The spectral radiance factor of the reflected light is detected simultaneously in the wavelength range from 200 nm to 2500 nm.

Spatially resolved measurements are realized by means of a photometric camera as detection system. The photometric camera measures luminance factors with a spatial resolution of 20 μm. As common in camera-based measurements, the determined RGB values are only valid for the present illumination conditions. Due to the importance of the standard illuminant $D65$, a filter is used to produce $D65$-like light with a correlated color temperature of 6500 K.

Chapter 4

Visual Appearance Research

In case of special effect colors, gaps in the knowledge about the essential visual appearance attributes cause problems in their perception-based characterization (section 1.1.3). For this problem, the understanding is extended in this chapter.

In addition, the need of the corresponding approach is explained. The number and nature of essential visual appearance attributes are intended to be identified (section 1.2.3, chapter 7).

For this purpose, section 4.1 gives an introduction to *visual perception* and *appearance attributes*. *Visual performance* and *vision testing* are introduced in section 4.2. Section 4.3 gives information about *standard conditions* for visual experiments and their *technical realization*. Information about *psychophysical experiments* and their *statistical evaluation* is given in section 4.4 and section 4.5, respectively.

4.1 Visual Perception and Appearance Attributes

The visual experience induced in the eye and interpreted in the brain is called visual perception as defined in the standard practices *ASTM E* 284-03*a* [8]. According to the same standard practice *ASTM E* 284-03*a* [8] and the standard practice *ASTM E* 1808-96 [2], visual appearance concerns the spectral and spatial perception of a visual stimulus in an environment specified by the geometric configuration of illumination and observation. A similar definition is given in the technical report *CIE TC*1-65 [120] written by the Technical Committee *TC*1-65 of the International Commission on Illumination (*CIE*). According to this technical report *CIE TC*1-65 [120] and the paper of *Eugène* [75], the visual perception is subdivided in appearance components for color, gloss, texture and translucency. This subdivision including visual appearance attributes for the description of the visual perception is shown in figure 4.1.

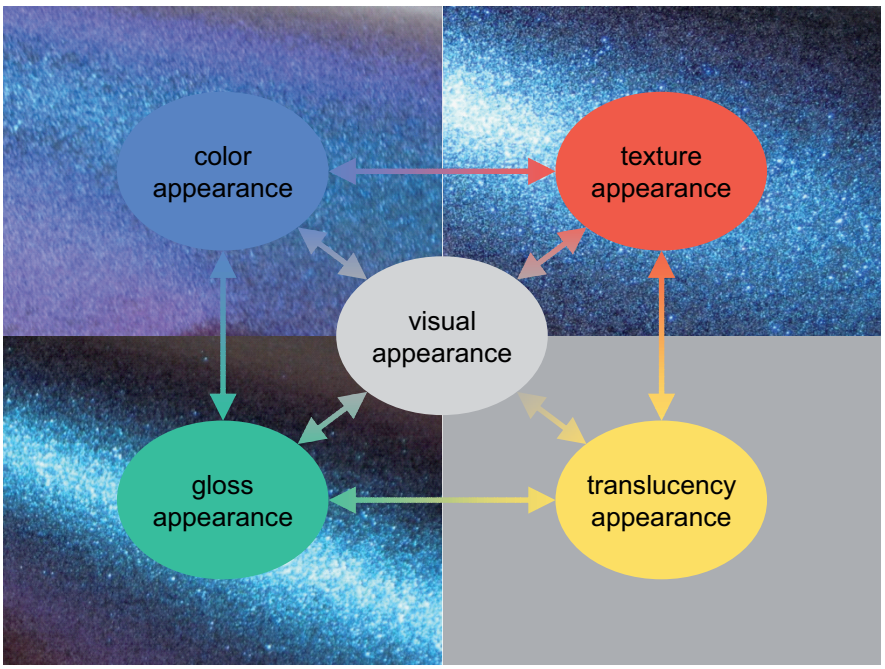

Figure 4.1: Subdivision of visual perception.

With the exception of translucency, the enlisted visual appearance components are perceived for printed special effect colors. All eligible appearance attributes describing the *color* (section 4.1.1), *gloss* (section 4.1.2) and *texture* (section 4.1.3) are presented in the following.

4.1.1 Color Attributes

Besides gloss (section 4.1.2) and texture (section 4.1.3) treated below, color is one of the fundamental components of our visual perception [120, 75]. Color describes a light source or an illuminated object in its spectral or wavelength-dependent properties [8].

The visual perception of color was extensively investigated by multiple color scientists such as *Young* [255], *Hering* [99], *Maxwell* [179], *Wright* [247], *Guild* [91], *Munsell* [189], *Judd* [135, 136, 137, 138, 139, 140] as well as *Stiles* and *Burch* [228]. The meaning of *hue*, *brightness*, *lightness*, *colorfulness*, *chromaticness*, *chroma* and *saturation* can be found in the standard practice *ASTM E* 284-03*a* [8] and in the books of *Fairchild* [76], *Hunt* [110] or *Hunter* and *Harold* [111].

For the description of light absorbing colors, three visual appearance attributes are necessary and sufficient. The well-established and most suitable color attributes are *hue*, *chroma* and *lightness*. The psychophysical function of these color attributes is known [21, 26].

In their book on special effect pigments, *Pfaff et al.* [204, 205] describe the *color shift* and the *lightness shift*. The *hue shift* was introduced by *Kehren* [145] as a color attribute expected to be important for printed special effect colors. The *hue angle shift* and the *chroma shift* can be defined in a similar way.

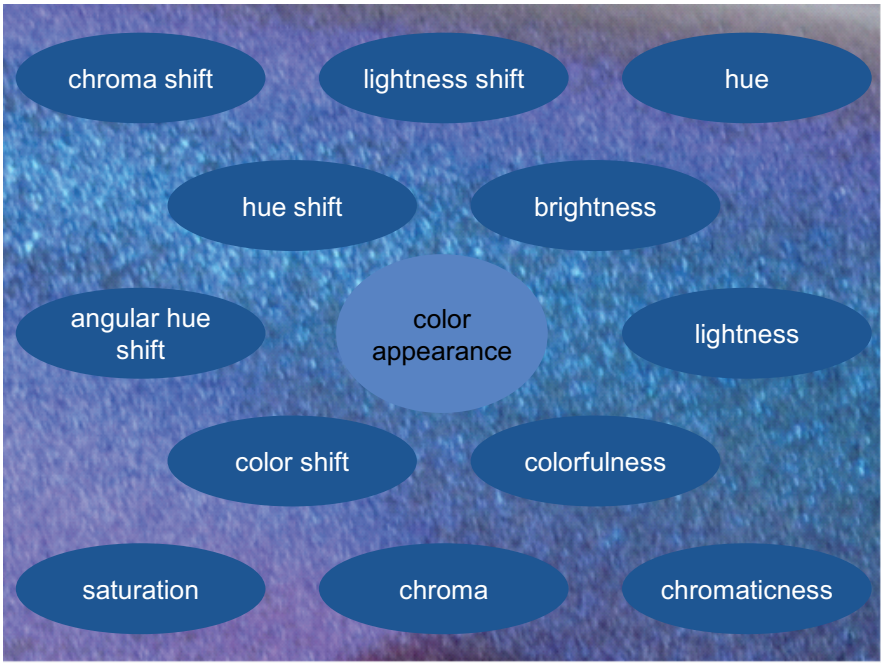

Figure 4.2: Color appearance and color attributes.

Figure 4.2 shows all mentioned color attributes for light and objects in general as well as for systems including special effect pigments. In the following sections, these color attributes are presented in detail.

Hue

The term hue is explained in the standard practice *ASTM E* 284-03*a* [8], the technical report *CIE TC*1-65 [120], the books of *Fairchild* [76], *Hunt* [110] and *Hunter* and *Harold* [111] as well as in the paper of *Judd* [136]. It is a visual perception attribute describing a color as red, yellow, green and blue or a mixture of two of them. So-called chromatic colors have a hue and a non-zero chroma. Achromatic colors have no hue and a chroma of zero.

In contrast to the chroma scale and the lightness scale, the hue scale has no natural zero point. Instead of the representation on a straight axis, the nature of hue is represented as a closed circle called hue circle. The circular representation of hue can be observed in several color order systems, such as the *Munsell* system [189], as well as in color appearance spaces, such as the *CIELCH* system [21, 26]. In the *CIELCH* system, hue is described by the so-called hue angle. The hue angle h°_{ab} is determined according to equation 4.1 [120].

$$h^{\circ}_{ab} = \arctan\left(\frac{b^*}{a^*}\right) \tag{4.1}$$

The symbols a^* and b^* are defined as the redness-greenness and yellowness-blueness value in the *CIELAB* system [21, 26], respectively. According to equation 4.2 and equation 4.3, both values are determined by the tristimulus values X, Y and Z of the object and X_n, Y_n and Z_n of the reference with the index n for normalization [120].

$$a^* = 500 \cdot \left(f\left(\frac{X}{X_n}\right) - f\left(\frac{Y}{Y_n}\right)\right) \tag{4.2}$$

$$b^* = 200 \cdot \left(f\left(\frac{Y}{Y_n}\right) - f\left(\frac{Z}{Z_n}\right)\right) \tag{4.3}$$

Regarding the quotient q of the object tristimulus values X, Y and Z and the reference tristimulus values X_n, Y_n and Z_n, two cases are distinguished. The function f of the quotient q serves as measure for the distinction of the both cases defined in equation 4.4.

$$f(q) = \begin{cases} \frac{1}{3} \cdot \left(\frac{29}{6}\right)^2 \cdot q + \frac{4}{29} & \text{if} \quad q \leq \left(\frac{6}{29}\right)^3 \\ \sqrt[3]{q} & \text{if} \quad q > \left(\frac{6}{29}\right)^3 \end{cases} \quad \text{with } q = \frac{X}{X_n}, \frac{Y}{Y_n}, \frac{Z}{Z_n} \tag{4.4}$$

Thus, the redness-greenness and yellowness-blueness axis in the $CIELAB$ system are an alternative representation of hue in combination with chroma. The term chroma is explained below.

Brightness

The stand practice $ASTM\ E\ 284\text{-}03a$ [8], the technical report $CIE\ TC1\text{-}65$ [120] and the books of $Fairchild$ [76] and $Hunt$ [110] define the term brightness. This color attribute describes the absolute amount of light either emitted by a light source or reflected or transmitted by an illuminated object. The brightness scale has a natural zero point. For a brightness of zero, no light is neither emitted, reflected nor transmitted. With the absolute amount of light, the visual perception increases from dim to bright.

Lightness

In contrast to the absolute character of brightness, the term lightness describes the perceived relative amount of light. According to stand practice $ASTM\ E\ 284\text{-}03a$ [8], the technical report $CIE\ TC1\text{-}65$ [120] and the books of $Fairchild$ [76] and $Hunt$ [110], lightness is a relative brightness. The term relative means that the absolute amount of light reflected or transmitted by an arbitrary object is referred to the absolute amount of light reflected or transmitted by an ideal reference. The ideal reference is a white reflector or a perfect transmitter. The mathematical connection of brightness and lightness is given by equation 4.5.

$$\text{lightness}\,(\text{object}) = \frac{\text{brightness}\,(\text{object})}{\text{brightness}\,(\text{reference})} \tag{4.5}$$

This definition sets the lower and upper limit of the lightness scale to zero and one, respectively. A dark object with a lightness of zero has a brightness of zero. A light object with a lightness equal to one has the same brightness as the reference.

For clarification of the difference between brightness and lightness, consider the following example. Imagine the same piece of a white paper in three different scenes. The scenes are your bedroom just illuminated by a bedside lamp, your bureau with a typical office illumination on the ceiling and your balcony flooded with natural sunlight from the cloudless sky. In the listed sequence, the brightness of the paper increases. Due to the increasing amount of incident light, an increasing amount of light can be reflected. The lightness of the paper remains constant. The increasing amount of light reflected by the white paper is referred to an equally increasing amount of light reflected by a white reference. Thus, the referencing of the object brightness to the reference brightness compensates the increase.

The relative character of lightness is also represented in color appearance spaces. In particular, this becomes clear in the definition of lightness L^* in the $CIELAB$ and $CIELCH$ system [21, 26]. As shown in equation 4.6, the tristmulus value Y of the object is normalized by the tristimulus value Y_n of the reference with the index n for normalization [120].

$$L^* = 116 \cdot f\left(\frac{Y}{Y_n}\right) - 16 \tag{4.6}$$

The case distinction function f is defined above in equation 4.4. This function is used to realize a case distinction.

Colorfulness

A further visual appearance attribute for color is colorfulness defined in the standard practice *ASTM E* 284-03*a* [8] and in the books of *Fairchild* [76], *Hunt* [110] and *Hunter* and *Harold* [111]. Colorfulness describes the perceived absolute amount of hue in the color of the considered light source or illuminated object. The colorfulness scale has a natural zero point for achromatic colors without hue. As mentioned before, chromatic colors have a hue and therefore non-zero colorfulness.

Chromaticness

The term chromaticness has the same meaning as the previously presented colorfulness. Compared to colorfulness, the color appearance attribute chromaticness is used less frequently. These both color attributes are defined in the standard practice *ASTM E* 284-03*a* [8].

Chroma

By analogy with lightness explained above, chroma is a relative color attribute. Thus, chroma is related to colorfulness in the same way as lightness is related to brightness. According to the standard practice *ASTM E* 284-03*a* [8], the technical report *CIE TC*1-65 and the books of *Fairchild* [76], *Hunt* [110] and *Hunter* and *Harold* [111], chroma is a relative colorfulness. As shown in equation 4.7, the chroma of an object is equal to its colorfulness divided by the brightness of the ideally reflecting or transmitting reference.

$$\text{chroma}\,(\text{object}) = \frac{\text{colorfulness}\,(\text{object})}{\text{brightness}\,(\text{reference})} \tag{4.7}$$

Chroma describes the deviation from the achromatic gray of the same brightness. Achromatic colors are located in the natural zero point of the chroma scale while chromatic colors are not located in the zero point. This becomes also clear in the definition of chroma C^*_{ab} in the *CIELCH* system according to equation 4.8 [120].

$$C^*_{ab} = \sqrt{(a^*)^2 + (b^*)^2} \tag{4.8}$$

Thus, chroma is equal to the *Euclidean* distance from the lightness axis. The redness-greenness value a^* and the yellowness-blueness value b^* were introduced above in equation 4.2 and equation 4.3, respectively.

Saturation

Saturation is also a relative colorfulness [8, 76, 110, 111, 136]. The saturation of an object is defined similar to chroma, as shown in equation 4.9.

$$\text{saturation}\,(\text{object}) = \frac{\text{colorfulness}\,(\text{object})}{\text{brightness}\,(\text{object})} \tag{4.9}$$

The only difference is in the definition of the reference. The reference for the saturation of an object is the object itself.

Color Shift or Color Flop

The term color shift is also known as color flop [180, 204, 205]. The color shift is a visual perception attribute for gonio-apparent surfaces like printed special effect colors. The visual appearance of gonio-apparent surfaces depends on the geometric configuration of light source and observer relative to the surface. Thus, the color shift describes the extent of the perceived geometry-induced color change. The perceived color change can be represented by a geometry-induced color difference [93, 94] in a first step. In a further step, the sum of geometry-induced color differences over a series of geometric configurations is used to represent the perceived color change.

To explain the geometry-induced color difference, imagine two color coordinates in the $CIELAB$ system [21, 26] given by the triplets (L_i^*, a_i^*, b_i^*) and $\left(L_j^*, a_j^*, b_j^*\right)$. The indices i and j specify the geometric configuration. Equation 4.10, equation 4.11 and equation 4.12 show the determination of the color component differences $\Delta L_{i,j}^*$, $\Delta a_{i,j}^*$ and $\Delta b_{i,j}^*$, respectively.

$$\Delta L_{i,j}^* = L_j^* - L_i^* \tag{4.10}$$

$$\Delta a_{i,j}^* = a_j^* - a_i^* \tag{4.11}$$

$$\Delta b_{i,j}^* = b_j^* - b_i^* \tag{4.12}$$

Using these color component differences, the color difference $\Delta E_{ab,i,j}^*$ [120] is defined as the *Euclidean* distance in the more or less perceptually uniform $CIELAB$ color space [234, 235]. The calculation of the *Euclidean* distance is shown by equation 4.13.

$$\Delta E_{ab,i,j}^* = \sqrt{\left(\Delta L_{i,j}^*\right)^2 + \left(\Delta a_{i,j}^*\right)^2 + \left(\Delta b_{i,j}^*\right)^2} \tag{4.13}$$

Haas [93, 94] used the geometry-induced color difference between the near-at-gloss geometry $45as15$ and the far-from-gloss geometry $45as45$ to represent the color shift in the first step. In the next step, the color shift is represented by the sum of geometry-induced color differences $\Delta E_{ab,i,i+1}^*$ called color difference sum $\Delta E_{ab,1,N}^*$. This summation is shown in equation 4.14

$$\Delta E_{ab,1,N}^* = \sum_{i=1}^{N-1} \Delta E_{ab,i,i+1}^* \tag{4.14}$$

The index i identifies the geometric configuration. Preferably, the geometric configurations are those belonging to an aspect or interference line. The terms aspect and interference line are defined in the books of *Maisch* and *Weigand* [172], *Glausch et al.* [86] and *Pfaff et al.* [204, 205] as well as in the thesis of *Hupp* [112, 113] and the paper of *Kehren* and *Dörsam* [144].

The index i ranges from 1 to N for the initial and final point of the aspect and interference line. The color difference sum is equal to the *Euclidean* length of the respective aspect or interference line.

Angular Hue Shift or Angular Hue Flop

The angular hue shift or angular hue flop is another visual appearance attribute for gonio-apparent surfaces. The angular hue shift is a color attribute for the extent of the changes in the hue angle caused by changes in the geometric configuration.

In the same way as the color shift, the angular hue shift can be represented by the sum of geometry-induced angular hue differences in the $CIELCH$ color system [21, 26] called angular hue difference sum ($AHDS$). Equation 4.15 defines the angular hue difference sum $\Delta h_{ab,1,N}^\circ$ for a series of N geometric configurations identified by the index i.

$$\Delta h_{ab,1,N}^\circ = \sum_{i=1}^{N-1} \left|\Delta h_{ab,i,i+1}^\circ\right| \tag{4.15}$$

The angular hue difference or hue angle difference $\Delta h^{\circ}_{ab,i,i+1}$ or $\Delta h^{\circ}_{ab,i,j}$ is defined in equation 4.16 as the difference of two hue angles $h^{\circ}_{ab,i}$ and $h^{\circ}_{ab,j}$.

$$\Delta h^{\circ}_{ab,i,j} = h^{\circ}_{ab,j} - h^{\circ}_{ab,i} \tag{4.16}$$

The sign of the hue angle difference indicates the direction of the rotation around the lightness axis. For a positive sign, the rotation from color coordinate i to color coordinate j is mathematically positive. The rotation from color coordinate i to color coordinate j is mathematically negative for a negative sign.

Hue Shift or Hue Flop

The term hue shift or hue flop is also used for gonio-apparent surfaces [180]. The hue shift describes the extent of the hue change induced by a geometry change.

Remember the definition of the angular hue difference sum (equation 4.15). Transfer this representation of the angular hue shift into a possible representation of the hue shift by the hue difference sum (HDS). According to *Kehren et al.* [145] equation 4.17, the hue difference sum $\Delta H^*_{ab,1,N}$ can be defined as the sum of $N-1$ hue differences $\Delta H^*_{ab,i,i+1}$ between N color coordinates for different geometric configurations identified with the indices i and $i+1$.

$$\Delta H^*_{ab,1,N} = \sum_{i=1}^{N-1} \Delta H^*_{ab,i,i+1} \tag{4.17}$$

Equation 4.18 gives information about the determination of the hue difference $\Delta H^*_{ab,i,j}$ using the color difference $\Delta E^*_{ab,i,j}$, the lightness difference $\Delta L^*_{i,j}$ and the chroma difference $\Delta C^*_{ab,i,j}$.

$$\Delta H^*_{ab,i,j} = \sqrt{\left(\Delta E^*_{ab,i,j}\right)^2 - \left(\Delta L^*_{i,j}\right)^2 - \left(\Delta C^*_{ab,i,j}\right)^2} \tag{4.18}$$

The color difference $\Delta E^*_{ab,i,j}$ and lightness difference $\Delta L^*_{i,j}$ were defined in equation 4.13 and in equation 4.10, respectively. Inserting them in the preceding equation 4.18 yields an equivalent expression for the hue difference given in equation 4.19.

$$\Delta H^*_{ab,i,j} = \sqrt{\left(\Delta a^*_{i,j}\right)^2 + \left(\Delta b^*_{i,j}\right)^2 - \left(\Delta C^*_{ab,i,j}\right)^2} \tag{4.19}$$

The redness-greenness difference $\Delta a^*_{i,j}$, and the yellowness-blueness difference $\Delta b^*_{i,j}$, were already defined above in equation 4.11 and equation 4.12, respectively. Equation 4.20 gives a comparable definition for the chroma difference on the basis of chroma $C^*_{ab,i}$, and $C^*_{ab,j}$, for the color coordinates i and j.

$$\Delta C^*_{ab,i,j} = C^*_{ab,j} - C^*_{ab,i} \tag{4.20}$$

The sign of the chroma difference gives information about the radial translation with respect to the lightness axis. A positive sign indicates an outwards directed translation from color coordinate i to color coordinate j. An inward directed translation from color coordinate i to color coordinate j is indicated by a negative sign.

Chroma Shift or Chroma Flop

A further visual perception attribute for gonio-apparent surfaces is the so-called chroma shift or chroma flop. The chroma difference sum (CDS) represents the perceived geometry-induced chroma change.

For a series of N geometric configurations, the chroma difference sum can be defined as the sum over $N-1$ chroma differences between the side by side color coordinates in the $CIELCH$ system [21, 26]. The mathematical expression for the chroma difference sum $\Delta C^*_{ab,1,N}$ is given in equation 4.21.

$$\Delta C^*_{ab,1,N} = \sum_{i=1}^{N-1} \left|\Delta C^*_{ab,i,i+1}\right| \tag{4.21}$$

The modulus of the chroma difference $\Delta C^*_{ab,i,i+1}$ eliminates negative signs. The chroma difference $\Delta C^*_{ab,i,j}$ is defined above in equation 4.20.

Lightness Shift or Lightness Flop

The lightness shift mentioned by *Pfaff et al.* [204, 205] and others [24, 82, 180] also known as lightness flop. It is related to the contrast gloss introduced below. Apart from the flop index specified in the technical report *CIE TC*1-65 [120] and the paper of *Rodrigues* [215], the lightness difference sum (*LDS*) is used to describe the geometry-induced lightness change of ordinary surfaces including gonio-apparent surfaces.

The sum of lightness differences between color coordinates of different configurations can serve as measure for the lightness shift. The lightness difference sum $\Delta L^*_{1,N}$ is expressed mathematically in equation 4.22.

$$\Delta L^*_{1,N} = \sum_{i=1}^{N-1} \left|\Delta L^*_{i,i+1}\right| \tag{4.22}$$

Due to the modulus, the lightness difference $\Delta L^*_{i,i+1}$ is always positive. The definition of the lightness difference $\Delta L^*_{i,j}$ is given above in equation 4.10.

4.1.2 Gloss Attributes

As color (section 4.1.1) and texture (section 4.1.3) explained above and below, respectively, gloss belongs to the fundamental components of our visual appearance [120, 75]. Our gloss perception describes the geometry-dependent properties of a surface [8, 111].

Besides others, such as *Phillips et al.* [208], *Leloup et al.* [163, 165, 164, 162] and *Fleming et al.* [81], the appearance of gloss was recently researched by *Wills et al.* [245] as well as by *Pellacini et al.* [200] and *Ferwerda et al.* [80]. In these publications, several visual appearance attributes are defined. For only some of them, the psychophysical function is known.

Apart from *specular gloss*, *contrast gloss*, *luster*, *bloom*, *haze*, *diffuseness* and *sheen*, the gloss attributes named *distinctness-of-image gloss*, *absence-of-bloom gloss*, *absence-of-texture gloss* and *surface-uniformity gloss* are defined in the standard practices *ASTM D* 4449-90 [4], *ASTM D* 523-89 [3], *ASTM D* 5767-95 [5], *ASTM E* 430-97 [9] and *ASTM E* 284-03*a* [8] or in the book of *Hunter* and *Harold* [111].

Pfaff et al. [204, 205] use the gloss attributes *metal* and *pearl gloss*. Metal and pearl gloss are relevant in the context of special effect pigments.

The generally known gloss attributes and those for systems with special effect pigments are shown in figure 4.3. All enlisted gloss attributes are defined in the following sections.

Specular Gloss

The visual appearance attribute called specular gloss describes the perceived luminance caused by specular reflection on the surface. This definition is given in the standard practices *ASTM D* 523-89 [1], *ASTM D* 523-89 [3], *ASTM E* 430-97 [9] and *ASTM E* 284-03*a* [8], in the technical report *CIE TC*1-65 [120], in the book of *Hunter* and *Harold* [111] and in the papers of *Ji et al.* [133], *Pellacini et al.* [200], *Ferwerda et al.* [80] and *Phillips et al.* [208]. A typical example for a surface with a high specular gloss is a mirror.

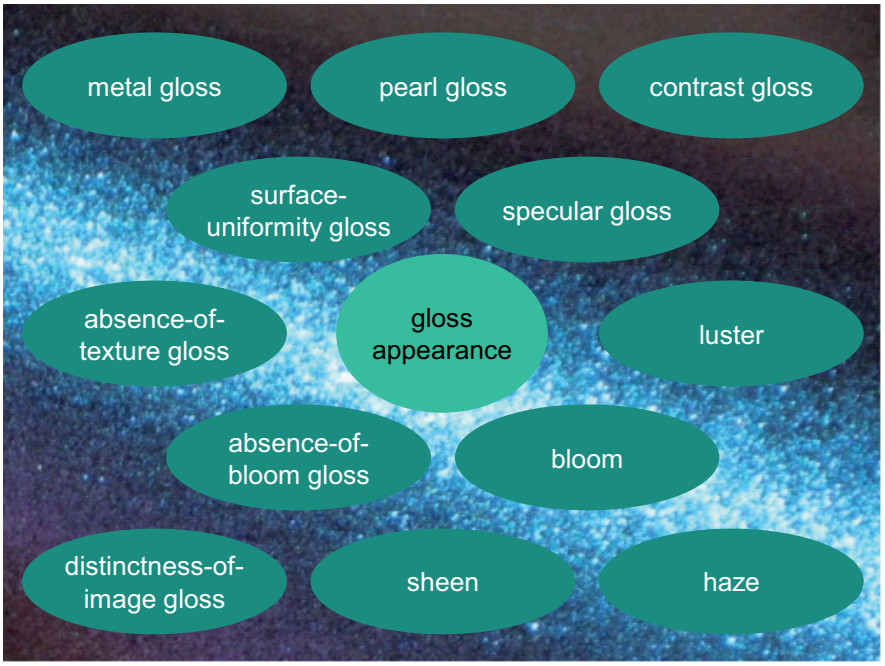

Figure 4.3: Gloss appearance and gloss attributes.

Contrast Gloss

The term contrast gloss is defined in the standard practice *ASTM E* 284-03*a* [8], the technical report *CIE TC*1-65 [120] and in the book of *Hunter* and *Harold* [111]. It is investigated in the studies of *Pellacini et al.* [200], *Ferwerda et al.* [80], *Phillips et al.* [208] and others [133, 161]. Contrast gloss is related to luster explained below. These both visual appearance attributes describe the perceived contrast in the luminance caused by specular reflection and off-specular reflection.

In more detail, the contrast gloss is the degree of dissimilarity between the luminance in specular and off-specular direction. This definition of contrast gloss is supported by figure 4.4.

Figure 4.4 shows a half metal cylinder with a partly unpolished (left part) and polished (right part) surface. In the unpolished half (left part), the luminance is high in specular direction and medium high in off-specular direction. The luminance is very high in specular direction and low in off-specular direction for the polished half (right part). Compared to the unpolished half, the dissimilarity in luminance is therefore higher in the polished half. Thus, the unpolished half has a lower contrast gloss than the polished half.

A uniform objective definition of contrast does not exist. Different mathematical formulas are in use. Some contrast formula are given in the standard practice *ASTM E* 284-03*a* [8]. A common formula defines the contrast as the quotient of the higher and lower luminance. The difference of the higher and lower luminance is another simple definition. The combination of these basic operations results in several possible definitions for contrast. In a physically reasonable definition, the difference of the higher and lower luminance is divided by the higher luminance.

This general definition of a contrast parameter based on the standard practice *ASTM E* 284-03*a* [8] can be transferred to a possible definition of a contrast gloss (CG) parameter. The parameter for contrast gloss P_{CG} is defined in equation 4.23.

$$P_{CG} = \frac{Y_G - Y_{FFG}}{Y_G} = 1 - \frac{Y_{FFG}}{Y_G} \tag{4.23}$$

The quotient of the far-from-gloss luminance Y_{FFG} and the gloss luminance Y_G is subtracted from one. Therefore, the contrast gloss parameter ranges from zero to one.

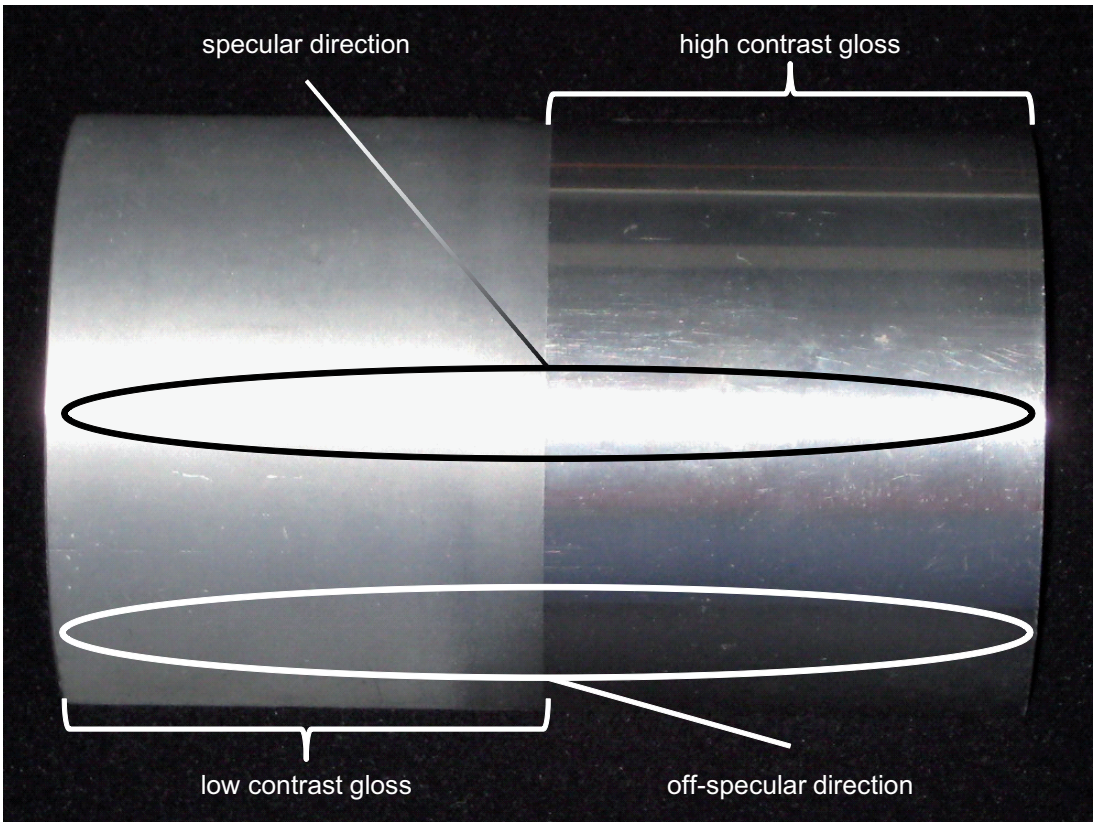

Figure 4.4: Partly unpolished and polished metal surface differing in contrast gloss.

Luster

The term luster is used in a similar context as the previously introduced visual appearance attribute contrast gloss. Thus, luster describes the increase of the perceived luminance in specular direction compared to the perceived luminance in off-specular directions. This definition is given in the standard practice *ASTM E* 284-03*a* [8], the technical report *CIE TC*1-65 [120], in the book of *Hunter* and *Harold* [111] as well as in the papers of *McCamy* [180, 181] and *Ji et al.* [133].

Bloom

As the terms haze and diffuseness considered below, the term bloom describes the perceived diffuse reflection near the specular direction. The standard practice *ASTM E* 284-03*a* [8], the technical report *CIE TC*1-65 [120] and the book of *Hunter* and *Harold* [111] mention this gloss attribute. The sensation of bloom, haze and diffuseness can be induced by a deposition on a surface like dust on a painted furniture or white frost on plants.

Haze

The term haze is used in similar to bloom and diffuseness explained above and below, respectively. Haze is defined in the standard practices *ASTM D* 523-89 [3], *ASTM E* 430-97 [9] and *ASTM E* 284-03*a* [8], the technical report *CIE TC*1-65 [120] as well as in the book of *Hunter* and *Harold* [111]. Haze was investigated in the studies of *Pellacini et al.* [200], *Ferwerda et al.* [80] and *Phillips et al.* [208].

Diffuseness

Diffuseness is used in the same context as bloom and haze considered above. Thus, the term diffuseness is used to describe the cloudy appearance near the specular direction. *Hunter* and *Harold* [111] introduced this gloss attribute.

Sheen

Sheen is a visual appearance attribute for the perceived amount of specular reflection at grazing angles. The standard practices *ASTM D* 523-89 [3], *ASTM E* 430-97 [9] and *ASTM E* 284-03*a* [8], the technical report *CIE TC*1-65 [120] and the book of *Hunter* and *Harold* [111] give a definition of sheen. It is also mentioned in the papers of *Pellacini et al.* [200], *Ferwerda et al.* [80], *Phillips et al.* [208] and *Ji et al.* [133]. Grazing angles are flat incidence and reflection angles with high values near 90° counted to the perpendicular on the sample surface.

Distinctness-Of-Image Gloss

The so-called distinctness-of-image gloss (*DOIG*) is a further visual appearance attribute. It is defined in the standard practices *ASTM D* 5767-95 [5], *ASTM E* 430-97 [9] and *ASTM E* 284-03*a* [8], in the technical report *CIE TC*1-65 [120] as well as in the book of *Hunter* and *Harold* [111]. It is investigated in the studies of *Pellacini et al.* [200], *Ferwerda et al.* [80], *Phillips et al.* [208] and others [24, 133, 161, 169]. The *DOIG* describes the perceived sharpness of an image reflected on the considered surface.

For a better imagination, think on a mirror in a bathroom. Apart from the possibility that you forgot your eye glasses or contact lenses, you usually see your face clear with sharp transitions. The mirror has a high *DOIG*. After a hot shower, the mirror might be steamed up. Thus, the mirror image is blurred to some extent. The *DOIG* is considerably lower.

Another example are metal surfaces. Two metal surfaces differing in the perceived *DOIG* are shown in figure 4.5.

The weakly polished metal surface shown in figure 4.5a has a low *DOIG*. A high *DOIG* is perceived for the strongly polished metal surface shown in figure 4.5b.

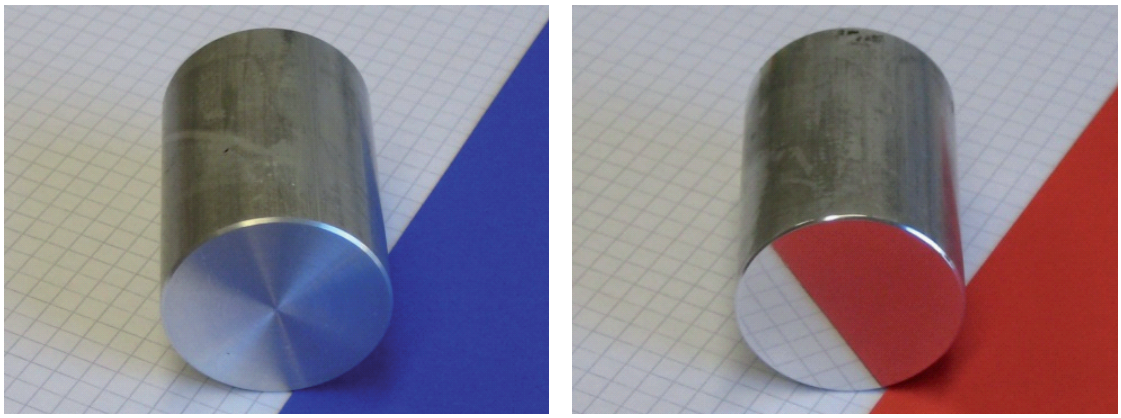

(a) Low *DOIG*. (b) High *DOIG*.

Figure 4.5: Metal surfaces differing in *DOIG*.

According to the standard practice *ASTM D* 5767-95 [5], the *DOIG* can be represented by a contrast-like parameter. The *DOIG* parameter is based on luminance measurements in the direction of specular reflection and between 0.2° and 0.4° off the direction of specular reflection. The gloss (G) luminance Y_G and the near-at-gloss (NAG) luminance Y_{NAG} are used to calculate the *DOIG* parameter P_{DOIG} as symbolized in equation 4.24 basing on the standard practice *ASTM D* 5767-95 [5].

$$P_{DOIG} = \frac{Y_G - Y_{NAG}}{Y_G} = 1 - \frac{Y_{NAG}}{Y_G} \tag{4.24}$$

This equation 4.24 for the *DOIG* parameter is comparable with equation 4.23 for the above introduced contrast gloss parameter. As the contrast gloss parameter, the *DOIG* parameter ranges from zero to one.

Absence-Of-Bloom Gloss

For the definition of the perception attribute called absence-of-bloom gloss, remember the explanations about bloom, haze and diffuseness given above. Thus, absence-of-bloom gloss describes the absence of the diffuse reflectance component adjacent to the direction of specular reflection. This definition in given in the standard practice *ASTM E* 284-03*a* [8], the technical report *CIE TC*1-65 [120], the book of *Hunter* and *Harold* [111] and in the paper of *Ji et al.* [133].

Absence-Of-Texture Gloss

The term absence-of-texture gloss is comparable with the term surface-uniformity gloss explained below. Both are visual perception attributes for the perceived homogeneity and uniformity of the surface as defined in the book of *Hunter* and *Harold* [111] as well as in the papers of *Pellacini et al.* [200], *Ferwerda et al.* [80] and *Phillips et al.* [208].

Surface-Uniformity Gloss

As mentioned above, surface-uniformity gloss and absence-of-texture gloss have the same meaning. According to the book of *Hunter* and *Harold* [111] and the paper of *Ji et al.* [133], these both visual attributes are defined as the smoothness of the surface and its freedom from texture.

Metal Gloss

According to *Pfaff et al.* [204, 205], the so-called metal gloss is a perception attribute for the visual sensation associated with the special gloss appearance of a metal surface. Metal gloss is

induced by the specular reflection from small mirrors. The small mirrors are either micro facets located at the object's surface or flaky pigments embedded in a transparent matrix. Aluminum flakes are added to cosmetics, plastics, industrial varnishes or printing inks to give the product a metal-like gloss appearance.

Pearl Gloss

The perception attribute called pearl gloss results from the association with the unique gloss appearance of a pearl as described by *Pfaff et al.* [204, 205]. The gloss of pearls seems to come from the deep inside of the pearl. The apparently three-dimensional gloss is induced by inter-reflections in the multi-layered structure of pearls. The pearl-like gloss appearance is imitated by means of special effect pigments.

4.1.3 Texture Attributes

In addition to color (section 4.1.1) and gloss (section 4.1.2) explained above, texture is one of the fundamental appearance components [120, 75]. Texture describes the location-dependent properties of a surface or its structure, pattern or topography [8].

Rao and *Lohse* [212] published results of their study on the appearance of texture. Twelve texture attributes were investigated in their suitability for describing the location-dependent properties of a surface. A wide range of textures were found to be representable by means of three dimensions. The first dimension correlates with *repetitiveness*, *randomness*, *directionality*, *regularity*, *orientation* and *uniformity*. The two texture attributes *contrast* and *directionality* are represented in the second dimension. The third dimension describes the *granularity*, *complexity* and *coarseness* of the considered texture.

In connection with special effect pigments, *Kirchner et al.* [154, 150, 152] and *Dekker et al.* [57] use texture attributes named *coarseness* and *glint*. The related terms *graininess* and *sparkle* are used by *Rentschler* [213], *Ďuricovič* and *Martens* [238], *Ďuricovič et al.* [237] and by *Ershov et al.* [73, 74].

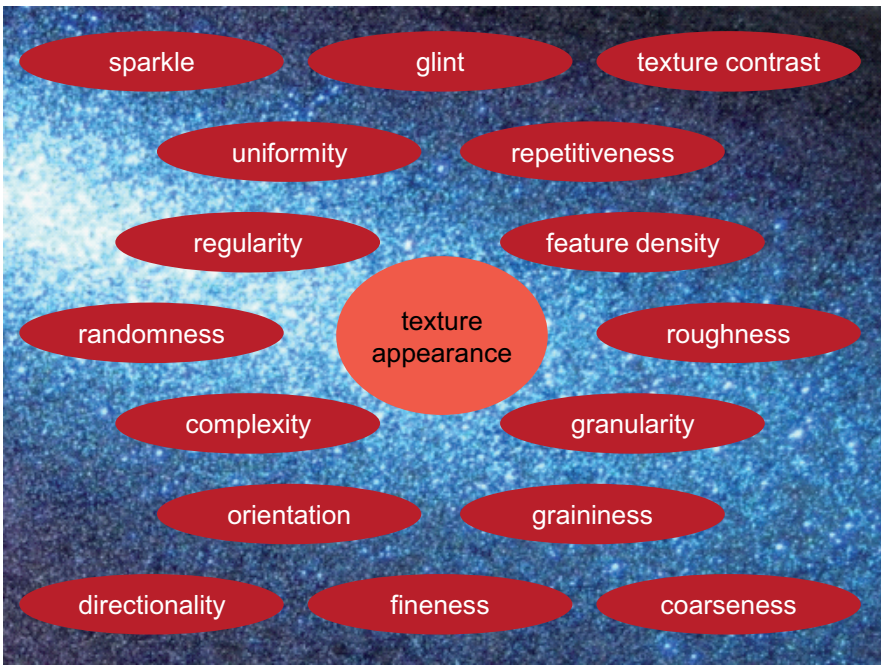

Figure 4.6: Texture appearance and texture attributes.

Figure 4.6 shows the universally valid texture attributes as well as those primarily used for systems with special effect pigments. All these texture attributes are explained in the next sections.

Texture Contrast

Remember the definitions of texture and contrast. Thus, the term texture contrast describes the degree of dissimilarity in the location-dependent properties. Among other texture attributes, *Rao* and *Lohse* [212] investigated the perceived texture contrast in their study on relevant texture dimensions. Some examples for a high texture contrast are dark rain clouds on a bright sunny sky, black letters on a white paper, white embroideries on a black fabric or a radiograph showing light bones on a dark X-ray screen.

As an especially illustrative example explaining the difference between a low and high texture contrast, imagine two beaches of fine grains of sand. The one beach consists of sand grains similar in color. The gray grains of sand have a medium lightness. From afar, the other beach has the same lightness. But, the one half of its sand grains is white and the other half of its sand grains is black. From near, the eye can visually resolve the individual grains of sand. Both beaches are not equal in texture. The first beach has no texture contrast. The texture contrast is maximal for the second beach.

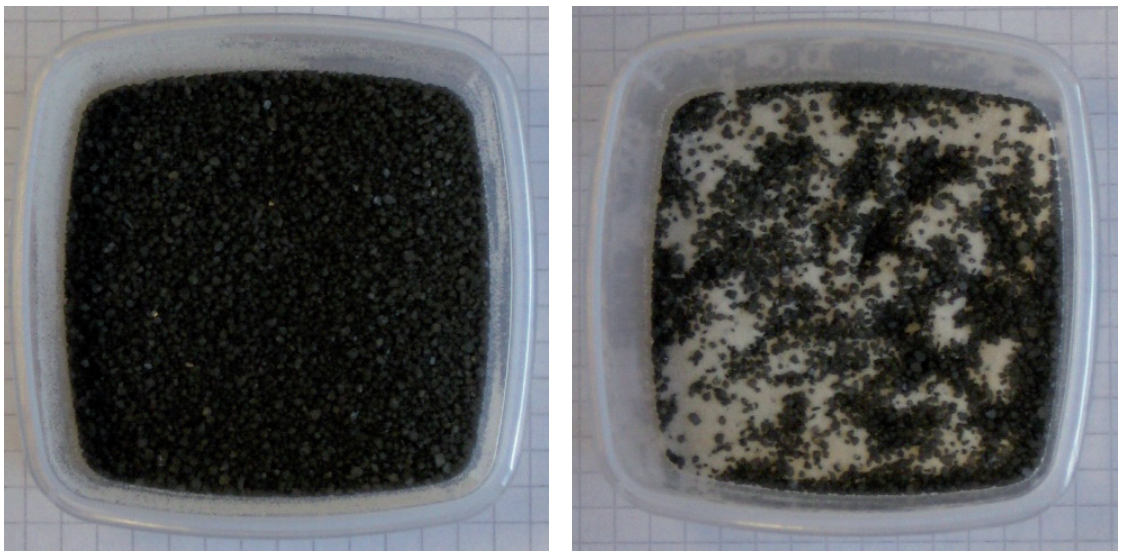

(a) Low texture contrast. (b) High texture contrast.

Figure 4.7: Particle systems differing in texture contrast.

In figure 4.7, the just given example of the two beaches differing in their lightness distribution is recreated by means of two particle systems. The system consisting of particles with nearly equal lightness (figure 4.7a) has a low texture contrast. The texture contrast is high for the system composed of light and dark particles (figure 4.7b).

Repetitiveness

The term repetitiveness has a similar meaning as the term feature density explained below. For the explanation, think of a total system composed of single components. For such a composed texture, repetitiveness describes the frequency of repetition. Typical examples for textures with considerable repetitiveness are wickerwork, woven tissues, meshed fabrics, brick walls and foamed soap. Such textures were investigated in the study of *Rao* and *Lohse* [212].

Feature Density

Feature density is a texture attribute with the same meaning as repetitiveness. Thus, feature density is the frequency of a feature per unit area. *Rao* and *Lohse* [212] investigated the visual perception of feature density in their study on texture appearance.

Roughness

According to *Rao* and *Lohse* [212], roughness is the opposite of smoothness. The roughness is a distance parameter used to quantify the quality of a surface topography. Shadowing and masking on elevated and recessed regions causes the impression of texture. Extreme examples are a smoothly polished steal and a rough stone wall, respectively. *Kwak* and *You* [160] and *Kitamura* [155] investigated the perception of roughness on samples of sand paper and of interior finishing materials like stucco, fabric and leather, respectively.

Granularity

As graininess considered below, granularity describes a non-uniformity caused by grains. Both texture attributes are defined in the paper of *McCamy* [181]. *Rao* and *Lohse* [212] considered the attribute granularity in their texture study. Due to its less frequent use, granularity is introduced below in the section on graininess in more detail.

Graininess

The texture attributes granularity and graininess describe the size of components into which a system can be subdivided. This definition is given in the paper of *McCamy* [181]. Some examples are salt, sugar, rice, peas, beans, popcorn and cornflakes. Sand and gravel are examples for less and more grainy systems, respectively. Figure 4.8 shows two containers filled with sand and gravel differing in graininess.

(a) Fine-grained sand. (b) Coarse-grained grave.

Figure 4.8: Particle systems differing in graininess.

A fine-grained system with a low graininess like sand (figure 4.8a) consists of many small components. In contrast to that, few large components are present in a coarse-grained system with a high graininess like gravel (figure 4.8b).

The graininess increases with an increasing particle size of the special effect pigments as found by *Rentschler* [213]. The graininess of blue special effect varnishes was determined in imaging measurements with the multi-angle spectrophotometers *BYK-mac* described in section 3.2.3.

Coarseness

Compared to granularity and graininess, the texture attribute coarseness definitely describes the composition of a system of few large components instead of many small components. The term coarseness is not only used for more or less grainy system like gravel or sand mentioned above. Coarseness also describes textures like fabric or foam. The perceived coarseness of natural and artificial textures was investigated by *Chamorro-Martínez et al.* [34] and *Gurnsey* and *Fleet* [92], respectively. *Kichner et al.* [154, 150, 152, 153] and *Dekker et al.* [57] investigated the coarseness perception of special effect varnishes under diffuse illumination.

Fineness

Fineness is the opposite of coarseness. Both texture attributes were investigated in the study of *Rao* and *Lohse* [212]. While coarseness is used for systems of few large components, fineness is used for systems of many small components.

Directionality

The texture attribute directionality is used to describe the existence and extend of a preferential direction in an arbitrary texture. A preferential direction is caused by a pronounced dependency on the considered direction. For example, the directionality of a wood grain depends on the growth of the tree. Among other texture attributes, *Rao* and *Lohse* [212] included this texture attribute in their study on the dimensionality of texture appearance. Furthermore, the perceived directionality was investigated *Shah et al.* [224, 223] and *Ji et al.* [132].

Orientation

In addition to the existence and extend of a preferential direction, the visual appearance attribute orientation describes the characteristics of the preferential direction in space. A brick wall, a stone pavement and a textile fabric have two orthogonal preferential directions. The orientation in textures of wooden surfaces, plant leafs or line drawings is more complex. The texture attribute orientation was also considered in the study of *Rao* and *Lohse* [212].

Complexity

The texture attribute named complexity is the opposite of simplicity. Complexity characterizes systems consisting of multiple different components in an intricate arrangement. Examples for textures with a high complexity are wooden surfaces, plant leafs or a line drawings. *Rao* and *Lohse* [212] investigated the perception of complexity.

Randomness

A further texture attribute considered by *Rao* and *Lohse* [212] and investigated by *Emrith et al.* [71] is called randomness. Random means that something is not definable, predictable or controllable. Thus, randomness assumes no order or coherence of the components preventing any pattern or combination in the system. Foam, clouds, leaves and grass are some examples for random textures. Randomness is inconsistent with regularity and uniformity explained in the following.

Regularity

The texture attribute called regularity is explained by means of the adjective regular. Regular describes that something reoccurs at fixed intervals or with a constant frequency to say it in other words. Such periodical repetitions can be found in the textures of a brick wall or a textile fabric. The perceived regularity of textures was studied by *Rao* and *Lohse* [212].

Uniformity

Furthermore, the term uniformity is a visual appearance attribute for a uniform type of textures investigated by *Rao* and *Lohse* [212]. Uniform implies that something is alike, equal, homogeneous or monotonous without diversity, variations, extremes or exclusions. As for regularity, examples are again the textures of a brick wall and a textile fabric.

Sparkle

Sparkle is defined in the standard practice *ASTM E* 430-97 [8] and considered in the papers of *Besold* [24], *Ďuricovič et al.* [238, 237], *Ershov et al.* [73, 74] and *Rentschler* [213]. It is a texture attribute for the perception of highlights in a surrounding. The tiny light spots are brighter than the surrounding.

Apart from self-luminous objects like stars in the sky, the bright flashes are caused by specular reflections on micro facets at the surface or on flaky pigments in a matrix. These bright points of light are clearly visible under intense directional illumination. For example, think on the sparkles caused by the reflection of sunlight at small waves on a calm sea.

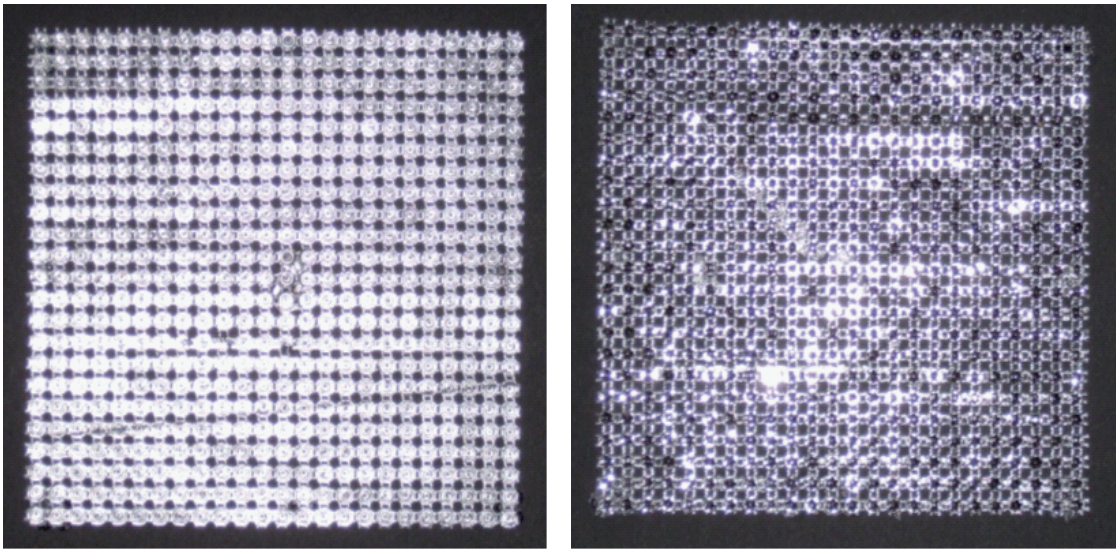

(a) Low sparkle intensity. (b) High sparkle intensity.

Figure 4.9: Decorative materials differing in sparkle intensity.

Figure 4.9 shows two samples of decorative materials with different sparkle intensities. The metallized, embossed and punched paper (figure 4.9a) appears to have a low sparkle intensity. An impression of a high sparkle intensity is induced by the same metallized, embossed and punched paper due to additional rhinestones (figure 4.9b).

Perception-related parameters for the perceived sparkle can be determined on the basis of bidirectional imaging measurements with instruments such as the multi-angle spectrophotometer *BYK-mac* described in section 3.2.3. The perception-related sparkle parameters are the sparkle area S_A, the sparkle intensity S_I and the sparkle grade S_G. The total size of the small, bright areas per unit area are called sparkle area. The sparkle intensity is specified as the intensity the

of small, bright light spots in relation to the intensity of the less bright surrounding. The sparkle area and the sparkle intensity are combined in the representative sparkle attribute called sparkle grade.

On samples of special effect varnishes, *Rentschler* [213] determined these sparkle parameters. Among the determined sparkle parameters and the realized geometric configurations, the sparkle intensity S_I for the geometry $15°/0°$ increases with an increasing particle size.

Glint

The term glint is defined in the standard practice *ASTM E* 430-97 [8] and in the paper of *McCamy* [181]. This texture attribute is used in the same context as the previously introduced term sparkle. Thus, glint is an appearance attribute for the local directional reflection of many small elements called glitters. On samples of special effect varnished, *Kichner et al.* [154, 150, 152, 153] and *Dekker et al.* [57] investigated the perceived glint under directional illumination.

4.2 Visual Performance and Vision Testing

For studies on the visual appearance, it is important to guarantee the visual performance of the participating subjects. Therefore, vision tests should be conducted previous to any kind of studies concerning visual appearance.

The visual performance regards two topics in equal measure. These both topics are namely visual acuity (section 4.2.1) as well as color vision (section 4.2.2). Therefore, they are treated in the following including visual acuity and color vision testing, respectively.

4.2.1 Visual Acuity

According to *Pedrotti et al.* [199], the word visual acuity describes the capability of the visual system to resolve fine details spatially. The acuteness of vision depends on the projection sharpness of the eye and the processing sensitivity of the brain. The limiting factors of the eye are the density of photoreceptors as well as the diffraction at the lens. Furthermore, external conditions like the intensity of the illumination and the contrast in the image have an influence in the visual acuity. In addition to these influencing factors, the visual acuity can be disturbed due to visual defects called hyperopia and myopia.

Hyperopia is also called farsightedness or longsightedness [199]. Thus, the focusing of near objects is difficult and a blurred image appears. The cause of hyperopia is a comparatively short eyeball or weakly curved lens. The optical power of cornea and lens is increased with eye glasses or contact lenses. Convex lenses with a positive dioptric value displace the focal point on the retina closer towards the lens.

Myopia is also known as nearsightedness or shortsightedness [199]. Distant objects cannot be focused resulting in the perception of a blurred image. A comparatively long eyeball or strongly curved lens is the cause of myopia. Apart from refractive surgery, eye glasses or contact lenses with a negative dioptric value are used to relocate the focal point. The negative optical power of the concave lens compensates the excess of the positive optical power.

The spatial resolution of the visual system is tested by means of different types of acuity tests [199]. In general, black symbols of variable sizes on a white background are observed from a specified distance of about six meters. The more or less common acuity tests belong to the classes of resolution, localization, detection and recognition tests. The most important *detection* and *recognition tests* are presented in the following.

Detection Test

In a detection test, the subject is asked to decide about the presence or absence of stimuli. The discrimination of any details of the target is not essential. Therefore, simple signs like a dot or a line and rotating letters like the *Landolt C* or the *Snellen E* are used as targets.

In the case of the simple signs, the existence of the dot or the line is assessed. The position of the gap in the *Landolt C* or of the limbs of the *Snellen E* is evaluated in the case of the rotating letters.

Recognition Test

The most common acuity tests are recognition tests. The subject is asked to recognize numbers or letters. The choice and design of the targets and their size in the assembly on the chart have to be elaborated carefully. The so-called *Snellen* letters were especially created for recognition tasks.

These letters are built up in a squared pattern of five by five units. The details, namely the lines and gaps, have a width of one unit. The size of the smallest correctly identifiable letter is used to determine the visual acuity.

4.2.2 Color Vision

The capability to perceive colors as an average observer is called color vision as described by *Berns* [21] and others [214, 219]. According to that, the term color vision deficiency describes any kind of deviation from the normal trichromatic color vision.

The reason for a color vision deficiency bases on the spectral performance of the photosensitive pigments in the cones on the retina. Their sensitivity to light of long, medium or short wavelengths is somehow disturbed. Compared to an observer with normal color vision, the respective colors red, green and blue are not correctly perceived by an observer with deficient color vision.

Besides the rare totally disturbed so-called monochromatism or monochromatic color vision, there are several types of partially disturbed color vision. These are either the real dichromatic color vision or the anomalous trichromatic color vision. Depending on the disturbed spectral region, the real dichromatism and the anomalous trichromatism are further distinguished in the following way [33, 219].

The terms protanopia and protanomaly describe the total and partial insensitivity to long-wave light usually inducing a sensation for the color red. The total and partial insensitivity to medium-wave light usually perceived as green is called deuteranopia and deutranomaly. Tritanopia and tritanomaly are the respective items for the total or partial insensitivity to blue perceived short-wave light.

The performance of color vision can be tested by means of color deficiency tests [21, 219]. Several color deficiency tests, such as the *Ishihara Color Deficiency Test*, the *Farnsworth-Munsell D*15 *Test* and the *Farnsworth-Munsell* 100 *Hue Test*, are common in vision research. These color deficiency tests are introduced in the following.

Ishihara Color Deficiency Test

The *Ishihara* Color Deficiency Test is conducted with several color charts developed by *Ishihara* [128, 239]. As described by *Berns* [21] and others [33, 219], *Ishihara* color charts are so-called pseudo-isochromatic plates. The adjective chromatic labels all colors with a chroma greater than zero. The extended adjective isochromatic describes colors with the same hue. Adding the prefix, pseudo-isochromatic signifies that the colors only seem to have the same hue. For observers with any kind of deficient color vision, specific pseudo-isochromatic colors are indistinguishable. Such pseudo-isochromatic colors are combined in the *Ishihara* color charts shown in figure 4.10 [128, 239].

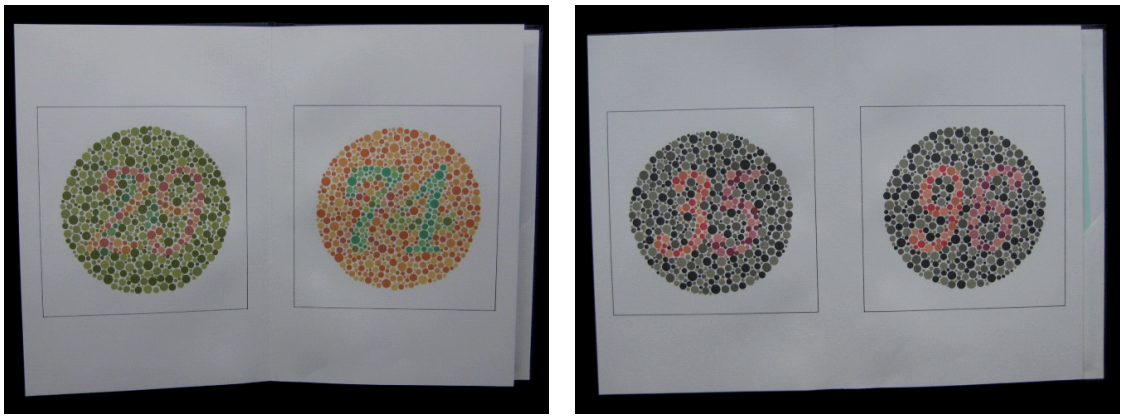

(a) 29 and 74.

(b) 35 and 96.

Figure 4.10: *Ishihara* Color Deficiency Test with pseudo-isochromatic plates [128, 239].

On each *Ishihara* color chart, multiple dots differing in color and size are arranged inside of a circle. These pseudo-isochromatic plates serve as a simple tool to detect deficiencies in the discrimination of red and green. Observers without any color deficiency are able to read numbers

and letters in the *Ishihara* color charts. The numbers and letters do not appear to observers with color-defective vision.

*Farnsworth-Munsell D*15 Test

Another simple test to detect color deficiencies is the so-called *Farnsworth-Munsell D*15 Test. As described by *Berns* [21] and others [27, 33] and as shown in figure 4.11, the *Farnsworth-Munsell D*15 Test consists of 16 colored caps differing in hue.

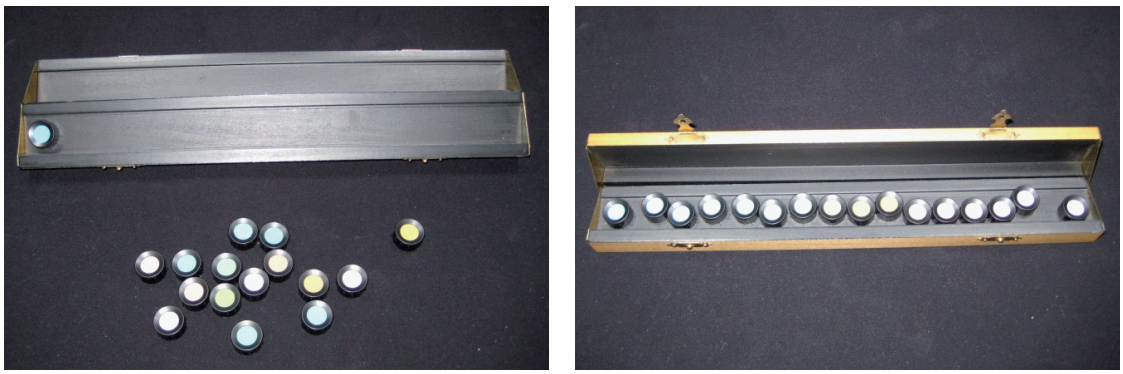

(a) Beginning. (b) Ending.

Figure 4.11: *Farnsworth-Munsell D*15 Test.

One of the colored caps is fixed at the left end of a bench serving as storing case. The subject is instructed to order the remaining 15 colored caps according to their hue. All observers with color-defective vision make mistakes in this ordering task. The task is solved correctly by observers with normal color vision.

Farnsworth-Munsell 100 Hue Test

The *Farnsworth-Munsell* 100 Hue Test is a further color deficiency test described by *Farnsworth* [77, 78] and others [21, 27, 33]. The equipment of the *Farnsworth-Munsell* 100 Hue Test includes 93 colored caps in four benches as shown in figure 4.12.

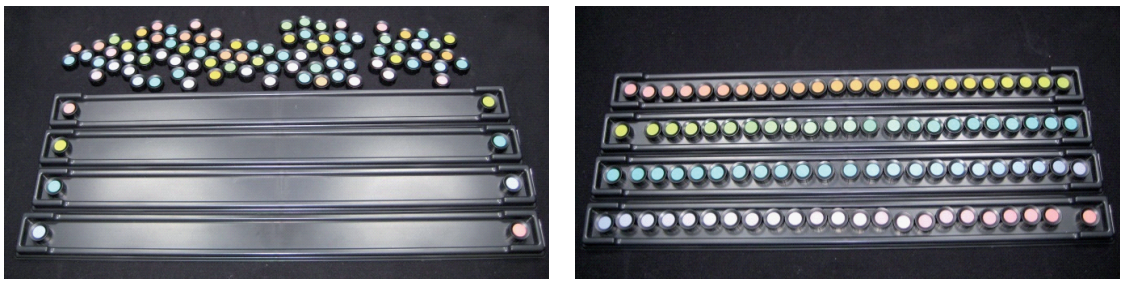

(a) Beginning. (b) Ending.

Figure 4.12: *Farnsworth-Munsell* 100 Hue Test.

At both ends of each bench, the first and the last colored cap with a specific hue is fixed in its position. The remaining 85 colored caps are not fixed and should be ordered according to their hue. This ordering task is solved without any mistakes or with few mistakes by subjects without any defects in color vision. In contrast, observers with a red-green or yellow-blue deficiency make systematic mistakes [241].

4.3 Standard Conditions and Technical Realization

The expression standard condition refers to the illumination and viewing conditions standardized by the International Commission on Illumination (CIE) as described in the technical report CIE $TC1$-65 [120] written by the Technical Committee $TC1$-65. These standard conditions are ideal concepts causing problems in their technical realization. In real applications, the characteristics of a standard illuminant (section 4.3.2) and a standard observer (section 4.3.1) are attempted to be realized as good as possible.

4.3.1 Light Source According to a Standard Illuminant

A standard illuminant is not a light source [219]. A light source is a real existing object emitting naturally or artificially generated electromagnetic radiation in the visible range. In contrast to that, a standard illuminant is a sequence of numbers representing the spectral power distribution of a light source. The spectral power distribution of a light source illuminating an arbitrary object has an influence in the perceived color.

A variety of standard illuminants was specified by the CIE [120]. Each standard illuminant is named with a capital letter and an optional number. Besides others, the collection includes standard illuminants for incandescent light and daylight.

The standard illuminant A represents the spectral power distribution of an incandescent lamp with a correlated color temperature (CCT) of 2856 K [219]. Technically, the standard illuminant is realized with a tungsten lamp in a system stabilized against temporal variations in the operation conditions. Due to the technical feasibility, simple optical instruments as those often used in printing industry work with standard illuminant A.

Another example for a technically realizable standard illuminant is the standard illuminant C [219]. The light emitted by a stabilized tungsten lamp is just led through a special filter. The filter manipulates the spectral power distribution towards the spectral power distribution of daylight with a CCT of 6750 K. Due to the nature of incandescent light, filtered incandescent light has no ultra violet (UV) component. Thus, the standard illuminant C represents an approximated daylight without UV component. The absence of UV radiation has no influence as long as non-fluorescent objects are considered. For objects containing optical brightening agents such as paper [142, 143], standard illuminant C is not the best choice.

The standard illuminants of the D series are suitable for optically brightened objects like paper [219]. Due to their use in printing and paper industry, the standard illuminants $D50$ and $D65$ are well-known representatives in the D series [21, 26]. In this notation, the letter D stands for daylight. The following number specifies the CCT in a hundredth $Kelvin$ (K). Thus, the standard illuminant $D50$ represents the spectral power distribution of a neutral white daylight with a CCT of 5000 K. The spectral power distribution of an average, bluish daylight with a CCT of 6500 K is represented by the standard illuminant $D65$. The slightly bluish coloring of standard illuminant $D65$ compared to the neutral white of standard illuminant $D50$ becomes clear in a comparison of the spectral power distributions. The spectral power distributions for all mentioned standard illuminants are shown in figure 4.13 [252].

The suitability of a standard illuminant for a specific application depends on the usage purpose of the considered object. For example, think on the application purposes of theater chairs compared to those of garden chairs. Normally, theater chairs stand indoors in closed rooms illuminated with incandescent lamps. Thus, standard illuminant A is the best choice for seat cushions of theater chairs. For seat covers for garden chairs, a standard daylight illuminant of the D series is more suitable. Usually, garden chairs are used outdoors in the open air illuminated by natural sunlight.

4.3.2 Visual Angle According to a Standard Observer

Remember that a standard illuminant is not a light source [219]. For a standard observer, this is valid in a similar way. Thus, a standard observer is not a human observer. A standard observer represents the spectral sensitivity functions of an average human observer. The spectral sensitivity

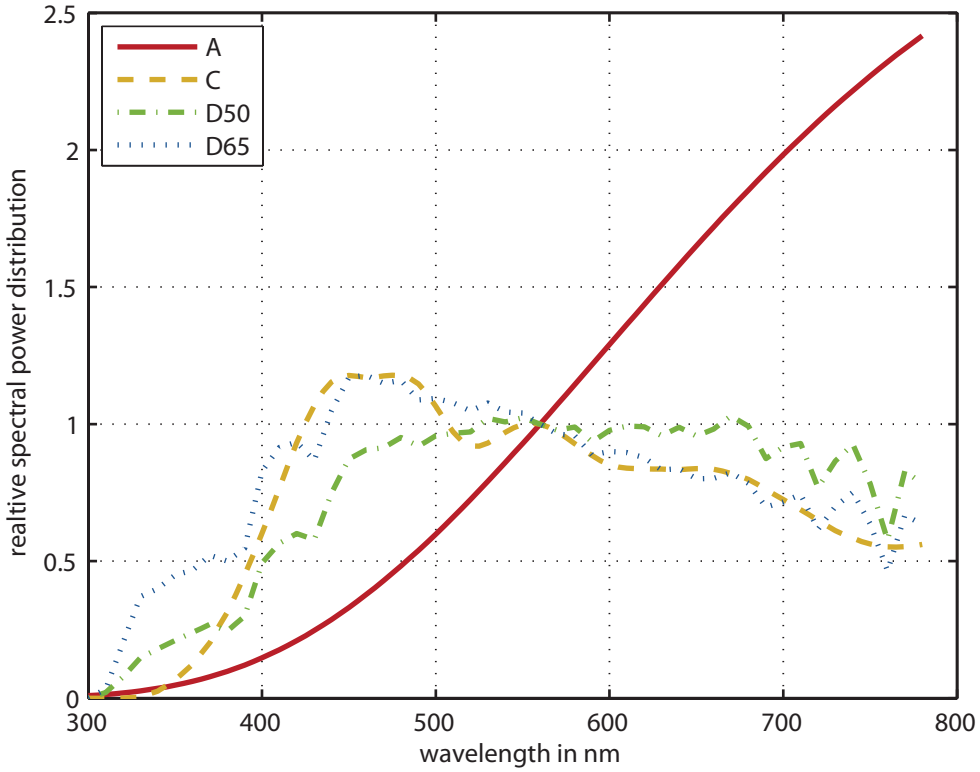

Figure 4.13: Spectral power distribution of standard illuminant A, C, $D50$ and $D65$ [252].

functions serve as spectral weighting factors for the light sensitivity of the three different cone types in the human eye. The three different types of cones are particularly sensitive in the range of short, medium or long wavelengths. Due to the spatially non-uniform distribution of the different cone types on the retina, the spectral sensitivity functions of the human eye depend on the visual angle [21, 26].

The *CIE* [120] specified two standard observers for visual angles of 2° and 10°. The spectral sensitivity functions of the 2° and 10° standard observer are shown in figure 4.14 [252].

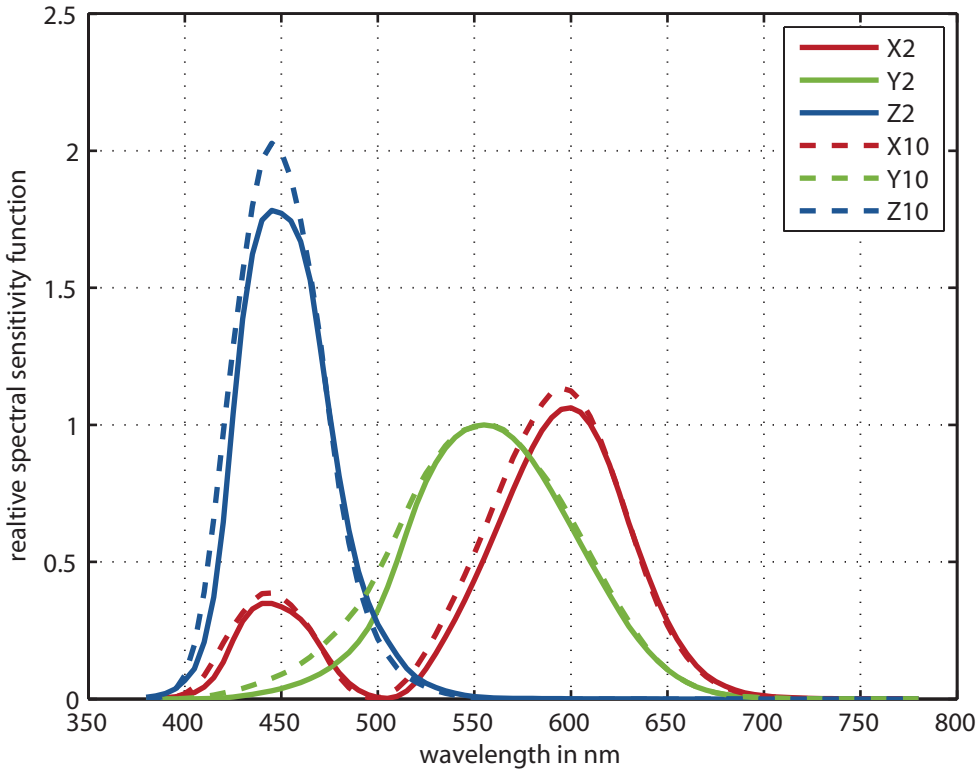

Figure 4.14: Spectral sensitivity functions of 2° and 10° standard observer [252].

The decision on the preference of the 2° or the 10° standard observer depends on the visual angle. The visual angle corresponds to the angular extend of an object seen from a specific distance as shown in figure 4.15.

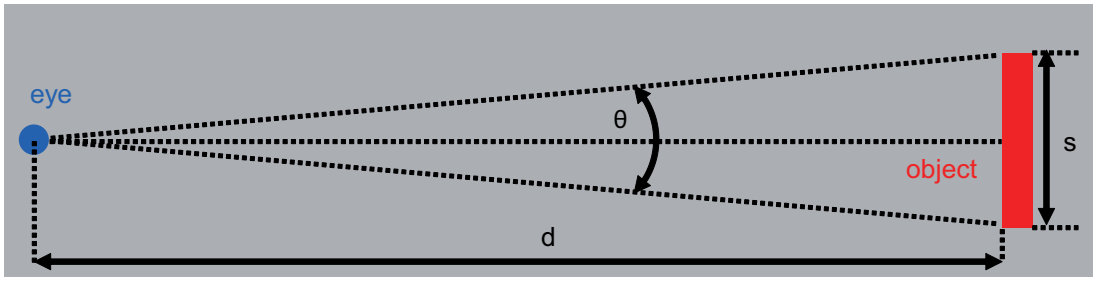

Figure 4.15: Visual angle.

The visual angle is labeled with the symbol θ. The letters s and d mark the object size and

the viewing distance, respectively. The mathematical relation between visual angle, object size and viewing distance is given in equation 4.25.

$$\tan\left(\frac{\theta}{2}\right) = \frac{s}{2 \cdot d} \tag{4.25}$$

Equation 4.25 permits an estimate of the viewing angle in an arbitrary application. Imagine a colored company logo. One time, it is pictured very small in the advertising of a newspaper. Another time, it is presented very big on a poster at the wall. For the small logo of about 14 mm in the newspaper regarded from a distance of about 40 cm, the viewing angle approximately measures 2°. A viewing angle of approximately 10° results for the big logo of about 70 cm on the poster seen from a distance of about 4 m. Thus, the present situation decides on the suitability of the 2° or the 10° standard observer.

4.4 Psychophysical Experiments

Visual experiments are a type of psychophysical experiments focusing on the visual component of the entire appearance. Such as chemistry, biology and other sciences, psychophysics focuses on the building and organizing of knowledge.

As the denomination indicates, the knowledge in psychophysics concerns the relation between psychological perceptions and physical parameters. This section gives some information about psychophysical experiments in general and about visual experiments in particular. For this purpose, the different *experiment categories* (section 4.4.1) differentiated first. For each experiment category, the most important *experimental methods* and *procedures* (section 4.4.2) are then introduced.

4.4.1 Experiment Categories

According to the standard practice *ASTM D* 2616-96 [2] and the book of *Fairchild* [76], psychophysical experiments can be sorted in two classes. The class of *threshold* and *matching experiments* is distinguished from the class of *scaling experiments*.

Threshold and Matching Experiments

In threshold and matching experiments described in the standard practice *ASTM D* 2616-96 [2] and the book of *Fairchild* [76], the relation between perceived magnitudes and physical measures is indirectly investigated on the basis of thresholds and matches, respectively. While a match indicates the perceptual equality of two stimuli, a threshold indicates their inequality. Apart from this difference, threshold and matching experiments are treated together.

In threshold and matching experiments, different types of thresholds are investigated by the use of different styles of presentation. The different *threshold types* and the different *presentation styles* are presented in the following.

Threshold Types The term threshold describes the detectability of a stimulus or a stimulus difference. Depending on the existence of a reference stimulus, two types of thresholds are distinguished. The *absolute* or *detection thresholds* as well as the *relative* or *difference thresholds* are mentioned in the book of *Engeldrum* [72] and presented in the following.

Absolute Thresholds or Detection Thresholds In contrast to relative thresholds, absolute thresholds are determined without the use of another stimulus as reference [72]. Absolute thresholds are also called detection thresholds. Detection thresholds are just perceptible stimuli.

Absolute or detection thresholds can be determined by the use of threshold and matching methods and procedures. Amongst others, these are the method of adjustment, the method of constant stimuli and the staircase procedure.

Relative Thresholds or Difference Thresholds In the case of using a reference stimulus for the determination, the threshold is assigned to be relative [72]. Relative thresholds are also called difference thresholds. Difference thresholds are just perceptibly different stimuli.

Multiple threshold and matching methods and procedures are available to determine relative or difference thresholds. For example, these are the method of adjustment, method of constant stimuli, the staircase procedure and several others.

Presentation Style Depending on the presentation of the evaluated stimuli, threshold and matching experiments can be conducted as a simultaneous or successive experiment as mentioned in the book of *Engeldrum* [72]. The following sections describe the characteristics of *simultaneous* and *successive presentation*.

Simultaneous Presentation As the designation suggests, the evaluated stimuli are presented at the same time in simultaneous threshold and matching experiments [72]. The simultaneous presentation is difficult to realize for some senses of our perception, such as the senses to hear, smell and taste. For the senses to feel and see, the realization of simultaneous threshold and matching experiments is easy.

In color science, simultaneous matching is common practice [190]. The simultaneous view of preferably two stimuli can be realized in two different ways. Either, both eyes look at both stimuli positioned in the total visual field. Or, each eye looks at one stimulus in separated fields of view.

Successive Presentation In contrast to the simultaneous presentation, all senses of our perception can be addressed in successive threshold and matching experiments [72]. The evaluated stimuli are presented one after the other.

Scaling Experiments

In contrast to threshold and matching experiments, scaling experiments directly connect the perceived relation between stimuli and the respective physical relations as described in the standard practice *ASTM E* 1808-96 [2] and the book of *Fairchild* [76]. For a set of stimuli with given physical measures, the perceived magnitudes are established in the scaling experiment.

The perceived magnitude of a stimulus is described on a scale. A scale specifies the arrangement of elements of a stimuli set according to evaluated appearance attributes. With respect to their mathematical utility, four different kinds of scales are defined in the standard practice *ASTM E* 1808-96 [2] and in the books of *Engeldrum* [72], *Fairchild* [76] and *Kuehni* [159]. These are *nominal*, *ordinal*, *interval* and *ratio scales*.

Categorical Scales In statistics, the term categorical data is used for data whose values are related to categories. Thus, categorical scales are scales with values belonging to categories. The categories might or might not stand in ordered relations. *Nominal* and *ordinal scales* are included in the class of *categorical scales*.

Nominal Scales Nominal scales are a type of categorical scales. Nominal scales are the simplest type of scales. All scales with names for the attributes of elements are called nominal scales [2, 72, 76, 159]. Thus, names are used to sort elements with the respective attributes in categories. In a corresponding scaling task, the subjects are asked to name the attributes of the elements or to decide about their belonging to a category with a given name.

Typical examples for nominal scales are the female or male gender and the blood groups A, B, AB or zero. The color of hair can be sorted to categories with the names blond, brown, black and red. The sorting of colors according to their hue in categories named red, orange, yellow, green, cyan, blue or violet is another example for a nominal scale.

Ordinal Scales The other type of categorical scales is called ordinal scales. Upon nominal scales, ordinal scales are the next less simple type of scales. By definition, an ordinal scale is a nominal scale with rankings of the relations of attributes [2, 72, 76, 159]. The categories do not only bear characteristic names. They do also stay in an ordered relation with other categories. The corresponding scaling task is a kind of sorting on the basis of logical operations. The subjects are asked to arrange specimen with increasing or decreasing amounts of the considered attribute.

For ordinal scales, multiple examples are possible. In marketing research, a service might be judged as excellent, very good, good, fair or poor. In attitudinal measurement, an acceptance can be expressed by strongly agree, agree, neither agree nor disagree, disagree, strongly disagree. Such ordinal scales expressing the personal attitude are also called rank scale or *Likert* scale [212]. Furthermore, school grades or quality classes range from good to bad. A color can be more or less chromatic or light.

Cardinal Scales In the mathematical context, cardinal numbers are a generalization of natural numbers. A cardinal number is used to describe the number of elements in a set but not their order. Cardinal scales are based on cardinal numbers. The class of *cardinal scales* includes *interval* and *ratio scales*.

Interval Scales Interval scales are a special type of cardinal scale. Interval scales are more complex than ordinal scales. Ordinal scales with equal intervals between attributes are called interval scales [2, 72, 76, 159]. The ordered relations between the elements are defined by relative distances. In the corresponding scaling task, the subject is asked to arrange specimen in consideration of their mutual distances.

Typical examples for interval scales are the calendar time and the geographic altitude. For both scales, the zero point is set arbitrarily. The birth of *Jesus Christ* and the sea level are not naturally given. Negative calendar times and geographical altitudes are possible. Further examples are the *Celsius* temperature and the *Fahrenheit* temperature. In contrast to the *Kelvin* temperature, both temperature scales have an arbitrary zero point and take negative values.

Ratio Scales The other type of cardinal scales are the so-called ratio scales. Ratio scales are the most complex type of scales. An interval scale with founded zero point is defined as ratio scale [2, 72, 76, 159]. The corresponding scaling task is a sorting task according to the absolute magnitude of the considered attribute. The subject is asked to arrange the specimen relative to the naturally given zero point.

In contrast to the previously mentioned *Celsius* temperature and *Fahrenheit* temperature, the *Kelvin* temperature has a naturally given zero point. Therefore, the *Kelvin* temperature is a good example for a ratio scale. Further examples are mass and length.

4.4.2 Experimental Methods and Procedures

Remember the distinction of threshold and matching experiments from scaling experiments. In *threshold* and *matching experiments*, perceived magnitudes are indirectly connected with physical measures. A direct connection of perceived magnitudes and physical measures is realized in *scaling experiments*. The respective experimental methods and procedures are presented in the following sections.

Threshold and Matching Methods and Procedures

As introduced in section 4.4.1 and described in the standard practice *ASTM E* 1808-96 [2] and in the book of *Fairchild* [76], threshold and matching experiments are based on the determination of thresholds and matches, respectively. Thresholds and matches are determined by the use of the most suitable amongst several existing methods and procedures. The *method of adjustment*, the *method of limits*, the *method of constant stimuli*, the *staircase procedure* and the procedures of *symmetric* and *asymmetric matching* are presented in the following.

Method of Adjustment or Method of Average Error The method of adjustment is explained in the standard practice *ASTM E* 1808-96 [2], the book chapter of *Ehrenstein* and *Ehrenstein* [70] and in the books of *Engeldrum* [72], *Fairchild* [76] and *Kuehni* [159]. It is a simple threshold method in the class of threshold and matching methods and procedures. The subject is asked to adjust the magnitude of the test stimulus until it is just perceivable or until it is just perceived to differ from a presented reference stimulus.

The task begins with a test stimulus considerably differing from the just perceivable stimulus or the reference stimulus. The subject varies the magnitude of the test stimulus until its acceptance. The subject accepts the adjustment when the test stimulus is just perceived or when both stimuli are just perceived to be different. The result is recorded as an absolute threshold or as a difference threshold between the test and reference stimulus.

The described action is repeated multiple times to obtain a representative mean deviation as sensitivity measure. Due to the multiple repetitions, the method of adjustment is also called method of average error.

Method of Limits or Method of Minimal Change The method of limits is also described in the standard practice *ASTM E* 1808-96 [2], the book chapter of *Ehrenstein* and *Ehrenstein* [70] and in the books of *Engeldrum* [72], *Fairchild* [76] and *Kuehni* [159]. As the method of adjustment, it is a rather simple variant among the threshold and matching methods and procedures. The method of limits is also called method of minimal change. Two types of this method are distinguished. These are namely the ascending and descending type.

In case of the ascending type, the presentation starts with a low surely non-detectable stimulus. The stimulus is gradually increased until the subject reports its detection. An example for the ascending type is the minimum detectable sound amplitude.

Compared to the ascending type, the descending type is conducted in the reverse direction. Beginning with a high certainly perceivable stimulus, the stimulus is decreased until it is not perceived anymore. Think on a visual acuity test with letters decreasing in size as an example.

In practice, the ascending and descending types are conducted in alternating sequences. The thresholds of all ascending and descending sequences are finally averaged. In the ascending and descending case, the threshold is equal to the level of the stimulus property at which the stimuli are just detected. The simplicity in the determination is a great advantage of this method.

The disadvantage of the ascending and descending type is the possible expectation or habituation of the subjects on the presented stimuli. The subject may predict the beginning or ending of the stimulus detection. In contrast, the subject may miss the beginning or ending of the stimulus. The resulting errors are called expectation and habituation error, respectively.

Expectation and habituation errors can be avoided by the use of the so-called staircase procedure. Apart from an alternation of ascending and descending sequences, the staircase procedure works with adapted starting stimuli approaching each other in the following sequences. Due to the approaching stimuli, the determined thresholds are quite precise. In one of the following sections, the staircase procedure is explained in more detail.

Method of Constant Stimuli Remember the method of limits and its disadvantage of expectation and habituation. The stimuli are presented in alternating ascending and descending sequences. A random stimuli presentation works around the problem of expectation and habituation. This is the advantage of the so-called method of constant stimuli. It is explained in the standard practice *ASTM E* 1808-96 [2], the book chapter of *Ehrenstein* and *Ehrenstein* [70] and in the books of *Engeldrum* [72], *Fairchild* [76] and *Kuehni* [159].

Previous to the session, several stimuli around the expected threshold are selected. In a random sequence, the selected stimuli are presented to the subject for multiple times. The subject is asked to decide about the perceptibility of the currently presented stimulus. One of the tested stimuli might be detected in about the half of its presentations. The magnitude of the stimulus with 50 % perceptibility is the searched threshold.

In the above explanation, the term stimulus can be replaced by stimulus difference. Furthermore, two or even three stimuli or stimuli differences can be presented simultaneously or successively (section 4.4.1) to the subject. Instead of the perceptibility of the presented stimulus, the subject can be asked for any other kind of forced choice, such as the preference for one stimulus of two presented stimuli.

For example, *Montag* and *Berns* [186, 187], *Montag* and *Wilber* [188] as well as *Fedutina* [79] presented a series of two stimulus pairs to their subjects. They asked them to identify the stimulus pair with the higher stimulus difference between the test and anchor pair.

Staircase Procedure As mentioned above, the staircase procedure originates from the method of limits. The staircase procedure is an alternation of the ascending and descending type of the method of limits with approaching start stimuli in the subsequent sequences. More precisely, the

staircase method works on the following way described in the standard practice *ASTM E* 1808-96 [2], the book chapter of *Ehrenstein* and *Ehrenstein* [70] and in the book of *Fairchild* [76].

In most cases, a staircase procedure starts with an easily detectable stimulus of a high magnitude. The stimulus magnitude decreases stepwise until the subject is not able any more to detect the stimulus. At this point, the magnitude of the stimulus increases step by step until the subject can again detect the stimulus. After several descending and ascending sequences, the values of the reversal point are averaged. On this way, precise thresholds can be determined.

Due to variations in the rules for decision and nomination, there are multiple forms of staircase procedures. Furthermore, the step size between the stimuli and the up-down switch can be adapted. Therefore, the obtained thresholds may vary to a great extent. To avoid variations, the staircase procedure should be designed carefully.

Symmetric Matching Remember the method of adjustment [2, 76] presented above as a pure threshold method. In this case, a pair of perceptually equal stimuli is presented to the subject. The subject is asked to manipulate the test stimulus until it is perceived to differ from the reference stimulus. In contrast to this, a pair of perceptually different stimuli can be presented to the subject. The subject should now modify the test stimulus until it equals to the reference stimulus. This kind of method is a clear matching method as defined in the books of *Fairchild* [76] and *Kuehni* [159].

The more precise designation as symmetric matching [30, 31] illustrates the following. For both stimuli, namely the reference stimulus and the test stimulus, all conditions potentially influencing the perception are equal. In case of a symmetric color matching [87, 170, 242, 251], these conditions include the illumination and observation of the colored object. Thus, the luminance level and spectral power distribution of the light source as well as the lightness and spectral reflectance of the background are identical.

Asymmetric Matching A further pure matching method described in the book of *Fairchild* [76] is the so-called asymmetric matching. In contrast to symmetric matching, not all of the above mentioned conditions are equal for both stimuli. With a specified condition for the reference stimulus, the condition of the test stimulus is systematically varied in asymmetric matching. The method of asymmetric matching is frequently performed in studies on the appearance of color [30, 29, 226, 56].

Apart from these studies on color appearance, *Fleming et al.* [81] studied the perception of surface reflection under different illumination conditions. Their subjects were asked to manipulate the reflectance properties of a test sphere in a test illumination condition until it visually matches a reference sphere in specified illumination conditions.

Scaling Methods and Procedures

According to the introduction in section 4.4.1, standard practice *ASTM E* 1808-96 [2] and the books of *Fairchild* [76] and *Kuehni* [159], perceived magnitudes and physical measures are directly connected in scaling experiments. In practice, the most suitable form of multiple available scaling methods and procedures is applied. In the following, *rank ordering*, *graphical rating*, *category scaling*, *paired comparison*, *magnitude estimation*, *magnitude production*, *ratio estimation* and *ratio production* are presented.

Rank Ordering or Rank-Order Method One of the scaling methods and procedures is the so-called rank ordering. The rank-order method works as explained in the standard practice *ASTM E* 1808-96 [2] and in the books of *Engeldrum* [72] and *Fairchild* [76].

The supervisor of the rank-order experiment presents a set of stimuli to the subject. The subject is asked to order the stimuli with regard to the magnitude of the requested attribute. The resulting sequence of the ordered stimuli represents the ordinal scale (section 4.4.1) of the tested attribute. With additional analysis steps under certain assumptions, an interval scale can be obtained on the basis of rank-order data.

Graphical Rating Among the scaling methods and procedures, the so-called graphical rating is a further type. As explained in the standard practice *ASTM E* 1808-96 [2] and in the books of *Engeldrum* [72] and *Fairchild* [76], this type bases on the following essential finding. For short distances, physical lengths are in linear relation to perceived lengths. Perceived lengths can be associated to perceived magnitudes of an attribute belonging to a stimulus.

The method of graphical rating works in the following way. By the supervisor of the experiment, the stimulus is presented to the subject. The subject associates the perceived magnitude of the tested attribute with the length of a distance on a scale with a specified zero and end point as anchors. The perceived length is marked as a position on the scale. The supervisor measures the physical length of the marker position. On this way, the interval scale of the considered attribute is directly determined.

In their study on the appearance of texture, *Rao* and *Lohse* [212] applied the method of graphical rating. Apart from tasks for naming and sorting, the subjects were asked to rate *Brodatz* textures [38, 166, 167, 174]. The well-known *Brodatz* texture database [193, 195, 194, 210] includes 111 different textures. A subset of 56 *Brodatz* textures [225, 232, 248, 253, 254] was rated in twelve texture attributes on a nine point *Likert* scale (section 4.4.1) [212].

Category Scaling A further scaling method is the so-called category scaling. It is described in the standard practice *ASTM D* 2616-96 [2], in the book chapter of *Ehrenstein* and *Ehrenstein* [70] and in the books of *Fairchild* [76] and *Kuehni* [159]. An experiment according to the method of category scaling is conducted in the following way.

A set of multiple stimuli differing in the magnitude of the considered attribute is presented to several subjects. All subjects are asked to assign each stimulus to the best matching category among some offered ones. For each stimulus, the number of assignments per category is counted over all subjects. The determined relation between the stimuli and categories results in an ordinal and interval scale (section 4.4.1) of the attribute.

Paired Comparison Furthermore, the scaling of an attribute can be realized by means of the method of paired comparison. This method is described in the standard practice *ASTM D* 2616-96 [2] and in the books of *Engeldrum* [72], *Fairchild* [76] and *Kuehni* [159]. In this scaling method, the selected stimuli are presented to multiple subjects for a choice of pairs. For each pair, the subject decides for which stimulus the considered attribute is more or less pronounced. Due to the repeated pairwise comparison of all stimuli, an interval scale of the considered attribute is obtained. The method of paired comparison is frequently applied in the visual appearance research [35, 90, 89, 100, 163, 192, 208, 245, 236].

For example, *Leloup et al.* [163] presented 15 pairs from a set of six achromatic glass samples illuminated with two light sources to the subjects and asked them to rate the glossiness of the right sample relative to the left sample.

Phillips et al. [208] showed a series of two randomly selected high dynamic range (HDR) and low dynamic range (LDR) images of glossy objects and requested for the identification of the object perceived to be glossier.

Furthermore, *Wills et al.* [245] presented several triplets of rendered images of the so-called *Stanford* bunny with different bidirectional reflectance distribution functions ($BRDF$) and asked for the indication of the test image being more similar to the reference image. In spite of the presentation of three images, this is a paired comparison. Only two stimuli are compared simultaneously. The simultaneous comparison of three stimuli is called triadic comparison, triadic combination or method of triads.

Magnitude Estimation The method of magnitude estimation is presented in the standard practice *ASTM E* 1808-96 [2], the book chapter of *Ehrenstein* and *Ehrenstein* [70] and in the books of *Engeldrum* [72], *Fairchild* [76] and *Kuehni* [159]. The labeling of this scaling method clearly describes its characteristic. The subject is asked to estimate the magnitude of an individual stimulus or the magnitude of a stimulus difference on a psychophysical scale. The psychophysical

scale can be the most meaningful ratio scale (section 4.4.1). The statistical method used in the subsequent evaluation depends on the type of the collected data. In case of estimates of individual stimuli, a regression analysis, a correlation analysis (CA), a principal component analysis (PCA) or a factor analysis (FA) are examples for suitable multivariate statistical methods. Multidimensional scaling (MDS) is a suitable multivariate statistical method for the evaluation of estimates of stimulus differences.

For example, *Pellacini et al.* [200] as well as *Ferwerda et al.* [80] applied the method of magnitude estimation in their psychophysical study on gloss appearance. Rendered images of achromatic spheres differing in gloss were estimated in two subsequent visual experiments. In the first experiment, the magnitude of the gloss difference between two spheres was estimated. The determined gloss difference estimates called dissimilarities were processed in MDS. As explained below in section 4.5.4, this multivariate statistical analysis gives information about the dimensionality of the underlying structure. Furthermore, MDS results in a spatial arrangement of the test stimuli called configuration. In the second experiment, individual spheres were estimated in their contrast gloss and distinctness-of-image gloss on ratio scales (section 4.4.1) from zero to 100. The collected individual estimates for both gloss attributes were evaluated in a regression analysis. In a regression analysis described below in section 4.5.4, hypothetical relationships between the perceived magnitude and physical parameters are tested on their validity. The found relationship is called psychophysical scaling function.

Leloup et al. [164] investigated the visual perception of specular gloss for directional and diffuse illumination using the method of magnitude estimation. They asked their subjects to estimate the glossiness of achromatic paint samples on a ratio scale. The zero point is defined as an imaginary sample without any perceived gloss. The perceived gloss of a physical reference presented at the beginning was set to a value of 100 units.

In place of numbers, the magnitude of the presented stimulus or stimulus difference can be estimated by means of another sensory or cognitive dimension. Such magnitude estimation experiments are called cross-modality matching [70]. Another modification of magnitude estimation is magnitude production explained in the following.

Magnitude Production The previously presented scaling method named magnitude estimation and the so-called magnitude production have some properties in common. Both methods work with magnitudes of individual stimuli or stimulus differences on ratio scales (section 4.4.1) of the considered attribute. In contrast to magnitude estimation using existing stimuli, magnitude production implies the generation of stimuli. The method of magnitude production works in the following way described in the standard practice *ASTM E* 1808-96 [2] and in the books of *Fairchild* [76] and *Kuehni* [159].

Previous to several sessions with multiple subjects, the supervisor defines the zero point and a reference point for the searched ratio scale of the considered attribute. In each session, the subject is asked to generate a stimulus or a stimulus difference of a given magnitude. The produced individual magnitudes or magnitude differences are evaluated as the estimated individual magnitudes or magnitude differences in magnitude estimation described above.

Ratio Estimation Remember the method of magnitude estimation explained above. Instead of estimating a magnitude, the subject can be asked to estimate a ratio. In this case, the method is called ratio estimation. It is presented in the standard practice *ASTM E* 1808-96 [2] and in the books of *Engeldrum* [72], *Fairchild* [76] and *Kuehni* [159]. The sessions of a ratio estimation experiment can be realized in two similar ways.

First, at least two of multiple available stimuli are simultaneously presented by the supervisor. The supervisor asks the subject to estimate the ratios among the presented stimuli. Last, multiple test stimuli and one reference stimulus are presented simultaneously to the subject. The subject is asked by the supervisor to select the test stimulus with a specified ratio relative to the reference stimulus.

On the basis of the data collected in multiple sessions with several subjects, a ratio scale

(section 4.4.1) is achieved. Alternative to the method of ratio estimation, a scaling experiment can be performed as ratio production described in the following.

Ratio Production With the relation of magnitude estimation and magnitude production in mind, ratio production is explained on the basis of ratio estimation. Compared to the use of existing stimuli in ratio estimation, stimuli are generated in ratio production. This scaling method is explained in the standard practice *ASTM E* 1808-96 [2] and in the books of *Fairchild* [76] and *Kuehni* [159]

In a ratio production session, the supervisor only presents a reference stimulus and specifies the wanted ratio. The subject generates a test stimulus of the given ratio with respect to the reference stimulus. With several subjects performing multiple sessions, a ratio scale (section 4.4.1) of the considered attribute is finally obtained.

4.5 Statistical Evaluation

For the evaluation of experimental results, various statistical measures and methods are available. In principle, univariate statistics are distinguished from multivariate statistics.

In univariate statistics, one single statistical variable is considered. Thus, any relations to other variables are neglected. In contrast to this, more than one statistical variable is considered in multivariate statistics. Here, potential relations between the variables and their conjoint variations are considered.

Subsequent to the well-known *univariate statistical measures* (section 4.5.1), several popular *multivariate statistical measures* (section 4.5.2) are introduced. Basing on the knowledge about the essential *associated statistical measures and methods* (section 4.5.3), the most important *multivariate statistical methods* (section 4.5.4) are explained.

4.5.1 Univariate Statistical Measures

Basing on the definition of the term univariate statistics, univariate statistical measures are statistical measures evaluated for one individual variable. Univariate measures are easy to handle and well established. The most important univariate statistical measures are the *arithmetic mean*, the *standard deviation* and the *variance* explained in the following.

Arithmetic Mean or Average Value

The arithmetic mean [59] is also called average value. It is an univariate statistical measure describing the central trend in a data set.

Imagine a data set comprising m sampled numbers $x_{i,k}$ of a random variable X_i. According to equation 4.26, the arithmetic mean A is equal to the sum of the sampled numbers divided by the size of the data set.

$$A(X_i) = \frac{1}{m} \sum_{k=1}^{m} x_{i,k} \tag{4.26}$$

In addition to the arithmetic mean, other mean values are known such as the geometric mean or the harmonic mean. Furthermore, the mode or the median might be used instead of the mean. The mode is defined to be the value at the maximum of the probability distribution. The value separating the lower and upper half of the probability distribution is called median.

Standard Deviation

On the basis of the previously introduced arithmetic mean (equation 4.26), the standard deviation [59, 60, 62] extends the characterization of a data set. The standard deviation describes the range of variation around the arithmetic mean. A narrow range of variation is described by a low standard deviation. A high standard deviation indicates a wide range of variation.

Remember the assumed data set composed of m sampled numbers $x_{i,k}$ for the random variable X_i and the arithmetic mean A. In equation 4.27, the standard deviation S is defined as the square root of its variance V.

$$S(X_i) = \sqrt{V(X_i)} = \sqrt{\frac{1}{m-1} \sum_{k=1}^{m} (x_{i,k} - A(X_i))^2} \tag{4.27}$$

Like the standard deviation, the variance is a measure for the variation of the sampled numbers around the arithmetic mean. In the following section, the variance is defined in detail.

Variance

As just mentioned in connection with the standard deviation (equation 4.27), the variance [59, 60, 61, 62] describes the range of variation around the arithmetic mean. Equation 4.28 specifies the calculation of the variance V as the square of the standard deviation S.

$$V(X_i) = (S(X_i))^2 = \frac{1}{m-1} \sum_{k=1}^{m} (x_{i,k} - A(X_i))^2 \tag{4.28}$$

The symbol m specifies the size of the sampled numbers $x_{i,k}$ in the considered data set. The arithmetic mean of the random variable X_i is again indicated with the symbol A.

Keep this definition of the variance in mind. It helps to understand the definitions of covariance and covariance matrix as well as of correlation coefficient and correlation matrix.

4.5.2 Multivariate Statistical Measures

Remember the definition of the term multivariate statistics. Thus, multivariate statistical measures consider more than one statistical variable simultaneously. Compared to univariate statistical measures, multivariate statistical measures are slightly more difficult and less common in use. The *covariance* or *covariance matrix* and the *correlation coefficient* or *correlation matrix* are well-known multivariate statistical measures introduced in the following.

Covariance

The so-called covariance [61] is a bivariate statistical measure included in the class of multivariate statistical measures. The term bivariate indicates the handling of two variables. The covariance C of the variables X_i and X_j with m sampled numbers $x_{i,k}$ and $x_{j,k}$ is defined in equation 4.29.

$$C(X_i, X_j) = S(X_i, X_j) = \frac{1}{m-1} \sum_{k=1}^{m} (x_{i,k} - A(X_i))(x_{j,k} - A(X_j)) \tag{4.29}$$

Set the index j equal to i and remember the definition of the variance of a variable X_i with m sampled numbers $x_{i,k}$ given in equation 4.28. Thus, the covariance for two identical variables is equal to the variance of the considered variable. This fact is revived in the definition of the covariance matrix given in the following section.

Covariance Matrix or Variance-Covariance Matrix

The multivariate covariance matrix S [61] is based on several bivariate covariances C (equation 4.29). Equation 4.30 defines the covariance matrix S for a number of n variables X_i.

$$S(X_1, \ldots, X_i, \ldots, X_n) = \begin{pmatrix} C(X_1, X_1) & \cdots & C(X_1, X_i) & \cdots & C(X_1, X_n) \\ \vdots & \ddots & \vdots & \ddots & \vdots \\ C(X_i, X_1) & \cdots & C(X_i, X_i) & \cdots & C(X_i, X_n) \\ \vdots & \ddots & \vdots & \ddots & \vdots \\ C(X_n, X_1) & \cdots & C(X_n, X_i) & \cdots & C(X_n, X_n) \end{pmatrix} \tag{4.30}$$

Due to the above mentioned connection of variance and covariance, the covariance matrix is also called variance-covariance matrix. The replacement of the bivariate covariances C by the univariate variances V is shown in equation 4.31.

$$S(X_1,\ldots,X_i,\ldots,X_n) = \begin{pmatrix} V(X_1) & \cdots & C(X_1,X_i) & \cdots & C(X_1,X_n) \\ \vdots & \ddots & \vdots & \ddots & \vdots \\ C(X_i,X_1) & \cdots & V(X_i) & \cdots & C(X_i,X_n) \\ \vdots & \ddots & \vdots & \ddots & \vdots \\ C(X_n,X_1) & \cdots & C(X_n,X_i) & \cdots & V(X_n) \end{pmatrix} \tag{4.31}$$

The covariance matrix is a statistical measure used for the determination of further statistical measures as well as for the execution of special statistical analyses. Two common application cases are the following ones.

For example, the covariance matrix is processed by calculating their eigenvalues and eigenvectors. Eigenvalues give information about the number of essential dimensions in a data set. The direction of maximal variations in the data set is given by the eigenvectors.

Another example for the evaluation of a data set using the covariance matrix is the so-called principal component analysis (PCA) [96]. The PCA is explained in section 4.5.4 on multivariate statistical methods.

Correlation Coefficient

The linear correlation coefficient [61] meant here is also called Pearson correlation coefficient. This correlation coefficient describes the strength and the direction of a linear relationship between two variables. Thus, the correlation coefficient is a bivariate statistical measure. For the both variables X_i and X_j, the linear correlation coefficient R is defined in equation 4.32.

$$R(X_i,X_j) = \frac{C(X_i,X_j)}{\sqrt{V(X_i)\,V(X_j)}} \tag{4.32}$$

According to that, the covariance C between both variables is divided by the square root of the product of the two variances V of both variables. By definition, the correlation coefficient is equal to one for two identical variables. For the more meaningful case of two different variables, the correlation coefficient takes values between minus and plus one.

A positive correlation coefficient near plus one indicates a strong correlation in the same direction. A strong correlation in the opposite direction is expressed by a negative correlation coefficient near minus one. A positive or negative correlation coefficient near zero stands for a weak correlation in the same or opposite direction, respectively.

Correlation Matrix

Remember the definition of the covariance matrix on the basis of covariances. In a similar manner, the correlation matrix K [61] is defined on the basis of correlation coefficients R (equation 4.32). In equation 4.33, the correlation matrix K is given for a number of n variables X_i.

$$K(X_1,\ldots,X_i,\ldots,X_n) = \begin{pmatrix} R(X_1,X_1) & \cdots & R(X_1,X_i) & \cdots & R(X_1,X_n) \\ \vdots & \ddots & \vdots & \ddots & \vdots \\ R(X_i,X_1) & \cdots & R(X_i,X_i) & \cdots & R(X_i,X_n) \\ \vdots & \ddots & \vdots & \ddots & \vdots \\ R(X_n,X_1) & \cdots & R(X_n,X_i) & \cdots & R(X_n,X_n) \end{pmatrix} \tag{4.33}$$

As mentioned above, the correlation coefficient for identical variables is equal to one. A simplified version of the correlation matrix is given in equation 4.34.

$$K(X_1,\ldots,X_i,\ldots,X_n)=\begin{pmatrix} 1 & \cdots & R(X_1,X_i) & \cdots & R(X_1,X_n) \\ \vdots & \ddots & \vdots & \ddots & \vdots \\ R(X_i,X_1) & \cdots & 1 & \cdots & R(X_i,X_n) \\ \vdots & \ddots & \vdots & \ddots & \vdots \\ R(X_n,X_1) & \cdots & R(X_n,X_i) & \cdots & 1 \end{pmatrix} \tag{4.34}$$

The application cases of the correlation matrix overlap with those of the covariance matrix. As the covariance matrix, the correlation matrix is used to calculate eigenvalues and eigenvectors or to perform a principal component analysis (PCA) [96].

Apart from the mentioned secondary application cases, the correlation matrix is primarily used in a correlation analysis. The direct processing in a correlation analysis is explained in section 4.5.4 on multivariate statistical methods.

4.5.3 Associated Statistical Measures and Methods

In connection with the above presented statistical measures and the below introduced statistical methods, further knowledge might be required. Therefore, this section gives some information about the *standard score*, the *explained* and *cumulated variance*, the *standardized residual sum of squares*, the *eigenvalue* and *eigenvector* as well as about the *Procrustes analysis*.

Standard Score or Z-Score

The statistical measure standard score is also named z-score. The letter z stands for the so-called z-distribution. The z-distribution is the well-known normal distribution with an arithmetic mean of zero and a standard deviation of one.

The sampled numbers $x_{i,k}$ with an arbitrary distribution can be transformed to standard scores $z_{i,k}$ with a normal distribution. The transformation for the standardization or normalization is given in equation 4.35.

$$z_{i,k}=\frac{x_{i,k}-A(X_i)}{S(X_i)} \tag{4.35}$$

In this transformation, the letter A labels the arithmetic mean of the random variable X_i. The standard deviation of the random variable X_i is labeled with the letter S. Due to the equality of the physical units belonging to arithmetic mean and standard deviation, the standard score is a dimensionless quantity.

Explained and Cumulated Variances

Imagine a set of n variances V given for a total number of n variables X_i and X_j identified by means of the indices i and j. The variables are sorted such that the variances descend from variable X_1 over variable X_i and X_j to variable X_n. Then, the explained variance V_e of variable X_j is equal to its variance V divided by the sum over all n variances V as expressed in equation 4.36.

$$V_e(X_j)=\frac{V(X_j)}{\sum_{i=1}^{n}V(X_i)} \tag{4.36}$$

Thus, the explained variance specifies the variance percentage of the considered variable on the total variance. As the variance, the explained variance decreases with an increasing index. In contrast to the explained variance, the cumulated variance increases with an increasing index. According to equation 4.37, the first j explained variances V_e are summed to get the cumulated variance V_c of variable X_j.

$$V_c(X_j) = \sum_{i=1}^{j} V_e(X_i) \tag{4.37}$$

In other words, the cumulated variance V_c of variable X_j is equal to the sum over the first j variances V divided by the sum over all n variances V. This alternative definition of the cumulated variance V_c of variable X_j is given in equation 4.38.

$$V_c(X_j) = \frac{\sum_{i=1}^{j} V(X_i)}{\sum_{i=1}^{n} V(X_i)} \tag{4.38}$$

Explained and cumulated variances are used in multivariate statistical methods (section 4.5.4), such as the principal component analysis (PCA) explained below. In a PCA, the explained and cumulated variances of the principal components give information about the number of essential principal components.

Standardized Residual Sum of Squares or *KruskalSTRESS*

In general terms, the standardized residual sum of squares ($STRESS$) is a measure for the quality of an arbitrary fitting [151]. In fitting, available data of an unknown structure are used to reproduce the underlying structure. With n available data d_i of the unknown structure and the associated fitted data δ_i of the reproduced structure, the $STRESS$ can be determined according to equation 4.39.

$$S = \frac{1}{c}\sqrt{\sum_{i=1}^{n} (\delta_i - d_i)^2} \tag{4.39}$$

The symbol c stands for a normalization constant, such as the square root of the sum of squares of the original data d_i. Due to the scaling constant, the $STRESS$ ranges from zero to one. A low $STRESS$ near zero indicates a good fit, while a bad fit is indicated by a high $STRESS$ near one.

A special form of the $STRESS$ is used in multidimensional scaling (MDS). MDS is one of the multivariate statistical methods (section 4.5.4) presented below. Equation 4.40 specifies the so-called $Kruskal\ STRESS$ [158] used in MDS.

$$S = \sqrt{\frac{\sum_{i=1}^{n}\sum_{j>i}^{n} (\delta_{i,j} - d_{i,j})^2}{\sum_{i=1}^{n}\sum_{j>i}^{n} d_{i,j}^2}} \tag{4.40}$$

In MDS (section 4.5.4), pairwise dissimilarities $d_{i,j}$ between the objects i and j are used to reproduce the so-called configuration of all n considered objects in space. In the reproduced spatial arrangement, the objects i and j are located in approximately correct distances $\delta_{i,j}$ to each other. The square root of the sum of squares of the original data $d_{i,j}$ is the scaling constant.

Eigenvalue and Eigenvector

Sometimes, the terms characteristic values and characteristic vectors are used instead of the terms eigenvalue and eigenvector, respectively. In psychophysics, eigenvalues and eigenvectors are used to characterize data sets in the following way.

Remember the covariance matrix and the correlation matrix introduced in section 4.5.2 on multivariate statistical measures. As announced above, the covariance matrix and the correlation matrix are used to calculate their eigenvalues and eigenvectors.

At this point, the calculation and interpretation of eigenvalues and eigenvectors is explained for an arbitrary square matrix. The considered n-by-n matrix A maximally has a number of n different non-zero eigenvalues and eigenvectors. All eigenvalues λ and eigenvector x should fulfill equation 4.41.

$$A \cdot x = \lambda \cdot x \tag{4.41}$$

For the calculation of eigenvalues and eigenvector, this equation is converted in a mathematically equivalent notation and supplemented by the n-by-n unit matrix E. The resulting equation 4.42 is called characteristic equation.

$$(A - \lambda \cdot E) \cdot x = 0 \tag{4.42}$$

All possible solutions of the characteristic equation can be found by solving the characteristic polynomial. The characteristic polynomial is given in equation 4.43.

$$det\,(A - \lambda \cdot E) = 0 \tag{4.43}$$

As mentioned above, a number of at most n different non-zero eigenvalues λ_i is obtained for an n-by-n square matrix A. The associated eigenvectors x_i are determined using equation 4.44.

$$(A - \lambda_i \cdot E) \cdot x_i = 0 \tag{4.44}$$

For the interpretation of the obtained eigenvalues and eigenvectors, the following facts should be known. An eigenvalue is a scalar quantity acting as scaling factor. Therefore, the eigenvalue carries information about the relative importance of the associated eigenvector. The product of the considered matrix and the eigenvector is parallel to the eigenvector itself. Thus, the eigenvector gives information about important preferential directions in the considered data set.

To come back to psychophysics, the information of eigenvalues and eigenvectors are used in the dimension reduction of an exploratory factor analysis (EFA) and in the scores determination in a principal component analysis (PCA). The eigenvalues and eigenvectors of the covariance matrix and the correlation matrix give information about the number of essential dimensions and the direction of maximal variations.

Procrustes Analysis

The *Procrustes* analysis is mainly used in connection with other multivariate statistical methods such as multidimensional scaling (MDS). As explained below, the configuration obtained in MDS is invariant against translation, scaling and rotation. Imagine two configurations generated in MDS. In principle, both configurations are similar. But, due to their different position, orientation and expansion, a direct comparison is difficult. This problem can be solved by means of a *Procrustes* analysis.

A *Procrustes* analysis generates a transform for one set of points to make it more comparable to another set of points named target matrix X. The set of points intended to be transformed is called reference matrix Y. The transformed matrix Z is received according to equation 4.45.

$$Z = t + s \cdot Y \cdot r \tag{4.45}$$

The transformation is described by three matrices. These are the translation matrix t, the scaling matrix s and the rotation matrix r. The spatial differences between the transformed matrix Z and the target matrix X are minimized during the *Procrustes* analysis using the least squares criterion.

4.5.4 Multivariate Statistical Methods

Basing on the previously generated knowledge about multivariate statistical measures, some multivariate statistical methods are introduced in the following. According to *Kohn* [156], asymmetric methods are distinguished from symmetric methods. In accordance with their purpose, they are rather called *confirmatory* or *hypothesis-testing methods* and *exploratory* or *structure-finding methods*, respectively.

Confirmatory Methods or Hypothesis-Testing Methods

The so-called confirmatory or hypothesis-testing methods are suitable when there is already some knowledge about the relations between variables [156]. An assumed hypothesis is proposed at the beginning and finally verified or falsified with the available data. Thus, a confirmatory data analysis has the objectives to test the validity of the proposed hypothesis and to estimate the confidence in the obtained result. The *regression analysis* and the *analysis of variance* are subsequently presented.

Regression Analysis The regression analysis is a confirmatory statistical method for testing hypotheses about relations between variables [156]. More precisely, suspected relations between a dependent variable and one or more independent variables are checked during a regression analysis.

A complete regression analysis includes the following steps. First, an arbitrary model is assumed to represent the relationship between the variables. The parameters of the selected model are then estimated from the available data. This main process step of fitting the model to the data of the variables is called regression. Finally, the quality of the presumed model is determined by means of specific tests.

Imagine an arbitrary model represented by the symbol f basing on model parameters labeled with the character a. The model parameters are also called regression coefficients. The dependent variable Y is a function of one or more independent variables X as expressed in equation 4.46.

$$Y = f\,(a, X) \tag{4.46}$$

The number of independent variables influences the complexity of the regression analysis. In the case of only one independent variable, the element X is simply a scalar and the regression analysis is reduced to a bivariate statistical method. For more than one independent variable, the element X is a vector and the regression analysis is a real multivariate statistical method.

In their study on the perception-based characterization of specular gloss, *Leloup et al.* [164] carried out a linear and a non-linear regression analysis with least-square fitting. The independent variables are the measured luminances of the reflected image and the sample background. The perceived surface gloss determined in a psychophysical experiment is the independent variable. Four regression models expected to be suitable were fitted to the data. An adjusted coefficient of determination was used to evaluate the quality of each regression model. The best-fitting regression model is the psychophysical function for specular gloss.

Analysis of Variance The term analysis of variance names a collection of confirmatory hypothesis-testing multivariate statistical methods [156]. All versions of the analysis of variance have in common that variances and other related test qualities are determined. These test qualities including variances give information about regularities in the considered data set. The complete variance in a dependent variable is divided in variance components originating from variations in different independent variables.

A simple type of the analysis of variance is just a statistical hypothesis test. Such a test is a statistical method to make a decision about the validity of an assumed hypothesis using available data. In case of the analysis of variance, the statistical test proves or disproves the hypothesis about the equality or inequality of the means belonging to two or more data groups. The hypothesis about the equality of all means is called null hypothesis. In other words, the null hypothesis says that all data groups are random samples of the same population. The opposite of the null hypothesis is named alternative hypothesis. Thus, the alternative hypothesis stands for at least one deviating mean or at least one non-random group.

Exploratory Methods or Structure-Finding Methods

Exploratory or also structure-finding methods are appropriate when there is no or few knowledge about the relations between variables [156]. A general structure is assembled or extracted from the present data and visualized in an appropriate diagram. In more detail, an exploratory data

analysis has the following objectives. A basis for an extended collection of data is prepared. The choice of suitable methods for further evaluations is assisted. A structure for subsequent steps in the evaluation is provided. Hypotheses about relations between variables are established. In the following, the *correlation analysis* (CA), the *multidimensional scaling* (MDS), the *principal component analysis* (PCA) and the *factor analysis* (FA) are introduced.

Correlation Analysis A well-known multivariate statistical method is the correlation analysis (CA). The term correlation describes the linear relationship between two variables. The presence, direction and intensity of a relationship are examined in a CA using correlation coefficients and correlation matrices introduced in section 4.5.2 and section 4.5.2, respectively. Due to the dealing with relationships, the structure-finding CA is related to the hypothesis-testing regression analysis introduced above.

CAs are frequently applied in psychophysical studies. Some examples in this context are the studies of *Rao* and *Lohse* [212], *Long* and *Leow* [167], *Wills et al.* [245] as well as of *Leloup et al.* [163].

The study of *Rao* and *Lohse* [212] focuses on the perception-based naming of textures. They carried out sorting and rating experiments. The sorting and rating data were processed in multidimensional scaling (MDS) explained next and in a CA. The result of the MDS and the CA is a three-dimensional space with coordinate axes correlated to texture attributes.

Long and *Leow* [167] took up the study of *Rao* and *Lohse*. They also generated a perceptual texture space and compared it to that of *Rao* and *Lohse* using a CA.

Wills et al. [245] carried out a study on the spatial representation of the perceived gloss. The appearance of gloss was also studied by *Leloup et al.* [163].

Multidimensional Scaling The so-called multidimensional scaling (MDS) is also a structure-finding method. It is explained in the books of *Engeldrum* [72], *Fairchild* [76] and *Kuehni* [159] as well as in the papers of *Jaworska* [131], *Kruskal* [158] and of *Venna* and *Kaski* [240]. In more detail, MDS is used to transfer known differences between objects in a spatial arrangement of points.

The input data for MDS are dissimilarities or perhaps similarities between stimuli. As output, MDS provides the so-called configuration and gives information about the dimensionality of the considered space.

The configuration is a geometric representation of the stimuli as points in a low-dimensional space. This low-dimensional representation provides a clearer insight in the underlying structure of relations [240]. The configuration is invariant against translation, rotation as well as scaling.

The quality of the configuration is described by a quality measure called standardized residual sum of squares ($STRESS$) [151, 158, 240]. The $STRESS$ is defined as the sum of remaining deviations over all stimuli pairs relative to the sum of input dissimilarities over all stimuli pairs (section 4.5.3, equation 4.39, equation 4.40). The remaining deviations are determined on the basis of a distance metric using the input dissimilarities and the resulting differences between the fitted points. The input dissimilarities and the resulting differences between the fitted points are intended to be equal. Thus, MDS is an optimization problem of the $STRESS$.

The $STRESS$ plotted versus the number of dimensions called scree plot is used to determine the dimensionality of the considered space. A significant improvement by adding a dimension is indicated by a sharp decline of the $STRESS$ between both dimensions. In contrast to that, a flat decline indicates an insignificant improvement. The number of dimensions at the transition from a significant to an insignificant improvement indicates the number of essential dimensions. Thus, the dimensionality of the underlying space is indicated by an inflection point in the scree plot. In psychophysic problems, the scree plot often has more than one inflection point and not that explicit inflection points. Due to the purely subjective judgment of the true inflection point, *Kruskal* [158] once named levels indicating excellence and tolerance. A $STRESS$ below 0.1 and 0.15 is excellent or tolerable, respectively.

The term MDS does not directly designate the multivariate statistical method. Several types of MDS are in use. These types are distinguished according to different classification criteria like the input data or the dissimilarity matrix and the distance model. The classification according to the input data results in a separation of metric MDS ($MMDS$) and non-metric MDS ($NMMDS$) [76]. The dissimilarity matrix and the distance model as classification criteria result in the distinction of classical MDS ($CMDS$), replicated MDS ($RMDS$), weighted MDS ($WMDS$) and generalized MDS ($GMDS$). In case of $CMDS$, one symmetric dissimilarity matrix is processed using the *Euclidean* distance metric.

MDS was applied in several psychophysical studies on visual appearance [80, 92, 167, 200, 212, 245]. *Pellacini et al.* [200], *Ferwerda et al.* [80] and *Wills et al.* [245] studied the visual appearance of gloss. *Rao* and *Lohse* [212], *Gurnsey* and *Fleet* [92] as well as *Long* and *Leow* [167] carried out studies on the perception of texture.

Principal Component Analysis The principal component analysis (PCA) is also a structure-finding method [55, 96, 231, 240, 246]. In multivariate statistics, the visualization of statistical data characterized by multiple variables is difficult. For more than three variables, there is a problem to visualize relationships between the variables in two- or three-dimensional plots. Due to the grouping of variables in high-dimensional data sets, it is possible to reduce the number of variables. Several original variables can be replaced with a single new variable.

The PCA searches for new variables with an enhanced force of expression. The new variables are based on a linear combination of the original variables. The linear combination accounts for most of the variations in the original variables. The new variables are called principal components. The principal components are an orthogonal basis for the data set. Due to the orthogonality of the principal components, there is no redundant information.

The total number of principal components is at most equal to the number of original variables. However, the first few principal components mostly characterize the original data. This becomes clear in the decrease and increase of the explained and cumulated variances (section 4.5.3, equation 4.38, equation 4.38), respectively. The very first principal component represented by an axis in space has the highest explained and lowest cumulated variance in the whole data set. For the second principal component, the explained variance is the highest among all axes being perpendicular to the first axis. The succeeding principal components have the highest explained variance possible on the condition that the considered principal component is orthogonal to all previous principal components.

In the following, the basic procedure of a PCA is explained. The procedure includes the standardization of the input data matrix, the determination of the covariance or correlation matrix, the calculation of eigenvalues and eigenvectors and the evaluation of the component coefficients and component scores.

The input data are present in the form of an m-by-n data matrix with m observations for n variables. The m-by-n data matrix is standardized using standard scores (section 4.5.3, equation 4.35).

The standardized data matrix is processed in the determination of the covariance (equation 4.31) or correlation (equation 4.34) matrix. The covariance matrix should be preferred for small differences between the variances of different variables [96]. For high differences between the variances of the different variables, the correlation matrix is more suitable.

As explained in section 4.5.2, the n-by-n covariance or correlation matrix is processed in the calculation of at most n eigenvalues (equation 4.43) and the associated eigenvectors (equation 4.44). The eigenvalues are used to decide about the number of essential principal components. The first i principal components are assumed to be sufficient to represent the data set.

The searched component coefficients are equal to the first i eigenvectors. The component coefficients specify the orientation of the principal component axes. The new variables are represented by the component coefficients. The component coefficients are further needed to calculate the composition scores. The composition scores matrix is equal to the product of the standardized data matrix and the n-by-i component coefficients matrix. Thus, the m-by-i composition scores

matrix contains m transformed observations for a number of i new variables. The component coefficients and composition scores are the output data of a PCA.

Subsequent to the PCA, one might continue with a rotation of the principal components. In principle, the orthogonal rotation is preferred over the oblique rotation. In contrast to the oblique rotation, the principal components remain uncorrelated during the orthogonal rotation. The reason of the orthogonal rotation (OR) lies in the enhanced interpretability of the underlying factors. By means of the OR, the absolute values of the component coefficients are maximized. For rotated principal components with few and high component coefficients, the identification or assignment of influencing factors is much easier. The successive application of a PCA and an OR is a special type of an exploratory factor analysis (EFA) explained below.

In their study on a perception-based space for texture, *Rao* and *Lohse* [212] applied a PCA on scale ratings of twelve texture attributes. In the PCA, they found out that none of the twelve texture attributes is superfluous. All twelve texture attributes are of a comparable importance. They are included in the principal components subsequently processed in a factor analysis.

Factor Analysis The so-called factor analysis (FA) described in the books of *Handl* [96], $Jolliffe$ [134] and *Tabachnick* and *Fidell* [231] originates from psychophysics. In addition to psychophysics, the FA is applied in any sciences dealing with large quantities of data. By means of a FA, a large set of multivariate data is fitted to a simple model representing the underlying structure.

Apart from a special version, the FA is a structure-finding method. For a clear differentiation from the confirmatory FA (CFA), the nomination as exploratory FA (EFA) is used in the following.

In an EFA, the variations in multiple observed variables are lead back to variations in a few unobserved variables. In other words, it is assumed that the observed variables depend on a smaller number of unobserved variables. The unobserved variables are not directly recognizable and therefore called latent factors. Due to their mutual influence on multiple variables they are also known as common factors. The observed variables are modeled as linear combinations of the latent factors. The model coefficients of the linear combination are called factor loadings.

In the EFA, the factors form the central field of activity. Three process steps need to be managed during an EFA. Subsequent to the determination of the number of essential factors, the respective factor loadings are then calculated. The factor loadings for the original factors are finally transformed into factor loadings for rotated factors.

First, the number of essential factors is determined. This happens on the basis of different tools with the associated criteria. A well-known tool is the so-called scree plot. In a scree plot, the eigenvalue is plotted versus its running number. The inflection point between a steep and flat descend in the eigenvalue indicates the number of essential factors [96]. Another tool works with the sum over the presumably essential eigenvalues divided by the sum over all existing eigenvalues. As soon as the quotient exceeds a level of 75 %, 80 % or 85 % the number of essential factors is reached [96].

After that, the respective factor loadings are calculated for all essential factors. In this process step, the assumed model equation just needs to be complied. The mathematical technique depends on the supposed model equation. For model equations in the simplest form, factor loadings are equal to the principal components. The principal components are again equal to the first few eigenvectors belonging to the essential eigenvalues. As mentioned above, the combination of a principal component analysis and a principal component rotation or factor rotation is a special type of an EFA. In case of another special type of an EFA, the calculation of factor loadings is based on maximum likelihood estimation. The maximum likelihood estimation is applied due to the somehow more complicated model equation. The model equation implies that all observed variables contain a component caused by an independent random variability. The so-called specific variance is unique to the considered observed variable.

At the end, the factors are rotated for an improved interpretability. The absolute values of the factor loading are maximized during the factor rotation. The recognition and description of

the represented properties is much easier for rotated factors with few and high factor loading. Generally, two rotation procedures are distinguished. These are the orthogonal rotation and the oblique rotation. Prior to the rotation, the original factors are uncorrelated. In case of an orthogonal rotation, this property is preserved. Therefore, orthogonally rotated factors can be interpreted independently. During an oblique rotation, the uncorrelated original factors become correlated. An independent interpretation of obliquely rotated factors is not possible. Thus, the orthogonal rotation is more suitable compared to the oblique rotation.

As already mentioned above, *Rao* and *Lohse* [212] used an EFA in combination with a PCA. By means of the EFA, they evaluated scale ratings of twelve texture attributes and generated an appearance-based space for texture characterization.

Chapter 5

Screen and Flexo Printing Samples

Remember, the first partial problem is the poorly researched influence of the printing parameters on the optical properties and visual appearance (section 1.1.1). A deeper insight into this problem is given in chapter 2.

In addition, the necessity of the corresponding approach is explained. In printing trials, a large set of special effect samples varying in the most important printing parameters will be produced (section 1.2.1). These printing samples will be used to generate a bidirectional reflectance and texture database and to identify the number and nature of the essential visual appearance attributes as described later in chapter 6 and chapter 7, respectively.

Now, section 5.1, section 5.2 and section 5.3 deal with the *preparation of printing components*, the *execution of the printing trials* and on the *identification of the printing samples*. Each of these sections is further divided in two subsections separating screen [146] and flexo [145] printing trials. This chapter is summarized with an overview about the *production of printing samples* in section 5.4.

5.1 Preparation of Printing Components

Previous to the printing trials, consumption materials and machine equipments have to be prepared. The consumption materials include printing substrates and printing inks. The necessary equipment components depend on the printing technology. Due to this dependence, the preparation of the *screen* (section 5.1.1) and *flexo* (section 5.1.2) *printing components* is described separately.

5.1.1 Preparation of Screen Printing Components

During the preparation of the screen printing trials, *printing substrates* were selected, *printing inks* were mixed and a *screen printing plate* was ordered. In the following, further information about the preparation of the screen printing trials is given.

White Glossy Coated Paper and Black Uncoated Paper

For the screen printing trials, two papers were selected. The black uncoated paper ($BUCP$) and the white glossy coated paper ($WGCP$) are specified in table B.1 and shown in figure 5.1a.

(a) Printing substrates. (b) Face cutting machine.

Figure 5.1: Printing substrates and face cutting machine *Polar* 78.

The white paper is produced by *Sappi Ltd.* and called *LuxoMagic*. This glossy coated art printing paper is normally used for high-quality printing products such as illustrated books, wall calendars or advertising posters. A grammage of 150 g/m^2 was selected for the screen printing trials.

The black paper manufactured by *Arjo Wiggins Fine Papers Ltd.* is named *PopSet*. This uncoated paper tinted black in bulk was selected to supersede a priming with a black light-absorbing ink. For the screen printing trials, a grammage of 120 g/m^2 is adequate.

Both papers were ordered as large-size sheets. The face cutting machine *Polar* 78 shown in figure 5.1b was used to cut handy sheets with edge lengths between 20 cm and 30 cm.

UV-Curing Special Effect Inks of 22 *BASF* Pigments

Altogether, the *BASF SE* Ludwigshafen provided 22 containers with different special effect pigments. The special effect pigments differ in material composition (table A.3, table A.4) and particle size. Therefore, table 5.1 enlists pigment classes and particle diameters of all used *BASF* pigments.

As introduced in section 2.1.3, special effect pigments are classified in silver white (SW), gold (G), iron oxide (IO), interference effect (IE), multi-color (MC) and sparkle (S) pigments. In this study, special effect pigments of all six pigment classes are included (table A.1).

Table 5.1: Special effect inks containing *BASF* pigments (concentration (*conc.*), silver white (*SW*), gold (*G*), iron oxide (*IO*), interference effect (*IE*), multi-color (*MC*), sparkle (*S*)).

code	name	class	diameter	*conc.*
BO90C0Z	*Black Olive*	*SW*	6 μm - 48 μm	19.2 %
F9G630L	*Firemist Blue*	*S*	5 μm - 300 μm	19.2 %
F9G680D	*Firemist Colormotion Blue Topaz*	*MC*	13 μm - 180 μm	19.2 %
F9G480D	*Firemist Colormotion Ruby*	*MC*	13 μm - 180 μm	19.2 %
F9G230L	*Firemist Gold*	*S*	5 μm - 300 μm	19.2 %
F9G830L	*Firemist Green*	*S*	5 μm - 300 μm	19.2 %
F9G130L	*Firemist Pearl*	*S*	5 μm - 300 μm	19.2 %
F9G430L	*Firemist Red*	*S*	5 μm - 300 μm	19.2 %
F9G730L	*Firemist Turquoise*	*S*	5 μm - 300 μm	19.2 %
F9G530L	*Firemist Violet*	*S*	5 μm - 300 μm	19.2 %
G9S130D	*Glacier Frost White*	*SW*	8 μm - 45 μm	19.2 %
L9A30D	*Lumina Aqua Blue*	*IE*	8 μm - 48 μm	19.2 %
L9232D	*Lumina Brass*	*G*	8 μm - 48 μm	19.2 %
L9359D	*Lumina Copper*	*IO*	8 μm - 48 μm	19.2 %
L9Y30D	*Lumina Gold*	*IE*	8 μm - 48 μm	19.2 %
L9G30D	*Lumina Green*	*IE*	8 μm - 48 μm	19.2 %
L9R30D	*Lumina Red*	*IE*	8 μm - 48 μm	19.2 %
L9680H	*Lumina Royal Blue*	*IE*	6 μm - 48 μm	19.2 %
L9450D	*Lumina Russet*	*IO*	8 μm - 48 μm	19.2 %
L9T30D	*Lumina Turquoise*	*IE*	8 μm - 48 μm	19.2 %
SF9332D	*Santa Fe Desert Blush*	*G*	8 μm - 48 μm	19.2 %
SF9832D	*Santa Fe Kiwi*	*G*	8 μm - 48 μm	19.2 %

Furthermore, a wide range of particle diameters is considered (table A.2). The smallest pigments measure between 6 μm and 48 μm in diameter. Diameters from 13 μm to 180 μm are those of medium sized pigments. Large sized pigments have diameters between 5 μm and 300 μm.

For each of the 22 containers, an amount of 55 g pigments was stirred with 220 g UV-curing binder. This binder is called *OMNIPLUS UL* 360 and provided by *Fujifilm Sericol GmbH*. Due to the increased viscosity, an amount of 11 g thinner was added. The thinner is named *UVIPLAST ZE* 834 and also provided by *Fujifilm Sericol GmbH*. Thus, the UV-curing screen printing inks are charged with 19.2 % of the special effect pigments by weight. This ink concentration is in accordance with the recommendations in literature [86, 204, 205].

Screen Printing Plate

Depending on the printed product, the screen printing unit described in section 5.2.1 is equipped with the respective screen printing plate. The screen printing plate consists of a frame stringed with a fabric. The selected fabric provided by *Sefar AG* is called *PET* 1500 $43/100 - 80Y$. The abbreviations specify the properties of the fabric. The abbreviation *PET* 1500 stands for a high modulus mesh of monofilament polyester with 43 *threads/cm* or 100 *threads/inch*, respectively. With a thread width of 80 μm, the resulting mesh width measures 149 μm. For most of the used pigments, the mesh width measures minimally 1.5 times the maximal particle size as recommended in literature [86, 204, 205]. The letter Y represents yellow and specifies the color of the threads. The open stencil area is a quadratic solid area with an edge length of 120 mm bordered by a non-printing margin.

5.1.2 Preparation of Flexo Printing Components

The preparation of the flexo printing trials includes the selection of *printing substrates*, the request for *printing inks*, the design of *digital masters* and the order of *printing plates*. The following sections give further information about the preparation of the flexo printing trials.

White Glossy and Matt Coated Paper

For the selection of the printing substrates, the influences of its roughness and porosity described in section 2.2.2 were considered. Thus, two wood-free coated art papers for high-quality printing products were selected. The coated papers called *LumiArt* and *LumiSilk* produced by *Stora Enso AG* differ in their surface finish as shown in table B.2 and figure 5.2a.

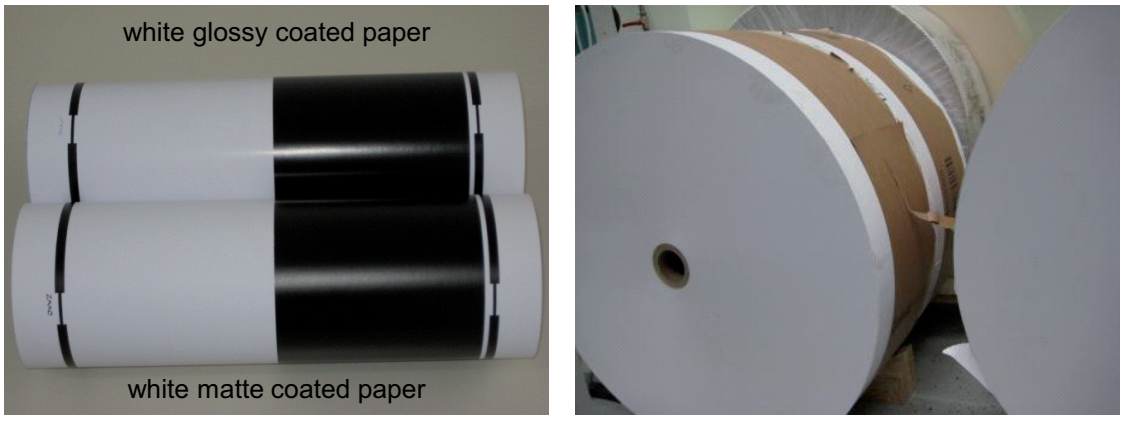

(a) Rolled samples. (b) Paper rolls.

Figure 5.2: White glossy and matte coated papers.

The glossy coated paper *LumiArt* has a smooth surface evoking a parallel orientation of the flaky special effect pigments [86, 204, 205]. Due to the well-aligned orientation, the color flop might be sharper and the gloss intensity higher compared to a matt coated paper.

For the matt coated paper *LumiSilk* having a rough surface, the pigments are oriented less parallel to each other [86, 204, 205]. In comparison with a glossy coated paper, the geometry-dependent color shift is expected to be a bit more blurry and the texture more distinctive.

The selected grammage of 120 g/m^2 represents applications at the upper limit of graphic printing and at the lower limit of package printing. Two 330 mm wide rolls of both papers shown in figure 5.2b were provided by the *Stora Enso Research Center Mönchengladbach*.

Water-Based Special Effect Inks of 28 *MERCK* Pigments

The *MERCK KGaA* Darmstadt provided 28 water-based inks containing special effect pigments of the product series *Iriodin*, *Colorstream* and *Miraval*. Apart from the product name, table 5.2 enlists the pigment class and the particle diameter of all selected *MERCK* pigments [145].

The classification of special effect pigments is introduced in section 2.1.3. All classes called silver white (SW), gold (G), iron oxide (IO), interference effect (IE), multi-color (MC) and sparkle (S) pigments are involved (table A.5). Overall, the assortment of *MERCK* pigments includes three to eight pigments of each of the six pigment classes.

Apart from the variety of pigment classes and so material compositions (table A.7, table A.8), a wide range of particle sizes is taken into account in this study (table A.6). The considered pigment diameters lie between 5 μm and 25 μm, 5 μm and 50 μm, 10 μm and 60 μm, 10 μm and 100 μm or between 20 μm and 100 μm.

The concentration of the pigments in the printing ink was chosen under consideration of the specifications in literature [86, 204, 205]. The concentration should be lower for large particles.

Table 5.2: Special effect inks containing *MERCK* pigments (concentration (*conc.*), silver white (*SW*), gold (*G*), iron oxide (*IO*), interference effect (*IE*), multi-color (*MC*), sparkle (*S*)) [145].

code	name	class	diameter	*conc.*
*I*123	*Iriodin Bright Lustre Satin*	*SW*	5 μm - 25 μm	25 %
*I*103	*Iriodin Rutile Sterling Silver*	*SW*	10 μm - 60 μm	25 %
*I*153	*Iriodin Flash Pearl*	*SW*	20 μm - 100 μm	25 %
*I*323	*Iriodin Royal Gold Satin*	*G*	5 μm - 25 μm	25 %
*I*305	*Iriodin Solar Gold*	*G*	10 μm - 60 μm	25 %
*I*300	*Iriodin Gold Pearl*	*G*	10 μm - 60 μm	25 %
*I*520	*Iriodin Bronze Satin*	*IO*	5 μm - 25 μm	25 %
*I*4504	*Iriodin Lava Red*	*IO*	5 μm - 50 μm	25 %
*I*500	*Iriodin Bronze*	*IO*	10 μm - 60 μm	25 %
*I*201	*Iriodin Rutil Fine Gold*	*IE*	5 μm - 25 μm	25 %
*I*211	*Iriodin Rutil Fine Red*	*IE*	5 μm - 25 μm	25 %
*I*221	*Iriodin Rutil Fine Blue*	*IE*	5 μm - 25 μm	25 %
*I*231	*Iriodin Rutil Fine Green*	*IE*	5 μm - 25 μm	25 %
*I*205	*Iriodin Rutil Platinum Gold*	*IE*	10 μm - 60 μm	25 %
*I*215	*Iriodin Rutil Red Pearl*	*IE*	10 μm - 60 μm	25 %
*I*225	*Iriodin Rutil Blue Pearl*	*IE*	10 μm - 60 μm	25 %
*I*235	*Iriodin Rutil Green Pearl*	*IE*	10 μm - 60 μm	25 %
*CF*1000	*Colorstream Autumn Mystery*	*MC*	5 μm - 50 μm	20 %
*CT*1001	*Colorstream Viola Fantasy*	*MC*	5 μm - 50 μm	20 %
*CT*1002	*Colorstream Arctic Fire*	*MC*	5 μm - 50 μm	20 %
*CT*1003	*Colorstream Tropic Sunrise*	*MC*	5 μm - 50 μm	20 %
*CT*1004	*Colorstream Lapis Sunlight*	*MC*	5 μm - 50 μm	20 %
*CT*1005	*Colorstream Pacific Lagoon*	*MC*	10 μm - 60 μm	20 %
*CT*1006	*Colorstream Royal Damask*	*MC*	10 μm - 60 μm	20 %
*M*5311	*Miraval Scenic White*	*S*	10 μm - 100 μm	15 %
*M*5320	*Miraval Scenic Gold*	*S*	10 μm - 100 μm	15 %
*M*5321	*Miraval Scenic Copper*	*S*	10 μm - 100 μm	15 %
*M*5325	*Miraval Scenic Turquoise*	*S*	10 μm - 100 μm	15 %

To a certain degree, the particle size correlates with the pigments class. The pigment class again correlates with the product series. Therefore, the product series was used as criterion for the realized ink concentration of the water-based flexo inks. Ink concentrations of 25 %, 20 % and 15 % by weight were realized for the product series *Iriodin*, *Colorstream* and *Miraval*, respectively.

Three Digital Master Layouts

Three digital masters were designed for three subsequent process sequences. In the following, the sequences are called priming, printing and finishing. The digital masters for the three process sequences are shown in figure 5.3 [145].

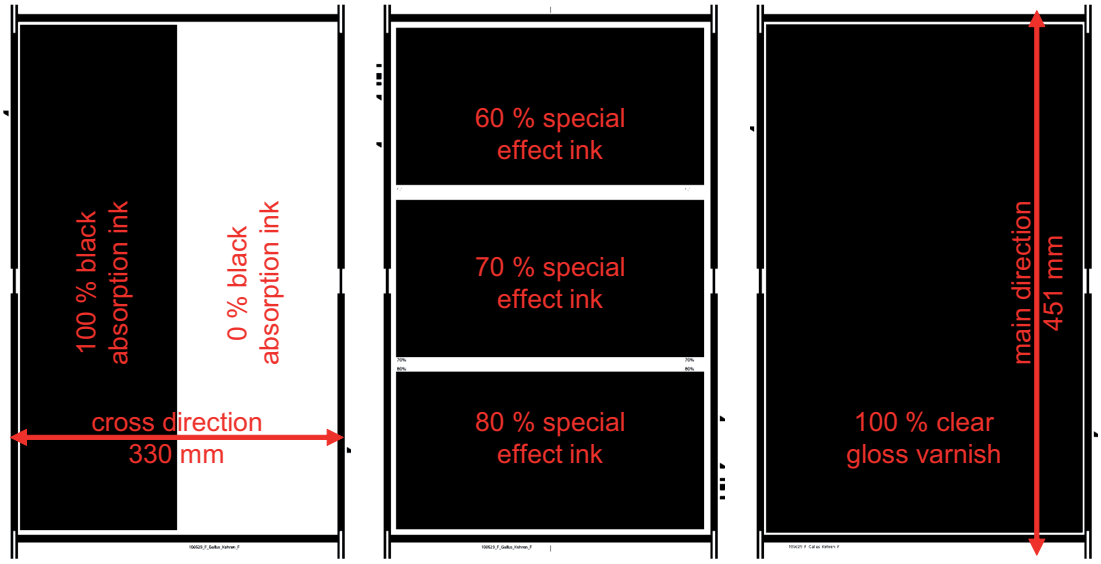

(a) Priming with water-based black light-absorbing ink.

(b) Printing with water-based special effect inks.

(c) Finishing with *UV*-curing clear gloss varnish.

Figure 5.3: Digital masters for the three process sequences [145].

Figure 5.3a shows the digital master layout for the priming sequence. The one half of the 330 *mm* wide paper web is printed with a black light-absorbing ink in solid. The remaining half is left white.

During the printing sequence, special effect inks are applied according to the pattern shown in figure 5.3b. Areas with tonal values of 60 %, 70 % and 80 % are provided in the non-primed white and primed black regions.

In preliminary printing tests with several special effect inks, a tonal value about 70 % yielded satisfying results. At low tonal values, the pigments are distributed uniformly resulting in a regular texture. However, the color shift is comparatively pale as mentioned in section 2.2.2. The color shift is most intense for a complete surface covering as in solid prints. At high tonal values, the pigments tend to build up agglomerates. For potential deviations from the optimal tonal value of 70 %, additional areas with tonal values of 60 % and 80 % were realized on the flexo printing plate.

The finishing sequence is an optional application used for the half number of printed special effect samples in each sample set. As shown in figure 5.3c, the sample is completely covered with a clear gloss varnish.

Three Flexo Printing Plates

As recommended in literature [86, 204, 205], three 1.14 *mm* thick photopolymer printing plates of *BASF SE* named *FAH D* were ordered. Figure 5.4 shows the three printing plates for the

priming (figure 5.4a), printing (figure 5.4b) and finishing (figure 5.4c) sequence.

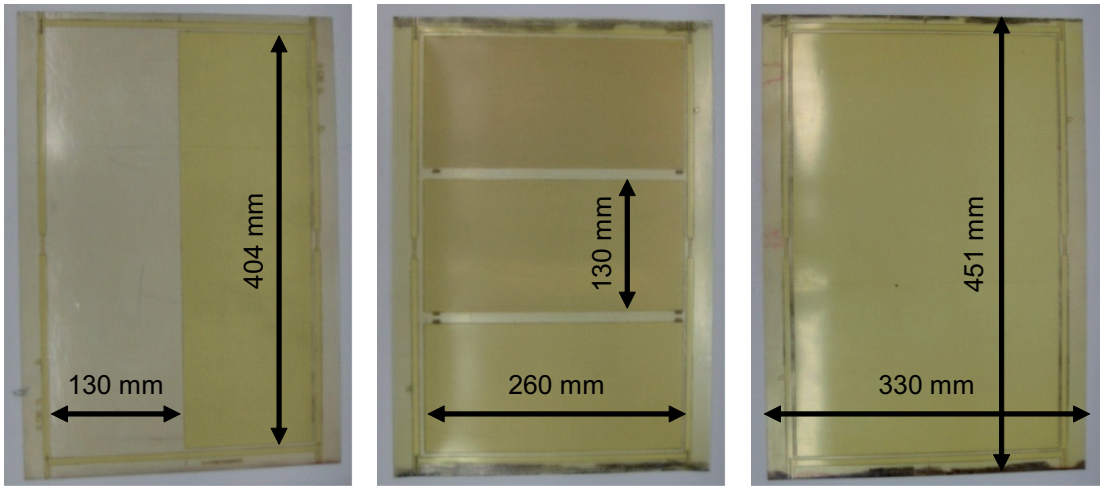

(a) Priming with water-based black light-absorbing ink.

(b) Printing with water-based special effect inks.

(c) Printing with UV-curing special effect inks.

Figure 5.4: Printing plates for the three printing sequences.

The printing plates measure 330 mm in cross direction and 451 mm in main direction. The main direction is equal to the transport direction of the substrate in the printing press. Its perpendicular direction also lying in the substrate plane is called cross direction. For each of the three printing sequences, the respective printing plate was mounted on the printing cylinder in the flexo printing unit of the modular web-fed printing press presented in section 5.2.2.

5.2 Execution of Printing Trials

A printing process is composed of at least one transferring-curing sequence. In a such sequence, the ink is first transferred on the substrate and subsequently cured. The transferring and curing can be realized in a discontinuous or continuous sequence in independent or connected process steps.

The screen and the flexo printing process differ in the number and continuity of transferring-curing sequences. The screen printing process is realized in a single discontinuous transferring-curing sequence. Three continuous transferring-curing sequences are passed in the flexo printing process. In the following sections, the *screen* (section 5.2.1) and *flexo* (section 5.2.2) *printing trials* conducted at the *Institute of Printing Science and Technology* (*IDD*) are described in detail.

5.2.1 Execution of Screen Printing Trials

As just mentioned, the screen printing process is a single discontinuous transferring-curing sequence. The transferring and curing of the printing inks is realized in a sheet-fed screen printing unit and a sheet-fed drying system, respectively. The transferring with the *screen printing unit* and the curing with the *combined drying system* are described in the following.

Screen Printing Unit

The prepared *UV*-curing special effect inks with *BASF* pigments were processed in screen printing previously described in section 2.2.1 [148, 149]. The used screen printing unit called *Kammann K15Q SL* is shown in figure 5.5.

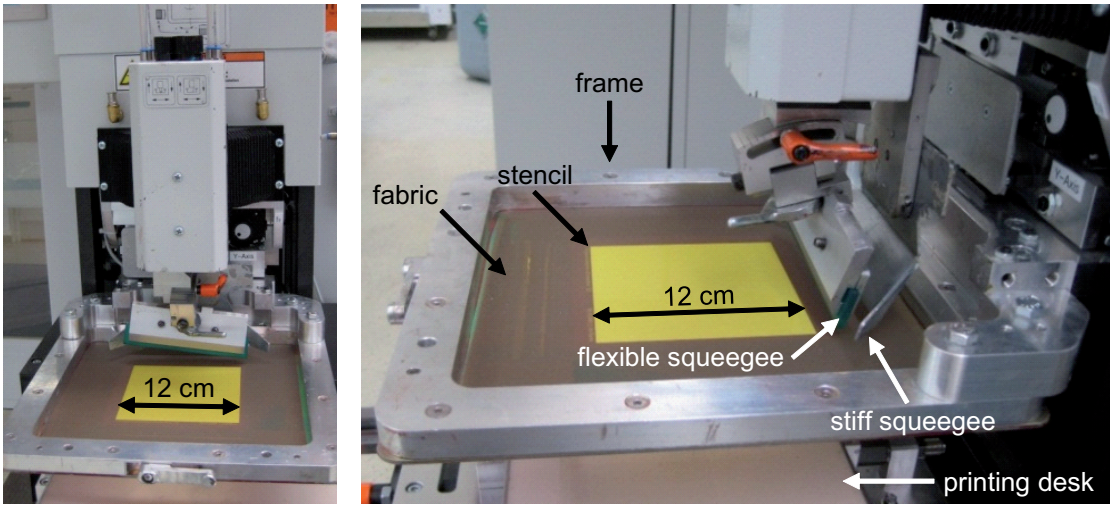

(a) Front view. (b) Side view.

Figure 5.5: Screen printing unit *K15Q SL* of *Kammann*.

The substrate is positioned on the printing desk and fixed by means of vacuum applied to the printing desk. Using a syringe, a specified amount of the respective printing ink is applied on the screen in front of the squeegees. The ink is transferred on the substrate in a four-stage motion.

Firstly, the application unit is moved to its lover position a few millimeters above the substrate placed on the printing desk. In the second stage, the stiff metal squeegee distributes the printing ink on the fabric fixed in the frame. The flexible polymer squeegee presses the ink through the meshes at the open areas of the stencil during the third stage. Finally, the application unit is lifted off from the substrate staying fixed on the printing desk.

The printed result is influenced by material parameters, equipment parameters as well as by process parameters. The selected materials including the two papers as printing substrates and

the prepared printing inks with 22 special effect pigments are described above in section 5.1.1. In the same context, related information is given on the screen printing plate. Apart from the screen printing plate, the equipment includes the flexible polymer squeegee. This flexible polymer squeegee is specified by a hardness of 65 *Shore*.

The machine settings such as the horizontal and vertical position and inclination of the frame and both squeegees were adjusted carefully. The vertical position of the screen influences the transfer of the ink on the substrate. The optimal distance of the frame to the printing desk depends on the thickness of the printing substrate. A small horizontal inclination of the screen relative to the substrate would result in a spatially non-uniform ink distribution and should be avoided. By means of the vertical position of the squeegees, their pressure on the fabric is regulated. Thereby, the distribution of the ink on the fabric and its pressing through the meshes are influenced. The same holds for their inclination. Furthermore, the advancing speed of the squeegees was adjusted and kept constant during all screen printing trials.

Combined Drying System

Subsequent to the application on the paper substrate, the *UV*-curing printing ink was dried. For the curing of the printing ink, the combined drying system of *IST Metz GmbH* shown in figure 5.6 was used.

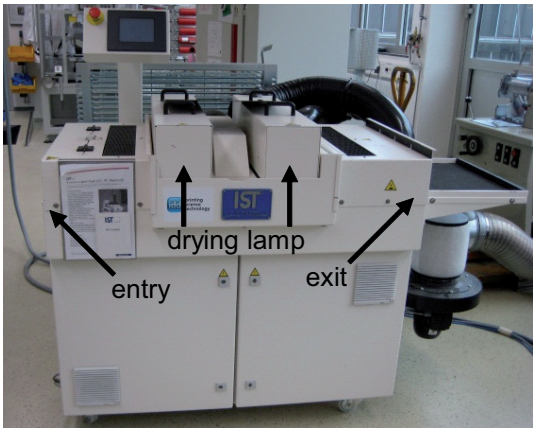

Figure 5.6: Combined drying system of *IST Metz GmbH*.

This dryer combines *UV*, *IR* and hot air drying units in a single device. The *UV* mode was used for the *UV*-curing special effect inks. On a conveyor belt, the sample is transported underneath the drying lamps. The transport velocity of the conveyor belt and the radiation power of the drying lamps were adjusted to the curing behavior of the applied printing ink.

Besides the ink system itself, the possible conveyor velocity and the necessary curing power depend on the absorption properties of the dissolved special effect pigments. The conveyor velocity and curing power should be low or high enough, respectively, that the cured ink sticks no more. For example, the curing of the printing ink with the dark, strongly light-absorbing pigments *Black Olive* 90*COZ* takes more energy than the one with the light, weakly light-absorbing pigments *Glacier Frost White* 9*S*130*D*. As reference point, a medium conveyor velocity of 20 m/min for a maximal curing power of 100 % was adequate for the samples with the pigments *Lumina Royal Blue* 9680*H* and *Lumina Turquoise* 9*T*30*D*.

5.2.2 Execution of Flexo Printing Trials

As mentioned above, the flexo printing process includes three continuous transferring-curing sequences. The flexo printing samples were produced on the modular web-fed printing press *Gallus RCS* 330-*HD*. The design of the 15 m long printing press is shown in figure 5.7.

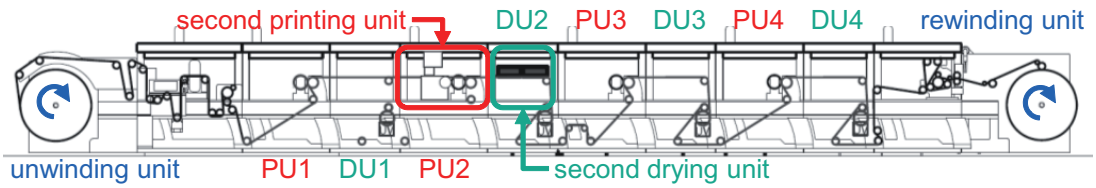

Figure 5.7: Sketch of web-fed printing press *Gallus RCS* 330-*HD*.

In this modular printing press, all conventional printing technologies described in section 2.2.1 are realized. Printing units (*PU*) for offset printing, gravure printing, flexo printing and screen printing can be combined in any desired order with drying units (*DU*) including *UV*, *IR* and hot-air dryers. For producing the flexo printing samples in the three mentioned sequences, the flexo printing unit and a combined drying unit were each installed in the second position as shown in figure 5.7 and figure 5.8a [145].

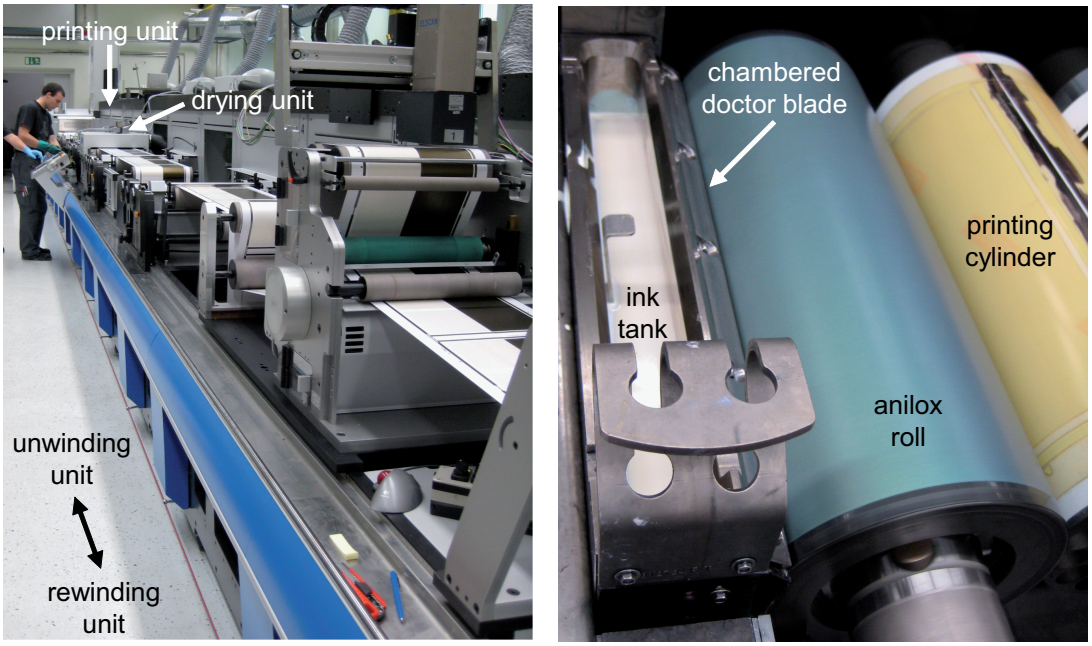

(a) Modular design. (b) Flexo unit.

Figure 5.8: Photos of web-fed printing press *Gallus RCS* 330-*HD* [145].

In figure 5.8b [145], the anilox roll is located between the chambered doctor blade system including the ink tank and the printing cylinder. According to recommendations in literature [86, 204, 205], the used anilox roll has a theoretical dispersing volume of 13 cm^3/m^2 and a cell size of 100 $lines/cm$. The theoretical dispersing volume and the cell size determine the amount of printing ink carried by the anilox roll. The ink dosage is also influenced by the pneumatically controlled doctor blade load. The air pressure defining the doctor blade load was adjusted and held constant on a medium level between 3 bar and 4.5 bar.

Furthermore, the printing process is specified by the machine speed. A machine speed of 80 m/min was possible during the priming with light-absorbing ink. In general, light-absorbing inks are easier to handle than special effect inks or clear gloss varnishes. Besides this, no intermediate process breaks were necessary for ink changes or unprinted intervals. This does not count for the printing and finishing sequence. Therefore, the machine speed was reduced to 40 m/min.

The dying unit was used in the combined hot-air and *IR* mode during the priming and printing sequence for drying the water-based black light-absorbing ink as well as the water-based special

effect inks. The *UV*-curing clear gloss varnish applied in the finishing sequence was thus cured by the *UV* lamps of the installed drying unit.

Between the three individual printing sequences, the paper roll was transported back from the rewinding unit at the end of the machine to the unwinding unit at the beginning of the machine. Figure 5.9 shows the results of each of the three printing sequences [145].

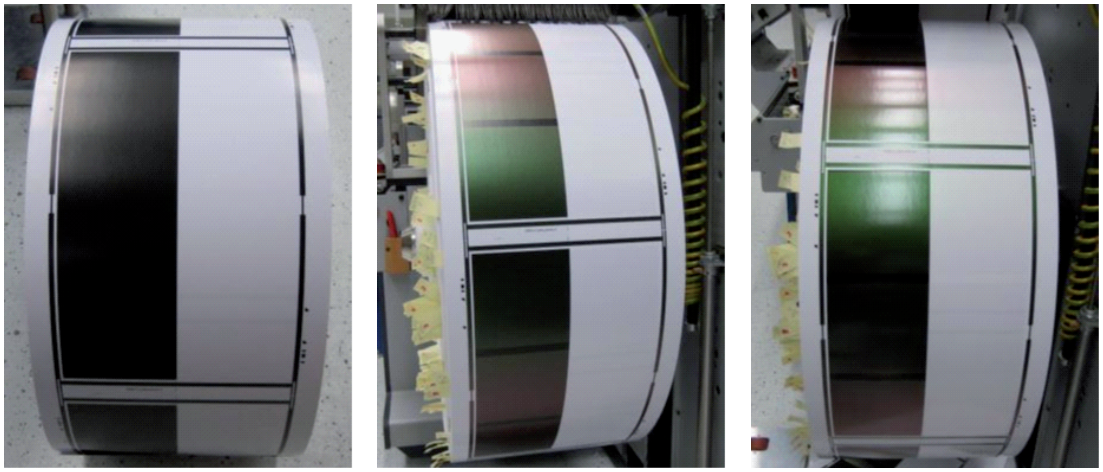

(a) Priming with water-based black light-absorbing ink.

(b) Printing with water-based special effect inks.

(c) Finishing with *UV*-curing clear gloss varnish.

Figure 5.9: Printing samples of the three printing sequences [145].

Further information about the *priming with black light-absorbing ink* (figure 5.9a), the *printing with special effect inks* (figure 5.9b) and the *finishing with a clear gloss varnish* (figure 5.9c) including the involved materials is given in the following sections.

Priming with a Water-Based Black Light-Absorbing Ink

As already mentioned and shown in figure 5.9a, the half of the paper web is covered with black light-absorbing ink in the first printing sequence. A water-based flexo ink called *Aqualabel Black* of *Siegwerk Druckfarben AG* was used.

The sense of the priming with a black light-absorbing ink is the manipulation of the optical properties and thus the visual appearance. The influence of the background color on the perceived color, gloss and texture are described in section 2.2.2.

Printing with 28 Water-Based Special Effect Inks

In the second sequence called special effect printing , 28 different special effect inks are applied on the partly primed paper in tonal values of 60 %, 70 % and 80 % as already shown in figure 5.9b.

The 28 special effect pigments were assorted in consideration of the preferences of typical customers and the applicability for flexo printing. The flexo printing process admits the application of inks with special effect pigments of particle sizes up to 200 μm as described in section 2.2.1. The size of the flaky particles decides about the concentration of the pigments in the printing ink [86, 204, 205]. As mentioned in section 5.1.2, ink concentrations of 25 %, 20 % and 15 % were realized for the *Iriodin*, *Colorstream* and *Miraval* pigments, respectively.

In addition to the process-related specifications, visual quality requirements have to be fulfilled. The visually relevant occupancy of the substrate with pigments (section 2.2.2) should be controlled without any manipulation of the process-related ink supply or pigment concentration. The tonal value is used as alternative control parameter.

Finishing with a *UV*-Curing Clear Gloss Varnish

The third printing sequence is an optional finishing with a clear gloss varnish. In this context, optional means the following. Only approximately the half number of the sample sheets of each paper-ink combination is finished with an *UV*-curing varnish as shown in figure 5.9c. The clear gloss varnish is called *Senolith* of *Weilburger Graphics GmbH*.

With the additional transparent layer, it is intended to smooth the printed surface. The varnishing influences the optical properties and visual appearance as explained in section 2.2.2.

5.3 Identification of Printing Samples

The post-processing of the printing trials includes the visual inspection of the samples on defects and their clear marking with labels. The inspection and marking is described in separate sections for the *screen* (section 5.3.1) and *flexo* (section 5.3.2) *printing samples*.

5.3.1 Identification of Screen Printing Samples

After screen printing and UV-curing, the screen printing samples were visually examined on defects. All acceptable samples were labeled with ink name, paper quality, varnishing state and background color. A dot is used to separate both features.

In table 5.1, abbreviations for all 22 special effect inks are already given. For the *paper quality*, the *varnishing state* and the *background color*, table 5.3 enlists the respective abbreviations.

Table 5.3: Abbreviations for the identification of screen printing samples.

identification	abbreviation	information
paper quality	$WGCP$	white glossy coated paper
	$BUCP$	black uncoated paper
varnishing state	UVS	unvarnished surface
background color	WPB	white paper background
	BPB	black paper background

A white glossy coated paper ($WGCP$) and a black uncoated paper ($BUCP$) were printed with the special effect inks. Previous or subsequent to the special effect printing, no light-absorbing ink or clear gloss varnish were applied, respectively. With respect to the paper quality, this results in a white paper background (WPB) or a black paper background (BPB) with an unvarnished surface (UVS).

The influence of the paper quality and the background color on the printed result is shown in figure 5.10. Figure 5.10a and figure 5.10b show both papers printed with special effect inks containing the $BASF$ pigments *Lumina Royal Blue* 9680H and *Lumina Turquoise* 9T30D, respectively.

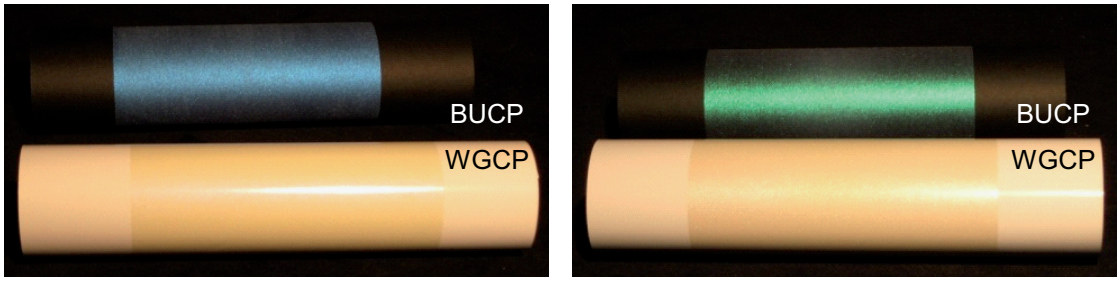

(a) *Lumina Royal Blue* 9680H. (b) *Lumina Turquoise* 9T30D.

Figure 5.10: Special effect inks printed on white glossy coated paper ($WGCP$) and black uncoated paper ($BUCP$).

The printing of 22 different special effect inks with $BASF$ pigments on two papers results in 44 application cases. For each application case, a number of about 20 samples free from defects is available in the whole screen printing sample set.

5.3.2 Identification of Flexo Printing Samples

Combining 28 special effect inks and two paper qualities, two varnishing states and two background colors yields 224 application cases for the flexo printing sample set. Out of more than 80 produced

samples per application case, a number of about 20 samples without any defects was selected and branded with abbreviations for their identification.

The sample identification contains information about the ink name, the paper quality, the varnishing state and the background color. The enlisted sample features are each separated by a dot.

Alphanumeric abbreviations like $I231$, $CT1003$ or $M5320$ for all 28 special effect inks are enlisted in table 5.2. The first letter I, C or M denotes the product series *Iriodin*, *Colorstream* and *Miraval*, respectively. The following number corresponds to the number in the pigment name. Table 5.4 enlists the respective abbreviations for both used *paper qualities*, both realized *varnishing states* as well as for both realized *background colors*.

Table 5.4: Abbreviations for the identification of flexo printing samples.

identification	abbreviation	information
paper quality	$WGCP$	white glossy coated paper
	$WMCP$	white matt coated paper
varnishing state	UVS	unvarnished surface
	GVS	glossy varnished surface
background color	WPB	white paper background
	BPB	black printed background

The abbreviations for paper quality, varnishing state and background color are explained by means of an example. Figure 5.11 shows a sample set for one special effect ink consisting of four sample sheets.

Two of the four sample sheets are based on the white glossy coated paper ($WGCP$). The two others are based on the white matt coated paper ($WMCP$). For both paper qualities, one of the two sample sheets has an unvarnished surface (UVS). The other one has a glossy varnished surface (GVS). On each sample sheet are test patches of printed special effect inks on the white paper background (WPB) as well as on the black printed background (BPB). In the following, only the test patches with a tonal value of 70 % are considered as framed in figure 5.11. The special visual appearance is satisfactory and exhibits no visible agglomeration.

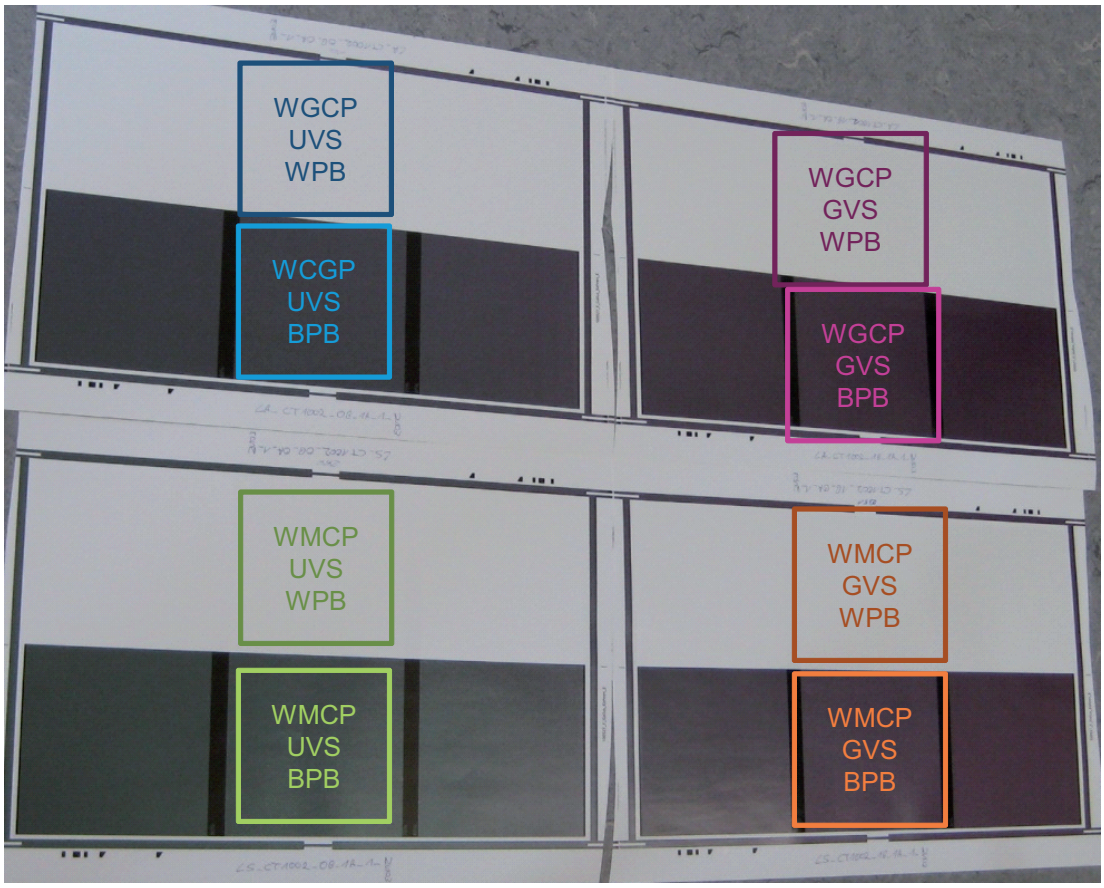

Figure 5.11: Sample set for one special effect ink with abbreviations for eight application cases differing in paper quality (white glossy coated paper ($WGCP$), white matt coated paper ($WMCP$)), varnishing state (unvarnished surface (UVS), glossy varnished surface (GVS)) and background color (white paper background (WPB), black printed background (BPB)).

5.4 Overview about the Production of Printing Samples

Finally, an overview is given about the production of the printing samples. The challenge in printing the samples in their suitability for the further objectives of this study. For the evaluation of the bidirectional reflectance and texture data (chapter 6) and the identification of the essential visual appearance attributes (chapter 7), the printing samples should vary in the printing parameters. The varied printing parameters and further important information is given in table 5.5.

Table 5.5: Printing trials.

printing technology	screen printing	flexo printing
printing press	*Kammann K15Q LS*	*Gallus RCS 330-HD*
special effect pigment	22 *BASF* pigments	28 *MERCK* pigments
special effect ink	22 *UV*-curing inks	28 water-based inks
printing substrate	white glossy coated paper, black uncoated paper	white glossy coated paper, white matt coated paper
background color	white paper background, black paper background	white paper background, black printed background
surface varnishing	unvarnished surface	unvarnished surface, glossy varnished surface
application cases	44 application cases	224 application cases

In *screen printing* on the printing press *Kammann K15Q LS* with 22 *special effect pigments* of *BASF SE*, the number of application cases was limited to the most representative assortment of 44 *application cases* [146]. A *white glossy* and *black uncoated paper* was printed with 22 *UV-curing special effect inks*.

A number of 224 *application cases* was realized [145] in *flexo printing* on the printing press *Gallus RCS 330-HD* with 28 *special effect pigments* of *MERCK KGaA*. A *white glossy* and *matt coated paper* was partially primed with a *black light-absorbing ink*, printed with one of 28 *water-based special effect inks* and optionally finished with a *clear gloss varnish*.

The special effect samples were produced for the investigation of their optical properties and visual appearance. In the following, the produced special effect samples are used in optical measurements and visual experiments.

The optical data measured in multiple geometric configurations are filed in a bidirectional reflectance and texture database (chapter 6). On the basis of the bidirectional reflectance and texture data, perception-related parameters are determined. The perception-related parameters are used to evaluate the influence of the varied printing parameters.

The visual data collected in different visual experiments are evaluated by means of statistical methods. The statistical evaluation gives information about the number and nature of the essential visual appearance attributes (chapter 7). Their psychophysical functions should be determined in a further study using samples with fine and specific variations in multiple printing parameters.

Chapter 6

Bidirectional Reflectance and Texture Database

The availability of measured or modeled bidirectional reflectance and texture distributions for the description of the complex bidirectional optical properties is the second partial problem (section 1.1.2). A better understanding of this problem is provided by chapter 3.

At the same place, the need of the corresponding approach is illustrated. It is intended to collect bidirectional reflectance and texture data for printed special effect colors (section 1.2.2). For this purpose, the screen and flexo printing samples previously produced according to chapter 5 are required.

In this chapter, the *measurements on the printing samples* (section 6.1) and the *structure of the bidirectional reflectance and texture database* (section 6.2) are described in detail. Furthermore, the *influence of the printing parameters* (section 6.3) on perception-related parameters is investigated and concluded (section 6.4).

6.1 Measurements on the Printing Samples

The samples of printed special effect colors were measured using different optical instruments. The measurements at the *Institute of Printing Science and Technology* (*IDD*) with commercial *multi-angle spectrophotometers* [147] are described in section 6.1.1. Section 6.1.2 describes the measurements at the *Physikalisch-Technische Bundesanstalt* (*PTB*) using a *robot-based gonioreflectometer* [147].

6.1.1 Measurements with Multi-Angle Spectrophotometers

For the screen printing sample set with 44 application cases as well as the flexo printing sample set with 224 application cases (section 5.3), seven measurements were carried out on four samples per application case. On the first sample, measurements were taken in four orientations of the instrument relative to the printed sample. The incidence direction of the multi-angle spectrophotometer was falling in line with the positive and negative machine direction as well as with the left and right cross direction of the printing press. On this way, the directionality caused by the directional application of the printing ink is taken into account. Three more measurements on three further samples were performed with the instrument axis aligning with the machine direction. This serves to comprise the statistical spread between individual samples.

Both sample sets were measured with two different multi-angle spectrophotometers (section 3.2.3) in a black painted room at the *Institute of Printing Science and Technology* (*IDD*). The *multi-angle spectrophotometer* $MA98$ (figure 3.6) was used for measurements of the screen printing samples. The flexo printing samples were measured with the *multi-angle spectrophotometer* *BYK-mac* (figure 3.7). Therefore, this section is divided in two subsections about multi-angle measurements on screen and flexo printing samples.

Measurements with Multi-Angle Spectrophotometer $MA98$

For the multi-angle measurements on the screen printing samples, the multi-angle spectrophotometer $MA98$ [147] of *X-Rite GmbH* was used (figure 3.6). For each of the 44 application cases, seven measurements were taken in all 19 geometric configurations. In addition to eleven in-plane geometries, this portable hand-held device performs spectral measurements in eight out-of-plane geometries (section 3.2.3).

Measurements with Upgraded Multi-Angle Spectrophotometer *BYK-mac*

The flexo printing samples were measured with the multi-angle instrument *BYK-mac* [147, 145] of *BYK-Gardner GmbH* (figure 3.7). Seven measurements were taken for all 224 application cases. The portable hand-held device performs spectral measurements in six geometries as well as imaging measurements in four geometries (section 3.2.3).

Spectral Multi-Angle Measurements with *BYK-mac* For an incidence angle of 45°, the spectral measurements are realized with six detectors located at aspect angles of −15°, 15°, 25°, 45°, 75° and 110°. As mentioned in section 3.2.2, the aspect angle corresponds to the angular difference between reflection angle and gloss angle. Spectral measurements serve to determine color coordinates.

The measured spectral reflectance factors are used to determine the color coordinates in the equivalent color systems *CIELAB* and *CIELCH* for the standard illuminant $D65$ and the 10° standard observer. The spectral reflectance factors as well as the color coordinates are recorded in the measurement report for all six geometric configurations.

Imaging Multi-Angle Measurements with *BYK-mac* The spatially resolved measurements are conducted with an in-build camera located perpendicular to the sample surface. As described in section 3.2.3, the sample is illuminated directionally under 15°, 45° and 75° counted

to the normal on the sample surface as well as diffusely by means of an integrating sphere. The photographed gray-scale pictures are internally used to calculate texture parameters.

Basing on the grabbed camera pictures, the measurement report also compasses texture parameters for sparkle and graininess. Sparkle intensity, sparkle area and sparkle grade are given in the measurement report for the three directional geometries. For the diffuse illumination, graininess is the relating enlisted texture parameter.

6.1.2 Measurements with Robot-Based Gonioreflectometer *ARGon*^{3}

For accurate bidirectional measurements on some selected samples (section 7.2.2), the three-dimensional appearance robot-based gonioreflectometer *ARGon*^{3} (figure 3.8b) was used. The samples were sent to the *Physikalisch-Technische Bundesanstalt* (*PTB*) and measured under the responsibility of *Andreas Höpe* and *Kai-Olaf Hauer*. As described in section 3.2.3 and the paper of *Atamas et al.* [12], the three-dimensional appearance robot-based gonioreflectometer *ARGon*^{3} is equipped with two types of detection systems. Apart from spectral measurements, imaging measurements are possible in any geometric configuration.

Due to the time-consuming positioning of light source and sample relative to the detection system, some limitations in the number and nature of the measurements are required. In this study, only some samples were measured in only some geometric configurations without repetitions and not in the image detection mode. On ten flexo printing samples selected as described in section 7.2.2, one-time spectral reflectance measurements were realized in 270 geometric configurations.

For all 270 geometric configurations, the light source and the printed sample are in a constant arrangement with an incidence direction ω_i of $(45°, 0°)$ to each other. The light source illuminates the printed sample under an incidence polar angle θ_i of 45° for an incidence azimuth angle ϕ_i of 0°. The 270 reflection directions ω_r were selected on the basis of 272 points evenly distributed on the surface of the half of the half sphere above the sample surface. In the quarter sphere, 272 points were organized in similar distances. From 272 reflection directions, two reflection directions had to be excluded due to geometrical and technical reasons. The coordinates of the 270 actually realized and 272 evenly distributed reflection directions ω_r are enlisted in table 6.1 as combinations of the reflection polar angle θ_r and the reflection azimuth angle ϕ_r.

Table 6.1: 270 (272) geometric configurations of bidirectional reflectance measurements with three-dimensional appearance robot-based gonioreflectometer *ARGon*^{3}.

ω_i		ω_r		n, $\Delta\phi_{r,j}$	
θ_i	ϕ_i	θ_r	$\phi_{r,1}$, $\phi_{r,2}$, $\phi_{r,3}$, $\phi_{r,4}$, …, $\phi_{r,n}$	n	$\Delta\phi_{r,j}$
45°	0°	0°	0°	1	0°
45°	0°	7.5°	0°, 45°, 90°, 135°, 180°	5	45°
45°	0°	15°	0°, 22.5°, 45°, 67.5°, …, 180°	9	22.5°
45°	0°	22.5°	0°, 15°, 30°, 45°, …, 180°	13	15°
45°	0°	30°	0°, 11.5°, 23°, 34.5°, …, 180°	17	11.5°
45°	0°	37.5°	0°, 9°, 18°, 27°, …, 180°	21	9°
45°	0°	45°	(0°, 7.5°,) 15°, 22.5°, …, 180°	23 (25)	7.5°
45°	0°	52.5°	0°, 7.5°, 15°, 22.5°, …, 180°	25	7.5°
45°	0°	60°	0°, 5°, 10°, 15°, …, 180°	37	5°
45°	0°	67.5°	0°, 5°, 10°, 15°, …, 180°	37	5°
45°	0°	75°	0°, 4.5°, 9°, 13.5°, …, 180°	41	4.5°
45°	0°	82.5°	0°, 4.5°, 9°, 13.5°, …, 180°	41	4.5°

For twelve reflection polar angles θ_r from 0° to 82.5° and a reflection polar angle resolution of 7.5°, j reflection azimuth angles $\phi_{r,j}$ are enlisted (table 6.1). The maximum number n is specific for the reflection polar angle θ_r and decides about the reflection azimuth angle resolution $\Delta\phi_{r,j}$.

The reflection azimuth angle resolution $\Delta\phi_{r,j}$ is equal to the difference of the reflection azimuth angles $\phi_{r,j+1}$ and $\phi_{r,j}$.

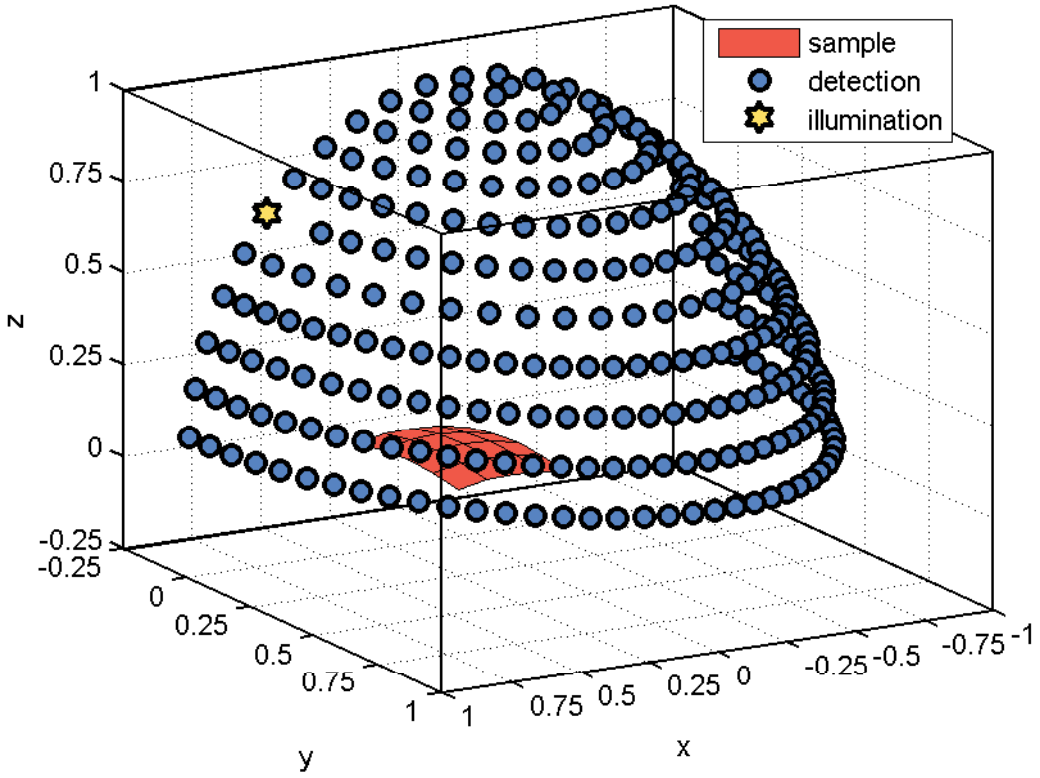

Figure 6.1: 270 geometric configurations of bidirectional reflectance measurements with three-dimensional appearance robot-based gonioreflectometer *ARGon*^{3}.

Figure 6.1 shows all 270 geometric configurations for an imaginary sample represented by a red plane. The yellow star indicates the constant position of the light source. All realized positions of the detection system are indicated by the blue circles.

6.2 Structure of the Bidirectional Reflectance and Texture Database

The measured reflectance spectra, the calculated color coordinates and the determined texture parameters are provided for other studies. In this study, the bidirectional reflectance and texture data will be used to evaluate the influence of the varied printing parameters (chapter 5). Due to the free availability for other studies and the better organization for this study, the determined data are filed in a database for printed special effect colors. Similarly, *Berns* [22, 23] and others [196, 36, 11] build up a database for artist materials. Further examples for such databeses are those of *Dana et al.* [52, 53, 54] and *Matusik et al.* [175, 178, 177].

The so-called bidirectional reflectance and texture database ($BRTD$) generated in the present study can be downloaded from the homepage (*www.idd.tu-darmstadt.de*) of the *Institute of Printing Science and Technology* (IDD) or requested by an e-mail ($office$@*idd.tu-darmstadt.de*, *doersam*@*idd.tu-darmstadt.de*) to the office or *Prof. Dr.-Ing. Edgar Dörsam.* The $BRTD$ is build up as a hierarchic structure using the numerical computing environment $MATLAB$ of the version $R2010a$. The tree structure consists of seven structure levels with one or two structuring criteria and several structuring cases as shown in figure 6.2 and listed in table 6.2.

Table 6.2: Structure of the $BRTD$.

level	criterion	case	abbreviation
1	printing technology, pigment producer	screen printing technology, pigment producer *BASF SE*	$BASF$
		flexo printing technology, pigment producer *MERCK KGaA*	$MERCK$
2	pigment series, product number	*Black Olive*, *Firemist*, *Glacier*, *Lumina* and *Santa Fe* for *BASF SE*	table 5.3
		Iriodin, *Colorstream* and *Miraval* for *MERCK KGaA*	table 5.4
3	paper quality	black uncoated paper for screen printing	$BUCP$
		white glossy coated paper for screen and flexo printing	$WGCP$
		white matt coated paper for flexo printing	$WMCP$
4	varnishing state	unvarnished surface for screen and flexo printing	UVS
		glossy varnished surface for flexo printing	GVS
5	background color	black paper or printed background for screen printing with $BUCP$ and flexo printing	BPB
		white paper background for screen printing with $WGCP$ and flexo printing	WPB
6	optical instrument	multi-angle spectrophotometer $MA98$ for screen printing	$MA98$
		multi-angle spectrophotometer *BYK-mac* for flexo printing	$BYKmac$
		robot-based gonioreflectomter $ARGon^3$ for flexo printing	$ARGon3$
7	instrument specifications, determined data	wavelength matrix for $MA98$, *BYK-mac* and $ARGon^3$	$LAMBDA$
		geometry matrix for $MA98$, *BYK-mac* and $ARGon^3$	$OMEGA$
		reflectance matrix for $MA98$, *BYK-mac* and $ARGon^3$	R
		color matrix for $MA98$, *BYK-mac* and $ARGon^3$	C
		sparkle matrix for *BYK-mac*	S
		graininess matrix for *BYK-mac*	G

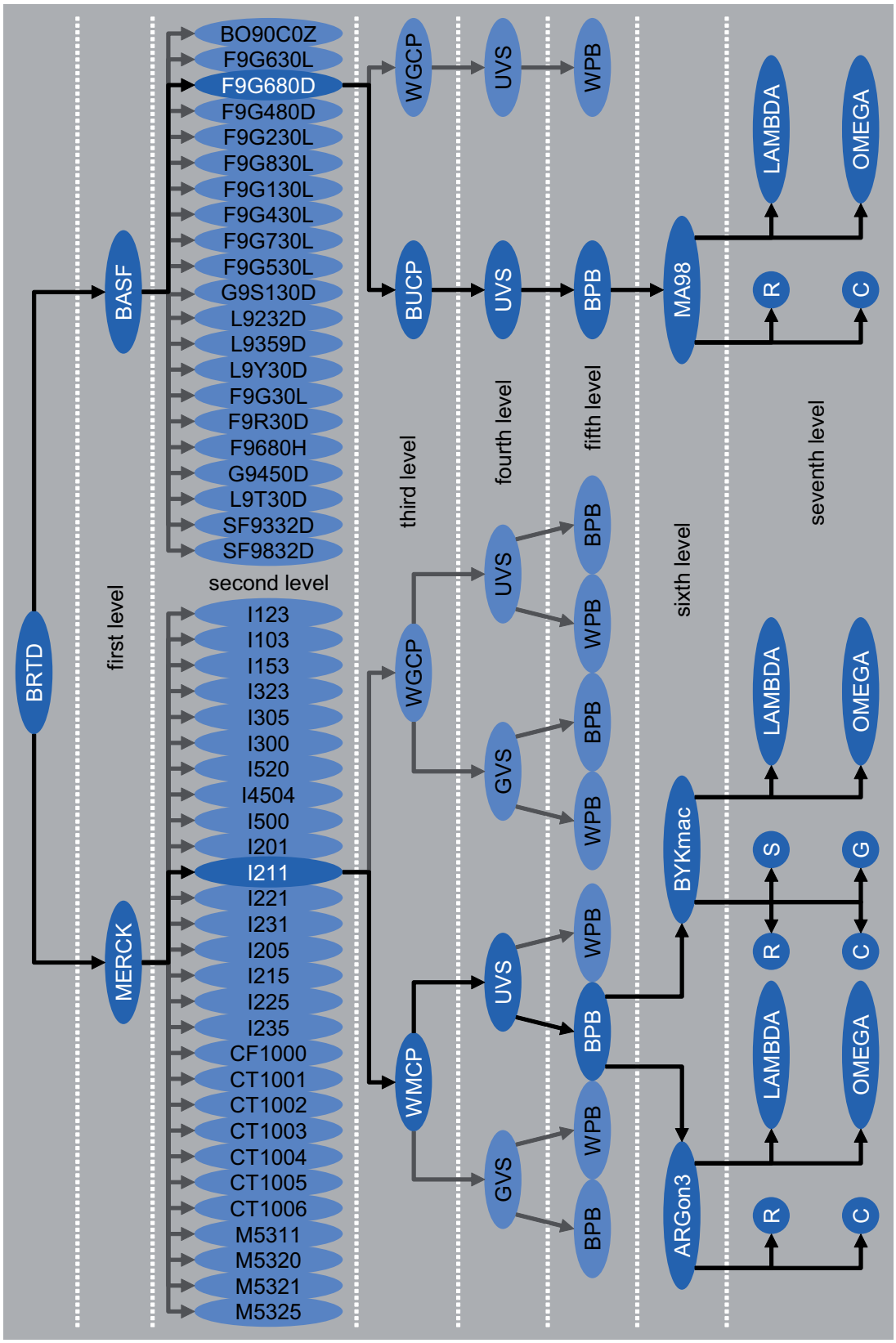

Figure 6.2: Structure of the *BRTD*.

The first structure level has the *printing technology* and the *pigment producer* (section 6.2.1) as structuring criterion. The *pigment series* and the *product number* (section 6.2.2) are specified on the second structure level. The third, fourth and fifth structure level is for the *paper quality* (section 6.2.3), the *varnishing state* (section 6.2.4) and the *background color* (section 6.2.5), respectively. The *optical instrument* (section 6.2.6) is the structuring criterion in the sixth structure level. On the seventh structure level, the *instrument specifications* and the *determined data* (section 6.2.7) are given. In the following, the structure levels and structuring criteria are used to remind the structuring cases and to explain the hierarchical structure of the *BRTD* in more detail.

6.2.1 First Structure Level for Printing Technology and Pigment Producer

The first structure level specifies the printing technology and the pigment producer (figure 6.2, table 6.2). The printing technology is either *screen* or *flexo printing*. The *BASF SE* or the *MERCK KGaA* is the pigment producer. Two combinations were realized in the printing trials described in chapter 5.

First Structure Level for Screen Printing with *BASF* Pigments

The *BASF* pigments were processed in screen printing. Section 5.1.1, section 5.2.1 and section 5.3.1 focuses on the preparation of printing components, the execution of the printing trials and on the identification of the printed samples, respectively.

First Structure Level for Flexo Printing with *MERCK* Pigments

Flexo printing was applied to process the *MERCK* pigments. The preparation of printing components, the execution of the printing trials and the identification of the printed samples are considered in section 5.1.2, section 5.2.2 and section 5.3.2, respectively.

6.2.2 Second Structure Level for Pigment Series and Product Numbers

The second structure level gives information about the pigment series and the product numbers (figure 6.2, table 6.2). These are specific designations of the pigment producers. For the two pigment producers *BASF SE* and *MERCK KGaA*, the pigment series and the product numbers are enlisted separately.

Second Structure Level for *BASF* Pigments

The 22 *BASF* pigments are named with the following pigment series and product numbers. Special effect pigments of the series *Black Olive* (*BO*), *Firemist* (*F*), *Glacier* (*G*), *Lumina* (*L*) and *Santa Fe* (*SF*) were used in this study (section 5.1.1, table A.1, table A.2, table A.3, table A.4). The ink code given in table 5.1 without the abbreviation of the pigment series is equal to the product number. This alphanumeric product number includes information about the substrate material, the interference color, the coating material, the absorption color, the surface treatment and the particle size.

Second Structure Level for *MERCK* Pigments

The pigment series and product numbers of the 28 *MERCK* pigments are the following ones. This study includes special effect pigments of the series *Iriodin* (*I*), *Colorstream* (*C*) and *Miraval* (*M*) (section 5.1.2, table A.5, table A.6, table A.7, table A.8). In table 5.2, the ink code consists of the abbreviation of the pigment series and the product number. Thus, the product number is a three-digit or four-digit number.

6.2.3 Third Structure Level for Paper Quality

On the third structure level, the structuring criterion is the paper quality (section 5.1, table B.1, table B.2). According to their quality, the used papers can be roughly described in the following way (table 5.3, table 5.4). Two white glossy coated papers ($WGCP$), a white matte coated paper ($WMCP$) and a black uncoated paper ($BUCP$) were used (figure 6.2, table 6.2).

In the screen printing trials described in section 5.1.1, a white glossy coated paper ($WGCP$) and a black uncoated paper ($BUCP$) were printed (table 5.3, table B.1).

As described in section 5.1.2 on the flexo printing trials, a white glossy coated paper ($WGCP$) and a white matte coated paper ($WMCP$) were used (table 5.4, table B.2).

6.2.4 Fourth Structure Level for Varnishing State

The varnishing state mentioned in section 5.2.2 and section 5.3.2 also serves as a structuring criterion (figure 6.2, table 6.2). On the fourth structure level, reflectance data for printing samples (table 5.4) with an unvarnished surface (UVS) are separated from those for samples with a glossy varnished surface (GVS). An unvarnished surface is existent for all screen printing samples and the half of the flexo printing samples. The other half of the flexo printing samples have a glossy varnished surface.

6.2.5 Fifth Structure Level for Background Color

On the fifth structure level, the background color mentioned in section 5.2.2 and section 5.3.2 is the structuring criterion (figure 6.2, table 6.2). The structuring cases include a white paper background (WPB), a black paper background (BPB) and a black printed background (BPB). The white paper background occurs for the white glossy coated paper in the screen printing sample set and for both papers in the flexo printing sample set (table 5.4). For the black uncoated paper in the screen printing sample set, the structuring case is always the black paper background. The black printed background occurs for both papers in the flexo printing sample set (table 5.4).

6.2.6 Sixth Structure Level for Optical Instrument

The optical instrument (section 3.2.3) used in the bidirectional measurement of the printed samples (section 6.1) is the structuring criterion on the sixth structure level (figure 6.2, table 6.2). The respective structuring cases are the multi-angle spectrophotometers $MA98$ and $BYK\text{-}mac$ (section 6.1.1) as well as the robot-based gonioreflectometer $ARGon^3$ (section 6.1.2).

6.2.7 Seventh Structure Level for Instrument Specifications and Determined Data

The seventh structure level separates the *instrument specifications* from the *determined data* (figure 6.2, table 6.2). These two structuring criteria and their structuring cases are treated in the following.

Seventh Structure Level for Instrument Specifications

The instrument specifications concern the spectral properties and the geometric configurations of the just mentioned optical instruments. The *wavelength* and *geometry specifications* are subsequently given.

Seventh Structure Level for Wavelength Specifications The instrument's spectral properties are specified by means of the wavelength range and the wavelength resolution. Both wavelength specifications are included in a 1-by-n_{LAMBDA} wavelength matrix called $LAMBDA$. The variable n_{LAMBDA} stands for the number of spectral measuring points being specific for each optical instrument.

The multi-angle spectrophotometer $MA98$ (section 3.2.3, section 6.1.1) detects the spectral reflectance in the wavelength range from 400 nm to 700 nm with a resolution of 10 nm. Thus, the associated wavelength matrix $LAMBDA$ is a 1-by-31 matrix.

For the multi-angle spectrophotometer *BYK-mac* (section 3.2.3, section 6.1.1), the wavelength matrix $LAMBDA$ is a 1-by-35 matrix. The spectral reflectance is detected in a wavelength range from 380 nm to 720 nm with a resolution of 10 nm.

With the robot-based gonioreflectometer $ARGon^3$ (section 3.2.3, section 6.1.2), the spectral reflectance was determined in a wavelength range from 363 nm to 848 nm with a resolution of 1 nm. This results in a 1-by-486 matrix as wavelength matrix $LAMBDA$.

Seventh Structure Level for Geometry Specifications The instrument's geometric configurations are specified by the use of the incidence and reflection direction introduced in section 3.1.3. As described in section 3.2.2, the direction of incidence and reflection is specified by the angles of illumination and detection, respectively. In a spherical coordinate system, the incidence and reflection angles each include the polar and azimuth angle. The incidence polar angle θ_i, the incidence azimuth angle ϕ_i, the reflection polar angle θ_r and the reflection azimuth angle ϕ_r are sufficient to describe the direction of incidence and reflection. The reflection direction of commercial multi-angle instruments is usually specified by means of the in-plane aspect angle θ_{as} and the at-specular aspect angle ϕ_{az}. Depending on whether it is a commercial multi-angle instrument or not, all six or just four angles are given in the m_{OMEGA}-by-n_{OMEGA} geometry matrix called $OMEGA$. The variables m_{OMEGA} and n_{OMEGA} correspond to the number of geometric configurations and to the number of specified angles, respectively.

In case of the commercial multi-angle spectrophotometer $MA98$, the geometry matrix $OMEGA$ is a 19-by-6 matrix. A number of 19 geometric configurations is realized in the instrumental setup as treated in section 3.2.3, section 6.1.1 and table C.1. In the just enlisted sequence, all six angles are given.

All six angles in the above enlisted sequence are also given for the multi-angle spectrophotometer *BYK-mac*. The spectral reflectance is measured in six geometric configurations enlisted in section 3.2.3, section 6.1.1 and table C.2. The geometry matrix $OMEGA$ is a 6-by-6 matrix.

The robot-based goniorflectometer $ARGon^3$ measures the spectral reflectance in an arbitrary number of geometric configurations as described in section 3.2.3. According to section 6.1.2 and table C.3, measurements in 270 geometric configurations were realized. For a fixed incidence direction, the reflection directions are evenly distributed in a half of the half space above the sample. Due to the complete geometric description with four angles, the geometry matrix $OMEGA$ is a 270-by-4 matrix.

Seventh Structure Level for Determined Data

The determined data include detected as well as calculated data. The detected data are reflectance spectra. The reflectance spectra were used to calculate color coordinates. Further calculated data are texture attributes based on imaging measurements. In the following, further information is given about the *detected reflectance spectra* as well as about the *calculated color coordinates* and the *calculated texture parameters*.

Seventh Structure Level for Detected Reflectance Spectra With all just mentioned instruments (section 3.2.3), the spectral reflectance was detected. The spectral reflectance is given as an m_R-by-n_R reflectance matrix R. The variables m_R and n_R indicate the number of geometric configurations and the number of spectral measuring points.

In the multi-angle spectrophotometer $MA98$ (section 6.1.1), 19 geometric configurations are realized. With a number of 31 spectral measuring points, the reflectance matrix R is a 19-by-31 matrix.

For the multi-angle spectrophotometer *BYK-mac* (section 6.1.1), the reflectance matrix R is a 6-by-35 matrix. The spectral measurements are performed in six geometric configurations and at 35 spectral measuring points.

With the robot-based gonioreflectometer *ARGon*^{3} (section 6.1.2), the spectral reflectance was detected in 270 geometric configurations. For 486 spectral measuring points, the reflectance matrix R is a 270-by-486 matrix.

Seventh Structure Level for Calculated Color Coordinates The color coordinates were calculated for the standard illuminant $D65$ and the 10° standard observer in the $CIELAB$ and $CIELCH$ color space. For both color spaces, one of the calculated color coordinates is the lightness L^*. The redness-greenness value a^* and the yellowness-blueness value b^* are the other color coordinates in the $CIELAB$ color space. In the $CIELCH$ color space, the other color coordinates are the chroma C^* and the hue angle $h°$. In the given sequence, these five color coordinates are combined in an m_C-by-5 color matrix C. The value m_C is equal to the instrument-specific number of geometric configurations.

In case of the multi-angle spectrophotometer $MA98$ (section 3.2.3, section 6.1.1), the color matrix C is a 19-by-5 matrix. For 19 geometric configurations, all five calculated color coordinates are given.

The color matrix C for the multi-angle spectrophotometer *BYK-mac* (section 3.2.3, section 6.1.1) is a 6-by-5 matrix. The five calculated color coordinates are given for all six realized geometric configurations.

The robot-based gonioreflectometer *ARGon*^{3} (section 3.2.3, section 6.1.2) was used to measure in 270 geometric configurations. Thus, the color matrix C is a 270-by-5 matrix containing all five color coordinates.

Seventh Structure Level for Calculated Texture Parameters Apart from the spectral detection system, the multi-angle spectrophotometer *BYK-mac* is equipped with an imaging detection system (section 3.2.3, section 6.1.1). On the basis of the spatial measurements, the instrument calculates texture parameters for *sparkle* and *graininess*.

Seventh Structure Level for Calculated Sparkle Parameters Three sparkle parameters are calculated on the basis of imaging measurements in three bidirectional geometries. These are the 15°/0°, 45°/0° and the 75°/0° geometry. The sparkle area S_A, the sparkle intensity S_I and the sparkle grade S_G are the three sparkle parameters (section 4.1.3). The calculated values are enlisted in a 3-by-3 sparkle matrix S. In the just given sequence, the geometric configuration and the sparkle parameter varies over the row and columns, respectively.

Seventh Structure Level for Calculated Graininess As described in section 3.2.3 and section 6.1.1, the texture parameter graininess G is based on an imaging measurement in the diffuse geometry $d/0°$. The diffuse illumination is realized by means of an integrating sphere. The imaging detection system is located perpendicular to the sample surface.

6.3 Influence of the Printing Parameters

We would like to know the influence of all printing parameters on the optical properties and so also on the visual appearance of printed special effect colors. The printing parameters are at least the particle size and the material composition of the special effect pigment, the roughness and porosity of the substrate, the background color, the varnishing state and the pigment occupancy (section 2.2.2). All optical properties are included in the spatially-varying bidirectional reflectance distribution (section 3.1.3). The visual appearance is described by multiple attributes for color, gloss and texture, such as the hue, chroma, lightness, hue shift, lightness shift, contrast gloss, distinctness-of-image gloss, texture contrast, sparkle, glint, graininess and coarseness (section 4.1).

The complete evaluation of all influencing factors is not possible due to the following reasons. The number and variability of the printing parameters is too high. The spatially-varying bidirectional reflectance distribution is not available as physically plausible model. The number and nature of the essential visual appearance attributes is widely unknown for printed special effect colors. Psychophysical equations are only known for some visual appearance attributes.

Some restrictions with regard to extent and feasibility are necessary. The set of printing parameters should be reduced to the representative ones. Instead of a bidirectional reflectance model, measured bidirectional reflectance and texture data can be used. Among the visual appearance attributes, only the most important ones should be considered. The visual appearance attributes can be represented by perception-related parameters.

This evaluation about the influencing factors covers the following printing parameters, bidirectional reflectance and texture data and perception-related parameters. The printing parameters are the special effect pigments, the paper quality, the background color and the varnishing state (section 5.1, section 5.2, section 5.3). Due to the great variety of 224 application cases, the flexo printing samples are preferred over the screen printing samples. The flexo printing samples were optically measured with the multi-angle spectrophotometer *BYK-mac* (section 3.2.3, section 6.1.1). The preference of the multi-angle spectrophotometer *BYK-mac* over the multi-angle spectrophotometer $MA98$ is justified by the additional determination of texture parameters. The color coordinates and texture parameters filed in the $BRTD$ (section 6.2) are used to determine the hue difference sum, lightness difference sum, relative luminance difference, sparkle and the graininess. The influence on these perception-related parameters for the appearance of *color* (section 6.3.1), *gloss* (section 6.3.2) and *texture* (section 6.3.3) is presented in the following.

6.3.1 Influence on Color Parameters

At first, the influence on color parameters is evaluated. Section 4.1.1 introduces a series of color attributes. Among the introduced color attributes, the geometry-dependent color is described by the color shift, angular hue shift, hue shift, chroma shift and by the lightness shift. The hue shift and the lightness shift are perceptually most important. Therefore, the influence on the *hue difference sum* and the *lightness difference sum* is evaluated in the following.

Influence on Hue Difference Sum

The visually unique appearance of the geometry-dependent color can be described by the angular hue shift or by the hue shift. As explained in section 4.1.1, the perceived angular hue shift and hue shift are assumed to be representable by the angular hue difference sum ($AHDS$) and hue difference sum (HDS) [145], respectively. For the following evaluations about the influence of the printing parameters, the HDS is preferred over the $AHDS$. The $AHDS$ is given in the angular units degrees ($^\circ$) or radians (rad). In contrast to this, the HDS sum is given in unit lengths of the $CIELAB$ or $CIELCH$ color space. The interpretation of $CIELAB$ or $CIELCH$ unit lengths is easier due to the well-known color difference. The definition of the HDS as the sum over the hue differences between color coordinates of different geometric configurations is given in equation 4.17.

For the considered flexo printing samples measured with the multi-angle spectrophotometer *BYK-mac*, the number of geometric configurations is six. As an illustrative example, the associated color coordinates of an arbitrary sample are plotted in the equivalent color spaces *CIELAB* and *CIELCH*. Its projection on the a^*b^* plane shown in figure 6.3 is used to explain the calculation of the *HDS*.

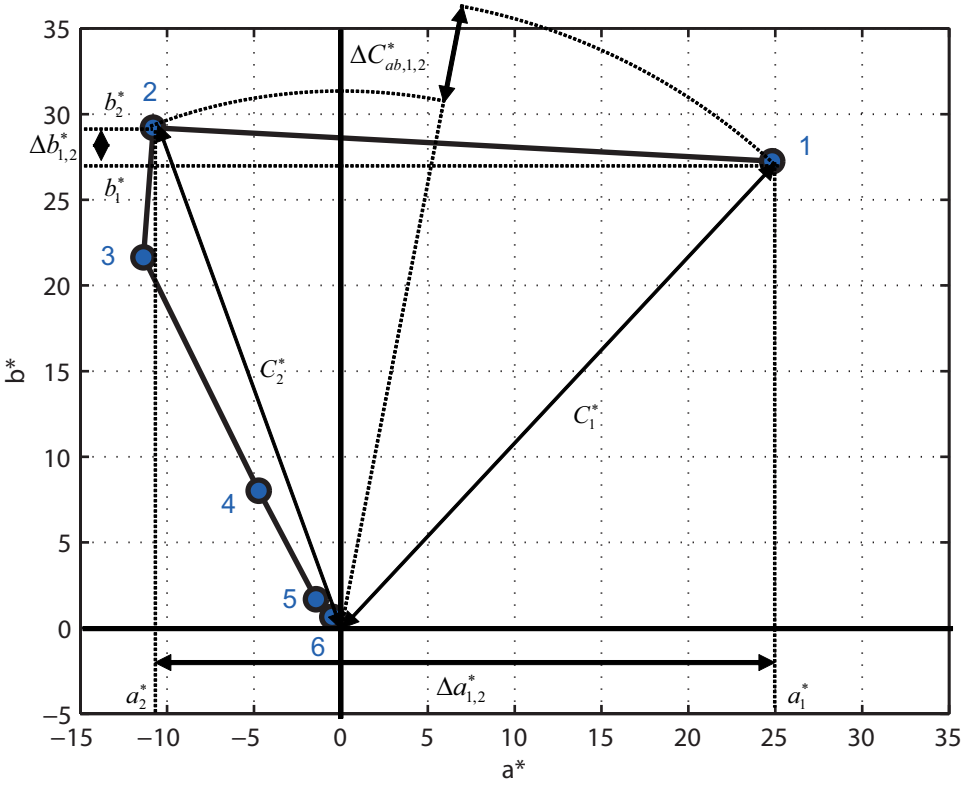

Figure 6.3: Calculation of the *HDS*.

For the calculation of the hue difference sum $\Delta H^*_{ab,1,6}$, the five inter-geometry hue differences $\Delta H^*_{ab,i,j}$ with i between one and five and j between two and six should be determined. The determination of the hue differences $\Delta H^*_{ab,i,j}$ is realized by means of equation 4.19 on the basis of the greenness-redness difference $\Delta a^*_{i,j}$, the blueness-yellowness difference $\Delta b^*_{i,j}$ and the chroma difference $\Delta C^*_{ab,i,j}$.

These three differences are calculated according to equation 4.11, equation 4.12 and equation 4.20 by using the greenness-redness value a^*_i and a^*_j, the blueness-yellowness value b^*_i and b^*_j as well as the chroma $C^*_{ab,i}$ and $C^*_{ab,j}$. These color data are filed in the generated *BRTD* for the six geometric configurations 45*as*-15, 45*as*15, 45*as*25, 45*as*45, 45*as*75 and 45*as*110.

For every application case, the just described procedure was passed through to calculate the *HDS* for any combination of the varied printing parameters. The influence of the *special effect pigment*, the *paper quality*, the *varnishing state* and the *background color* on the *HDS* is subsequently evaluated in detail.

Influence of Special Effect Pigment on Hue Difference Sum The *HDS* is assumed to be influenced by the special effect pigment (section 2.1.1, section 2.1.3). For the silver white (*SW*), gold (*G*), iron oxide (*IO*) and sparkle (*S*) pigments, the *HDS* is expected to be low compared to the other special effect pigments. A somehow higher *HDS* is suspected for the interference

effect (IE) pigments. For the multi-color (MC) pigments, the HDS is expected to be the highest among the investigated special effect pigments. The designations of the pigment classes are the basis of these assumptions (section 2.1.3). The assumptions are verified by means of figure 6.4.

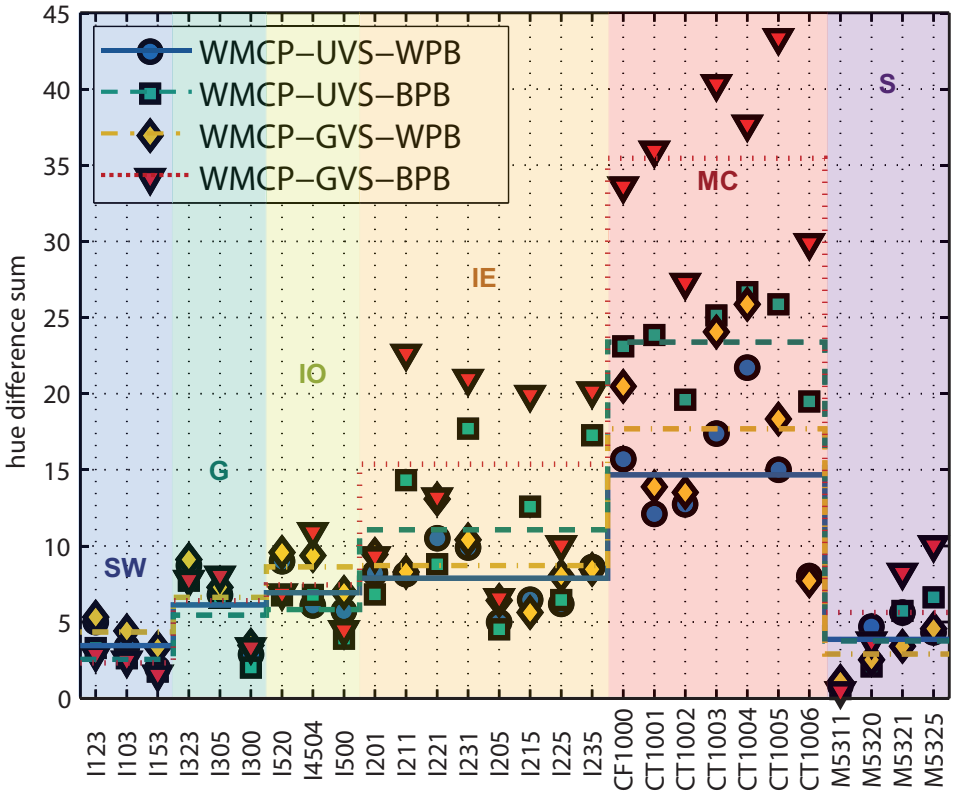

Figure 6.4: HDS of flexo printing samples for all application cases (table 5.4, table 6.2) with white matt coated paper ($WMCP$) [145].

For all application cases with the white matt coated paper ($WMCP$), figure 6.4 shows the HDS for the individual pigment types as well as the mean of the HDS for the different pigment classes. The HDS of the individual pigments is indicated by the data points. The stairs curves indicate the mean class HDS.

In comparison with the other pigment classes, the mean class HDS is low for the silver white (SW), gold (G), iron oxide (IO) and the sparkle (S) pigments. For the interference effect (IE) pigments, the mean class HDS is slightly higher. Among all pigment classes, the mean class HDS of the multi-color (MC) pigments is maximal.

The significant dependence of the HDS on the pigment class (section 2.1.3, table A.5) is caused by differences in the choice and combination of the pigment's substrate material (table A.7) with one or more coating materials (table A.8). The refractive indices of the substrate material and the coating materials as well as the number and thickness of the high-refractive coating layers have an influence on the character and strength of the optical effect of thin-layer interference (section 2.1.2, section 2.1.3). A pronounced interference effect is responsible for a high determined HDS or a high perceived hue shift.

For a global consideration of the influence of all other printing parameters, the mean of the HDS over all 28 special effect pigments is calculated. The mean HDS is shown in figure 6.5 for all combinations of paper quality, varnishing state and background color.

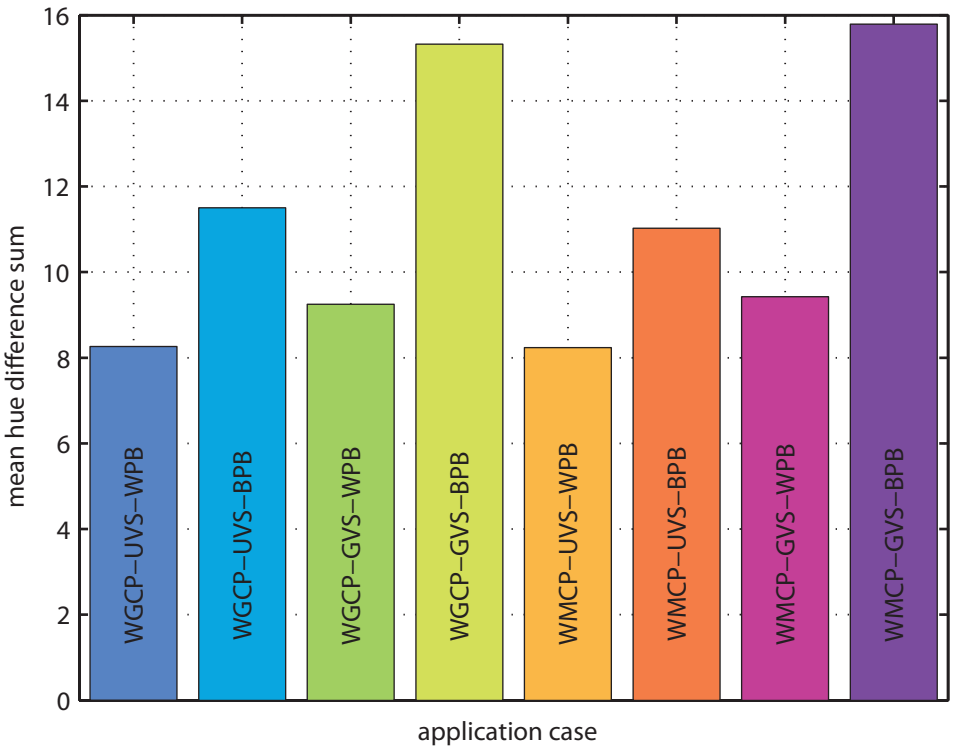

Figure 6.5: Mean HDS of flexo printing samples for all application cases (table 5.4, table 6.2) differing in paper quality (white glossy coated paper ($WGCP$), white matt coated paper ($WMCP$)), varnishing state (unvarnished surface (UVS), glossy varnished surface (GVS)) and background color (white paper background (WPB), black printed background (BPB)).

Influence of Paper Quality on Hue Difference Sum On the basis of experiences gained in preliminary tests, it is expected that the paper quality has an influence on the HDS (section 2.2.2). For the white glossy coated paper, the HDS is assumed to be higher than for the white matt coated paper. The mean HDS shown in figure 6.5 is used for the verification of this expectation.

The mean $HDSs$ for the white glossy coated paper ($WGCP$) are comparable to the mean $HDSs$ for the white matt coated paper ($WMCP$). Against the above assumption, the paper quality has no significant influence on the HDS.

The reason for insignificant influence of the paper quality on the HDS must be the comparably small differences in the roughness and porosity of both papers (section 2.2.2). The selection of the papers is a compromise between highest possible differences in the substrate properties and the most realistic representation of industrial applications.

Influence of Varnishing State on Hue Difference Sum The influence of the varnishing state on the HDS is assumed to be negligible (section 2.2.2). This assumption is checked by means of figure 6.4 showing the HDS and the mean class HDS and by means of figure 6.5 showing the mean HDS.

In figure 6.4, the $HDSs$ and mean class $HDSs$ for the unvarnished surface (UVS) are lower than those for the glossy varnished surface (GVS). Compared to the unvarnished surface (UVS), the mean $HDSs$ for the glossy varnished surface (GVS) in figure 6.5 are higher, too.

Against the expectation (section 2.2.2), the varnishing state has an influence on the HDS. The rather small differences must be caused by the following difference between the unvarnished and the glossy varnished surface.

In case of the unvarnished surface, the flaky pigments stick out of the ink layer to some extent. Apart from the pigment substrate and the binder matrix, the ambient air forms a boundary with the high-refractive coating layer. For the air-coating boundary, the difference in the indexes of refraction is very high. The difference in the indexes of refraction is very high is medium high for the substrate-coating and the binder-coating boundary. Very and medium high differences in the refraction index result in different interference effect colors. In consideration of the number of boundaries for the different material combinations, the intense interference effect color induced by the medium high refraction index difference is influenced by the interference effect color induced by the very high refraction index difference.

For the glossy varnished surface, the pigments are completely embedded in the ink layer and under the varnishing layer. Instead of the ambient air, the high-refractive coating layer forms a boundary with the varnishing layer. As for the substrate-coating and the binder-coating boundary, the difference in the refraction indexes for the varnish-coating boundary is medium high. The always medium high difference in the index of refraction induces a specific interference effect color. This intense interference effect color is not influenced resulting in a high HDS.

Influence of Background Color on Hue Difference Sum The expectation about the influence of the background color on the HDS is the following (section 2.2.2). For the white paper background, the HDS is expected to be lower than for the black printed background. The influence of the background color on the HDS is evaluated by means of figure 6.4 and figure 6.5.

Figure 6.4 shows significantly lower $HDSs$ and mean class $HDSs$ in case of the white paper background (WPB). In accordance with this, the mean HDS in figure 6.5 are significantly higher for the black printed background (BPB).

This finding is compatible with the above assumption. The reason for the significant influence of the background color on the HDS is the scattering and absorption of the white paper and black printed background, respectively (section 2.2.2).

Influence on Lightness Difference Sum

As a measure for the perceived lightness shift, the lightness difference sum (LDS) explained in section 4.1.1 can be used. According to equation 4.22, the lightness difference sum $\Delta L^*_{1,N}$ is defined as the sum of the absolute lightness differences $\Delta L^*_{i,i+1}$ between the lightness L^*_i and L^*_{i+1}. The

index i and $i+1$ specifying different geometric configurations ranges from one to $N-1$ and from two to N, respectively.

In the present case, the geometric configurations are those realized in the multi-angle spectrophotometer *BYK-mac* used for the measurements on the flexo printing samples. For the six geometric configurations $45as$-15, $45as15$, $45as25$, $45as45$, $45as75$ and $45as110$, the generated $BRTD$ provides the lightness L_i^* with i between one and six. The lightness L_i^* and L_j^* with i between one and five and j between two and six are used to calculate the lightness difference according to equation 4.10. The five lightness differences $\Delta L_{i,j}^*$ with i between one and five and j between two and six are summed up to yield the lightness difference sum $\Delta L_{1,6}^*$.

On the depicted way, the LDS is determined for all applications cases combining a *special effect pigment* with a *paper quality*, a *varnishing state* and a *background color*. In the following, the influence of the varied printing parameters on the LDS is highlighted.

Influence of Special Effect Pigment on Lightness Difference Sum It is assumed that the special effect pigment has no significant influence on the LDS (section 2.1.1, section 2.1.3). This assumption is checked by means of figure 6.6 showing the LDS for all application cases with the white glossy coated paper ($WGCP$).

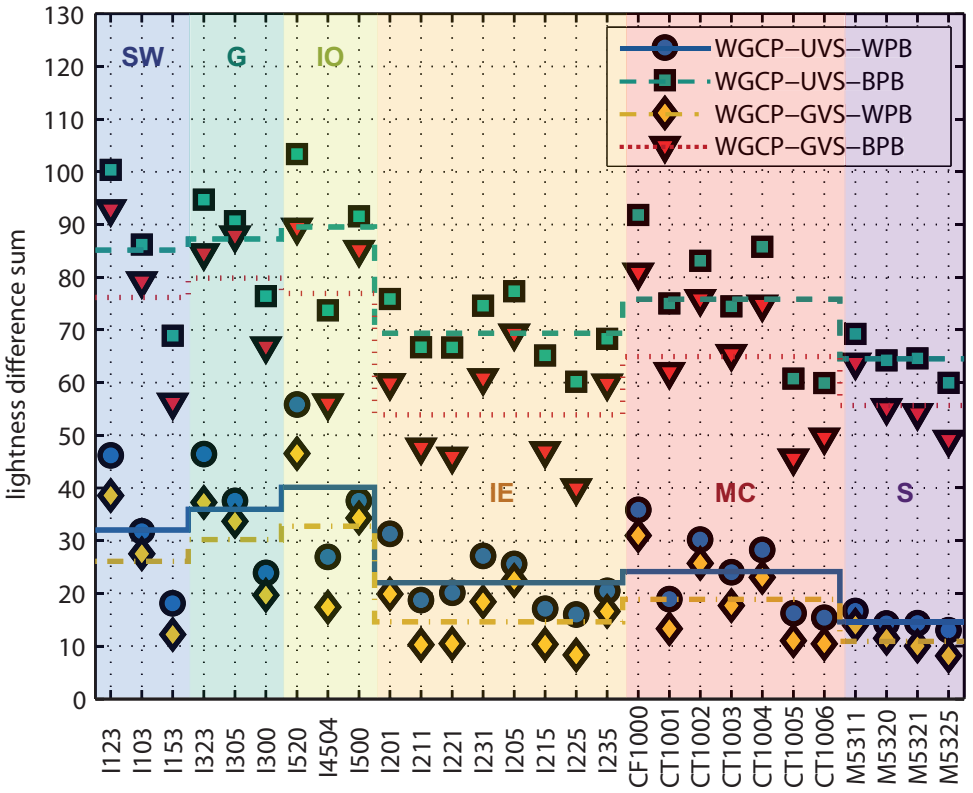

Figure 6.6: LDS of flexo printing samples for all application cases (table 5.4, table 6.2) with white glossy coated paper ($WGCP$).

In addition to the LDS for the individual pigment types, figure 6.6 shows the mean of the LDS over the special effect pigments of the different pigment classes. A mean class LDS for the pigment classes is represented by a stairs curve.

Among the pigment classes, the mean class LDS is rather low for the interference effect (IE), multi-color (MC) and the sparkle (S) pigments (figure 6.6). For the silver white (SW), gold (G)

and iron oxide (IO) pigments, the mean class LDS is rather high compared to the other pigment classes.

The mean of the LDS over all 28 special effect pigments is calculated for a global evaluation about the influence of the other printing parameters. Figure 6.7 shows the mean LDS for all application cases varying in paper quality, varnishing state and background color.

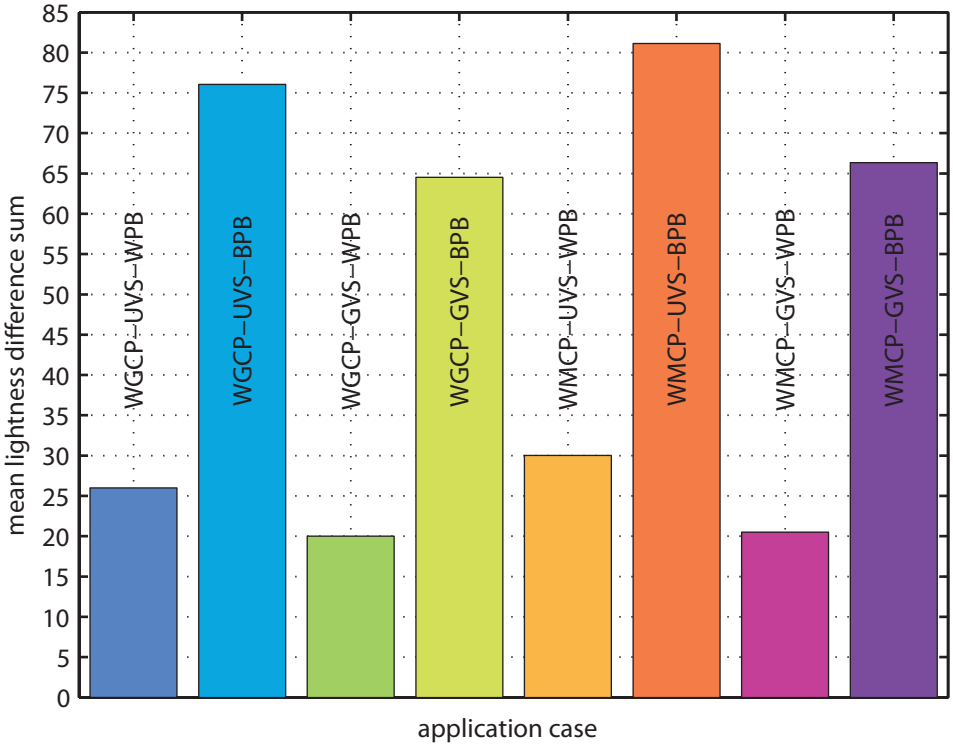

Figure 6.7: Mean LDS of flexo printing samples for all application cases (table 5.4, table 6.2) differing in paper quality (white glossy coated paper ($WGCP$), white matt coated paper ($WMCP$)), varnishing state (unvarnished surface (UVS), glossy varnished surface (GVS)) and background color (white paper background (WPB), black printed background (BPB)).

Influence of Paper Quality on Lightness Difference Sum The LDS for the white glossy coated paper is expected to be slightly higher than the LDS for the white matt coated paper (section 2.2.2). This influence of the paper quality on the LDS is assumed to be negligible.

As shown in figure 6.7, the influence of the paper quality on the LDS depends on the varnishing state. For the unvarnished surface (UVS), the mean $LDSs$ of the white glossy coated paper ($WGCP$) are somehow lower than the corresponding mean $LDSs$ of the white matt coated paper ($WMCP$). In case of the glossy varnished surface (GVS), the mean $LDSs$ for both paper qualities is almost equal.

Both findings are against the just given expectation (section 2.2.2). Without varnishing the surface, a white glossy coated paper ($WGCP$) results in a lower LDS than a white matt coated paper ($WMCP$). The described effect is masked by means of an additional varnish layer on the ink layer. Probably, the LDS is not the appropriate parameter to represent the perceived lightness shift. Instead of the parameter itself, the geometric configurations considered in the determination are insufficient. The geometric configurations realized in the multi-angle spectrophotometer BYK-

mac do not include a specular geometry.

Influence of Varnishing State on Lightness Difference Sum For the unvarnished surface, the LDS is assumed to be lower than for the glossy varnished surface (section 2.2.2). To check this perception-based assumption, figure 6.6 showing the LDS and the mean class LDS as well as figure 6.7 showing the mean LDS are consulted.

In figure 6.6, the LDSs and the mean class LDSs for the unvarnished surface (UVS) are higher than the respective ones for the glossy varnished surface (GVS). The mean LDS in figure 6.7 show the same influence of the varnishing state on the mean LDS.

This result is against the perception-based expectation (section 2.2.2). The LDS seems to be inappropriate to represent the perceived lightness shift. In more detail, the geometric configurations used in the determination are not sufficient. A specular geometry is missing in the assortment of geometric configurations realized in the multi-angle spectrophotometer *BYK-mac*.

Influence of Background Color on Lightness Difference Sum It is expected that the lightness difference sum is lower for the white paper background and higher for the black printed background (section 2.2.2). Figure 6.6 and figure 6.7 are used to check this expectation.

The LDS and the mean class LDS shown in figure 6.6 are lower for the white paper background (WPB). To the same extent, the mean LDS is higher for the black printed background (BPB) as shown in figure 6.7.

This finding corresponds to the assumption given above (section 2.2.2). Due to the high lightness difference between the specular highlight and the surrounding, the background color has a significant influence on the LDS.

6.3.2 Influence on Gloss Parameter

In the following, the influence on the metal to pearlescent gloss of printed special effect colors is evaluated. Several gloss attributes are defined in section 4.1.2. Basing on the study of *Pellacini et al.* [200] and *Ferwerda et al.* [80], the contrast gloss (CG) and distinctness-of-image gloss ($DOIG$) are expected to be essential for the characterization of the visual appearance of printed special effect colors. These gloss attributes can be represented by the contrast gloss (CG) parameter P_{CG} and distinctness-of-image gloss ($DOIG$) parameter P_{DOIG} basing on the standard practice *ASTM E* 284-03*a* [8] and *ASTM D* 5767-95 [5], respectively.

The parameters P_{CG} and P_{DOIG} for contrast gloss (CG) and distinctness-of-image gloss ($DOIG$) are defined in equation 4.23 and equation 4.24, respectively. The definitions include the far-from-gloss luminance Y_{FFG}, the near-at-gloss luminance Y_{NAG} and the gloss luminance Y_G. In contrast to the far-from-gloss luminance Y_{FFG} and the near-at-gloss luminance Y_{NAG}, the gloss luminance Y_G is not available from the $BRTD$. The multi-angle spectrophotometer *BYK-mac* is not equipped with a detection system in specular direction.

Instead of the contrast gloss (CG) parameter and the distinctness-of-image gloss ($DOIG$) parameter, an alternative gloss parameter called relative luminance difference (RYD) is used to evaluate the influence of the printing parameters. The calculation of the RYD is explained by means of figure 6.8.

In this polar plot, the angular coordinate indicates the aspecular angle. The radius vector specifies the determined luminance. According to *Kehren et al.* [145], equation 6.1 defines the relative luminance difference ΔY_r on the basis of the available far-from-gloss (FFG) luminance Y_{FFG} and the available near-at-gloss (NAG) luminance Y_{NAG}.

$$\Delta Y_{r,FFG,NAG} = \frac{(Y_{NAG} - Y_{FFG})}{Y_{NAG}} = 1 - \frac{Y_{FFG}}{Y_{NAG}} \tag{6.1}$$

The far-from-gloss luminance Y_{FFG} is set equal to the lower value of the luminance Y_{45as75} and $Y_{45as110}$ for the geometric configurations $45as75$ and $45as110$. The higher value of the luminance $Y_{45as-15}$ and Y_{45as15} for the geometric configurations $45as$-15 and $45as15$ is set equal to the

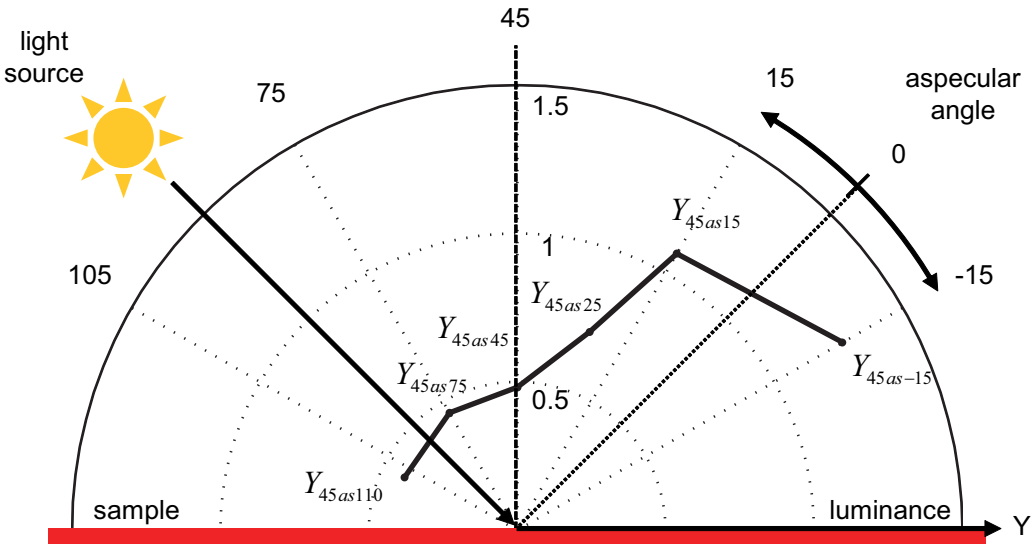

Figure 6.8: Calculation of the RYD.

near-at-gloss luminance Y_{NAG}. These definitions of the far-from-gloss luminance Y_{FFG} and the near-at-gloss luminance Y_{NAG} are expressed mathematically in equation 6.2 and in equation 6.3, respectively.

$$Y_{FFG} = min\left(Y_{45as75}, Y_{45as110}\right) \tag{6.2}$$

$$Y_{NAG} = max\left(Y_{45as-15}, Y_{45as15}\right) \tag{6.3}$$

The geometry-dependent luminance $Y_{45as\Theta_{as}}$ for in-plane aspect angles Θ_{as} of $-15°$, $15°$, $75°$ and $110°$ can be calculated from the corresponding lightness $L^*_{45as\Theta_{as}}$ filed in the $BRTD$. The transformation of equation 4.5 for the lightness L^* results in equation 6.4 for the luminance Y.

$$Y = Y_n \cdot f^{-1}\left(\frac{1}{116} \cdot (L^* + 16)\right) \tag{6.4}$$

The symbol Y_n specifies the normalization luminance for the given set of standard illuminant and standard observer. The case distinction function f given in equation 4.4 is transformed to the inverse case distinction function f^{-1} given in equation 6.5.

$$f^{-1}(q) = \begin{cases} 3 \cdot \left(\frac{26}{29}\right)^2 \cdot \left(q - \frac{4}{29}\right) & \text{if} \quad q \leq \frac{6}{29} \\ q^3 & \text{if} \quad q > \frac{6}{29} \end{cases} \quad \text{with } q = \frac{X}{X_n}, \frac{Y}{Y_n}, \frac{Z}{Z_n} \tag{6.5}$$

The inverse case distinction function f^{-1} (equation 6.5) is inserted in the formula for the luminance Y (equation 6.4). This insertion results in equation 6.6.

$$Y = \begin{cases} Y_n \cdot \frac{3}{116} \cdot \left(\frac{6}{29}\right)^2 \cdot L^* & \text{if} \quad L^* \leq 8 \\ Y_n \cdot \left(\frac{1}{116} \cdot (L^* + 16)\right)^3 & \text{if} \quad L^* > 8 \end{cases} \tag{6.6}$$

By the use of equation 6.1, equation 6.2, equation 6.3 and equation 6.6, the RYD was determined for all application cases differing in the printing parameters. The influence of the *special effect pigment*, the *paper quality*, the *varnishing state* and the *background color* on the RYD is subsequently considered in detail.

Influence of Special Effect Pigment on Relative Luminance Difference

As in case of the above considered LDS, the RYD is not assumed to be significantly influenced by the special effect pigment (section 2.1.1, section 2.1.3). This assumption is checked by means of figure 6.9 and figure 6.10.

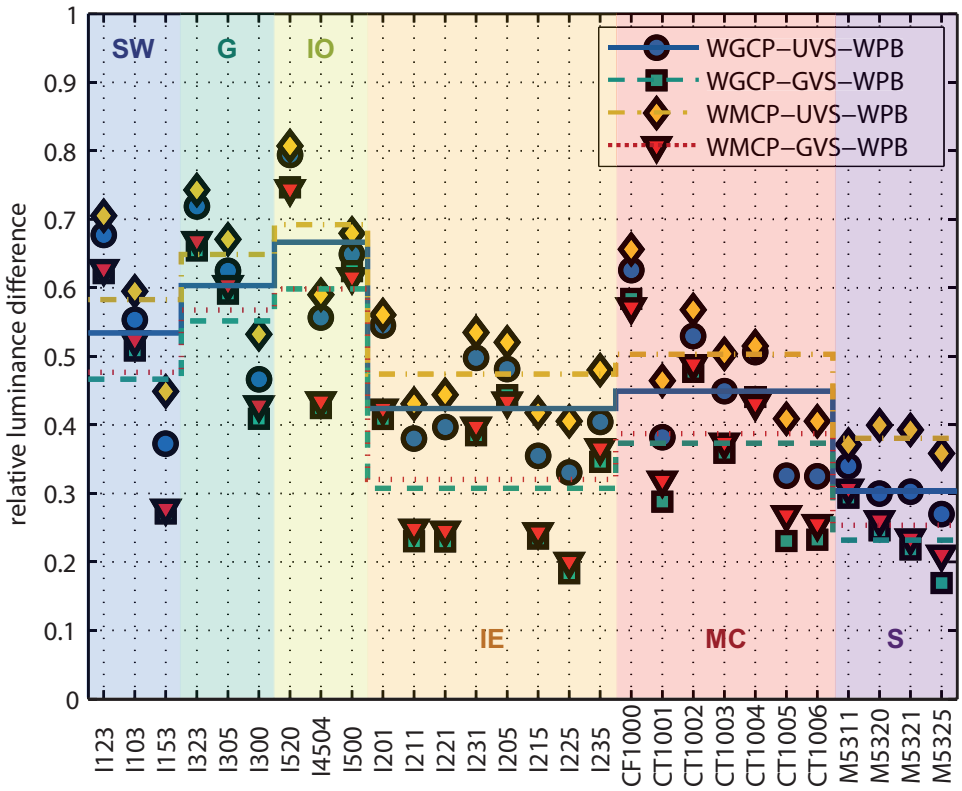

Figure 6.9: RYD of flexo printing samples for all application cases (table 5.4, table 6.2) with white printed background (WPB) [145].

Figure 6.9 and figure 6.10 show the RYD for all application cases with the white paper background (WPB) and the black printed background (BPB), respectively. The data points show the RYD of the individual pigment types. The individual $RYDs$ were averaged over the special effect pigments belonging to the same pigment class. The mean class $RYDs$ are represented by a stairs curve.

Per definition (equation 6.1), the RYD can take values between zero and one. For the white paper background (WPB, figure 6.9), the RYD and the mean class RYD cover a wide range from 0.169 to 0.807 and from 0.232 to 0.692, respectively, around the center of the defined range. In contrast to that, the RYD and the mean class RYD are in a small range from 0.929 to 0.993 and from 0.953 to 0.991, respectively, at the upper end of the defined range for the black printed background (BPB, figure 6.10). The significant dependence of the RYD on the background color is even visible in the influence of the special effect pigments on the RYD. The influence of the special effect pigment is therefore described separately for both background colors.

In case of the white paper background (WPB, figure 6.9), the mean class RYD increases from a comparably low level for the sparkle (S) pigments on a medium level for the interference effect (IE) and multi-color (MC) pigments on a comparably high level for the silver white (SW), gold (G) and iron oxide (IO) pigments. In a slightly different order, the mean class RYD increases from a comparably low level for the interference effect (IE) pigments on a medium level for the multi-

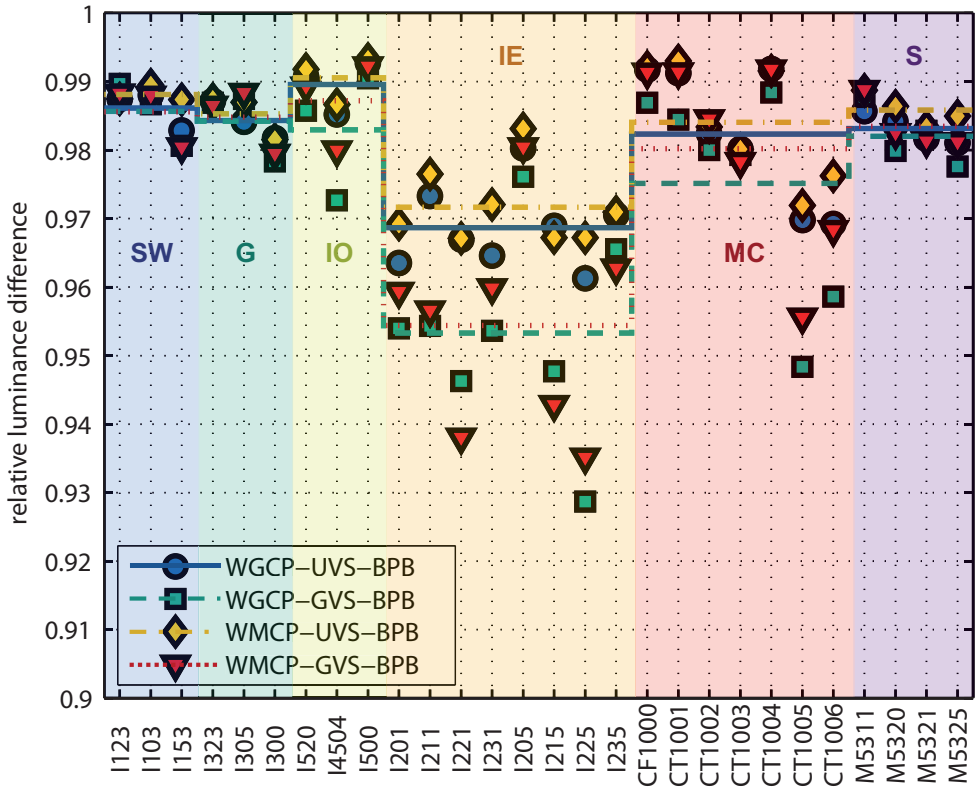

Figure 6.10: RYD of flexo printing samples for all application cases (table 5.4, table 6.2) with black printed background (BPB) [145].

color (MC) and sparkle (S) pigments on a comparably high level for the gold (G), silver white (SW), and iron oxide (IO) pigments in case of the black printed background (BPB, figure 6.10). The background color-induced differences in the order of the pigment classes from a comparably low to a comparably high RYD must be caused by the differences in the typical class-specific material composition.

To get a better overview about the influence of paper quality, varnishing state and background color, the mean of the RYD over the 28 special effect pigments is determined. The mean of the RYD is shown in figure 6.11 used for further evaluations about the influence of the other printing parameters.

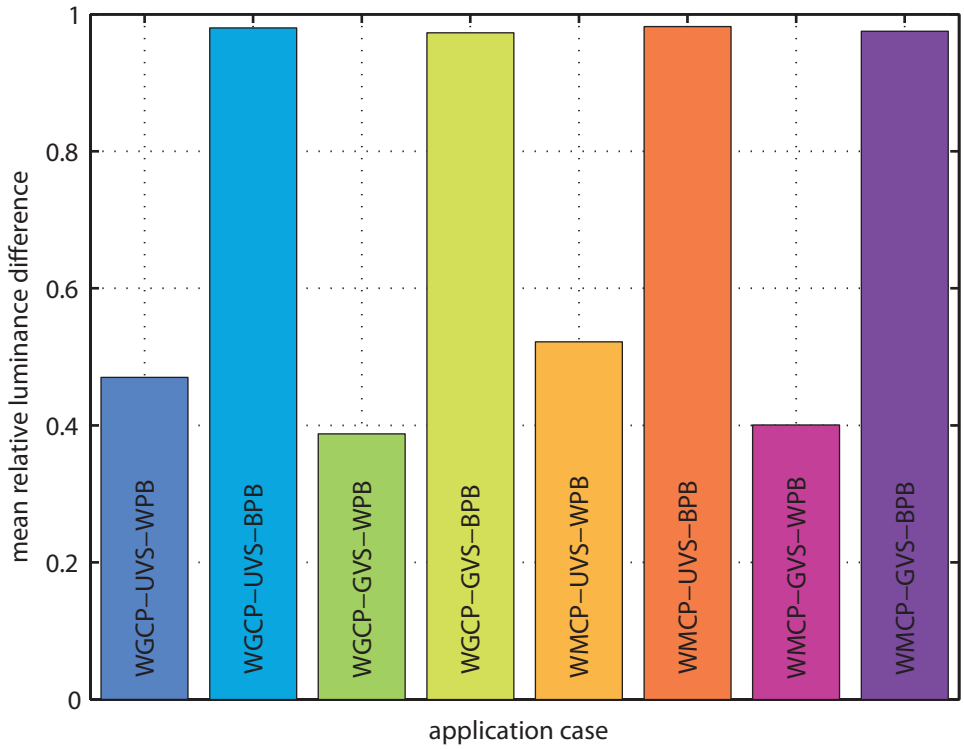

Figure 6.11: Mean RYD of flexo printing samples for all application cases (table 5.4, table 6.2) differing in paper quality (white glossy coated paper ($WGCP$), white matt coated paper ($WMCP$)), varnishing state (unvarnished surface (UVS), glossy varnished surface (GVS)) and background color (white paper background (WPB), black printed background (BPB)).

Influence of Paper Quality on Relative Luminance Difference

The influence of the paper quality on the RYD is expected to be negligible (section 2.2.2). If at all present, the RYD for the white glossy coated paper is assumed to be slightly higher than for the matt coated paper. Figure 6.9, figure 6.10 and figure 6.11 are used to check this assumption.

As already worked out by means of figure 6.9 and figure 6.10, the background color has a significant influence on the RYD. The significant influence of the background color is expressed in the background color-dependent influence of the paper quality. Compared to the paper quality, the influence of the background color on the RYD is more pronounced.

For the white paper background (WPB), the RYD and the mean class RYD shown in figure 6.9 are slightly lower for the white glossy coated paper ($WGCP$) than for the white matt coated paper

($WMCP$). In consideration of the displayed range, the RYD and the mean class RYD of both paper qualities are similar in case of the black paper background (BPB) as shown in figure 6.10. Figure 6.11 showing the mean RYD for all application cases confirms these findings.

In a way, these findings are against the expectation given above (section 2.2.2). Probably, the contrast gloss and distinctness-of-image gloss are not appropriately represented by the RYD. In addition to the near-at-gloss luminance and the far-from-gloss luminance, the gloss luminance should be known. An optical instrument such as the multi-angle spectrophotometer *BYK-mac* needs to be equipped with a detection system in specular direction.

Influence of Varnishing State on Relative Luminance Difference

On the basis of the perceived gloss, it is assumed that the varnishing state has a significant influence on the RYD (section 2.2.2). For the unvarnished surface, the RYD should be significantly lower than for the glossy varnished surface. Apart from figure 6.9 and figure 6.10 showing the RYD and the mean class RYD, figure 6.11 showing the mean RYD is used to check the expectation.

The significant influence of the background color worked out by means of figure 6.9 and figure 6.10 is found again in the background color-dependent influence of the varnishing state. The influence of the background color on the RYD is more pronounced compared to the varnishing state. Due to this dependence, the influence of the varnishing state is evaluated separately for both background colors.

In case of the white paper background (WPB), figure 6.9 shows a higher RYD and mean class RYD for the unvarnished surface (UVS) compared to the glossy varnished surface (GVS). According to figure 6.10 only showing a narrow band at the upper limit of the defined range, the varnishing state has no influence in case of the black printed background (BPB). These findings are confirmed by figure 6.11.

The above assumption is not verified by means of the determined RYD (section 2.2.2). Perhaps, the RYD is not the appropriate parameter to represent the gloss attributes contrast gloss or distinctness-of-image gloss. In more detail, the near-at-gloss luminance and the far-from-gloss luminance are not sufficient to determine a gloss parameter. The gloss luminance should be determined with an optical instrument such as the multi-angle spectrophotometer *BYK-mac*. This instrument is not equipped with a detection system in specular direction.

Influence of Background Color on Relative Luminance Difference

The background color is assumed to have a significant influence on the RYD (section 2.2.2). The RYD is expected to be low for the white paper background. For the black printed background, the RYD is assumed to be high.

This assumption is already verified above by means of figure 6.9 and figure 6.10 showing the RYD and the mean class RYD for the white paper background (WPB) and the black printed background (BPB), respectively.

For the white paper background (WPB), a wide range around the center of the defined range from zero to one is studded with data points and crossed by stairs curves. The data points and stairs curves for the black printed background (BPB) are all massed together in a narrow range near one at the upper limit. In figure 6.11 showing the mean RYD for all application cases as bars along the same axis, this difference becomes much clearer.

This finding is in accordance with the expectation (section 2.2.2). In near-at-gloss directions, incident light is reflected specularly at the surface of the ink layer. Incident light passing the ink layer is reflected by a white background and absorbed by a black background. The presence or absence of reflected light in far-from-gloss directions results in a low or high RYD, respectively.

6.3.3 Influence on Texture Parameters

Finally, the determined texture parameters are used to evaluate the influence on the perceived texture. Some perception-based texture attributes are introduced in section 4.1.3. As in case

of the parameters for color and gloss, the influence on texture parameters are evaluated for the flexo printing samples (section 5.1.2, section 5.2.2, section 5.3.2). The flexo printing samples were measured with the multi-angle spectrophotometer *BYK-mac* (section 3.2.3, section 6.1.1). Only the multi-angle spectrophotometer *BYK-mac* determines texture parameters. These are three sparkle parameters in each three geometric configurations and the graininess in the diffuse geometry. The influence on *sparkle* and *graininess* are considered separately.

Influence on Sparkle Parameters

In section 4.1.3, a definition of the texture attribute sparkle is given. The term sparkle describes the appearance of small, bright light spots in a less bright surrounding. As just mentioned, the multi-angle spectrophotometer *BYK-mac* was used to determine three sparkle parameters in three bidirectional geometries on all flexo printing samples.

The sparkle parameters are the sparkle area, the sparkle intensity and the sparkle grade (section 4.1.3). The sparkle area specifies the total size of the small, bright areas per unit area. The sparkle intensity is equal to the intensity of the small, bright light spots relative to the intensity of the less bright surrounding. Scaling the product of the sparkle grade and the sparkle intensity results in the sparkle grade used as a combined representative sparkle attribute.

The geometric configurations are the 15°/0°, 45°/0° and the 75°/0° geometry (section 3.2.3, section 6.1.1). The angles 15°, 45° and 75° are the incidence angles counted to the perpendicular on the sample surface. With a reflection angle of 0°, the image detection system is located perpendicular to the sample surface.

The influence cannot be evaluated for all nine combinations of the three sparkle parameters and the three geometric configurations. For all nine combinations, the overall results about the general influence are similar. The three sparkle parameters for the 15°/0° geometry are preferred over those for the 45°/0° and 75°/0° geometry. For the 45°/0° and 75°/0° geometry, all sparkle parameters for the white paper background are near zero or equal to zero, respectively. Meanwhile, all sparkle parameters for the black printed background are considerably different from zero. The intended conjoint evaluation of a sparkle parameter for both background colors is not possible. Therefore, the sparkle parameters for the 15°/0° geometry are used in the following evaluations about the influence of *special effect pigment*, *paper quality*, *varnishing state* and *background color*.

Influence of Special Effect Pigment on Sparkle It is assumed that the special effect pigments have an influence on all three sparkle parameters (section 2.1.1, section 2.1.3). The sparkle area, the sparkle intensity and thus also the sparkle grade are expected to be influenced by the particle size and material composition in the following way.

The sparkle area is expected to correlate with the particle size. In more detail, the sparkle area should be proportional to the particle area times the pigment concentration. In this rather simple way of view, non-parallel alignments and mutual overlaps are neglected. Furthermore, identical particle thicknesses and material densities are assumed. According to some simple calculations presented below, the sparkle area should be lower for the smaller but higher concentrated interference effect pigments and higher for the larger but lower concentrated sparkle pigments.

The sparkle intensity is assumed to depend on the material composition. To say it in more detail, the sparkle intensity should be rather low or high for special effect pigments based on a less even natural mica or a more even synthetic substrate, respectively. For example, the sparkle intensity should be lower for the mica-based interference effect pigments and higher for the borosilicate-based sparkle pigments.

This leads to the assumption that particle size and material composition have an influence on the sparkle grade. The particle size and material composition are interlinked pigment class-specific parameters. The sparkle grade is a function of the sparkle area and the sparkle intensity. The dependence of the sparkle area on the particle size and the dependence of the sparkle intensity on the material composition verifies the influence of the particle size and the material composition on the sparkle grade.

The first both assumptions about the influence of the particle size and the substrate material and thus also the last assumption are checked by means of the determined sparkle data. For the 15°/0° geometry, the sparkle area and intensity are shown in figure 6.12 and figure 6.13, respectively.

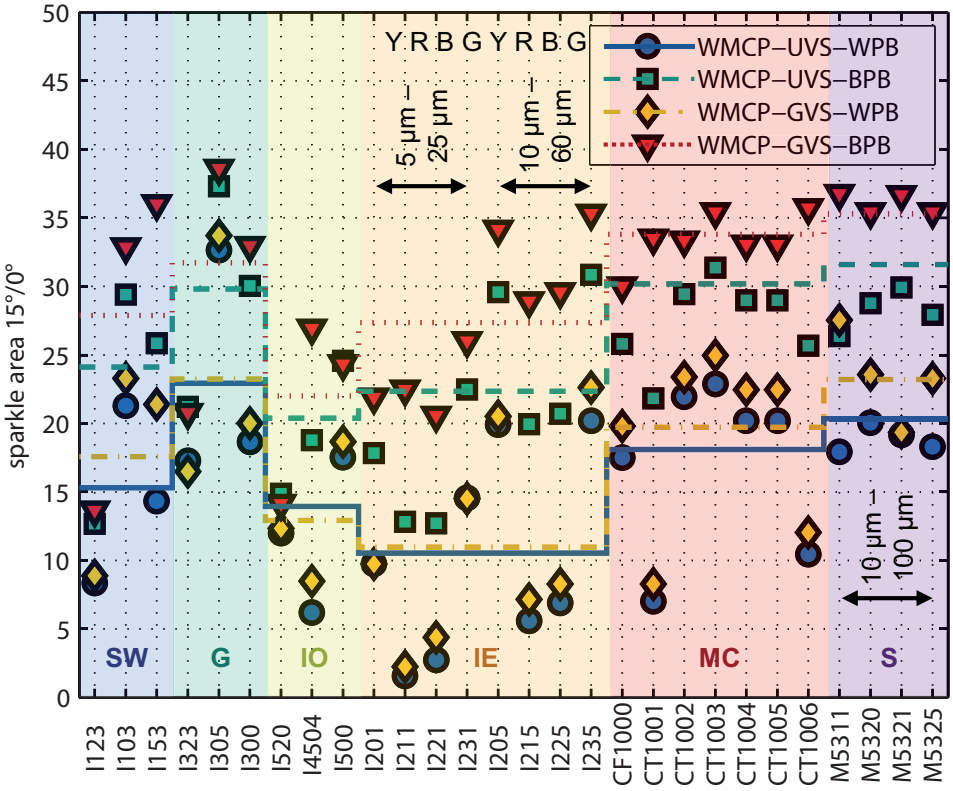

Figure 6.12: Sparkle area for 15°/0° geometry of flexo printing samples for all application cases (table 5.4, table 6.2) with white matt coated paper ($WMCP$) [145].

With respect to figure 6.12 and figure 6.13, the sparkle area for the white matt coated paper ($WMCP$) and the sparkle intensity for the white glossy coated paper ($WGCP$) for the 15°/0° geometry are shown as data points. The stairs curves show the mean class sparkle area and the mean class sparkle intensity, respectively.

The assumption about the influence of the particle size on the sparkle area is checked at first using figure 6.12. As expected, the mean class sparkle area for the smaller but higher concentrated interference effect (IE) pigments is lower than for the larger but lower concentrated sparkle (S) pigments.

The first and last four interference effect (IE) pigments measure between 5 μm and 25 μm and between 10 μm and 60 μm in diameter (section 5.1.2, table 5.2, table A.6), respectively. For average particle sizes of 15 μm and 35 μm, the particle areas are 177 μm^2 and 962 μm^2 assuming that the pigments are shaped like circular platelets. With a pigment concentration of 25 %, the concentration-related effective particle area is 44 μm^2 and 241 μm^2.

For the sparkle (S) pigments measuring between 10 μm and 100 μm (section 5.1.2, table 5.2, table A.6), the mean particle diameter is 55 μm and the associated particle area is 2376 μm^2. The relation to the pigment concentration of 15 % results in an effective particle area of 356 μm^2.

For the interference effect (IE) pigments, the roughly estimated concentration-related effective particle area is smaller than for the sparkle (S) pigments. This comparison between interference effect and sparkle pigments confirms the assumed proportionality of the sparkle area with the

product of particle area and pigment concentration. But, some confusion about the assumed proportionality arises in the following comparisons between the first and last four interference effect pigments.

For the first four interference effect pigments $I201$, $I211$, $I221$ and $I231$ measuring between 5 μm and 25 μm, the sparkle area is lower than for the last four interference effect pigments $I205$, $I215$, $I225$ and $I235$ measuring between 10 μm and 60 μm (figure 6.12). But, the sparkle area varies among the first and last four interference effect pigments despite an equal particle size and pigment concentration. For the both red (R) interference effect pigments $I211$ and $I215$ and the both blue (B) interference effect pigments $I221$ and $I225$, the sparkle area is lower than for the both yellow (Y) interference effect pigments $I201$ and $I205$ and the both green (G) interference effect pigments $I231$ and $I235$. This pigment-dependent pattern should be born in mind.

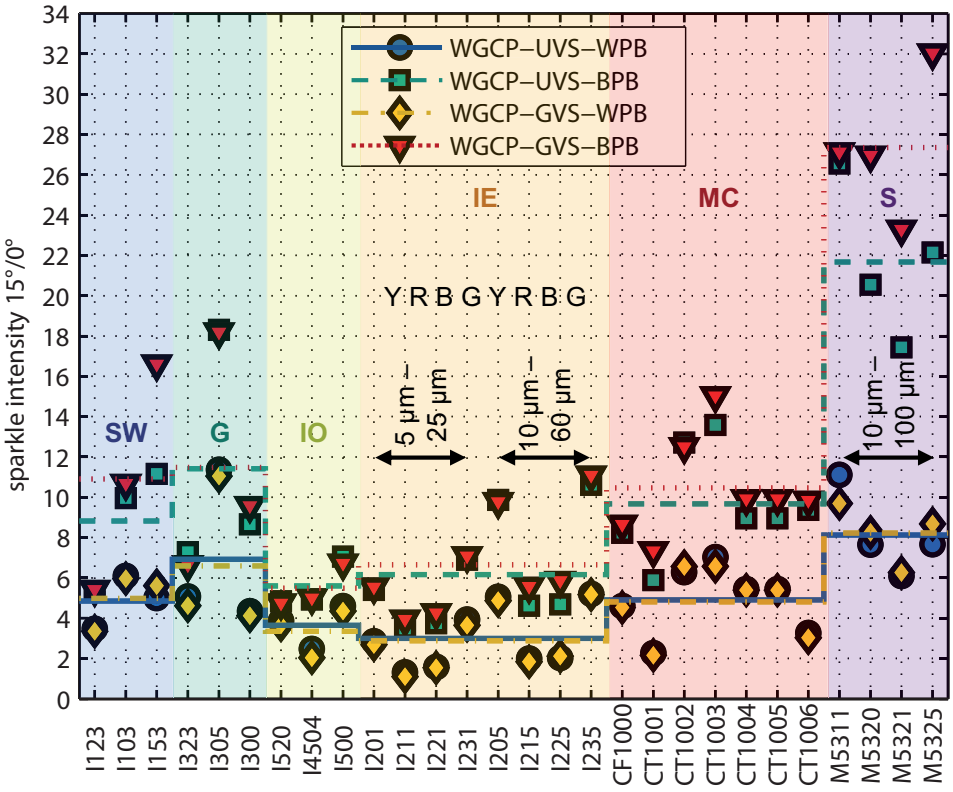

Figure 6.13: Sparkle intensity for 15°/0° geometry of flexo printing samples for all application cases (table 5.4, table 6.2) with white glossy coated paper ($WGCP$) [145].

Now, the expectation about the influence of the substrate material is checked by means of figure 6.13. In accordance with the expectation, the sparkle intensity for the mica-based interference effect (IE) pigments is lower than for the borosilicate-based sparkle (S) pigments [145]. Remember the pigment-dependent pattern just found for the sparkle area. As in case of the sparkle area, the sparkle intensity is lower for the both red (R) and blue (B) interference effect pigments $I211$, $I215$, $I221$ and $I225$ than for the both yellow (Y) and green (G) interference effect pigments $I201$, $I205$, $I231$ and $I235$. This finding is revived below in the evaluation about the influence on graininess.

The final check of the influence of particle size and material composition on the sparkle area is superfluous. As mentioned above, the verification comes along with the verified influence of the particle size on the sparkle area and the verified influence of the material composition on the sparkle intensity.

Due to the one-dimensional representation of sparkle area and sparkle intensity, the sparkle

grade is useful for the evaluation of the influence of paper quality, varnishing state and background color. For global evaluations about the influence of these printing parameters, the mean of the sparkle grade over the 28 special effect pigments is shown in figure 6.14.

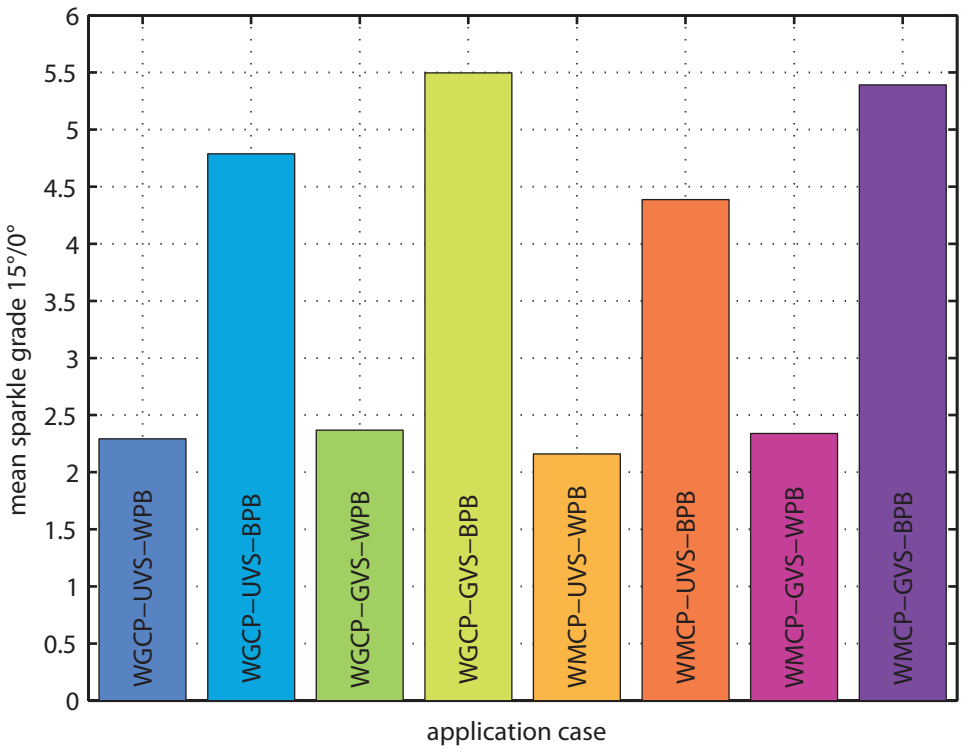

Figure 6.14: Sparkle grade for 15°/0° geometry of flexo printing samples for all application cases (table 5.4, table 6.2) differing in paper quality (white glossy coated paper ($WGCP$), white matt coated paper ($WMCP$)), varnishing state (unvarnished surface (UVS), glossy varnished surface (GVS)) and background color (white paper background (WPB), black printed background (BPB)).

Influence of Paper Quality on Sparkle Concerning the paper quality, a negligible influence on the sparkle parameters is assumed (section 2.2.2). This assumption is checked by the use of the mean sparkle grade shown in figure 6.14.

The mean sparkle grades for the white glossy coated paper ($WGCP$) are slightly higher than for the white matt coated paper ($WMCP$). The paper quality has a certain influence on the sparkle grade.

On the even surface of the glossy coated paper, the special effect pigments are aligned more parallel than on the less even surface of the matt coated paper (section 2.2.2). The more or less parallel orientation results in a more or less regular texture.

Influence of Varnishing State on Sparkle The influence of the varnishing state on all sparkle parameters is expected to be negligible (section 2.2.2). With respect to the sparkle area, the sparkle intensity and the sparkle grade, figure 6.12, figure 6.13 and figure 6.14 are used to check the assumed negligible influence of the varnishing state.

The sparkle area and the mean class sparkle area shown in figure 6.12 as well as the sparkle intensity and the mean class sparkle intensity [145] shown in figure 6.13 are somehow lower for the unvarnished surface (UVS) than for the glossy varnished surface (GVS). The same influence is found for the mean sparkle grade shown in figure 6.14 due to its reliance on the sparkle area and the sparkle intensity. Compared to the white paper background (WPB), the difference induced by the varnishing state is higher for the black printed background (BPB).

To a certain degree for the white paper background, but especially for the black printed background, this finding is against the above expectation (section 2.2.2). The reason for the influence of the varnishing state on the sparkle is not known.

Influence of Background Color on Sparkle It is assumed that the background color has no influence on the sparkle area. The sparkle intensity is expected to be influenced by the background color. For the white paper background, the sparkle intensity should be lower than for the black printed background. Due to the combination of sparkle area and sparkle intensity, the background color should have an influence on the sparkle grade (section 2.2.2). The three assumptions for the sparkle area, the sparkle intensity and the sparkle grade are checked by the use of figure 6.12, figure 6.13 and figure 6.14, respectively.

In figure 6.12, the sparkle area and the mean sparkle area are significantly lower for the white paper background (WPB) than for the black printed background (BPB). This finding is against the above expectation. The lightness of the background color has an influence on the sparkle area. The same influence, but in accordance with the expectation, is found for the sparkle intensity and the mean class sparkle intensity [145] shown in figure 6.13 as well as for the mean sparkle grade shown in figure 6.14.

Influence on Graininess

The texture attribute graininess is introduced in section 4.1.3. The perceived size of the components in a system is specified by the graininess.

The graininess of all flexo printing samples was determined with the multi-angle spectrophotometer *BYK-mac* and filed in the $BRTD$. By means of these data, the influence of the *special effect pigment*, the *paper quality*, the *varnishing state* and the *background color* is evaluated.

Influence of Special Effect Pigment on Graininess As just mentioned, the texture attribute graininess specifies the size of the components in a system. In the present case, the printed special effect ink is the system and the individual special effect pigments are the components. Thus, the graininess should somehow correlate with the particle size (section 2.1.1, section 2.1.3). Low and high particle sizes are expected to result in a lower and higher graininess, respectively. This expectation about the influence of the particle size on the graininess is checked by means of figure 6.15.

In figure 6.15, the pigment-specific graininess and the mean class graininess are shown for all application cases with the white matt coated paper ($WMCP$). Data points and stairs curves represent the pigment-specific graininess and the mean class graininess, respectively.

The pigment-specific graininess as well as the mean class graininess show significant fluctuations. Against the above expectations, no clear correlation with the particle size can be observed. Apart from the particle size, the used special effect pigments differ in their material composition (section 2.1.1). The influence of particle size and material composition on the graininess needs to be considered in connection. A detailed consideration of both pigment parameters is realized by means of comparisons between and within the classes of interference effect (IE) and sparkle (S) pigments (section 2.1.3).

The particle size of the interference effect pigments used in this study lies between 5 μm and 25 μm or between 10 μm and 60 μm (table 5.2, table A.6). An interference effect pigment is a composition of a natural mica substrate and coating layers of tin dioxide and titanium dioxide (table A.7, table A.8). The used sparkle pigments measure between 10 μm and 100 μm (table 5.2,

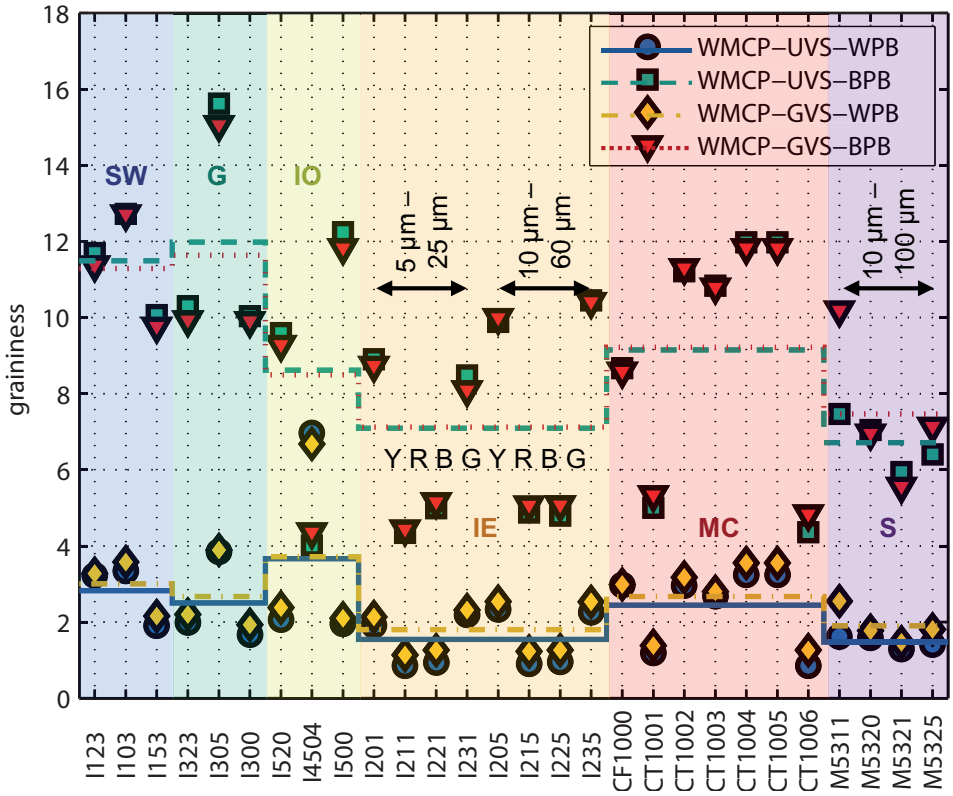

Figure 6.15: Graininess of flexo printing samples for all application cases (table 5.4, table 6.2) with white matt coated paper ($WMCP$).

table A.6). Sparkle pigments are composed of a synthetic borosilicate substrate and silicon dioxide, tin dioxide and titanium dioxide coatings (table A.7, table A.8).

In spite of the different particle size and the different material composition, the mean class graininess of the interference effect (IE) and sparkle (S) pigments is equal (figure 6.15). Either, both classification parameters, the particle size and the material composition, have an opposite compensating influence on the graininess. Or, none of the two classification parameters, neither the particle size nor the material composition, have an influence on the graininess.

The comparison between the pigment classes is extended by a comparison within the pigment classes. The graininess of different interference effect or sparkle pigments is not equal although their particle size and material composition is the same (figure 6.15). In addition to particle size and material composition, there must be another influencing parameter. The additional parameter compensates the inter-class variations and causes the intra-class variations in the graininess.

The influence of this additional parameter is especially noticeable for the first four interference effect pigments $I201$, $I211$, $I221$ and $I231$ measuring between 5 μm and 25 μm as well as for the last four interference effect pigments $I205$, $I215$, $I225$ and $I235$ measuring between 10 μm and 60 μm. For both particle size ranges, the graininess is comparably low for the red (R) interference effect pigments $I211$ and $I215$ and for the blue (B) interference effect pigments $I221$ and $I225$. In contrast to that, the both yellow (Y) interference effect pigments $I201$ and $I205$ and the both green (G) interference effect pigments $I231$ and $I235$ have a comparably high graininess. A similar pigment-dependent pattern is found for the other texture parameters and also for the lightness. For the sparkle area and the sparkle intensity, this finding is mentioned above and shown in figure 6.12 and figure 6.13. Although not considered in detail, the following fact should be mentioned about the lightness. The lightness is lower for the red and blue interference effect pigments. For the yellow and green interference effect pigments, the lightness is higher.

The intended global consideration about the influence of the other printing parameters suggests to average the graininess over all 28 special effect pigments. The mean graininess is shown in figure 6.16 for all application cases varying in the paper quality, the varnishing state and the background color.

Influence of Paper Quality on Graininess The paper quality is expected to have no significant influence on the graininess (section 2.2.2). This expectation is checked by means of figure 6.16 showing the mean graininess.

The mean graininess for the white glossy coated paper ($WGCP$) resembles to the mean graininess for the white matt coated paper ($WMCP$). As just assumed, the paper quality has no influence on the graininess (section 2.2.2).

Influence of Varnishing State on Graininess The varnishing state is supposed to have no significant influence on the graininess (section 2.2.2). The graininess and the mean class graininess shown in figure 6.15 as well as the mean graininess shown in figure 6.16 are used to check this assumption.

In figure 6.15, the graininess and the mean class graininess for the unvarnished surface (UVS) and for the glossy varnished surface (GVS) are equal. In figure 6.16, the mean graininess for the unvarnished surface (UVS) resembles to the mean graininess for the glossy varnished surface (GVS). Thus, the varnishing state has no influence on the graininess (section 2.2.2).

Influence of Background Color on Graininess The expectation about the influence of the background color on the graininess is the following (section 2.2.2). For the white paper background, the graininess should be lower than for the black printed background. Figure 6.15 showing the graininess and the mean class graininess as well as figure 6.16 showing the mean graininess are used to verify the expectation on the influence of the background color.

For the white paper background (WPB), the graininess and the mean class graininess (figure 6.15) as well as the mean graininess (figure 6.16) are lower. A higher graininess and mean class

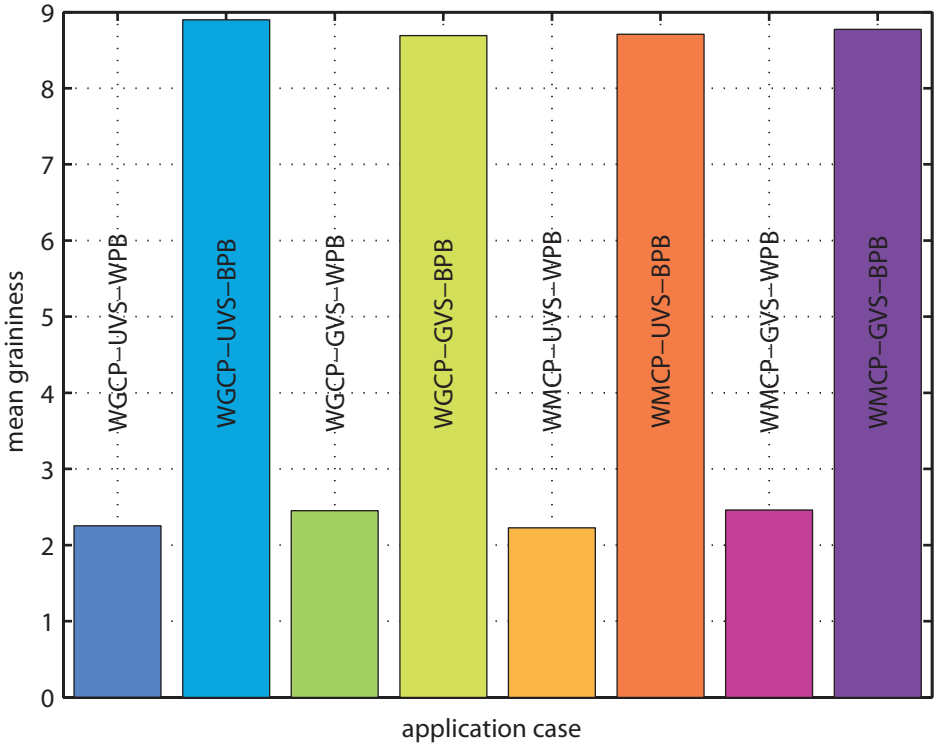

Figure 6.16: Mean graininess of flexo printing samples for all application cases (table 5.4, table 6.2) differing in paper quality (white glossy coated paper ($WGCP$), white matt coated paper ($WMCP$)), varnishing state (unvarnished surface (UVS), glossy varnished surface (GVS)) and background color (white paper background (WPB), black printed background (BPB)).

graininess (figure 6.15) as well as a higher mean graininess (figure 6.16) occurs for the black paper background (BPB). This finding is in accordance with the above assumption (section 2.2.2).

6.4 Conclusion on the Influence of Printing Parameters

This chapter is finished with a conclusion about the influence of the varied printing parameters (chapter 5). Their influence on the visual appearance was determined by means of perception-related parameters.

Due to the number of application cases and the availability of texture data, the influence evaluation was conducted for the flexo printing samples measured with the multi-angle spectrophotometer *BYK-mac*. In flexo printing, special effect inks containing 28 different *MERCK* pigments of six different classes were applied on two paper grades partially primed with a black light-absorbing ink and optionally finished with a clear gloss varnish. The special effect pigments are silver white (SW), gold (G), iron oxide (IO), interference effect (IE), multi-color (MC), sparkle (S) pigments. The printing substrate is a white glossy coated paper ($WGCP$) or a white matt coated paper ($WMCP$). A white paper background (WPB) and a black printed background (BPB) were realized by means of the partial priming. The optional finishing results in an unvarnished surface (UVS) or a glossy varnished surface (GVS).

The perception-related parameters were determined on the basis of the bidirectional reflectance and texture data. The bidirectional reflectance and texture database includes reflectance spectra, color coordinates and texture parameters determined in spectral and imaging measurements in multiple geometric configurations. The color coordinates were used to calculate the hue difference sum (HDS), the lightness difference sum (LDS) and the relative luminance difference (RYD). These perception-related parameters were assumed to represent the visual appearance attributes hue shift, lightness shift and contrast gloss or distinctness-of-image gloss. The perceived sparkle (S) and graininess (G) were assumed to be represented by the sparkle area, sparkle intensity, sparkle grade and graininess.

Thus, the influence of the special effect pigment, the paper quality, the varnishing state and the background color on the hue difference sum (HDS), the lightness difference sum (LDS), the relative luminance difference (RYD), the sparkle (S) and the graininess (G) was evaluated. The following summary about the influence of the printing parameters on the perception-related parameters is supported by table 6.3.

As expected, the perception-related parameters are influenced by the *special effect pigment*. The interference effect (IE) and multi-color (MC) pigments induce a medium high and very high hue difference sum (HDS, table 6.3), respectively. The same influence was found by *Haas* [93, 94] using the geometry-induced color difference (section 4.1.1) as perception-related parameter for the hue shift. Both perception-related parameters, the hue difference sum (HDS) and the geometry-induced color difference, are suitable to represent the perceived hue shift. Compared to the other pigment classes such as the interference effect (IE) pigments, the sparkle (S) parameters are high for the sparkle (S) pigments, as the designation suggests. However, the comparably large sparkle (S) pigments have a similar graininess (G) as the comparably small interference effect (IE) pigments. Thus, the graininess is not only influenced by the particle size of the special effect pigment. Another influence might be its material composition.

The *paper quality* has no significant influence on all considered perception-related parameters (table 6.3). Apparently, the two wood-free coated art papers are too similar in their roughness and porosity to induce significant differences in the hue difference sum (HDS) and in the perception-related texture parameters sparkle (S) and graininess (G). Especially for the lightness difference sum (LDS) and the relative luminance difference (RYD), this finding is against the expectations based on own experiences and the findings of *Haas* [93, 94]. The lightness difference sum (LDS) and the relative luminance difference (RYD) do not adequately represent the perceived lightness shift and contrast gloss or distinctness-of-image gloss. For this purpose, lightness or luminance measurements in specular direction are necessary. In contrast to the gloss meter *Vipgloss*-1 of *FAG* used by *Haas* [93, 94] to determined the so-called gloss number, the multi-angle spectrophotometer *BYK-mac* is not equipped with a detection system in specular direction.

The statement about the unsuited representation of the perceived lightness shift or contrast gloss and distinctness-of-image gloss by the calculated lightness difference sum (LDS) and relative luminance difference (RYD) is confirmed by the findings about the influence of the *varnishing*

Table 6.3: Influence of special effect pigment (silver white (SW), gold (G), iron oxide (IO), interference effect (IE), multi-color (MC), sparkle (S)), paper quality (white glossy coated paper ($WGCP$), white matt coated paper ($WMCP$)), varnishing state (unvarnished surface (UVS), glossy varnished surface (GVS)) and background color (white paper background (WPB), black printed background (BPB)) on hue difference sum (HDS), lightness difference sum (LDS), relative luminance difference (RYD), sparkle (S) and graininess (G)).

pigment class	paper quality	varnishing state	background color
$HDS(SW) \approx HDS(G) \approx HDS(IO) \approx HDS(S) < HDS(IE) < HDS(MC)$	$HDS(WGCP) \approx HDS(WMCP)$	$HDS(UVS) < HDS(GVS)$	$HDS(WPB) < HDS(BPB)$
$LDS(IE) \approx LDS(MC) \approx LDS(S) < LDS(SW) \approx LDS(G) \approx LDS(IO)$	$LDS(UVS,WGCP) < LDS(UVS,WMCP)$, $LDS(GVS,WGCP) \approx LDS(GVS,WMCP)$	$LDS(GVS) < LDS(UVS)$	$LDS(WPB) < LDS(BPB)$
$RYD(S) \approx RYD(IE) \approx RYD(MC) < RYD(SW) \approx RYD(G) \approx RYD(IO)$	$RYD(WPB,WGCP) < RYD(WPB,WMCP)$, $RYD(BPB,WGCP) \approx RYD(BPB,WMCP)$	$RYD(WPB,GVS) < RYD(WPB,UVS)$, $RYD(BPB,UVS) \approx RYD(BPB,GVS)$	$RYD(WPB) < RYD(BPB)$
$S(IE) < S(S)$	$S(WGCP) \approx S(WMCP)$	$S(UVS) < S(GVS)$	$S(WPB) < S(BPB)$
$G(IE) \approx G(S)$	$G(WGCP) \approx G(WMCP)$	$G(UVS) \approx G(GVS)$	$G(WPB) < G(BPB)$

state. For the unvarnished surface (UVS), the lightness difference sum (LDS) and the relative luminance difference (RYD) are higher than for the glossy varnished surface (GVS, table 6.3). This is not in accordance with the perception and the findings of $Haas$ [93, 94]. The gloss number determined with the gloss meter $Vipgloss$-1 of FAG is increased by an additional finishing with a gloss varnish. Concerning the varnishing state, $Haas$ [93, 94] also found that the glossy varnishing increases the the geometry-induced color difference (section 4.1.1). The same influence is found in the present study. The hue difference sum (HDS) is lower for the unvarnished surface (UVS) than for the glossy varnished surface (GVS).

The influence of the *background color* is very pronounced. In comparison with to the white paper background (WPB), all considered perception-related parameters are significantly higher for the black printed background (BPB, table 6.3). With respect to the background color, the scattering and the absorption are the reason in case of the hue difference sum (HDS). In case of the lightness difference sum (LDS), the relative luminance difference (RYD), the sparkle (S) and the graininess (G), the contrast between the more or less bright areas is the reason. This fact was already considered in the study of $Haas$ [93, 94] in the context of the homogeneity of the printed special effect colors. Instead of the white background of the printing substrate, the homogeneity was visually assessed for the black background realized by priming with a black light absorbing ink.

Chapter 7

Number and Nature of Essential Attributes

The third partial problem is the incomplete perception-based characterization of special effect colors with visual appearance attributes (section 1.1.3). Chapter 4 provides a deeper understanding of this problem.

Furthermore, it clarifies the necessity of the respective approach. In visual experiments and statistical evaluations, the number and nature of the essential visual appearance attributes will be identified (section 1.2.3). The previously produced screen and flexo printing samples described in chapter 5 are needed for this purpose.

At first, the *methodical concept* (section 7.1) is explained and the *experimental conditions* (section 7.2) are defined in this chapter. After that, the conduction of the *visual experiments* (section 7.3) is described and the *statistical evaluation* of the collected datasets (section 7.4) is presented. Finally, the results about the number and nature of the *essential visual appearance attributes* are summarized and compared to the results of other studies (section 7.5).

7.1 Designing the Methodical Concept

Any psychophysical study is based on a methodical concept. The methodical concept includes psychophysical experiments and statistical evaluations. Multiple experimental procedures are introduced in section 4.4. Section 4.5 presents important statistical evaluation methods. For this study on the visual appearance of printed special effect colors, suitable psychophysical experiments and statistical evaluations were composed in a methodical concept as already presented by *Kehren et al.* [146]. This methodical concept is shown in figure 7.1.

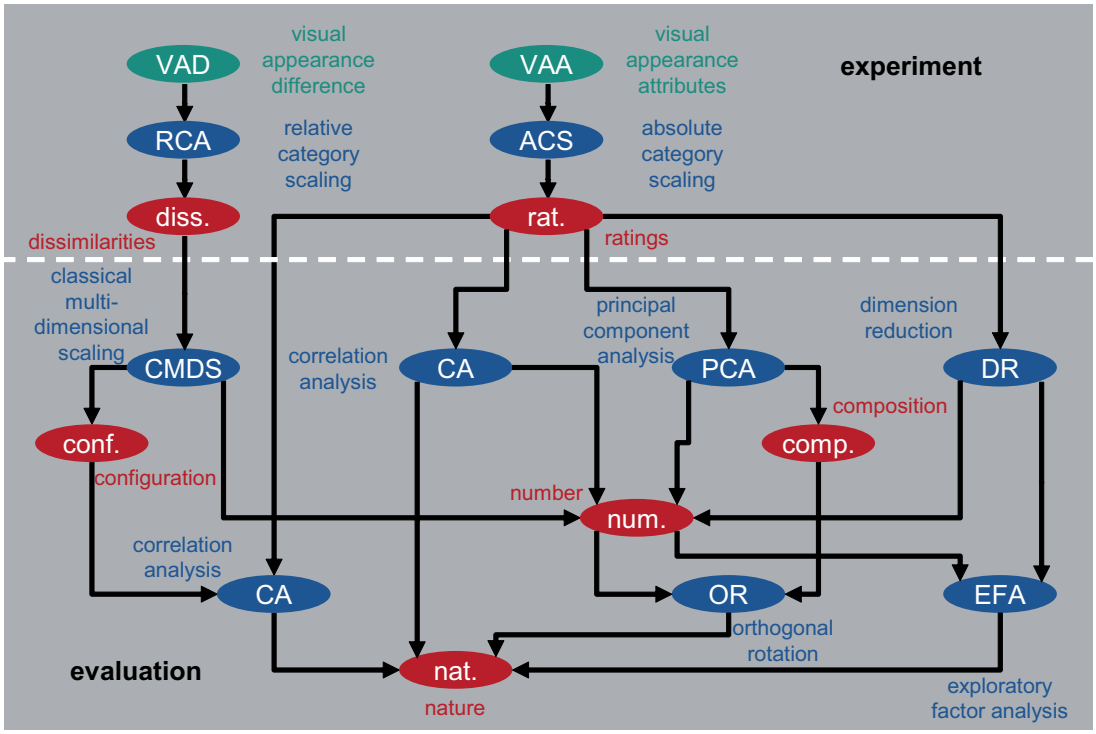

Figure 7.1: Methodical concept including visual experiments and statistical evaluations [146].

The green ellipses represent the estimated dimension. The experimental procedure and the evaluation method are represented by the blue ellipses. The red ellipses represent the collected data, the interim results and the final results. The abbreviations for the specifications in the ellipses are itemized in table 7.1.

The estimated dimension is either the total visual appearance difference (VAD) or a set of twelve visual appearance attributes (VAA) expected to be essential. The relative category scaling (RCS) and the absolute category scaling (ACS) is the associated experimental procedure. The collected data are dissimilarity (*diss.*) matrices or rating (*rat.*) matrices, respectively. The classical multidimensional scaling ($CMDS$), two correlation analyses (CA), a principal component analysis (PCA) followed by an orthogonal rotation (OR) and an exploratory factor analysis (EFA) based on a dimension reduction (DR) are the evaluation methods. The configuration (*conf.*) and the composition (*comp.*) are interim results. The final results are the number (*num.*) and nature (*nat.*) of essential attributes.

The ellipses for the estimated dimensions and the experimental procedures including the collected data are separated from the statistical evaluations including the interim and final results. The separation of experiment and evaluation is realized by means of a white broken line. The ellipses are connected with black arrows indicating their sequence in the methodical concept. In the following, the sequences in the methodical concept are explained in two separate sections. Section 7.1.1 focuses on the *visual experiments* including the collected data. The *statistical evaluations*

Table 7.1: Abbreviations for the specification of the methodical concept.

specification	abbreviation	information
estimated dimension	VAD	visual appearance difference
	VAA	visual appearance attributes
experimental procedure	RCS	relative category scaling
	ACS	absolute category scaling
collected data	*diss.*	dissimilarity matrix
	rat.	rating matrix
evaluation method	$CMDS$	classical multidimensional scaling
	CA	correlation analysis
	PCA	principal component analysis
	OR	orthogonal rotation
	DR	dimension reduction
	EFA	exploratory factor analysis
interim result	*conf.*	configuration
	comp.	composition
final result	*num.*	number of essential attributes
	nat.	nature of essential attributes

including the obtained results are treated in section 7.1.2.

7.1.1 Visual Experiments and Collected Datasets

Two versions of category scaling experiments described in section 4.4.2 and in literature [2, 70, 76] were conducted subsequently. The first experiment is called *relative category scaling* (RCS) of total *visual appearance differences* (VAD). The *absolute category scaling* (ACS) of *visual appearance attributes* (VAA) designates the second experiment.

Relative Category Scaling of Visual Appearance Differences

In the relative category scaling (RCS) experiment explained by *Ehrenstein* and *Ehrenstein* [70], the selected samples (section 7.2.2) are presented to the subject in all possible pairs of different samples. For each of the sample pairs, the subject is asked to estimate the magnitude of the total visual appearance difference (VAD) on a scale from zero to ten (figure 7.1 and table 7.1). The number zero stands for no difference. The number ten denotes the maximal difference in the whole sample set. All estimates are noted in an upper triangular matrix called dissimilarity (*diss.*) matrix.

Absolute Category Scaling of Visual Appearance Attributes

For the absolute category scaling (ACS) experiment described by *Ehrenstein* and *Ehrenstein* [70], twelve visual appearance attributes (VAA) expected to be essential are selected from the amount of the theoretically possible ones (section 7.2.1). For all selected samples (section 7.2.2), the subject is asked to assign numbers from zero to ten for the perceived magnitude of the visual appearance attribute (VAA) currently considered (figure 7.1, table 7.1). The rating zero has the meaning of no magnitude, one of a very small magnitude and so on. The rating ten stands for the maximal magnitude over the sample set. The ratings are combined to the so-called rating (*rat.*) matrix with 14 or 20 rows for the samples and twelve columns for the attributes.

7.1.2 Statistical Evaluation and Obtained Results

Different types of multivariate statistical evaluation methods described in section 4.5.4 were applied on the determined visual data. At first, the *dissimilarities* (*diss.*) are processed in *classical*

multidimensional scaling (*CMDS*) resulting in the so-called *configuration* (*conf.*). The configuration is further processed in a *correlation analysis* (*CA*) in combination with the *ratings* (*rat.*). Another *correlation analysis* (*CA*) is exclusively applied on the *ratings* (*rat.*). The ratings are also processed in a *principal component analysis* (*PCA*). The resulting *composition* (*comp.*) is then subjected to an *orthogonal rotation* (*OR*). Finally, the results are checked by means of a *dimension reduction* (*DR*) followed by an *exploratory factor analysis* (*EFA*).

Classical Multidimensional Scaling of Dissimilarities

In the style of *Rao* and *Lohse* [212], *Long* and *Leow* [167], *Pellacini et al.* [200], *Ferwerda et al.* [80] and *Wills et al.* [245], multidimensional scaling (*MDS*) was applied to evaluate dissimilarity data. By means of classical *MDS* (*CMDS*), the averaged difference estimates collected in the dissimilarity (*diss.*) matrix are converted in the so-called configuration (*conf.*, figure 7.1, table 7.1). As described in section 4.5.4, the configuration is the best fitting spatial arrangement of the samples. The measure for the residual error called standardized residual sum of squares (*STRESS*) [151, 158] is plotted against the number of dimensions. An inflection point in the *STRESS* curve or the dropping below the level of tolerance or excellence indicate the number of essential dimensions. Thus, the dimensionality of the underlying appearance space is found out.

Correlation Analysis of Configuration and Ratings

Until now, the numbered axes of the appearance space representing the just determined configuration (*conf.*) have no perception-based labels. In a comparable case, *Rao* and *Lohse* [212] applied a correlation analysis (*CA*) explained in section 4.5.4. Thus, a *CA* between the coordinates of the samples in the configuration (*conf.*) and the respective ratings (*rat.*) of the visual appearance attributes is the solution (figure 7.1, table 7.1). Between the configuration matrix and the rating matrix, the correlation matrix is determined. A high absolute correlation coefficient with a sufficient p-value significance allow the assignment of the considered visual appearance attribute to the considered configuration axis.

Correlation Analysis of Ratings

The selection of visual appearance attributes assessed in the visual experiments includes twelve hypothetically meaningful attributes for color, gloss and texture. Three of them are entitled with two related attributes. Obviously, the color attribute lightness flop (*dL*) and the gloss attribute contrast gloss (*CG*) seem to have the same meaning. Therefore, lightness flop and contrast gloss (*dLCG*) are treated together. The same holds for the texture attributes graininess and coarseness (*GC*) as well as sparkle and glint (*SG*). Maybe, such a relation also exists for other visual appearance attributes among the hypothetically meaningful attributes. As in the study of *Rao* and *Lohse* [212], such inter-attribute correlations can be identified by means of a correlation analysis described in section 4.5.4. Thus, a correlation analysis (*CA*) is applied on the rating (*rat.*) matrix (figure 7.1, table 7.1). A high absolute correlation coefficient with an adequate p-value significance points out an inter-attribute correlation. A significant inter-attribute correlation allows the subsumption of the considered visual appearance attributes.

Principal Component Analysis of Ratings and Orthogonal Rotation of Configuration

In addition to their processing in the previously considered correlation analyses, the ratings (*rat.*) are evaluated in a principal component analysis (*PCA*) followed by an orthogonal rotation (*OR*, figure 7.1, table 7.1). As mentioned in section 4.5.4, *Rao* and *Lohse* [212] applied a *PCA* in their study. During the *PCA*, the eigenvalues and eigenvectors belonging to the covariance or correlation matrix of the rating (*rat.*) matrix are determined. The eigenvalues plotted against their index give information about dimensionality of the underlying space. The eigenvectors with a running number up to the number of essential dimensions are set equal to the component coefficients of

the principal components. For their easier interpretation, the principal components are subjected to an OR.

Dimension Reduction and Exploratory Factor Analysis of Ratings

In a bipartite sequence comparable to the PCA combined with the OR, the ratings ($rat.$) are processed in a dimension reduction (DR) and an exploratory factor analysis (EFA, figure 7.1, table 7.1). The EFA described in section 4.5.4 was applied by *Rao* and *Lohse* [212]. The dimensionality is again determined by means of the eigenvalue plot. Instead of calculating the component coefficients of the principal components, the EFA continues with the calculation of the factor loadings. For the number of essential dimensions, the factor loadings are calculated on the basis of maximum likelihood estimation. The subsequent OR of the factors simplifies their interpretation.

7.2 Specifying the Experimental Conditions

Previous to any experiments, the relevant conditions need to be specified. In the present case, the experimental conditions include the *estimated attributes* (section 7.2.1), the *assessed samples* (section 7.2.2) and the *experimental equipment* (section 7.2.3). The itemized experimental conditions are subsequently treated.

7.2.1 Estimated Attributes

Remember the scientifically known visual appearance attributes presented in section 4.1. Not all of the presented visual appearance attributes are essential for the appearance characterization of printed special effect colors and testable in visual experiments. Therefore, a subset of visual appearance attributes was first selected and then adapted. The *selection* and *adaption* are described in the following.

Attribute Selection

Apart from translucency attributes being not essential for printed special effect colors, section 4.1 presents all visual appearance attributes mentioned in literature. These scientifically known visual appearance attributes are the basis for a selection of visual appearance attributes expected to be essential for printed special effect colors. All selected *color*, *gloss* and *texture attributes* are shown in figure 7.2.

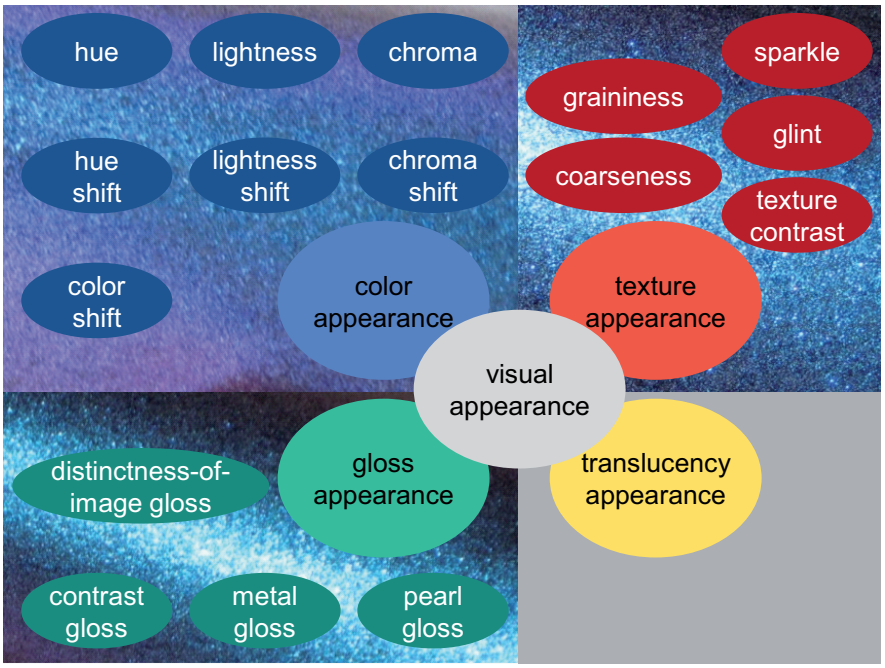

Figure 7.2: Selected visual appearance attributes.

The visual appearance attributes are sorted in groups for the perception of color, gloss and texture. According to this appearance grouping, the selection of color, gloss and texture attributes expected to be meaningful is now justified in detail.

Color Attribute Selection In the standard practice *ASTM E* 284-03*a* [8], in the books of *Fairchild* [76] *Hunt* [110], *Hunter* and *Harold* [111] and *Pfaff et al.* [204, 205] as well as in the papers of *Eugène* [75], *Judd* [136, 137, 138, 139, 140] and others [91, 145, 189, 228, 247], twelve color attributes are mentioned altogether (section 4.1.1). These scientifically known color

attributes are hue, brightness, lightness, colorfulness, chromaticness, chroma and saturation for systems colored with light-absorbing pigments. For systems with special effect pigments, they are extended by the color shift, angular hue shift, hue shift, chroma shift and lightness shift.

As mentioned above, the number and nature of essential color attributes is known well for light absorbing colors. The three color attributes hue, chroma and lightness allow the complete color characterization of an object without superfluous information. Therefore, hue, chroma and lightness are included in the set of visual appearance attributes expected to be essential for printed special effect colors (figure 7.2). In a single number, the hue specifies the proportions of red or green and yellow or blue in the considered color. The attribute lightness is preferred over brightness due to the relative character. The same explanation holds for the preference of chroma over colorfulness and chromaticness. Like chroma, saturation is a relative measure. But, saturation is related to the considered color itself while chroma is related to an ideal reference.

The full color description of systems including special effect pigments with these three color attributes is not sufficient. The color shift, hue shift, chroma shift and the lightness shift are expected to be additional essential color attributes for systems with special effect pigments (figure 7.2). The so-called color shift or color flop describes the total geometry-induced difference in color. The separate geometry-induced differences for hue, chroma and lightness are specified by the hue shift, chroma shift and the lightness shift.

Gloss Attribute Selection In total, twelve gloss attributes are named in the standard practices *ASTM D* 4449-90 [4], *ASTM D* 523-89 [3], *ASTM D* 5767-95 [5], *ASTM E* 430-97 [9] and *ASTM E* 284-03*a* [8], the books of *Hunter* and *Harold* [111] and *Pfaff et al.* [204, 205] as well as in the papers of *Eugène* [75], *Pellacini et al.* [200], *Ferwerda et al.* [80], *Fleming et al.* [81], *Leloup et al.* [163, 164], *Phillips et al.* [208] and *Wills et al.* [245] (section 4.1.2). For ordinary glossy surfaces, the contrast gloss, specular gloss, luster, bloom, haze, diffuseness, sheen, distinctness-of-image gloss, absence-of-bloom gloss, absence-of-texture gloss and surface-uniformity gloss are known. The metal gloss and the pearl gloss are used in the connection with special effect pigments.

Among the scientifically known gloss attributes, specular gloss and sheen are absolute characters. Specular gloss and sheen describe the perceived amount of specular reflection for arbitrary and flat incidence and reflection angles. As mentioned in the comparison of lightness with brightness and of chroma with colorfulness and chromaticness, relative measures are preferred over absolute measures. Therefore, contrast gloss and luster are preferred over specular gloss and sheen. Contrast gloss and luster indicate the gloss-induced lightness variation of dark and light areas. Due to the higher application frequency and the better self-declaration, the term contrast gloss is preferably set on the list of hypothetically essential appearance attributes (figure 7.2).

Apart from contrast gloss, distinctness-of-image gloss was found to be essential for the characterization of arbitrary glossy surfaces [80, 200]. Thus, distinctness-of-image gloss is also included in the list of hypothetically essential appearance attributes (figure 7.2). The gloss-induced transition sharpness of dark and light areas is described by means of the distinctness-of-image gloss.

The remaining ordinary gloss attributes are obviously not essential for printed special effect colors. Haze, bloom and absence-of-bloom gloss are used in the context of diffuse reflections near the specular direction inducing a cloudy appearance. The presence or absence of a cloudy appearance is not an outstanding property of printed special effect colors. The same holds for the smoothness and homogeneity of printed special effect colors. The respective gloss attributes are named absence-of-texture gloss and surface-uniformity gloss.

In addition to contrast gloss and distinctness-of-image gloss, the list of hypothetically essential appearance attributes is extended with metal gloss and pearl gloss (figure 7.2). These two gloss attributes are used for the characterization of systems including special effect pigments. Metal gloss and pearl gloss specify the intensity of the gloss sensation associated with the visual appearance of a metal object and a pearl, respectively.

Texture Attribute Selection Altogether, in the standard practice *ASTM E* 284-03*a* [8] and papers of *Eugène* [75], Ďuricovič *et al.* [238, 237], *Ershov et al.* [73, 74], *Kirchner et al.* [154,

150, 152], *Rao* and *Lohse* [212], *Rentschler* [213] a number of 16 texture attributes were found (section 4.1.3). Most of them, the texture contrast, repetitiveness, feature density, roughness, granularity, graininess, coarseness, fineness, directionality, orientation, complexity, randomness, regularity and uniformity are used for a wide range of ordinary textures. In connection with special effect pigments, the texture attributes sparkle and glint are mentioned.

In the large number of scientifically known texture attributes, the selection of texture attributes expected to be essential seems to be difficult at the first view. At the second view, several attributes for arbitrary textures can be excluded. Among others, these are the repetitiveness and the feature density. In case of printed special effect colors, the texture is not composed of texture elements being repeated after a certain sequence or having a specific number per unit area. Furthermore, the textures of printed special effect colors have a certain directionality and orientation. In principle, directionality and orientation is for itself not remarkable. Among themselves, directionality and orientation are very similar. The similarity among the textures is also an exclusion criterion for the roughness, complexity, randomness, regularity and uniformity.

Among the remaining attributes for arbitrary textures, granularity, graininess, coarseness and fineness describe the same property. The described property is the dimension of the components in the system. Due to the frequency and proportionality, graininess and coarseness were added to the list of visual appearance attributes expected to be meaningful (figure 7.2). This list also includes the texture contrast describing the location-dependent lightness variation of dark and light areas.

Apart from these ordinary texture attributes, sparkle and glint are obviously essential for the characterization of systems with special effect pigments in their texture (figure 7.2). Both texture attributes describe the perceived intensity concerning small, bright light spots in a dark, uniform surrounding area.

Attribute Adaption

Not all visual appearance attributes expected to be meaningful (figure 7.2) are experimentally testable. The limiting factors concern the definability of the visual appearance attribute and the design of the psychophysical scale as well as the level of the task's difficulty and the power of the subject's concentration.

For some of the mentioned visual appearance attributes, it is difficult to give a precise definition. The distinction of one attribute to another attribute causes sometimes particular problems. The affected attributes should be treated together.

Usually, psychophysical scales like the lightness and chroma scale have a linear shape. This is not true for the hue scale being circular in shape. In such special cases the non-linear scale should be sampled by the use of an alternative individual attribute or an alternative attribute set.

A further occasion for searching for alternatives might be induced by a too difficult task. The level of the task's difficulty should be designed in accordance with the subject's abilities [58]. Apart from a preceding training on samples, the task can be designed in a way that either a group of attributes or even the total set of attributes is evaluated together.

Despite an adequate level of difficulty, the subject gradually gets tired during the experiment. Therefore, an experimental session including instructions should not take more than one hour [58]. Without mentioning the possibility of dividing the whole session in two or more sub-sessions, less important visual appearance attributes can be omitted.

Therefore, the visual appearance attributes expected to be meaningful were subjected to an adaption resulting in a set of experimentally testable attributes. The visual appearance attributes tested in the visual experiments of this study are shown in figure 7.3 and enlisted in table 7.2.

Figure 7.3 and table 7.2 separate the visual appearance attributes for color, gloss and texture from each other. This separation is picked up in the structure of the following sections with more detailed explanation about the adaption of the *color*, *gloss* and *texture attributes*.

Color Attribute Adaption Remember the color attributes expected to be meaningful (figure 7.2). These are hue, chroma, lightness, color shift, hue shift, chroma shift and lightness shift.

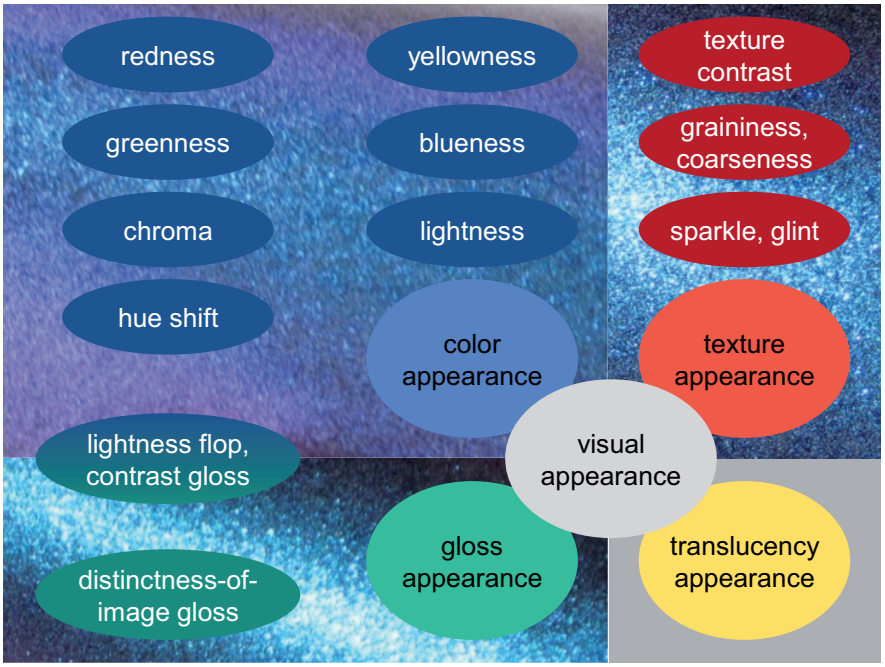

Figure 7.3: Adapted visual appearance attributes.

Table 7.2: Adapted visual appearance attributes.

visual appearance	abbreviation	visual appearance attribute
color appearance	ap	redness
	bp	yellowness
	an	greenness
	bn	blueness
	C	chroma
	L	lightness
	dH	hue shift
	dL	lightness shift
gloss appearance	CG	contrast gloss
	$DOIG$	distinctness-of-image gloss
texture appearance	TC	texture contrast
	GC	graininess and coarseness
	SG	sparkle and glint

As mentioned above, the psychophysical scale of hue is of a circular nature. Compared to circular scales, the sampling of linear scales is preferred in the conduction and evaluation of a psychophysical experiment. Therefore, the color attribute hue (figure 7.2) is replaced by the experimentally testable color attributes redness, yellowness, greenness and blueness (figure 7.3).

Among the other enlisted color attributes, chroma, lightness and hue shift were directly set on the list of experimentally testable appearance attributes (figure 7.3). Like hue, the attributes chroma and lightness belong to the fundamental color attributes. But, due to the linear character of the chroma and lightness scale, there are no experimental limitations necessitating an adaption. The psychophysical scale of the hue shift is also linear in shape. This is also valid for the color shift, chroma shift and lightness shift.

Nevertheless, the color shift, chroma shift and the lightness shift were not directly added to the set of experimentally testable appearance attributes. For printed special effect colors, the hue shift seems to be the most meaningful shift attribute to describe their geometry-dependent color appearance. The change in the perceived hue induced by a change in the geometric configuration is specified by the hue shift. The hue shift is perceptually unique due to the rare occurrence for ordinary objects. Compared to the hue shift, the chroma shift and lightness shift occur for any chromatic or glossy surface and are therefore perceptually not unique. The chroma shift and the lightness shift mean that a color is getting more or less chromatic or bright, respectively. Apart from the perceptually less unique chroma shift and lightness shift, the perceptually most unique hue shift is included in the total color shift. In the total color shift, the contribution of the hue shift may go down next to the chroma and lightness shift. Therefore, the hue shift is the first choice shift attribute on the list of experimentally testable appearance attributes (figure 7.3).

The list of experimentally testable appearance attributes (figure 7.3) also includes the lightness shift, but not in its original form. The lightness shift describes the geometry-induced lightness change. The perceived lightness difference between specular and off-specular reflection is called contrast gloss. Due to the similar meaning, lightness flop and contrast gloss are treated together as an intermediate color-gloss attribute (figure 7.3).

Gloss Attribute Adaption As just explained, the contrast gloss is listed together with the lightness shift among the experimentally testable appearance attributes (figure 7.3). Apart from the contrast gloss and distinctness-of-image gloss, the metal gloss and pearl gloss were selected as gloss attribute expected to be meaningful (figure 7.2).

As in case of the contrast gloss, the importance of the distinctness-of-image gloss in the characterization of the gloss appearance is experimentally proven [80, 200]. The experimental validation justifies the inclusion of the distinctness-of-image gloss in the set of experimentally testable appearance attribute (figure 7.3).

Such an experimental importance proof does not exist for metal gloss and pearl gloss. Furthermore, the definition of these gloss attributes themselves and the associated psychophysical scales is somehow too indistinct. In consideration of the number of visual appearance attributes and the availability of qualified subjects, metal gloss and pearl gloss are not estimated in the visual experiments.

Texture Attribute Adaption During the selection of texture attributes expected to be meaningful (figure 7.2), the texture contrast, the graininess and coarseness as well as the sparkle and glint were expected to be essential for the texture characterization of printed special effect colors. All enlisted texture attributes expected to be meaningful are included in the set of experimentally testable appearance attributes (figure 7.3). The texture contrast does not require any adaption. Due to their similar meaning, graininess and coarseness as well as sparkle and glint were each joined to a combined texture attribute.

7.2.2 Assessed Samples

The present section focuses on the printing samples assessed in the visual experiments. Important information on the *selection* and *preparation* of the samples is given in the following.

Sample Selection

For the visual experiments, adequate subsets of samples are selected from the two sets of screen and flexo printing samples (section 5.4). The *selection aspects* and the *selected samples* are subsequently presented.

Selection Aspects The selection process bases on three aspects with different significance. These aspects are the algorithm-based *spectral sorting*, the *visual specialty* and the *combination diversity*.

Spectral Sorting The first aspect is the result of an algorithm sorting the samples according to the dissimilarity of their spectral reflectance. The applied sorting algorithm was developed by *Hardeberg* [97] to select a set of filters for multi-spectral imaging. For such applications, filters with maximal differences in their spectral transmittance are most qualified. With maximally different spectral properties, the maximal number of colors is represented.

The same holds for the maximal difference in the spectral reflectance of samples intended to be used for visual experiments. Therefore, the sorting algorithm was applied on the reflectance data of the multi-angle measurements. For this purpose, the spectral reflectance factors of the different geometric configurations were just stringed together.

The result of the spectral sorting is an importance ranking of the printing samples in both sample sets. For the screen printing samples, the first eleven items in the ranking list were picked for visual validation. Visually, the picked samples do considerably differ in color. The same was tested and validated for the first 14 items in the ranking list for the set of flexo printing samples. The primary selection of eleven and 14 samples, respectively, was extended by the use of two further selection aspects explained in the following.

Visual Specialty The second selection aspect is the special visual appearance of several samples. For both sample sets, all samples were spread out on a table and visually evaluated in their specialty.

Some samples catch your eye due to a large geometry-induced color shift. A pronounced color shift especially occurs for the samples printed with special effect inks containing multi-color pigments. Samples printed with special effect inks containing sparkle pigments are also visually interesting. Due to the big particles, an intense sparkling effect is induced.

If not already covered by the first aspect in spectral sorting, such visually unique samples were marked down. Some of the earmarked samples were added to the already selected samples considering the third aspect.

Combination Diversity The third selection aspect concerns the diversity in the combination of the varied printing parameters. Besides the special effect pigment, the paper quality, the varnishing state and the background color were varied (section 5.4).

Remember the following parameter combinations for the both sample sets. The special effect inks with 22 different *BASF* pigments were applied on a white glossy and a black uncoated paper in screen printing. In flexo printing, special effect inks with 28 different *MERCK* pigments were applied on a white glossy and matt coated paper with a partial priming using a black absorption ink and an optional finishing using a clear gloss varnish.

For example, consider unselected but earmarked samples with a visually special multi-color or sparkle pigment differing in at least one of the other printing parameters. Apart from the special effect pigment, differences in the paper quality, the varnishing state and the background color are considered.

Selected Samples During the sample selection, both sample sets are treated independently. This section gives an overview of the *selected screen* and *flexo printing samples*.

Selected Screen Printing Samples In fourfold version, 14 samples were extracted from the whole set of screen printing samples. For the selection of the first eleven samples, the mentioned spectral sorting algorithm was used. Three more screen printing samples were selected on the basis of the visual specialty and the combination diversity. All 14 selected screen printing samples differing in special effect pigment (table 5.1), paper quality, varnishing state and background color (table 5.3) are enlisted in table 7.3 [146].

Table 7.3: Screen printing samples differing in the printing parameters (table 5.3) special effect pigment (table 5.1), paper quality (white glossy coated paper ($WGCP$), black uncoated paper ($BUCP$)), varnishing state (unvarnished surface (UVS)) and background color (white paper background (WPB), black paper background (BPB)) selected for visual experiments [146].

sample code	pigment code	paper quality	varnishing state	background color
$B01$	$G9S130D$	$WGCP$	UVS	WPB
$B02$	$F9G680D$	$BUCP$	UVS	BPB
$B03$	$L9232D$	$BUCP$	UVS	BPB
$B04$	$L9G30D$	$BUCP$	UVS	BPB
$B05$	$L9T30D$	$BUCP$	UVS	BPB
$B06$	$SF9832D$	$WGCP$	UVS	WPB
$B07$	$SF9832D$	$BUCP$	UVS	BPB
$B08$	$F9G480D$	$BUCP$	UVS	BPB
$B09$	$L9680H$	$BUCP$	UVS	BPB
$B10$	$L9A30D$	$BUCP$	UVS	BPB
$B11$	$L9450D$	$WGCP$	UVS	WPB
$B12$	$F9G730L$	$WGCP$	UVS	WPB
$B13$	$BO90C0Z$	$WGCP$	UVS	WPB
$B14$	$F9G130L$	$WGCP$	UVS	WPB

The letter B for $BASF$ and the number between one and 14 simplify the sample identification. All screen printing samples are shown in figure 7.4 to give an overview of the covered visual appearance range [146].

In addition to an arrow for the printing direction, the letter and the number were marked on each sample. Then, all samples cut to the maximum possible size of 120 mm times 120 mm were prepared for the visual experiments as explained below.

Selected Flexo Printing Samples In total, the sample set of visually studied flexo printing samples spans 20 samples in fourfold version. The first 14 samples were selected on the basis of the spectral sorting algorithm. Under consideration of the visual specialty and the combination diversity, six further samples were selected. Table 7.4 enlists all 20 selected flexo printing samples differing in the special effect pigment (table 5.2), paper quality, varnishing state and background color (table 5.4).

For simplification, the letter M for $MERCK$ and a number from one to 20 were assigned to the samples. As an illustration of the covered visual appearance range, figure 7.5 shows all selected flexo printing samples.

The shown flexo printing samples were labeled with the respective letter and number as well as with an arrow indicating the machine direction. After cutting to the maximum possible size of 130 mm in square, the samples were prepared as explained in the following section.

Sample Preparation

Each of the selected samples being available in at least fourfold version is prepared in two different shapes. So-called planar samples were prepared with two of the available individual samples. Two

Figure 7.4: Screen printing samples selected for visual experiments [146].

Table 7.4: Flexo printing samples differing in the printing parameters (table 5.4) special effect pigment (table 5.2), paper quality (white glossy coated paper ($WGCP$), white matt coated paper ($WMCP$)), varnishing state (unvarnished surface (UVS), glossy varnished surface (GVS)) and background color (white paper background (WPB), black printed background (BPB)) selected for visual experiments and bidirectional measurements with the three-dimensional appearance robot-based gonioreflectometer $ARGon^3$.

sample code	pigment code	paper quality	varnishing state	background color
$M01$	$I123$	$WMCP$	UVS	WPB
$M02$	$I323$	$WMCP$	UVS	BPB
$M03$	$I4504$	$WMCP$	GVS	WPB
$M04$	$I211$	$WMCP$	UVS	BPB
$M05$	$CF1000$	$WMCP$	GVS	BPB
$M06$	$CT1002$	$WMCP$	GVS	BPB
$M07$	$CT1004$	$WMCP$	GVS	BPB
$M08$	$CT1003$	$WMCP$	GVS	BPB
$M09$	$I231$	$WMCP$	UVS	BPB
$M10$	$M5320$	$WMCP$	UVS	WPB
$M11$	$I500$	$WGCP$	GVS	WPB
$M12$	$I211$	$WGCP$	GVS	WPB
$M13$	$I520$	$WMCP$	GVS	BPB
$M14$	$I201$	$WMCP$	GVS	BPB
$M15$	$CT1005$	$WGCP$	GVS	WPB
$M16$	$CT1006$	$WMCP$	GVS	WPB
$M17$	$I225$	$WGCP$	GVS	WPB
$M18$	$M5311$	$WGCP$	UVS	BPB
$M19$	$I305$	$WGCP$	UVS	BPB
$M20$	$M5320$	$WMCP$	GVS	BPB

Figure 7.5: Flexo printing samples selected for visual experiments and bidirectional measurements with the three-dimensional appearance robot-based gonioreflectometer *ARGon*^{3}.

more individual samples were prepared as rolled samples. Information about the composition and the dimensions of the *planar* and *rolled samples* is subsequently given.

Planar Samples The planar samples are composed of the printing sample and a black paper. Both components were exactly trimmed to squares and carefully fixed with a few drops of an adhesive. Local corrugations of the paper due to an extensive amount of the liquid adhesive should be avoided. Figure 7.6 shows the composition and indicates the dimensions.

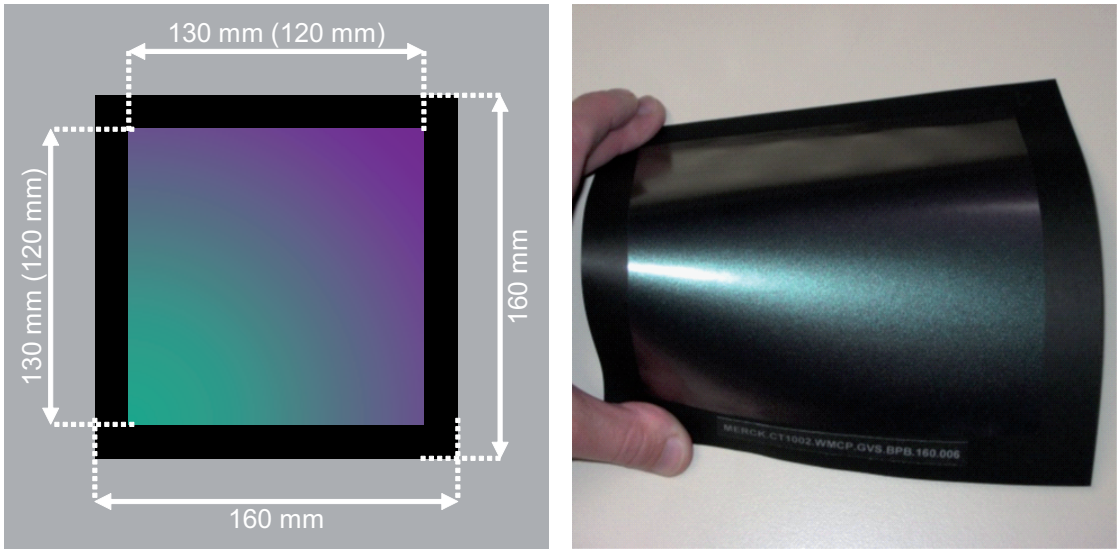

(a) Sketch. (b) Photo.

Figure 7.6: Planar sample.

A printing sample measures 120 *mm* or 130 *mm* in square for the screen and flexo printing samples, respectively. The printing sample is supported by a black paper. The dimensions of 160 *mm* times 160 *mm* were used for the black paper support. Black paper is the same paper already used in the screen printing trials. The protruding seam of the black paper allows the handling of the sample without touching the printed region. Furthermore, the seam provides space for labeling with the previously presented sample code.

The planar samples were used for visual experiments in the multi-angle test bench realizing a variety of geometric configurations. The multi-angle test bench is explained in section 7.2.3.

Rolled Samples In their composition the so-called rolled samples are similar to the planar samples. In addition to the black paper, a paper core serves as support for the printing samples. To avoid wrinkles, the rolled sample was gradually built up from the paper core over the black paper to the printing sample. The resulting sample is shown in figure 7.7.

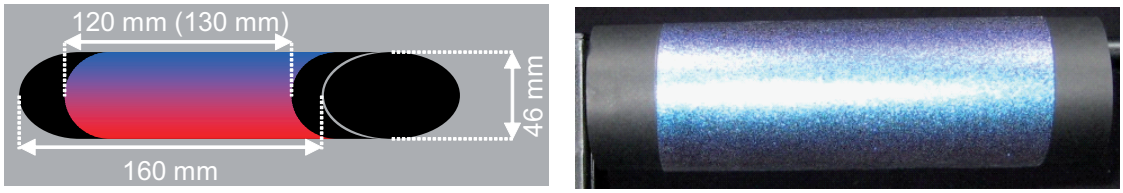

(a) Sketch. (b) Photo.

Figure 7.7: Rolled sample.

The dimensions of the printing sample and the black paper are mentioned above. The cylinder

measures 46 *mm* in diameter. This dimension is connected with the viewing distance over the visual angle. For a visual angle of 10°, the viewing distance measures 241 *mm* or 264 *mm* counted to the surface or center, respectively. The sample should exactly lie in the visual field. For such well-defined conditions, the perceivable information is comparable to that of the 10° standard observer.

Due to the curvature of the rolled sample, multiple geometric configurations are simulated simultaneously. Thus, the rolled samples are suitable for experiments in the color matching light booth presented in section 7.2.3.

7.2.3 Experimental Equipment

The experimental equipment serves as a tool for the repeatable setting and exact compliance of the experimental conditions. Apart from the spectral power distribution of the illuminant and the viewing angle of the observer the experimental conditions include the geometric configuration of light source and sample relative to the observer. These experimental conditions were realized in two different experimental setups. The modified commercial *color matching light booth Spectra Light III* and a *multi-angle test bench* developed at the *Institute of Printing Science and Technology* (*IDD*) are described in the following.

Modified Commercial Color Matching Light Booth *Spectra Light III*

As mentioned in the paper of *Kehren et al.* [146], the main component of the first experimental setup [146] is the commercial color matching light booth *Spectra Light III* of *X-Rite GmbH*. Usually, such color matching light boots are designed for visual experiments on more or less matte absorbing colors. The colored samples positioned in the medium-gray cabin are illuminated from above and viewed from ahead.

Most color matching light booths such as that one used in this study are equipped with more than one sets of light sources and special filter foils. Multiple standard illuminants can be simulated on this way. In the present case, a pair of filtered tungsten halogen lamps simulating standard illuminant $D65$ (section 4.3) was selected. The two 750 W tungsten halogen lamps including the two average north sky daylight filters are positioned behind a dispersing plate. Due to the dispersing plate, the light falling on the sample is more or less diffuse.

The commercial color matching light booth *Spectra Light III* was modified to the present requirements. The deviations from the mentioned standard requirements for visual experiments are based on the unique optical properties and visual appearance of printed special effect colors. The geometry-dependent color, the metal to pearlescent gloss and the clearly visible texture require the following measures.

The geometry-dependent color and the metal to pearlescent gloss come along with local colored highlights. To avoid their reflection on the otherwise medium-gray cabin walls, the commercial color matching light booth *Spectra Light III* was enhanced by means of a light-absorbing wall covering. The black wall covering consists of corrugated cardboard covered by black self-adhesive velour foil reducing inter-reflections. The cabin faced with the absorbing wall covering is shown figure 7.8.

Due to the geometry-dependent color and clearly visible texture, angular and translational displacements should be avoided. The precise geometric arrangement requires further extending measures at the commercial color matching light booth *Spectra Light III*. The mutual orientation and distance of sample and observer were adjusted by means of a sample holder and a chin rest shown figure 7.8. For individual evaluations or side-by-side comparisons, the sample holder allows the placement of one sample or two samples, respectively. The chin rest is fixed at the table of the modified commercial color matching light booth *Spectra Light III*. It is adjustable in its horizontal and vertical direction. The sample holder and the chin rest ensured a viewing distance of 241 *mm* and 264 *mm* counted to the surface or the center, respectively. For a rolled sample measuring 46 *mm* in diameter, the visual angle (section 4.3.2) is equal to 10°. For more detailed

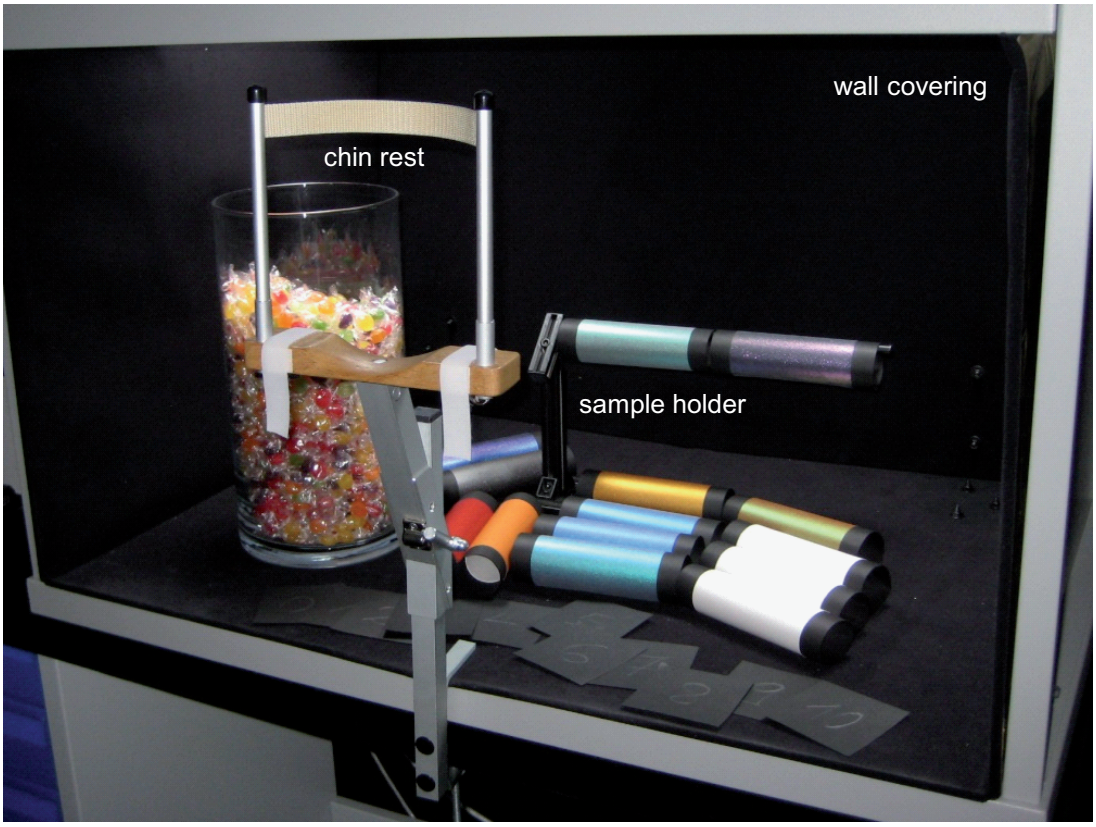

Figure 7.8: Important components of the modified commercial color matching light booth *Spectra Light III*.

information, the geometric setup of the modified commercial color matching light booth *Spectra Light III* is shown in figure 7.9 [146].

Figure 7.9 labels four geometric configurations by two numbers separated by a slash. The first number is equal to the incidence angle. The reflection angle is given by the second number. Both angles are counted relative to the surface normal. With the assumption that only directional light is vertically falling from the ceiling onto the sample, the incidence angle covers a range from $-40°$ to $90°$. In reality, the directed light is superimposed by diffuse light. For the same geometry sequence, the viewing angle lies between $90°$ and $-49°$.

To sum up, the important features of the modified commercial color matching light booth are the following ones. A filtered light source allows a more or less diffuse illumination in accordance with standard illuminant $D65$ (section 4.3). The viewing distance results in a visual angle according to $10°$ standard observer (section 4.3.2). The range of geometric configurations realized with a rolled sample lies between $-40°/90°$ and $90°/-49°$.

Multi-Angle Test Bench

The second experimental setup is a custom-made multi-angle test bench developed and evaluated by the students *Vogt* [243], *Bettner* [25], *Sperber* [227] and *Becher et al.* [19] at the *Institute of Printing Science and Technology* (*IDD*). It simulates multiple geometric configurations of light source, sample and detection system such as a multi-angle spectrophotometer or gonioreflectometer. The construction of the multi-angle test bench is in the style of the robot-based gonioreflectometer (*RGon*) and the three-dimensional appearance robot-based gonireflectometer ($ARGon^3$) of the *Physikalisch-Technische Bundesanstalt* (*PTB*, section 3.2.3).

Thus, the light source rotates on a circular path around the also rotating sample in the center of the circle. Due to the degrees of freedom in the motions of light source and sample holder, the position of the detection system or observer is held fixed. The constant position is the most ergonomic solution for the subject participating in the visual experiment [227]. For this experimental setup, the at least required components are a light source, a sample holder and a chin rest. These important components are shown in figure 7.10.

The light source itself is incorporated in the illumination unit (figure 7.10). In addition to the light source, the illumination unit includes a transformer, filter foil, lamp housing and a bi-pin connector. The light source is a narrow flood halogen bulb called $Q50MR16/CG/47/36$. *SoLux* halogen lamps are made by *Eiko Ltd.* under the license from *Tailored Lighting Inc.* as listed in table 7.5.

Table 7.5: Multi-angle test bench.

unit	component	specification	manufacturer
illumination unit	light source	$Q50MR16/CG/47/36$	*SoLux, Eiko Ltd.*
	transformer	*Halotronic HTM-75*	*Osram AG*
drive unit	stepper motor	$ST5918L3008\text{-}B$	*Nanotec Electronic GmbH & Co. KG*
	planetary gear	$GPLE60\text{-}1S\text{-}8$	
	incremental encoder	$WEDL5541\text{-}B06$	
control unit	positioning control	$SMCI33\text{-}1$	*Nanotec Electronic GmbH & Co. KG*
	connection cable	$ZK\text{-}WEDL\text{-}8\text{-}500\text{-}S$	
	charging capacitor	$Z\text{-}K4700/50\text{-}2$	

In the product specification $Q50MR16/CG/47/36$, the number 50 stands for the consumed electrical power of $50\ W$. The joined expression $MR16$ specifies the casing shape as a mini reflector abbreviated with the letters MR. The abbreviation CG means covered glass and specifies the lens type. The numbers 47 and 36 stand for a correlated color temperature of $4700\ K$ and a beam angle of $36°$, respectively. The stated correlated color temperature of $4700\ K$ as well as the radiant exitance of $1484\ W/m^2$, the average live time of $4000\ h$ and the color rendering index of 99 are only valid for the intended voltage of $12\ V$. For an increased voltage of $13.35\ V$, the

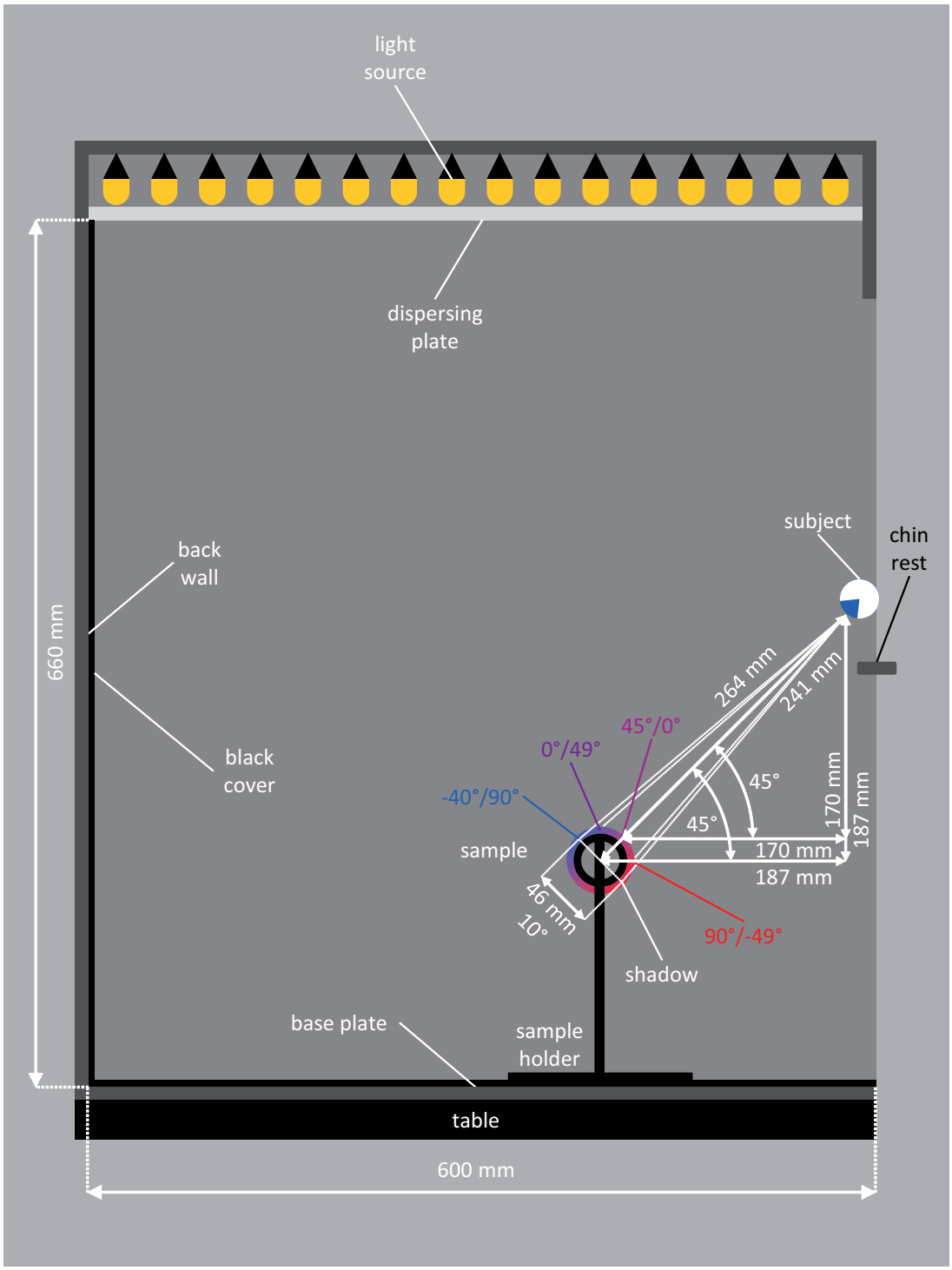

Figure 7.9: Geometric setup in the modified commercial color matching light booth *Spectra Light III* with a rolled sample to simulate multiple geometric configurations between $-40°/90°$ and $90°/-49°$ [146].

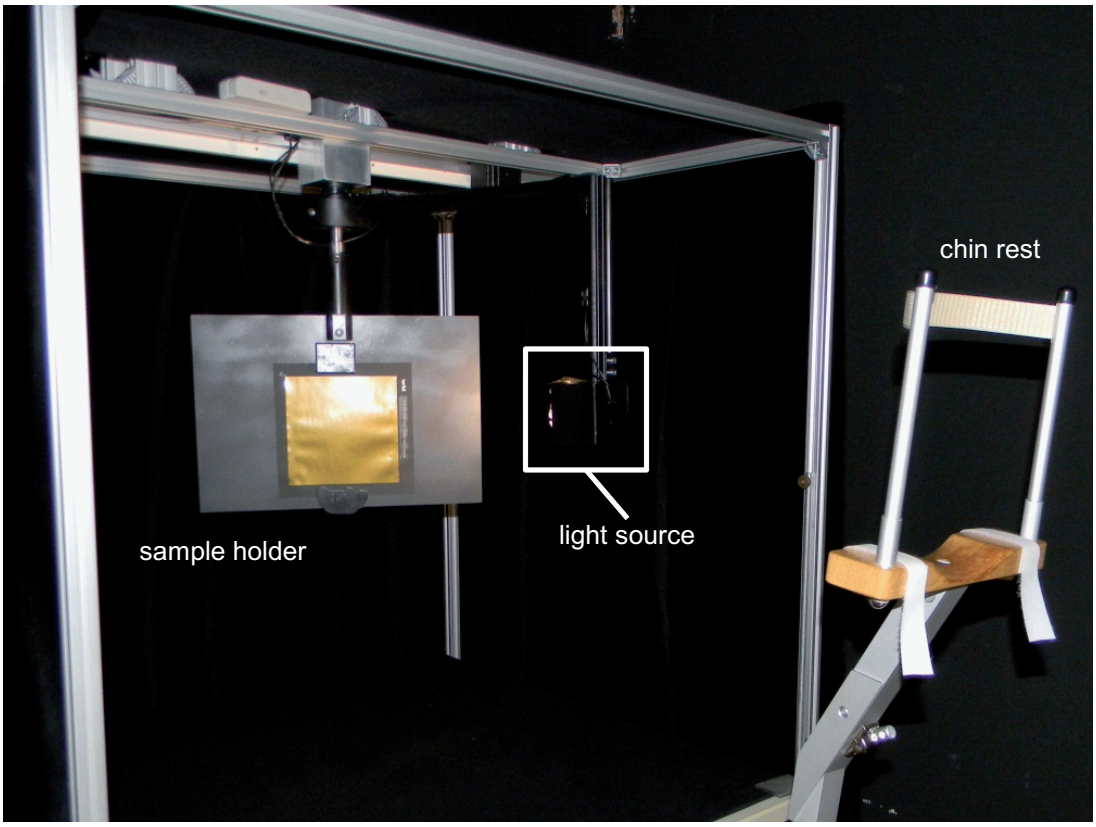

Figure 7.10: Important components of the multi-angle test bench developed at the *Institute of Printing Science and Technology* (*IDD*).

correlated color temperature is about 5000 K. In the present case, a small transformer named *Halotronic HTM*-75 of *Osram AG* (table 7.5) was used to increase the voltage to 13.35 V and thereby the correlated color temperature to 5000 K. For a further increase of the correlated color temperature to 6500 K for example, a filter foil can be fixed at the glass lens. In spite of the black painting on the back side of the reflector casing, some light is emitted through the reflector casing. An enclosure for the lamp was necessary to shield the escaping light. In the black painted lamp housing (figure 7.10), there is a standard bi-pin connector appropriate to the bi-pin base of the halogen bulb. The lamp housing with bi-pin connector and halogen bulb is mounted on a rectangular screwed strut profile. This aluminum profile moves the light source on a circular path around the sample holder. A circle radius of 330 mm achieves the complete illumination of the sample holder.

As the designation suggests, the task of the sample holder (figure 7.10) is to hold the sample in a specified position. This is achieved by means of a metal plate and two permanent magnets. Both are painted in black to avoid disturbing reflections. The metal plate measures 330 mm in width and 230 mm in height. One or two printed samples fixed on a 160 mm times 160 mm black paper support can be illuminated and viewed. For the printed samples cut to rectangles with edge lengths of 130 mm or 120 mm, a viewing distance of 743 mm and 686 mm, respectively, results in a visual angle of 10°. The exact distance and orientation of the subject to the sample is realized using a chin rest (figure 7.10). The chin rest is fixed in the desired position and the subject sits on a height-adjustable chair. Figure 7.11 shows the experimental setup in detail.

Apart from the light source, the sample holder and the chin rest, further mechanical and electrical components are required. These are the frame and the covering as well as the drive unit and the control unit.

The frame is based on an ordinary table measuring 800 mm in square. All four legs of the table are extended upward beyond the top of the table with aluminum profiles. The upper ends of the vertical aluminum profiles are connected with horizontal aluminum profiles. The vertical and horizontal profiles are the frame of the illuminated and observed space. Despite its installation in a black painted room without windows, the test space is protected against unintentionally incident light. All sides except that in the direction of observation are covered with a curtain of black velvet. The top of the cabin and also the top of the table are covered with black self-adhesive velour foil supported by corrugated board.

The drive unit is installed on the top of the cabin. The whole drive unit includes two identical subunits. The components of both subunits are a stepper motor ($ST5918L3008\text{-}B$) with planetary gear ($GPLE60\text{-}1S\text{-}8$) and incremental encoder ($WEDL5541\text{-}B06$) provided by *Nanotec Electronic GmbH & Co. KG* (table 7.5). Using a toothed belt, one of the motor-gear units is connected with a hollow shaft moving the light source. The other motor-gear unit is directly connected with a solid shaft for the motion of the sample holder.

The control unit is located under the table. As the drive unit, it includes two identical subunits. The components are each a motor positioning control ($SMCI33\text{-}1$), a connection cable ($ZK\text{-}WEDL\text{-}8\text{-}500\text{-}S$) and a charging capacitor ($Z\text{-}K4700/50\text{-}2$) also provided by *Nanotec Electronic GmbH & Co. KG* (table 7.5). The test bench is driven with a lap top computer using the system design software *LabVIEW* of *National Instruments Germany GmbH*.

All standardized geometric configurations specified in the standard practices *ASTM E* 2194-03 [7] and *DIN* 6175-2:2001-03 [64] are taken into account in the computer program. The currently desired geometric configurations are selectable in a drop-down menu. However, not all implemented geometric configurations are useful in terms of direct glare and realizable in terms of time. The usability of all realized geometric configurations was checked during some pilot tests. Figure 7.12 shows six geometric configurations judged as reasonable for the visual experiments.

The successively set geometric configurations are those with the labels $45as\text{-}15$, $45as15$, $45as25$, $45as45$, $45as75$ and $45as110$ introduced in section 3.2.2. The corresponding views of the subject on the sample are shown in figure 7.13.

The multi-angle test bench was developed and evaluated in several student projects [19, 25, 227, 243]. A student assistant assembled the components and generated the program for the successive setting of the different geometric configurations.

Summing up the specific properties of the custom-made multi-angle test bench yields the following list. The sample is illuminated with a directed beam of unfiltered light having a spectral power distribution like that of the standard illuminant $D50$. The 10° standard observer is realized by an adjustment of the visual angle or rather the viewing distance for a specific sample size. Among the great variety of mechanically realized geometric configurations, six standardized geometric configurations without direct glare were included in the program. The program successively runs the geometric configurations $45as$-15, $45as15$, $45as25$, $45as45$, $45as75$ and $45as110$.

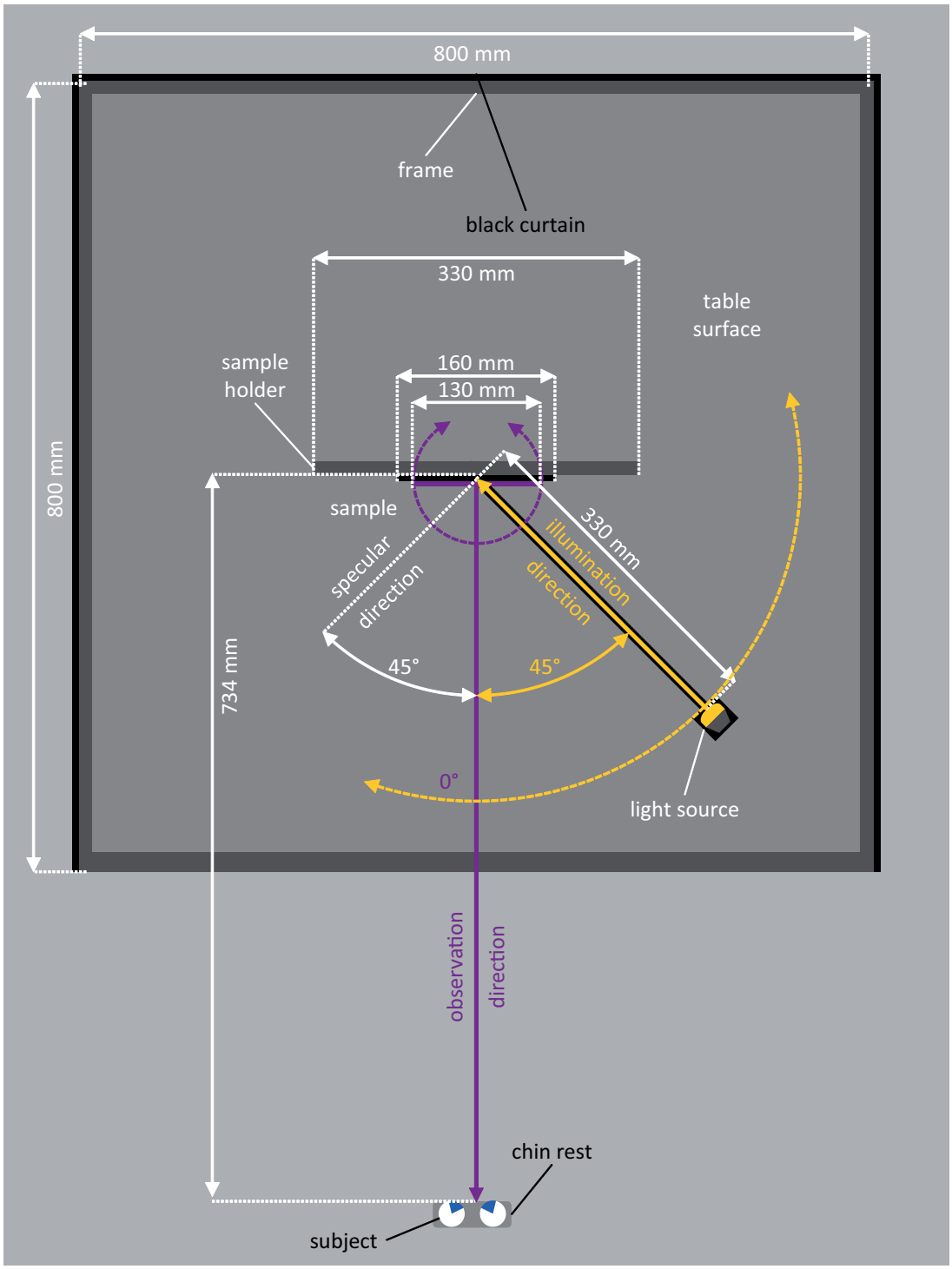

Figure 7.11: Geometric setup in the multi-angle test bench developed at the *Institute of Printing Science and Technology* (*IDD*) to realize multiple geometric configurations such as 45*as*45 with a planar sample.

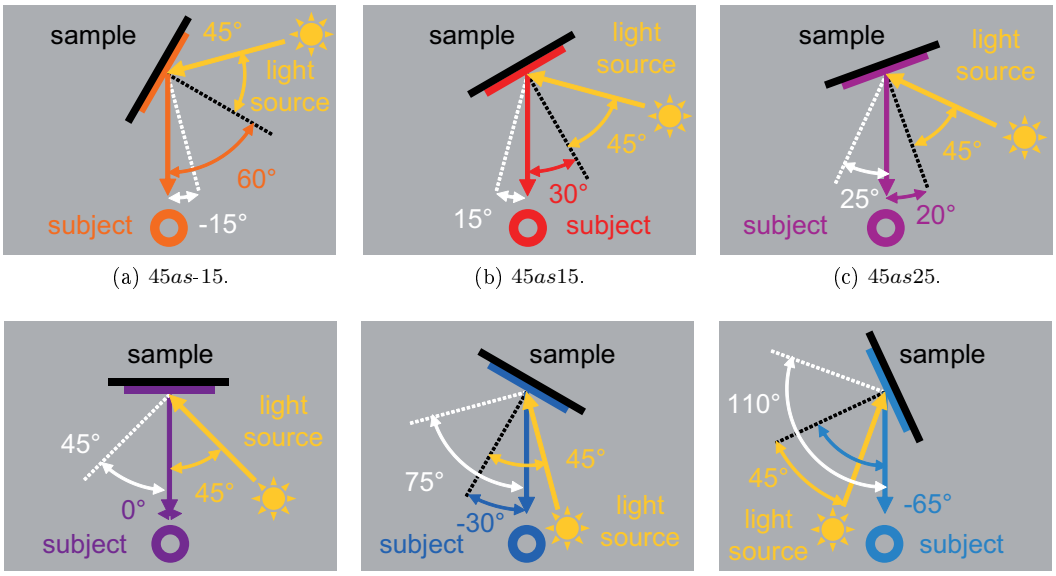

(a) 45*as*-15. (b) 45*as*15. (c) 45*as*25.

(d) 45*as*45. (e) 45*as*75. (f) 45*as*110.

Figure 7.12: Sketches of geometric configurations in the multi-angle test bench.

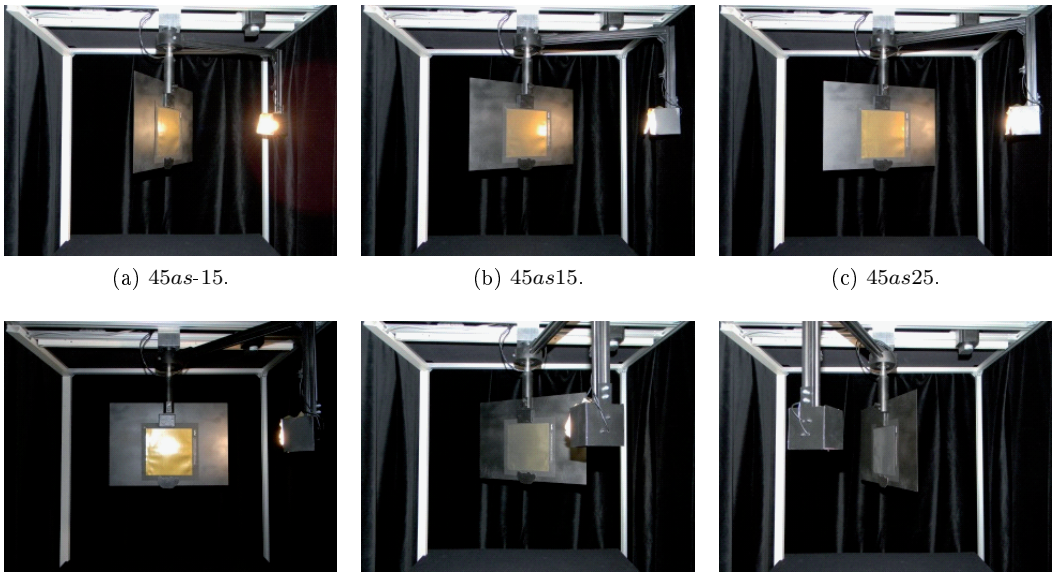

(a) 45*as*-15. (b) 45*as*15. (c) 45*as*25.

(d) 45*as*45. (e) 45*as*75. (f) 45*as*110.

Figure 7.13: Photos of geometric configurations in the multi-angle test bench.

7.3 Conducting the Visual Experiments

This section focuses on the execution of the visual experiments. A series of three experimental trails was conducted. Due to the resemblances of these three trials, the descriptions overlap. Therefore, the information about the execution of the visual experiments is presented in sections called *trial specification* (section 7.3.1) and *participating subjects* (section 7.3.2).

7.3.1 Trial Specification

As just mentioned, a series of three trials was executed in succession. The successively conducted trials are characterized by four specifications. The trial specification bases on the specifications of the experimental conditions given above in section 7.2. These specifications are namely the experimental procedure, the estimated dimension, the experimental equipment and the sample set. For each trial specification, two alternatives were realized. Both alternatives per specification including the respective abbreviation are listed in table 7.6.

Table 7.6: Abbreviations for the specification of trials.

specification	abbreviation	information
procedure	RCS	relative category scaling
	ACS	absolute category scaling
dimension	VAD	visual appearance difference
	VAA	visual appearance attributes
equipment	$CMLB$	color matching light booth
	$MATB$	multi-angle test bench
samples	$OB14$	14 rolled screen printing samples
	$IM20$	20 planar flexo printing samples

The experimental method (section 7.1) is either the relative category scaling (RCS) or the absolute category scaling (ACS). The visual appearance difference (VAD) or visual appearance attributes (VAA) are the psychophysical scales (section 7.2.1). As experimental setup (section 7.2.3), the color matching light booth ($CMLB$) and the multi-angle test bench ($MATB$) are available. A number of 14 rolled screen ($OB14$) or 20 planar flexo ($IM20$) printing samples were assembled in two separate sample sets (section 7.2.2).

With four specifications and two alternatives, 16 combinations are possible in total. Among the large number of possible combinations, the most useful combinations need to be identified. The combinations should make a physical sense and have an adequate extent. The identification of reasonable combinations was realized in a two-step procedure. The *primary* and *secondary trial combinations* are explained in the following.

Primary Trial Combinations

The primary selection was realized on trial combinations of two individual specifications. The primary combinations are the *experimental procedure* and the *estimated dimension* as well as the *experimental equipment* and the *sample set*. The sense and extent of these primary combinations are subsequently treated.

Primary Trial Combinations of Procedure with Dimension The primary combination of the two alternatives for the experimental procedure and the two alternatives for the estimated dimension results in four possible combinations. In table 7.7, these four primary procedure-dimension combinations are assessed in their sense and extent.

The absolute category scaling (ACS) of the visual appearance difference (VAD) makes no sense. Visual appearance differences can be only estimated for stimulus pairs. However, individual stimuli are considered in an absolute category scaling experiment.

Table 7.7: Primary trial combinations of procedure with dimension.

primary trial combination		procedure	
		RCS	*ACS*
dimension	*VAD*	good sense, right extent	no sense, right extent
	VAA	good sense, high extent	good sense, right extent

In contrast to that, a relative category scaling (*RCS*) experiment works with stimulus pairs. Thus, the requirement concerning the physical sense is fulfilled for the relative category scaling of visual appearance differences (*VAD*). The relative category scaling of total visual appearance differences also fulfills the condition concerning an adequate extent. A number of m samples can be combined to $m \cdot (m-1)/2$ different pairs of different samples. The $m \cdot (m-1)/2$ difference estimates are filed in a symmetric m-by-m dissimilarity matrix. For 14 screen or 20 flexo printing samples these are 91 or 190 difference estimates per subject, respectively.

The visual appearance attributes are estimated for individual stimuli. Therefore, the absolute category scaling (*ACS*) of visual appearance attributes (*VAA*) makes a physical sense. Apart from the physical sense, the absolute category scaling of visual appearance attributes has an adequate extent. For each of m samples, each of n attributes is estimated. This results in an m-by-n rating matrix. For 14 screen or 20 flexo printing samples and twelve attributes, each subject gives 168 or 240 difference estimates, respectively.

In contrast to the three already mentioned combinations, the extent is too high for the relative category scaling (*RCS*) of visual appearance attributes (*VAA*). Each visual appearance attribute should be estimated for each sample pair. Remember the number of $m \cdot (m-1)/2$ different pairs of different samples for m samples. With a number of n visual appearance attributes, this results in $n \cdot m \cdot (m-1)/2$ difference ratings. For twelve visual appearance attributes and 14 screen printing samples or 20 flexo printing samples, these are 1092 or 2280 difference estimates, respectively.

To sum up, the procedure-dimension combinations of the relative category scaling (*RCS*) with the visual appearance difference (*VAD*) and of the absolute category scaling (*ACS*) with the visual appearance attributes (*VAA*) are appropriate. In the secondary trial combinations, these both primary trial combinations are treated again.

Primary Trial Combinations of Equipment with Samples Four primary combinations are obtained for two alternatives in the experimental equipment and two alternatives in the sample set. The sense and extent of these equipment-samples combinations are assessed in table 7.8.

Table 7.8: Primary trial combinations of equipment with samples.

primary trial combination		equipment	
		CMLB	*MATB*
samples	*OB*14	good sense, right extent	no sense, right extent
	*IM*20	no sense, right extent	good sense, right extent

Trials in the color matching light booth (*CMLB*) on the planar flexo printing samples (*IM*20) as well as trials in the multi-angle test bench (*MATB*) on the rolled screen printing samples (*OB*14) make no sense. The reason lies in the simultaneous or successive simulation of multiple geometric configurations during the visual experiment. A change in the geometric configuration results in a change in the optical properties and visual appearance.

In the color matching light booth, the stationary sample is illuminated more or less directional from above and viewed obliquely from the side. For a planar sample, only one single geometric

configuration can be realized simultaneously and successively. A simultaneous simulation of multiple geometric configurations can be realized by means of a rolled sample. Thus, trials in the color matching light booth ($CMLB$) on the rolled flexo printing samples ($OB14$) make sense.

In case of the multi-angle test bench, the rotating sample is illuminated by an also rotating light source and viewed by a stationary subject. For a rolled sample, the simulation of multiple geometric configurations is realized simultaneously and successively. The rotation of the light source and a rolled sample is superfluous. The rotation of the light source and a planar sample is necessary. For the planar sample, multiple geometric configurations are simulated successively. Therefore, the requirement to make sense is fulfilled for trials with the multi-angle test bench ($MATB$) on planar flexo printing samples ($IM20$).

Apart from the physical sense, the extent should be adequate. This is the case for all equipment-samples combinations. The number of successively simulated geometric configurations as well as the number of individual samples and sample pairs was already limited during the equipment design, the sample design and the sample selection. For the color matching light booth, the number of successively realized geometric configurations is equal to one. Six carefully selected geometric configurations are successively simulated in the multi-angle test bench. As mentioned above, a number of m samples can be combined to a number of $m \cdot (m-1)/2$ different pairs of different samples. For the sample sets of 14 screen and 20 flexo printing samples, the number of sample pairs is 91 and 190, respectively.

Thus, the equipment-samples combinations of the color matching light booth ($CMLB$) with the rolled flexo printing samples ($OB14$) and of the multi-angle test bench ($MATB$) with the planar flexo printing samples ($IM20$) are suitable. These both primary trial combinations are further assessed in the secondary trial combinations.

Secondary Trial Combinations

The secondary combinations are based on the primary combinations identified to make physical sense and to have an adequate extend. Both reasonable procedure-dimension combinations are combined with both meaningful equipment-samples combinations. This results in four secondary combinations of an experimental procedure, an estimated dimension, a test equipment and a sample set. All procedure-dimension-equipment-samples combinations are assessed in their sense and extent, as shown in table 7.9.

Table 7.9: Secondary trial combinations of procedure and dimension with equipment and samples.

secondary trial combination		procedure, dimension	
		RCS-VAD	*ACS-VAA*
equipment, samples	*CMLB-OB14*	good sense, right extent	good sense, right extent
	MATB-IM20	good sense, high extent	good sense, right extent

All secondary trial combinations make sense. In addition to the physical sense, the extent needs to be adequate. Among the secondary trial combinations, the relative category scaling (RCS) of visual appearance differences (VAD) in the multi-angle test bench ($MATB$) on 20 planar flexo printing samples ($IM20$) causes the highest extent.

In the relative category scaling experiment, a series of sample pairs is presented to the subject and estimated in their total visual appearance difference. In the multi-angle test bench, the samples or sample pairs are successively shown in six geometric configurations. The presentation and estimation of a number of 190 sample pairs for a number of 20 individual samples results in a comparably high extent.

Due to the higher extent, the other trials are preferred against the trial *RCS-VAD-MATB-IM20*. The three preferred trials are namely the *trial RCS-VAD-CMLB-OB14*, the *trial ACS-VAA-CMLB-OB14* and the *trial ACS-VAA-MATB-IM20*. These three trials were conducted

in this study. Therefore, they are described in the following paragraphs in more detail.

Secondary Trial Combination *RCS-VAD-CMLB-OB*14 The trial *RCS-VAD-CMLB-OB*14 is the relative category scaling (*RCS*) of the visual appearance difference (*VAD*) in the color matching light booth (*CMLB*) on 14 rolled screen printing samples (*OB*14). At the beginning of the trial, some formal things are treated. The formal things include a request of personal data, tests of the visual performance and explanations of the experimental task. Subsequent to the formal part, a short training phase and the actual test phase follow.

In the training phase, all 14 rolled screen printing samples are positioned in the experimental area of the color matching light booth. In front of the color matching light booth, the subject takes place on an office chair to have a good look on the samples spread out in the experimental area. The subject is allowed to touch the samples at the edges consisting of the black paper support. The supervisor asks the subject to identify the sample pair or pairs with the maximal total visual appearance difference in the whole sample set. The identified sample pair or pairs are the reference for the maximal value of ten on the psychophysical scale describing the total visual appearance difference. The minimal value of zero stands for no total visual appearance difference. The linking of the perceived difference and the scale value is trained on several sample pairs. When the subject is familiar with the task, the training phase finishes and the test phase begins.

During the test phase, the subject sits still on the office chair with the head positioned on the chin rest. The subject's task is to look at the sample pair and to give the respective estimate. The supervisor undertakes the handling of the samples and the listing of the estimates. All 91 possible pairs of different samples are successively positioned on the sample holder. As soon as both samples are positioned on the sample holder, the subject gives the difference estimate.

The estimated difference in the total visual appearance is noted in a 14-by-14 upper triangular matrix called dissimilarity matrix. The dissimilarity matrix has 14 rows and columns for 14 rolled screen printing samples. The matrix element in row k and column l or row l and column k corresponds to the estimated difference between sample k and l. Two samples produced in the same conditions were assumed to be perceived identical. Thus, the elements on the decreasing diagonal of the dissimilarity are equal to zero. The dissimilarity matrix is evaluated in classical multidimensional scaling (*CMDS*, section 4.5.4, section 7.4.1, section 7.4.2).

Secondary Trial Combination *ACS-VAA-CMLB-OB*14 The absolute category scaling (*ACS*) of twelve visual appearance attributes (*VAA*) in the color matching light booth (*CMLB*) on 14 rolled screen printing samples is shortly terminated as trial *ACS-VAA-CMLB-OB*14. As mentioned above, the formal things are treated at the beginning. Some personal data are requested, the visual performance is tested and the experimental task is explained. A short training phase is followed by the actual test phase.

At the beginning of the training phase, the subject takes seat in front of the color matching light booth. In the experimental area of the color matching light booth, all 14 rolled screen printing samples are spread out to give an overview about their visual appearance. The subject is asked to sort the samples in an ascending order with respect to the currently considered visual appearance attribute. Apart from stringing them together, the samples can be arranged side by side to indicate an equally perceived intensity of the visual appearance attribute. Subsequent to the sorting, numbers ranging from zero to ten are assigned to individual samples or sample groups. In other words, more than one sample can get the same rating. The combined sorting and rating is expected to result in a better accuracy. The described task is trained on sample subsets and attribute subsets in the training phase until the subject is familiar with the sorting and rating.

In contrast to the training phase, the sorting and rating sequence is conducted with all 14 rolled screen printing samples and subsequently for all twelve visual appearance attributes. Furthermore, the subject's estimates of the visual appearance attributes are noted for the test phase. The attribute estimates are noted in the rating matrix. In the present case, the rating matrix is a 14-by-12 matrix. It has 14 rows for the 14 rolled screen printing samples and twelve columns for the twelve visual appearance attributes. The evaluation of the rating matrix includes two correlation

analyses (CA), a principal component analysis (PCA) followed by an orthogonal rotation (OR) as well as an exploratory factor analysis (EFA) based on a dimension reduction (DR, section 4.5.4, section 7.4.1, section 7.4.2).

Secondary Trial Combination *ACS-VAA-MATB-IM20* The abbreviation as trial ACS-VAA-$MATB$-$IM20$ labels the absolute category scaling (ACS) of twelve visual appearance attributes (VAA) in the multi-angle test bench ($MATB$) on 20 planar flexo printing samples. Like the others, this trial starts with some formal things. Questions, tests and information concerning personal data, the visual performance and the experimental task are included in the formal part of the trial. This formal part is followed by a short training phase and the actual test phase.

For training, the color matching light booth is needed. The color matching light booth provides enough space to spread out all 20 planar flexo printing samples. Furthermore, the experimental area of the multi-angle test bench is oriented vertical. The fixation of the samples with permanent magnets is inappropriate for training. The subject is asked to pick up and tilt the samples to view them in different geometric configurations. The supervisor demands for some estimates of the twelve selected visual appearance attributes until the subject is familiar with the task.

The task is the same in the test phase. Here, the multi-angle test bench is used to hold and rotate the printed sample and the light source. In front of the multi-angle test bench, an office chair is provided for the subject. The subject's head is positioned in the chin rest while a sequence of six geometric configurations is simulated. The subject just looks at the rotating sample and subsequently estimates the intensity of six from twelve selected visual appearance attributes. The visual appearance attributes redness, yellowness, greenness, blueness, lightness and chroma are estimated in the first session part. The first part is temporally separated from the second part or performed by another subject. In the second session part, the remaining six visual appearance attributes are estimated. These are namely the hue shift, the lightness shift and contrast gloss, the distinctness-of-image gloss, the texture contrast, the graininess and coarseness as well as the sparkle and glint.

The estimates are noted in two partial 20-by-6 rating matrices with 20 rows for 20 planar flexo printing samples and six columns for six from twelve visual appearance attributes. Two partial 20-by-6 rating matrices for different attribute subsets were joined together to one total 20-by-12 rating matrix. The total 20-by-12 rating matrix has 20 rows for 20 planar flexo printing samples and 12 columns for 12 visual appearance attributes. The rating matrix is evaluated in two correlation analyses (CA), a principal component analysis (PCA) with a subsequent orthogonal rotation (OR) as well as in an exploratory factor analysis (EFA) based on a dimension reduction (DR, section 4.5.4, section 7.4.1, section 7.4.2).

7.3.2 Participating Subjects

This section focuses on the subjects participating in the visual experiments on printed special effect colors. The *features* of the subjects, the *requirements* on the subjects and the *instructions* to the subjects are presented in the following.

Subject Features

The population of subjects includes subjects of male and female gender, a wide range of age and diverse degrees of experience in visual perception and psychophysics experiments. Due to the difficulties in the quantitative evaluation of experience, the following information is limited to gender and age. An overview about *gender* and *age* of the participating subjects is given in table 7.10.

For the gender, the number of female subjects and male subjects as well as the total number of subjects are enlisted. The distribution of the age is characterized by the use of the minimum age, the maximum age, the average age and the standard deviation. These values are each given for all three experiments characterized by the experimental procedure, the estimated dimension, the experimental equipment and the sample set.

Table 7.10: Gender and age of subjects for the three trials specified by the experimental procedure (relative category scaling (RCS), absolute category scaling (ACS)), the estimated dimension (visual appearance difference (VAD), visual appearance attributes (VAA)), the experimental equipment (color matching light booth ($CMLB$), multi-angle test bench ($MATB$)) and the sample set (14 rolled screen printing samples ($OB14$), 20 planar flexo printing samples ($IM20$)).

trial	procedure	RCS	ACS	ACS
	dimension	VAD	VAA	VAA
	equipment	$CMLB$	$CMLB$	$MATB$
	samples	$OB14$	$OB14$	$IM20$
gender	female	14 subjects	9 subjects	14 subjects
	male	24 subjects	13 subjects	20 subjects
	total number	38 subjects	22 subjects	34 subjects
age	minimal	23 years	25 years	22 years
	maximal	63 years	49 years	46 years
	average	34.5 years	31.4 years	25.7 years
	standard deviation	9.7 years	5.8 years	4.6 years

Gender In the trial *RCS-VAD-CMLB-OB*14, 38 subjects were employed. Amongst them, there are 14 female and 24 male subjects [146].

A subset of 22 subjects participated in the trial *ACS-VAA-CMLB-OB*14. This subset includes nine female and 13 male subjects [146].

In the trial *ACS-VAA-MATB-IM*20, 34 subjects took place. This group is composed of 14 female and 20 male subjects.

Age For the trial *RCS-VAD-CMLB-OB*14, the average age is equal to 34.5 years. The standard deviation is 9.7 years. The minimal age and maximal age is 23 years and 63 years, respectively [146].

An average age of 31.4 years is obtained for the trial *ACS-VAA-CMLB-OB*14. In this case, the standard deviation is 5.8 years. The age ranged from 25 years to 49 years [146].

For the trial *ACS-VAA-MATB-IM*20 the mean age is 25.7 years. The associated standard deviation is 4.6 years. The minimum and maximum value of the age is 22 years and 46 years, respectively.

Subject Requirements

Apart from their majority, the requirements on the participating subjects concern their visual performance. All subjects should have a normal or corrected-to-normal *visual acuity* as well as a non-deficient *color vision*.

Visual Acuity To check the visual acuity, at least one of three available visual acuity tests was used. The visual acuity tests are namely the *Landolt C* Detection Test, the *Snellen E* Detection Test and the *Snellen* Letters Recognition Test. These visual acuity tests are presented in section 4.2.1.

Color Vision The color vision was checked with at least two of three available color deficiency tests. The *Ishihara* Color Deficiency Test [128, 239], the *Farnsworth-Munsell D*15 Test [241] and the *Farnsworth-Munsell* 100 Hue Test [77, 78, 241] are introduced in section 4.2.2. All subjects passed the *Ishihara* Color Deficiency Test and the *Farnsworth-Munsell D*15 Test. On a voluntary basis, the *Farnsworth-Munsell* 100 Hue Test was performed by interested subjects.

Subject Instructions

The instructions to the participating subjects include general information on psychophysical experiments as well as special information on this visual experiment with printed special effect colors. The *general* and *special information* on *psychophysical* and *visual experiments*, respectively, are listed in the following.

General Information on Psychophysical Experiments The general information on psychophysical experiments concerns the voluntariness, confidentiality, privacy and harmlessness. Thus, the subjects may leave the running experiment and withdraw given responses. The supervisors should keep data confidential and note the ethical guidelines [58].

All subjects recruited on a voluntary basis sign a consent form before they participate in the psychophysical experiment. With their signature, they give their consent to begin the psychophysical experiment. They confirm to be informed that they may leave the experiment at any time. Furthermore, they confirm to know that they are able to forbid the usage of their responses.

The subjects in all cases are free to withdraw from the experiment at any time. The individual responses of all subjects are only used for statistical calculations. The results obtained from all subjects will be kept strictly confidential. A single subject will not be identified in any kind of publication. On this way, the anonymity of each subject is preserved.

In these experiments, only subjects of full age are allowed to participate. The only requirement on the participating subjects is their normal visual performance. This includes a normal color vision as well as normal or corrected to normal visual acuity.

The conducted procedures of the psychophysical experiment are completely harmless. All experiments are conducted in full agreement with the so-called ethic guidelines [58]. These ethic guidelines were established by the *Deutsche Gesellschaft für Psychologie e. V.* (*DGPs*).

Special Information on this Visual Experiment Among others, the special information on this visual experiment concern the experimental equipment (section 7.2.3) as well as the assessed samples (section 7.2.2). The construction of the experimental setup and the production of the printed samples are shortly explained.

Furthermore, some precise information is given on the assumed trisection of the visual appearance in color, gloss and texture (section 4.1). The three visual appearance domains including the selected and adapted visual appearance attributes were explained in detail and trained on several samples (section 7.2.1).

Finally, the experimental procedure (section 7.3) is explained with precise instructions about the asked questions and possible answers. Any questions of the subject about the visual experiment or additional things, such as the statistical evaluation (section 7.4), were answered by the supervisor as good as possible.

7.4 Evaluating the Collected Datasets

The evaluation of the collected datasets includes several multivariate statistical analyses. These are namely a classical multidimensional scaling ($CMDS$), two correlation analyses (CA), a principal component analysis (PCA) followed by an orthogonal rotation (OR) and an exploratory factor analysis (EFA) based on a dimension reduction (DR). The properties and procedures of the multivariate statistical methods are explained in section 4.5.4.

Section 7.1 introduces the connection of these multivariate statistical methods via interim results. These are the configuration and the composition. In spite of the acting as an interim result, the number of essential correlates is rather a final result. A final result is also the nature of essential correlates. They are also included in the so-called methodical concept shown in detail in figure 7.1. In the following, the *interim* and *final results* are presented in section 7.4.1 and section 7.4.2, respectively.

7.4.1 Interim Results

As mentioned above, the interim results are the so-called *configuration* and *composition*. They are obtained by means of *classical multidimensional scaling* and a *principal component analysis* of the dissimilarity matrix and the rating matrix, respectively. Apart from some information about the preparing of the matrices and about the realization of the analyses, the interim results are presented in the following.

Configuration from Classical Multidimensional Scaling

In the trial $RCS\text{-}VAD\text{-}CMLB\text{-}OB14$, visual appearance differences (VAD) between two samples of the 14 rolled screen printing samples ($OB14$) were estimated in a relative category scaling (RCS) experiment using the color matching light booth ($CMLB$). For each subject, the collected difference estimates of the total visual appearance were noted in symmetric 14-by-14 dissimilarity matrices. An integer scale ranging from zero to ten was given as basis for the relative category scaling of the visual appearance differences. By some subjects, the ten or even the nine were not used. Therefore, the dissimilarity matrix of each subject was normalized. Normalization means that the maximal value in the dissimilarity matrix was set to be equal to one. The normalized dissimilarity matrices of all subjects were averaged.

By the use of classical multidimensional scaling ($CMDS$), the averaged dissimilarity matrix was converted in the so-called configuration. As explained in section 4.5.4 on $CMDS$, the configuration is the best fitting spatial arrangement of the samples. The configuration for the trial $RCS\text{-}VAD\text{-}CMLB\text{-}OB14$ is shown in figure 7.14 and figure 7.15.

Figure 7.14 shows the projection of the configuration on the plane spanned by the first and second configuration dimension [146]. Apart from the data points, photos of the samples and labels of the visual appearance attributes are included in figure 7.14 and figure 7.15. The additional photos of the samples simplify the interpretation of the configuration. The interpreted results are clarified by the additional labels.

In the configuration, local grouping of samples with similar visual appearance attributes occurs [146]. Especially for the well-known color attributes, the local grouping becomes quite clear by means of the photos.

The white samples $B01$, $B12$ and $B14$ with a perceptually high lightness (L) are grouped in the upper right corner of the projected configuration. In the first quadrant, the coordinate values are positive for the first two configuration dimensions. For these light samples $B01$, $B12$ and $B14$, the coordinate values in the first configuration dimension are higher than in the second configuration dimension.

The samples $B03$, $B06$ and $B07$ with a perceptually medium to high yellowness (bp) and redness (ap) as well as the sample $B11$ with a perceptually very high redness (ap) have a perceptually high chroma (C). The named samples $B03$, $B06$, $B07$ and $B11$ are located in the lower third of

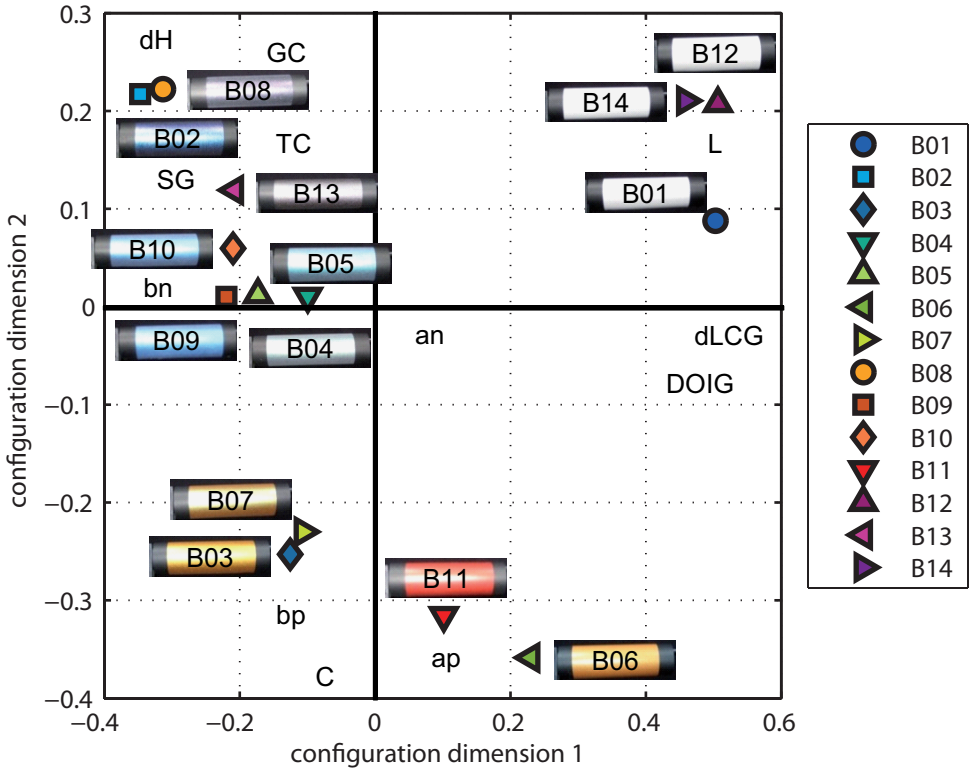

Figure 7.14: Configuration in first and second dimension for trial *RCS-VAD-CMLB-OB*14 (table 7.6) with local groups of printing samples with similar visual appearance attributes (table 7.2) [146].

figure 7.14 expressed by high negative values in the second configuration dimension. In the first configuration dimension, their coordinate values are near zero.

In the second configuration dimension, the coordinate values are near zero for the blue samples $B09$ and $B10$ and the green samples $B04$ and $B05$. The samples $B09$ and $B10$ and also the sample $B02$ with a perceptually high blueness (bn) have high negative values in the first configuration dimension. The samples $B04$ and $B05$ with a perceptually high greenness (an) lie somewhat nearer at the zero point of the projected configuration.

The hue shift (dH) is perceived to be high for the samples $B02$ and $B08$. For sample $B02$, the hue shifts from cyan over blue to violet. The intense violet shifts toward a pale orange for the sample $B08$. The samples $B02$ and $B08$ with a perceptually high hue shift are located in the upper left corner of the projected configuration. In the second quadrant, the coordinate values are negative for the first configuration dimension and positive for the second configuration dimension.

In contrast to the color attributes, the photos do not illustrate the gloss and texture attributes very well. Nevertheless, the grouping of the samples according to their perceived gloss and texture is presented.

The color-gloss attributes named lightness shift and contrast gloss ($dLCG$) as well as the gloss attribute called distinctness-of-image gloss ($DOIG$) are perceived to be high for the samples $B01$, $B06$, $B11$, $B12$ and $B14$. The enlisted samples have an even surface. Incident light is mainly reflected in specular direction. The samples $B01$, $B06$, $B11$, $B12$ and $B14$ are all located in the right half of the projected configuration. In the first and fourth quadrant, the coordinate values of the first configuration dimension are positive.

All texture attributes are perceptually high for the samples $B02$ and $B08$. The sample $B13$ is perceived to have a medium to high texture contrast (TC), graininess and coarseness (GC) as well as sparkle and glint (SG). The special effect pigments have a large particle size. The individual pigments are visible from the adjusted viewing distance. The flaky pigments are not completely embedded in the binder matrix. Small bright light spots are perceived. As mentioned above, the samples $B02$ and $B08$ as well as the sample $B13$ are located in the upper left corner of figure 7.14.

A certain degree of grouping is also observed in the projection of the configuration on the plane spanned by the third and fourth configuration dimension shown in figure 7.15. The grouping according to the estimated color, gloss and texture attributes is shortly presented.

The samples $B01$, $B12$ and $B14$ with a perceptually high lightness (L) are located near the center of the projected configuration. Their coordinate values in the third configuration dimension are exceptionally near at zero. The same holds for the gray sample $B13$ and one of the three orange samples namely the sample $B03$. The orange samples $B03$, $B06$ and $B07$ with a perceptually medium to high yellowness (bp) and redness (ap) have low negative or positive coordinate values in the third configuration dimension and more or less low negative coordinate values in the fourth configuration dimension. The only purely red sample $B11$ is located in the upper left corner of figure 7.15. In the second quadrant, the coordinate values of the third and fourth configuration dimension are negative and positive, respectively. Among all samples, the red sample $B11$ is perceived to have the maximal chroma (C). A grouping with other samples with a perceptually high chroma, such as the samples $B03$, $B06$ and $B07$, cannot be observed.

As mentioned above, the hue shift is perceived to be high for the samples $B02$ and $B08$. These both samples are located in the middle of the left half in figure 7.15. In the second and third quadrant, the coordinate values in the third configuration dimension are negative. The samples $B02$ and $B08$ stand out due to their pronounced texture correlates. Texture contrast (TC), graininess and coarseness (GC) as well as sparkle and glint (SG) are perceptually high for the sample $B13$. Despite its perceptual similarity, sample $B13$ is not located next to the samples $B02$ and $B08$. For the color-gloss attribute named lightness shift and contrast gloss ($dLCG$) as well as the gloss attribute called distinctness-of image gloss ($DOIG$), no noticeable grouping occurs.

The detection of the consistency concerning the forming of local groups is the interim result about the configuration obtained in $CMDS$. The configuration is further processed in a correlation analysis (CA). The CA gives information about the nature of essential visual appearance attributes. The nature and number of essential visual appearance attributes are final results. Before considering any final results, a further interim result is presented. This result concerns the

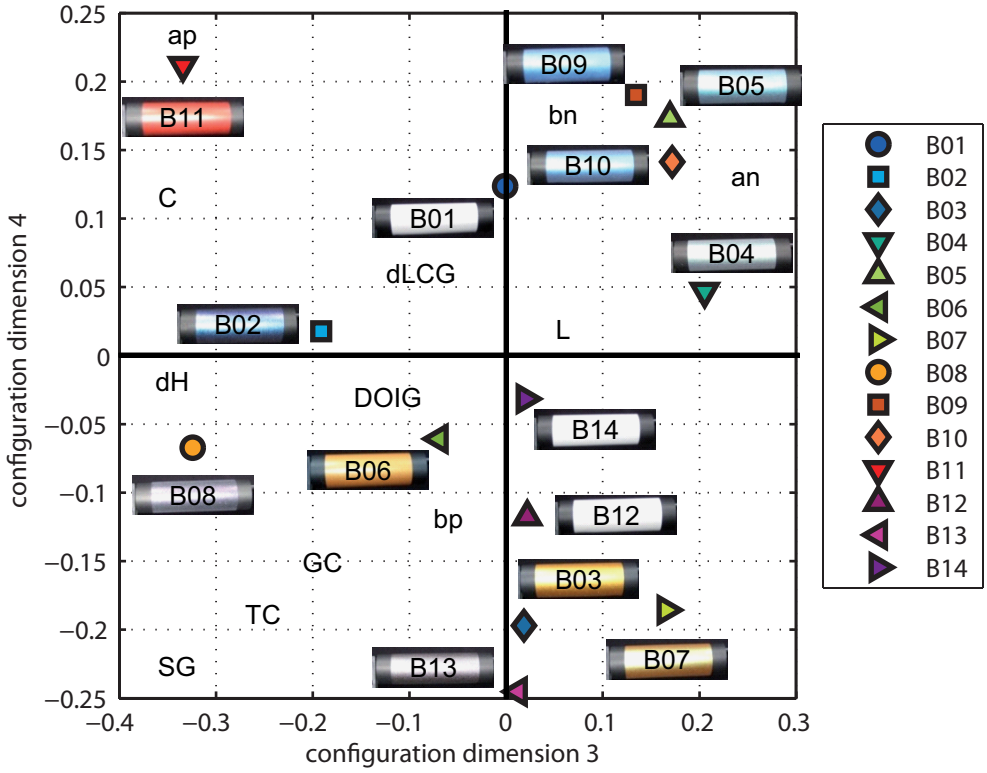

Figure 7.15: Configuration in third and fourth dimension for trial *RCS-VAD-CMLB-OB*14 (table 7.6) with local groups of printing samples with similar visual appearance attributes (table 7.2).

composition generated in a principal component analysis.

Composition from Principal Component Analysis

In the trials *ACS-VAA-CMLB-OB*14 and *ACS-VAA-MATB-IM*20, twelve visual appearance attributes (*VAA*) were estimated in an absolute category scaling experiment (*ACS*). On the one hand, 14 rolled screen printing samples (*OB*14) were scaled in the color matching light booth (*CMLB*). On the other hand, the multi-angle test bench (*MATB*) was used to scale 20 planar flexo printing samples. For each subject, the absolute estimates of the visual appearance attributes were stored in 14-by-12 and 20-by-12 rating matrices. The visual appearance attributes were rated on an integer scale ranging from zero to ten. By some subjects, the ten or even the nine on the scale were not used for some visual appearance attributes. Therefore, each of the twelve columns of the rating matrix was normalized. In the course of the normalization, the maximal value in each column of the rating matrix was set to be equal to one. Subsequent to that, the normalized rating matrices were averaged over all subjects. Finally, all columns of the average rating matrix were standardized using the z-score transformation introduced in section 4.5.3. By means of the standardization, the ratings of each column are centered to the mean value and scaled to the standard deviation. The scaling to the standard deviation ensures an equal weighting of all variables. Variables with comparably high variations do not dominate the results.

On the standardized rating matrix, a principal component analysis (*PCA*) was applied to obtain the principal composition. The principal composition is a spatial arrangement of the samples. The samples are arranged along orthogonal axes of maximal variation, as explained in section 4.5.4. In figure 7.16 and figure 7.17, the principal compositions for trial *ACS-VAA-CMLB-OB*14 and trial *ACS-VAA-MATB-IM*20 are shown as a projection on the first and second composition dimension.

The composition for trial *ACS-VAA-CMLB-OB*14 is shown in figure 7.16. In figure 7.16 and also in figure 7.17, photos of the samples and labels of the visual appearance attributes are included. Even at this point, the photos simplify the interpretation. The labels clarify the results here as well. As in case of the configuration, the composition points out the grouping of visually similar samples. Only the most important groups are enlisted at this point.

The lightness shift or contrast gloss (*dLCG*) and the distinctness-of-image gloss (*DOIG*) are perceptually high for the samples *B*01, *B*06, *B*11, *B*12 and *B*14 being located in the second and third quadrant. The white samples *B*01, *B*12, and *B*14 grouped in the third quadrant stand out from the other samples due to the perceptually high lightness (*L*). Perceptually, the hue shift (*dH*) is high for the samples *B*02 and *B*08 being positioned next to each other in the fourth quadrant. The samples *B*02, *B*08 and *B*13 in the fourth quadrant have a perceptually high texture contrast (*TC*), graininess or coarseness (*GC*) and sparkle or glint (*SG*).

The local grouping for further attributes and in the further components is not discussed for the trial *ACS-VAA-CMLB-OB*14. For trial *ACS-VAA-MATB-IM*20, the effect of local grouping can be also observed.

Figure 7.17 shows the composition for trial *ACS-VAA-MATB-IM*20. Only the most obvious cases of local grouping are enlisted in the following.

The golden samples *M*02, *M*14, *M*19 and *M*20 with a perceptually high yellowness (*bp*) are located close to each other in the first and second quadrant. In the third and fourth quadrant, the turquoise samples *M*07 and *M*09 having a perceptually high greenness (*an*) and blueness (*bn*) are somehow separated from the other samples. The separation of the white samples *M*01, *M*10, *M*12, *M*16 and *M*17 in the second and third quadrant is also quite obvious explained by their perceptually high lightness (*L*). The perceptually high hue shift (*dH*) of the samples *M*05, *M*06, *M*08 and *M*15 causes a preferred positioning in the first and fourth quadrant. There is also group of the samples *M*07, *M*08, *M*14, *M*15 and *M*20 justified by their perceptually high lightness difference or contrast gloss (*dLCG*) and distinctness-of-image gloss (*DOIG*).

The consistency of the just presented composition and also the grouping in the before introduced configuration are just interim results. As the configuration, the composition is further processed to obtain final results. The further processing of composition is just an orthogonal

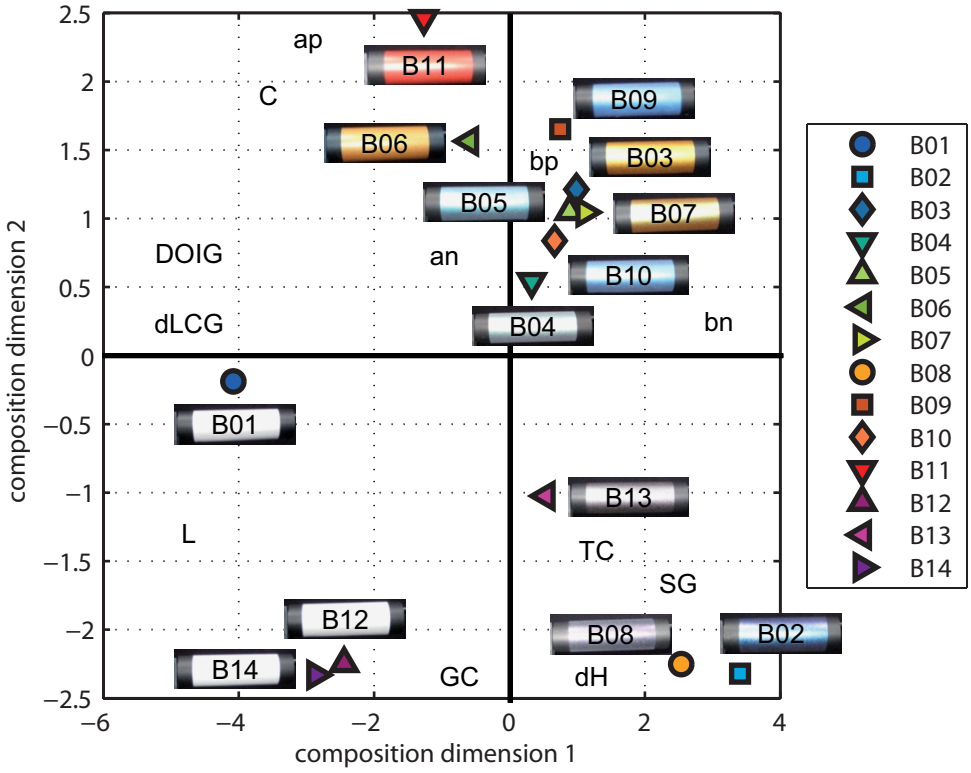

Figure 7.16: Composition in first and second dimension for trial *ACS-VAA-CMLB-OB*14 (table 7.6) with local groups of printing samples with similar visual appearance attributes (table 7.2).

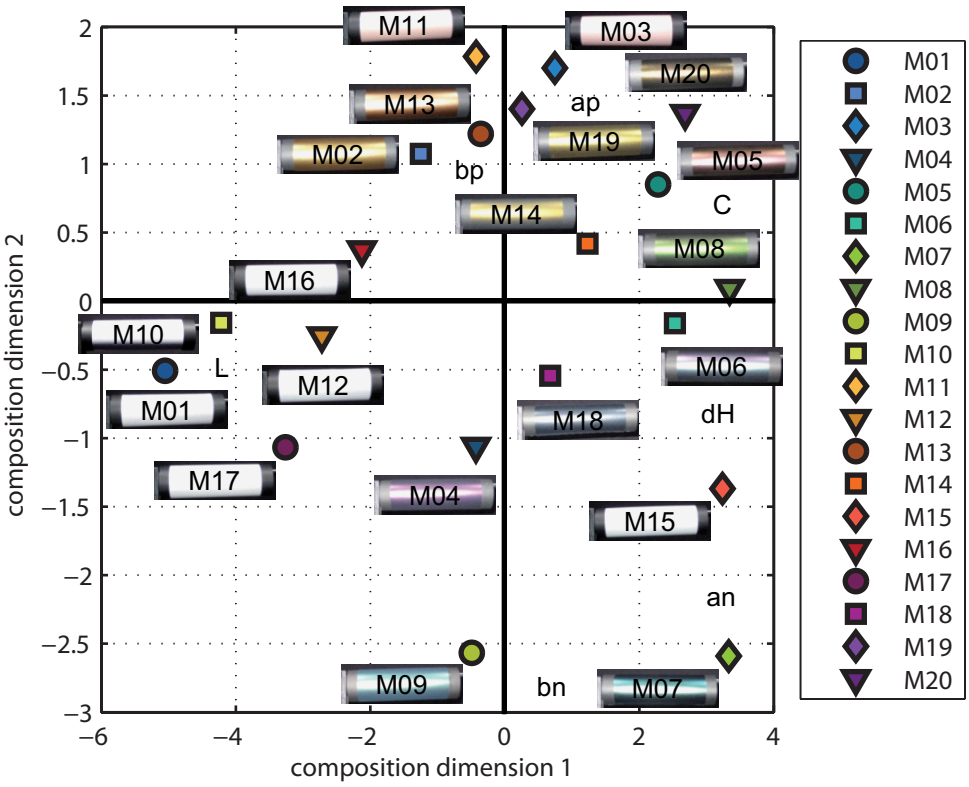

Figure 7.17: Composition in first and second dimension for trial *ACS-VAA-MATB-IM*20 (table 7.6) with local groups of printing samples with similar visual appearance attributes (table 7.2).

rotation (OR). The OR simplifies the interpretation of the nature of essential visual appearance attributes.

7.4.2 Final Results

The final results concern the *number* and *nature* of essential visual appearance correlates. Their quantification and nomination is presented in the following.

Number of Essential Attributes

There are different statistical methods to find the number of essential visual appearance attributes. These include *classical multidimensional scaling*, a *principal component analysis* and a *dimension reduction*. The application of the enlisted multivariate statistical methods is explained. Naturally, their results about the number of essential correlates are subsequently presented.

Number of Essential Attributes from Classical Multidimensional Scaling As described in section 7.4.1, the configuration was obtained by means of classical multidimensional scaling ($CMDS$). The configuration is the spatial arrangement of the samples (section 4.5.4). Even in the best fitting spatial arrangement, an error remains. The remaining error of the best fitting result is called standardized residual sum of squares ($STRESS$) [151, 158]. The plot of the $STRESS$ against number of dimensions is named scree plot. The scree plot of the trial $RCS\text{-}VAD\text{-}CMLB\text{-}OB14$ is shown in figure 7.18 [146].

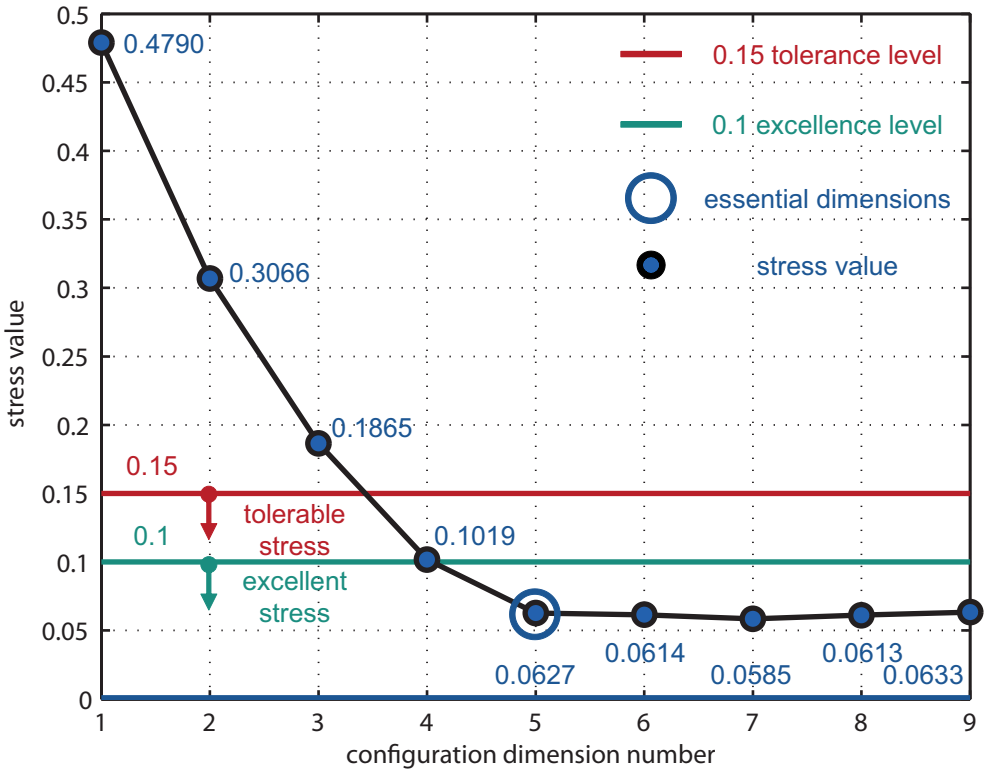

Figure 7.18: Scree plot of $STRESS$ for trial $RCS\text{-}VAD\text{-}CMLB\text{-}OB14$ (table 7.6) [146] with 0.1 excellence and 0.15 tolerance level according to *Kruskal* [131].

With an increasing number of dimensions, a steady decrease of the $STRESS$ is observed. As explained in section 4.5.4, the shape of the scree plot gives information about the number of essential dimensions. The number of essential dimensions is indicated by an inflection point between a steep and a flat decrease in the $STRESS$. Despite this rather subjective approach, an interpretation is given at this point. In the present case, the encircled point in figure 7.18 can be interpreted as inflection point. Thus, the dimensionality of the underlying visual appearance space is five.

Based on the height of the associated $STRESS$, the goodness of fit can be referred to be excellent or tolerable. In general, the goodness of fit is considered as excellent for $STRESS$ less than or equal to 0.1. For $STRESS$ less than or equal to 0.15, the goodness of fit is regarded as tolerable. Such statements about the excellence or tolerance of $STRESS$ were once formulated by $Kruskal$ [131].

The criterion concerning the inflection point and the criterion concerning the excellence level are fulfilled for a number of five configuration dimensions [146]. Based on the evaluation using $CMDS$, a number of five dimensions are essential for the characterization of the visual appearance of printed special effect colors.

Number of Essential Attributes from Principal Component Analysis In the principal component analysis, the eigenvalues and eigenvectors belonging to the covariance or correlation matrix of the rating matrix are determined. The plot of the eigenvalues against their index indicates the dimensionality of the underlying space (section 4.5.4). The eigenvalue plot is also considered in the dimension reduction treated in the next paragraph. The principal component analysis treated in this paragraph provides another tool to decide about the number of essential components. Therefore, the eigenvalue plot is considered in the next paragraph on the dimension reduction. In this paragraph on the principal component analysis, the explained and cumulated variance are used to get information about the number of essential attributes.

For a specific principal component, the explained variance is equal to the variance of the component itself divided by the sum of variances over all components. On the basis of the explained variances, the respective cumulated variances are determined. The cumulated variance of a specific principal component corresponds to the sum over the explained variances whose number is smaller than and equal to the number of the considered principal component. The explained and cumulated variances were determined for trial $ACS\text{-}VAA\text{-}CMLB\text{-}OB14$ and trial $ACS\text{-}VAA\text{-}MATB\text{-}IM20$. In figure 7.19 and figure 7.20, respectively, the explained and cumulated variances are plotted against the component.

The explained and cumulated variances for the trial $ACS\text{-}VAA\text{-}CMLB\text{-}OB14$ are shown in figure 7.19. For an increasing component number, the explained variance decreases steadily. A slightly flatter decrease between component four and five is followed by a slightly steeper decrease between component five and six. This observation itself allows no clear statement about the dimensionality of the visual appearance space of printed special effect colors. In addition to the explained variances, the cumulated variances should be considered. The cumulated variance increases steadily with an increasing number of principal components (figure 7.19). Between the fourth and fifth principal component and between the fifth and sixth principal component, the cumulated variance exceeds the level of 0.9 and 0.95, respectively. Thus, more than 90 % and 95 % of the total variance in the data set is explained by the first five or six principal components as indicated by the circles in figure 7.19. Additional principal components do not increase the cumulated variance significantly. Five or six dimensions are sufficient to represent the rating data for the trial $ACS\text{-}VAA\text{-}CMLB\text{-}OB14$. By means of the rating data for trial $ACS\text{-}VAA\text{-}MATB\text{-}IM20$, this result is checked.

Figure 7.20 shows the explained and cumulated variances for trial $ACS\text{-}VAA\text{-}MATB\text{-}IM20$. With an increasing number of components, the explained and cumulated variance steadily decrease and increase, respectively. The very steep decrease of the explained variance between the component one and two is followed by several slightly flatter and steeper decreases in an alternating sequence (figure 7.20). As indicated by the circles in figure 7.20, the cumulated variance of

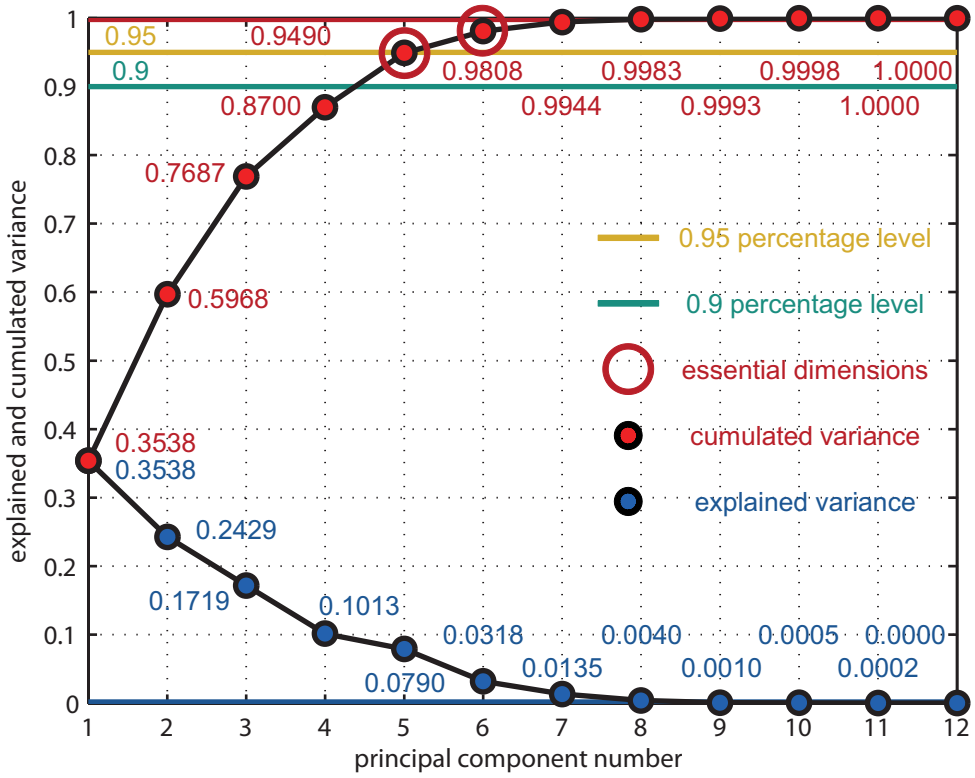

Figure 7.19: Explained and cumulated variances for trial *ACS-VAA-CMLB-OB*14 (table 7.6) with 0.9 and 0.95 percentage level.

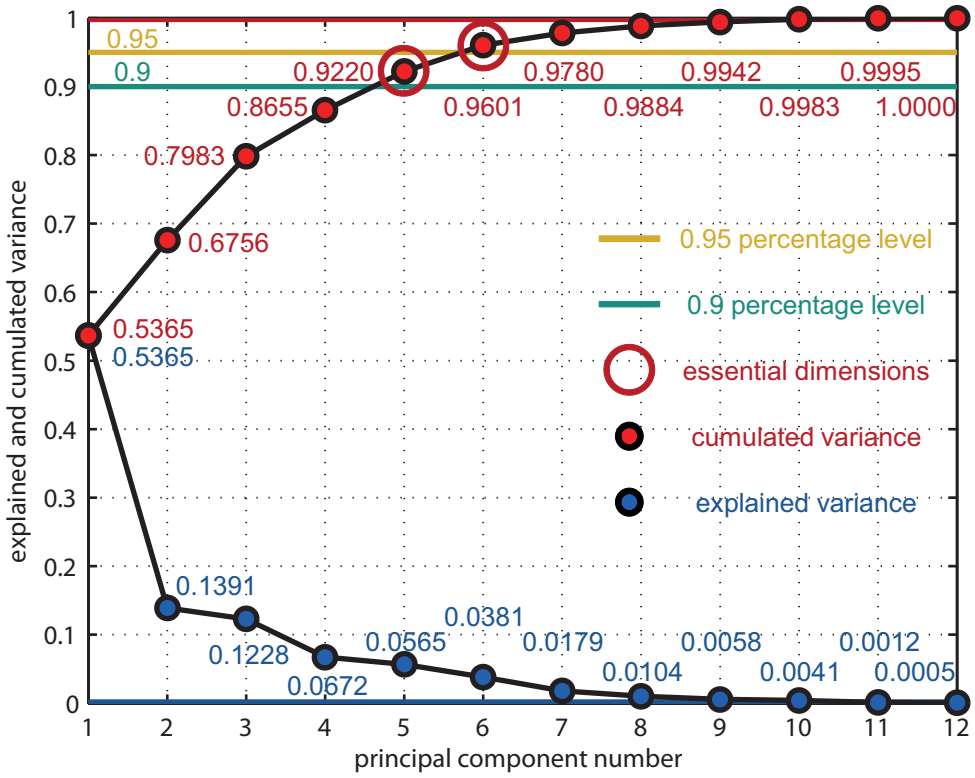

Figure 7.20: Explained and cumulated variances for trial *ACS-VAA-MATB-IM*20 (table 7.6) with 0.9 and 0.95 percentage level.

component five and six is higher than the value 0.9 and 0.95, respectively. A percentage of more than 90 % and 95 % of the total variance is explained by the principal components one to five or one to six.

Summing up, the result for trial *ACS-VAA-MATB-IM*20 about the number of essential dimensions is consistent with the result for the trial *ACS-VAA-CMLB-OB*14. The evaluation based on a principal component analysis results in a number of five or six essential dimensions to characterize the visual appearance of printed special effect colors to a percentage of 0.9 and 0.95, respectively.

Number of Essential Attributes from Dimension Reduction As a principal component analysis, a dimension reduction works with eigenvalues determined for the covariance or correlation matrix of the rating matrix (section 4.5.4). The eigenvalues were calculated and evaluated for both matrices. For both matrices the result about the number of essential dimensions is identical. In the derivation and presentation of the result, the correlation matrix is preferred over the covariance matrix. In case of the covariance matrix, variables with comparably high variances dominate the results [96]. This problem is avoided by using of the covariance matrix for the determination of eigenvalues.

The eigenvalues belonging to the correlation matrix are plotted against their index to find out the dimensionality of the underlying space. The scree plots for the trials *ACS-VAA-CMLB-OB*14 and *ACS-VAA-MATB-IM*20 are shown in figure 7.21 and figure 7.22, respectively.

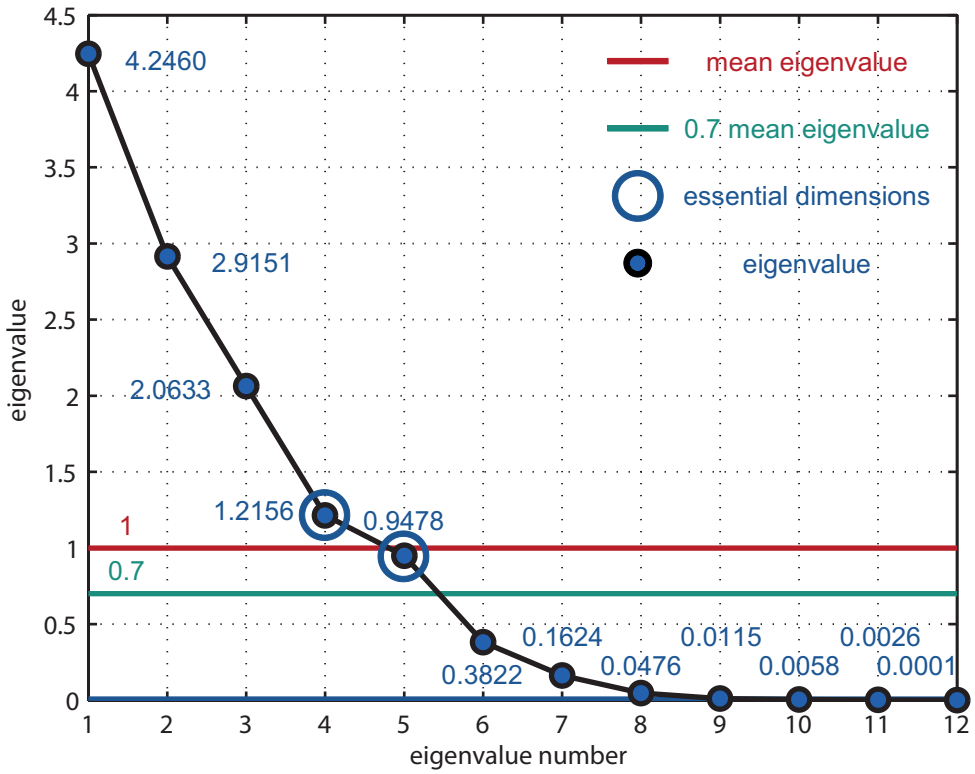

Figure 7.21: Scree plot of eigenvalue of correlation matrix for trial *ACS-VAA-CMLB-OB*14 (table 7.6) with mean and 0.7 mean eigenvalue level according to *Kaiser* and the *Jolliffe* criterion [96].

Figure 7.21 shows the eigenvalue plotted against the running number for trial *ACS-VAA-*

*CMLB-OB*14. A steady decrease of the eigenvalue with an increasing number of dimensions is observed. The decrease is slightly flatter and slightly steeper between dimension four and five and between dimension five and six, respectively. Inflection points between a steep and a flat decrease indicate the number of essential dimensions (section 4.5.4). The transition from a steeper to a flatter decrease occurs for a number of four and six dimensions. Four or six dimensions may be essential for the perception-based characterization of printed special effect colors.

For further conclusions, the *Kaiser* criterion and the *Jolliffe* criterion described in the book of *Handl* [96] are applied. According to the *Kaiser* criterion, the number of required dimensions is equal to the number of eigenvalues being higher than the average eigenvalue. The average eigenvalue is always equal to one in case of working with the correlation matrix. As shown by the circle in figure 7.21, a number of four eigenvalues are higher than the average eigenvalue of one. An aggravated and therefore preferred form of the *Kaiser* criterion is the *Jolliffe* criterion. The *Jolliffe* criterion implies that the number of necessary dimensions is equal to the number of eigenvalues being higher than 0.7 times the average eigenvalue. In the present case, a number of five eigenvalues are higher than 0.7 as shown by the circle in figure 7.21.

Finally, the inflection point criterion, the *Kaiser* criterion and the *Jolliffe* criterion are considered together. Four dimensions seem to be insufficient while the sixth dimension is probably superfluous. Thus, the number of essential dimensions is set equal to five for trial *ACS-VAA-CMLB-OB*14. For trial *ACS-VAA-MATB-IM*20, the same three criteria are consulted.

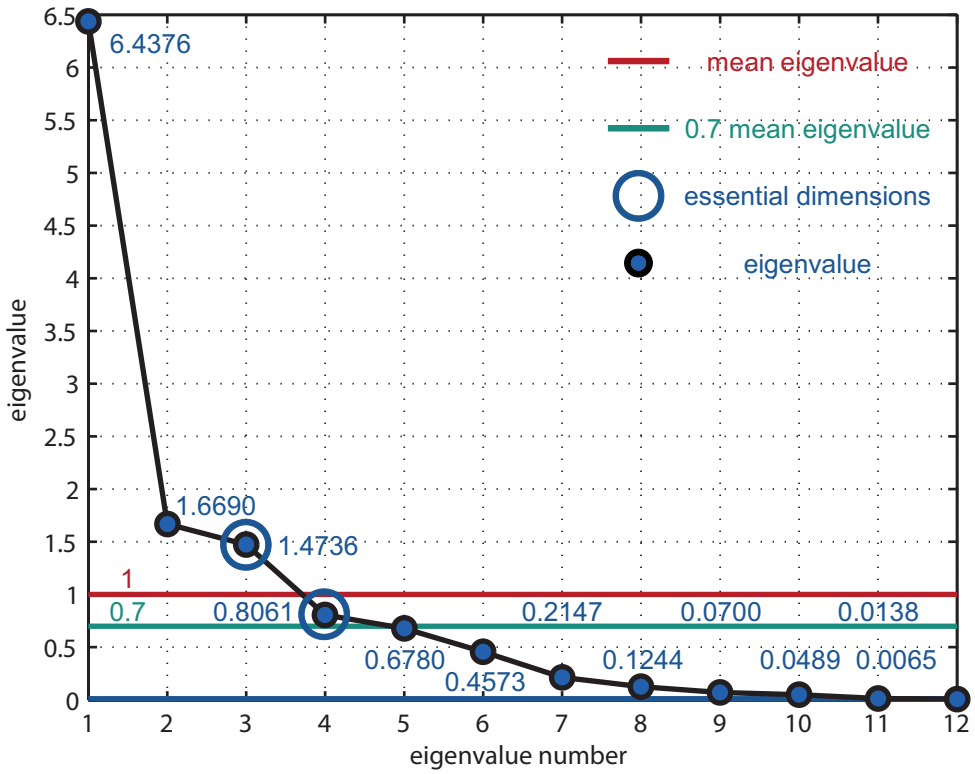

Figure 7.22: Scree plot of eigenvalue of correlation matrix for trial *ACS-VAA-MATB-IM*20 (table 7.6) with mean and 0.7 mean eigenvalue level according to *Kaiser* and the *Jolliffe* criterion [96].

The eigenvalue for the trial *ACS-VAA-MATB-IM*20 is shown in figure 7.22. With an increasing number of dimensions, the eigenvalue decreases steadily. The very steep decrease between dimension one and two is followed by a very flat decrease between dimension two and three. In a

similar way, slightly steeper decreases between dimension three and four and between dimension six and seven are followed by slightly flatter decreases between dimension four and five and between dimension seven and eight. Thus, the inflection points at dimension two, four and seven let expect the number of essential dimensions.

As indicated by the circles in figure 7.22, a number of three and four eigenvalues are higher than one and 0.7, respectively. Thus, three and four dimensions are essential according to the $Kaiser$ and $Jolliffe$ criterion. Considering the $Kaiser$ and $Jolliffe$ criterion together with the inflection point criterion, two or three dimensions might be insufficient. In contrast to that, seven dimensions seem to over-determine the visual appearance.

In summary, the evaluation of the trials $ACS\text{-}VAA\text{-}CMLB\text{-}OB14$ and $ACS\text{-}VAA\text{-}MATB\text{-}IM20$ using dimension reduction yields comparable results. With respect to mentioned trials, a number of five or four dimensions are essential for the visual appearance description of printed special effect colors.

Nature of Essential Attributes

The nature of visually relevant perception attributes was investigated by means of several different statistical methods. The applied statistical methods are two *correlation analyses*, a *principal component analysis* followed by an *orthogonal rotation* and an *exploratory factor analysis* based on a *dimension reduction*. In the following sections, the results about the nature of the essential attributes are presented.

Nature of Essential Attributes from Correlation Analysis of Configuration and Ratings Remember the configuration calculated for the trial $RCS\text{-}VAD\text{-}CMLB\text{-}OB14$ (section 7.4.1). The dissimilarities determined in the relative category scaling (RCS) experiment of the total visual appearance difference (VAD) were processed in multidimensional scaling. The determined configuration represents the printed samples in an appearance space (section 4.5.4).

The representation of the samples in the appearance space is based on coordinate points. The associated coordinate axes are equal to the directions of maximal variation considering the requirement on their mutually orthogonal orientation. Thus, the axes have a perception-based meaning. But, they are just identified with numbers. Instead of the perception-based numbers, perception-based labels are desired. These perception-based labels might be the visual appearance attributes (VAA) rated in the absolute category scaling (ACS) experiment. For the trial $ACS\text{-}VAA\text{-}CMLB\text{-}OB14$, the ratings of the visual appearance attributes are available.

The visual appearance attributes can be assigned to the appearance space axes by means of a correlation analysis. Thus, the correlation matrix between the sample coordinates of trial $RCS\text{-}VAD\text{-}CMLB\text{-}OB14$ and the attribute ratings of trial $ACS\text{-}VAA\text{-}CMLB\text{-}OB14$ is determined. The correlation coefficients are plotted as colored bars in the vertical direction of a three-dimensional coordinate system. A connection of the attributes with the axes is indicated by high absolute correlation coefficients. The p-value decides about their significance. The significance levels are displayed as horizontal planes in the three-dimensional plot of colored bars. Projections on the horizontal planes from below and above only include significantly negative and positive correlation coefficients, respectively. These projections are shown in figure 7.23 and figure 7.24 [146].

Figure 7.23 shows significantly negative correlation coefficients below the negative significance level of -0.55 with p-values below 0.05. A significantly negative correlation can be especially observed in the first both dimensions. For the first dimension, the variation is maximal over the total visual appearance. The variation over the total visual appearance decreases with an increasing dimension number.

Graininess and coarseness (GC), blueness (bn), texture contrast (TC) and hue shift (dH) show a significantly negative correlation with the first dimension. With the second dimension, significantly negative correlation occurs for yellowness (bp), redness (ap) and chroma (C). Apart from the second dimension, redness (ap) also correlates significantly negative with the third dimension. With the fourth dimension, sparkle and glint (SG) are correlated significantly negative. For the

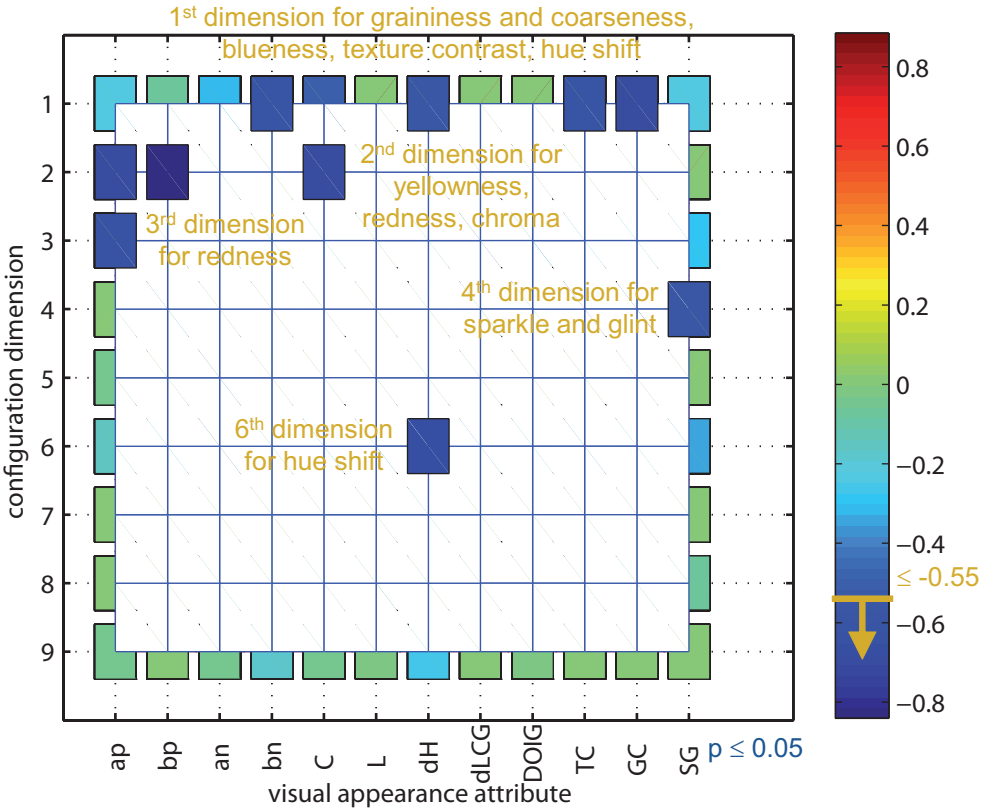

Figure 7.23: Significantly negative correlation coefficients between configuration dimensions and visual appearance attributes (table 7.2) below the negative significance level of -0.55 with p-values below 0.05 for trial $RCS\text{-}VAD\text{-}CMLB\text{-}OB14$ and $ACS\text{-}VAA\text{-}CMLB\text{-}OB14$ (table 7.6) [146].

tested attributes, no significantly negative correlation was found for the fifth dimension. For the sixth dimension, significantly negative correlation occurs with the hue shift [146]. For the remaining dimensions seven, eight and nine, there was found neither a significantly negative nor a significantly positive correlation.

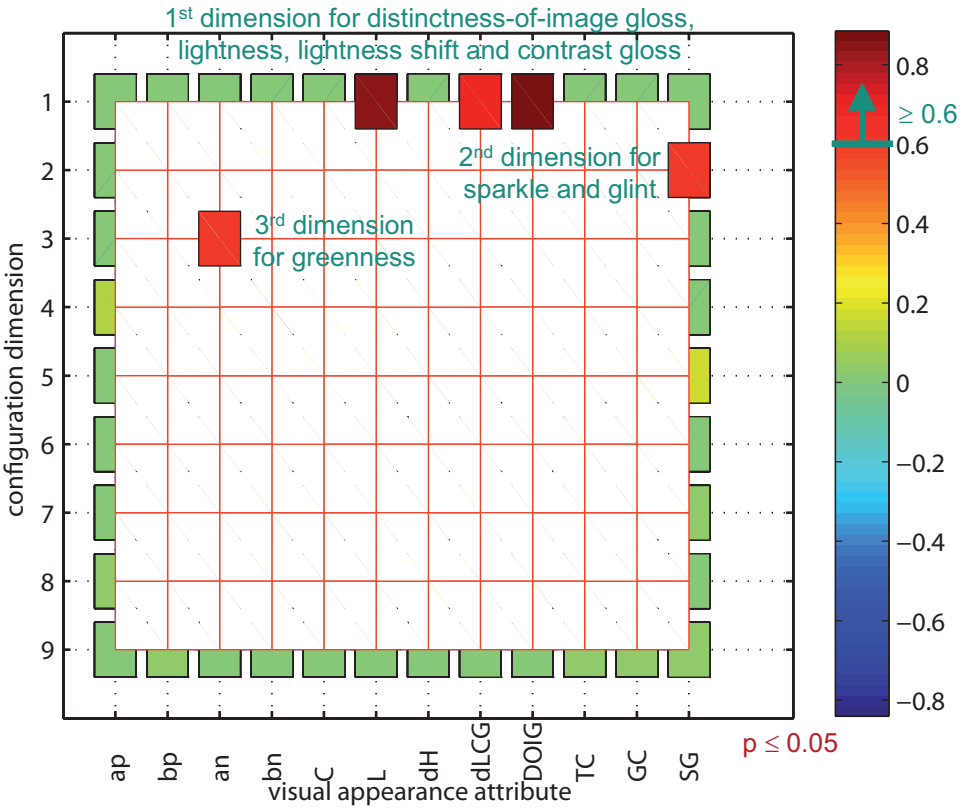

Figure 7.24: Significantly positive correlation coefficients between configuration dimensions and visual appearance attributes (table 7.2) above the positive significance level of 0.6 with p-values below 0.05 for trial $RCS\text{-}VAD\text{-}CMLB\text{-}OB14$ and $ACS\text{-}VAA\text{-}CMLB\text{-}OB14$ (table 7.6) [146].

Significantly positive correlation coefficients above the positive significance level of 0.6 with p-values below 0.05 are shown in figure 7.24. With the first dimension, three visual appearance attributes are correlated significantly positive. These are the color attribute named lightness (L), the color-gloss attribute named lightness shift and contrast gloss ($dLCG$) as well as the gloss attribute named distinctness-of-image gloss ($DOIG$). The texture attribute called sparkle and glint (SG) is in significantly positive correlation with the second dimension. The third dimension is correlated significantly positive with greenness (an) [146].

The following should be said to sum up the results of the correlation analysis on the configuration and ratings. For the first two to three dimensions, the most significant correlations are observed. At least one significant correlation occurs for all tested visual appearance attributes. Thus, all tested visual appearance attributes are somehow relevant for the perception-based description of printed special effect colors. Further attributes not tested in this study might be relevant.

Nature of Essential Attributes from Correlation Analysis of Ratings As explained in section 7.2.1 on the selection and adaption of the estimated visual appearance attributes, some of the attributes can be treated together. Some examples for visual appearance attributes with

an obviously identical meaning are reminded. Lightness flop and contrast gloss ($dLCG$), graininess and coarseness (GC) as well as sparkle and glint (SG) are treated together. Some further resemblances in the psychophysical meaning of the estimated attributes can be expected.

Any kind of resemblance was tested by means of a correlation analysis applied on the rating matrices obtained in the absolute category scaling (ACS) experiments of the visual appearance attributes (VAA). For the trail $ACS\text{-}VAA\text{-}CMLB\text{-}OB14$ and the trial $ACS\text{-}VAA\text{-}MATB\text{-}IM20$, the correlation matrices were determined. In a three-dimensional coordinate system, the determined correlation coefficients are displayed as colored bars in the vertical direction. An inter-attribute correlation is pointed out by a high absolute correlation coefficient with a low p-value. The p-value specifies the negative and positive significance level visualized as horizontal planes in the considered coordinate system. To show only the significantly negative and positive correlation coefficients, the three-dimensional plot of colored is projected on the horizontal plane from below and above, respectively.

These projections including only the significant correlation coefficients are shown in figure 7.25, figure 7.26, figure 7.27 and figure 7.28. Figure 7.25 and figure 7.26 show significant correlation coefficients with p-values below 0.05 for the trial $ACS\text{-}VAA\text{-}CMLB\text{-}OB14$.

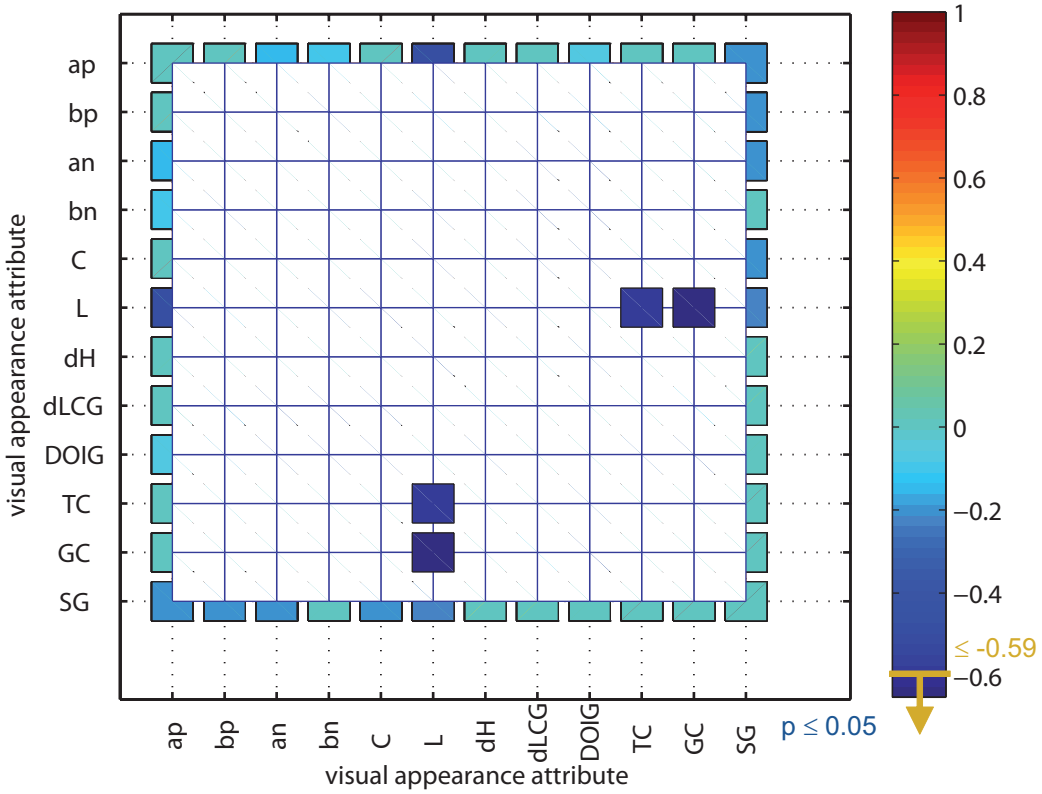

Figure 7.25: Significantly negative correlation coefficients between visual appearance attributes (table 7.2) below the negative significance level of -0.59 with p-values below 0.05 for trial $ACS\text{-}VAA\text{-}CMLB\text{-}OB14$ (table 7.6).

The significantly negative correlation coefficients below the negative significance level of -0.59 are shown in figure 7.25. Only the correlation of the color attribute lightness (L) with the texture attributes graininess or coarseness (GC) and texture contrast (TC) is significantly negative. For the same p-value of 0.05, some more cases of significantly positive correlation occur.

Figure 7.26 shows these significantly positive correlation coefficients above the positive significance level of 0.54. For the interpretation, please note the following self-evident fact. The

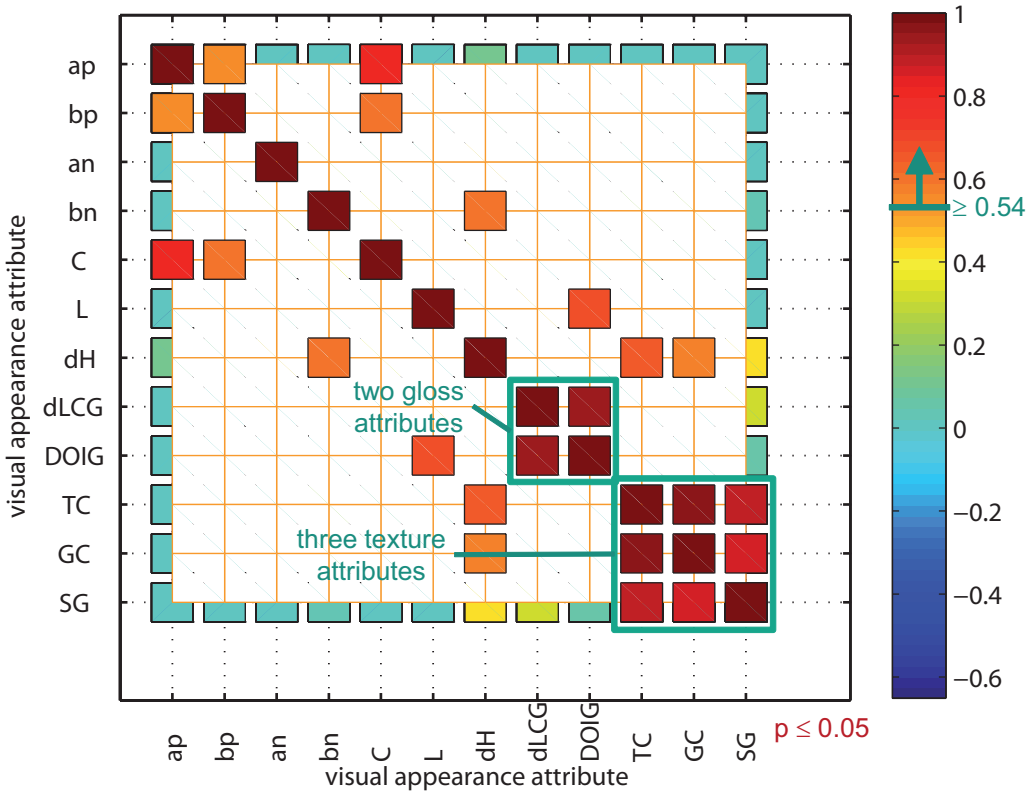

Figure 7.26: Significantly positive correlation coefficients between visual appearance attributes (table 7.2) above the positive significance level of 0.54 with p-values below 0.05 for trial *ACS-VAA-CMLB-OB*14 (table 7.6).

correlation coefficient between to identical variables is always equal to one. Apart from these insignificantly ideal correlations of the visual appearance attributes with themselves, several significantly positive correlations occur.

The significance of positive correlation is particularly high in the following four cases. Three of these four cases are the three combinations of all three texture attributes. The distinction of texture contrast (TC), graininess and coarseness (GC) as well as sparkle and glint (SG) is superfluous as indicated by the frame in figure 7.26. One single texture attribute might be sufficient. At this point, there is an important thing to note. No statement can be given about untested texture attributes like roughness, granularity, fineness and others (section 4.1.3, section 7.2.1).

For the untested color attributes, especially the chroma shift, the same thing is true. The same also applies to the untested gloss attributes such as metal gloss and pearl gloss. The tested gloss attributes lightness shift or contrast gloss ($dLCG$) and distinctness-of-image gloss ($DOIG$) show a positive correlation with a particularly high significance. Their combination is the fourth of the above mentioned cases. The distinction of these two gloss attributes is superfluous highlighted by the frame in figure 7.26. It might be sufficient to characterize printed special effect colors with one single gloss attribute.

Apart from these inter-texture-attribute correlations and inter-gloss-attribute correlations, further significantly positive correlations occur. However, some of these significantly positive correlations are not based on the visual perception of printed special effect colors. The reason for the significantly positive correlations is rather the quantity and quality of the estimated samples.

For example, redness (ap) and chroma (C) show a significantly positive correlation. This is not a perception-induced correlation, but a result of the small and uneven stimulus set. Perceptually, sample $B11$ (figure 7.4) has a high redness and a high chroma. A medium to high redness and a high chroma is also perceived for the three orange samples $B03$, $B06$ and $B07$ (figure 7.4). Apart from the medium to high redness and the high chroma, the orange samples $B03$, $B06$ and $B07$ have a perceptually medium to high yellowness. Therefore, yellowness is correlated significantly positive with redness and chroma.

The significantly positive correlation of lightness (L) and distinctness-of-image gloss ($DOIG$) is another example for the stimulus-set-based correlation. The three white samples $B01$, $B12$ and $B14$ (figure 7.4) have a perceptually high lightness. Due to their even surface, a directional illumination results in a sharp gloss reflex perceived as high distinctness-of-image gloss.

Further examples are the significantly positive correlations of hue shift (dH) with blueness (bn), with texture contrast (TC) and with graininess or coarseness (GC). For the significantly positive correlation of hue shift and blueness, the sample $B02$ (figure 7.4) is responsible. Sample $B02$ is characterized by a hue shift from cyan over blue to violet. Furthermore, the texture contrast as well as the graininess and coarseness are perceptually pronounced for sample $B02$. Apart from sample $B02$, sample $B08$ (figure 7.4) is characterized by a perceptually high hue shift, texture contrast and graininess or coarseness.

These unwanted sample-set-based correlations should be differentiated from the desired perception-induced correlations. The results on perception-based correlations are concluded not yet. For the confirmation of the results for trial $ACS\text{-}VAA\text{-}CMLB\text{-}OB14$, we look at trial $ACS\text{-}VAA\text{-}MATB\text{-}IM20$. For the trial $ACS\text{-}VAA\text{-}MATB\text{-}IM20$, the significant correlation coefficients with p-values below 0.005 are shown in figure 7.27 and figure 7.28.

Figure 7.27 shows the significantly negative correlation coefficients below the negative significance level of -0.65. As for the trial $ACS\text{-}VAA\text{-}CMLB\text{-}OB14$, only a few significantly negative correlations occur for the trial $ACS\text{-}VAA\text{-}MATB\text{-}IM20$. Lightness ($L$) correlates significantly negative with chroma (C), sparkle and glint (SG), graininess and coarseness (GC) and with texture contrast (TC). Remember the above statement about the significantly negative inter-attribute correlations for trial $ACS\text{-}VAA\text{-}CMLB\text{-}OB14$. The correlation coefficients for the combinations of lightness (L) with graininess or coarseness (GC) and with texture contrast (TC) are significantly negative. This corresponds to the finding for trial $ACS\text{-}VAA\text{-}MATB\text{-}IM20$. We conclude that the texture attributes are correlated significantly negative with lightness. Small bright spots are perceived to be more intense on a dark background.

In spite of an identical p-value of 0.05, the following was determined for trial $ACS\text{-}VAA\text{-}$

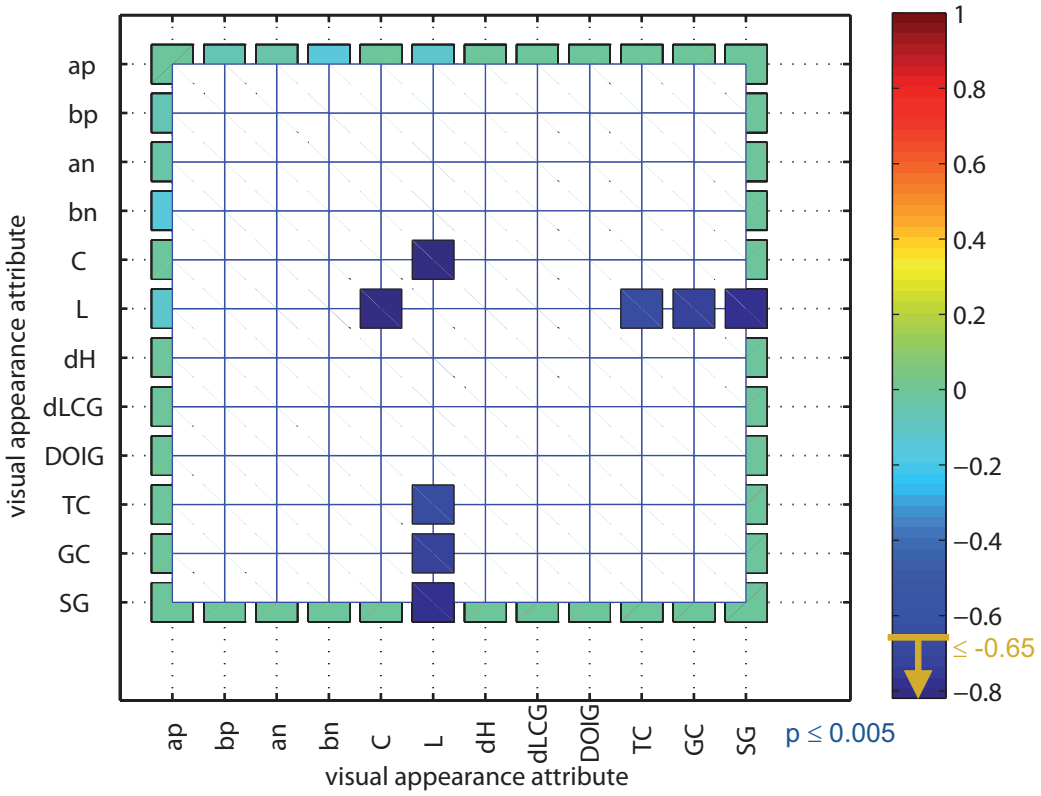

Figure 7.27: Significantly negative correlation coefficients between visual appearance attributes (table 7.2) below the negative significance level of -0.65 with p-values below 0.005 for trial *ACS-VAA-MATB-IM*20 (table 7.6).

*CMLB-OB*14. Compared to the significantly negative correlation, several more significantly positive correlations occur. This also holds for trail *ACS-VAA-MATB-IM*20 considering a comparably low p-value of 0.005.

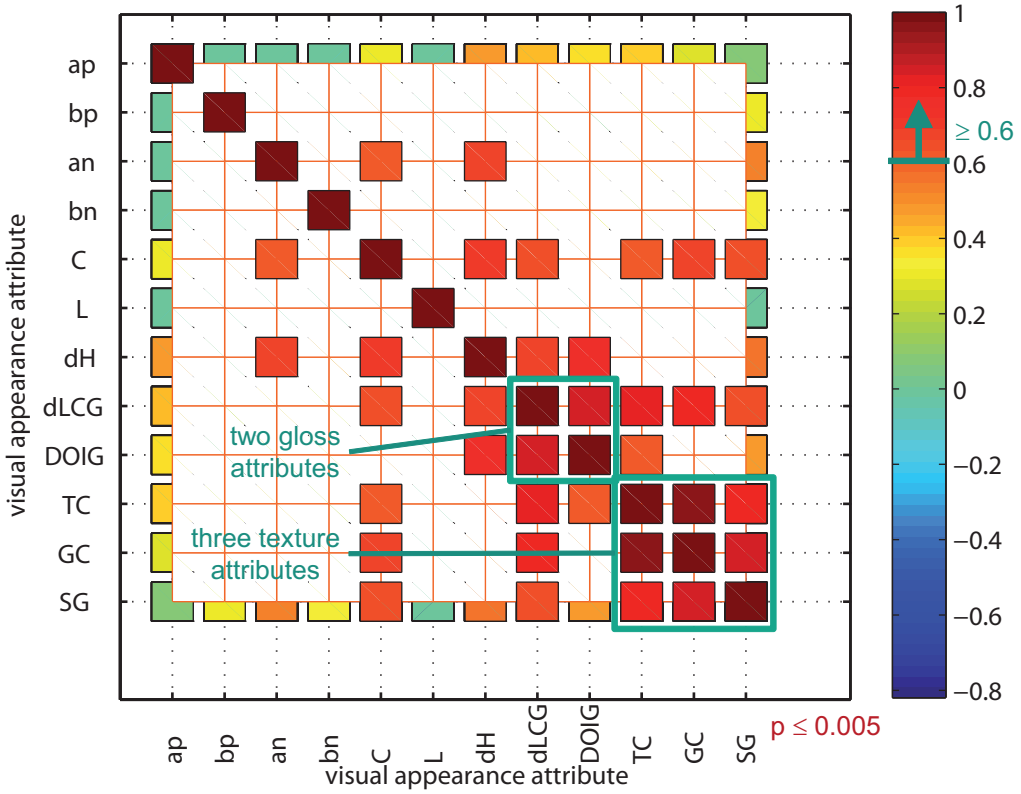

Figure 7.28: Significantly positive correlation coefficients between visual appearance attributes (table 7.2) above the positive significance level of 0.6 with p-values below 0.005 for trial *ACS-VAA-MATB-IM*20 (table 7.6).

All significantly positive correlation coefficients above the positive significance level of 0.6 are shown in figure 7.28. Remember, the correlation coefficients are equal to one for the combinations of an attribute with itself. Apart from the self-evident but insignificantly ideal correlations, the following significantly positive correlation should be mentioned.

Noticeable are again the significantly positive inter-texture-attribute correlations as well as the significantly positive inter-gloss-attribute correlations as highlighted by the frames in figure 7.28. Texture contrast (*TC*), graininess and coarseness (*GC*) as well as sparkle and glint (*SG*) are correlated significantly positive. A significantly positive correlation also occurs for lightness shift or contrast gloss (*dLCG*) with distinctness-of-image gloss (*DOIG*). These are the obviously perception-induced correlations. As for the trial *ACS-VAA-CMLB-OB*14, the perception-based correlations should to be distinguished from the sample-set-induced correlations. The sample-set-based correlations are not that obvious for the trial *ACS-VAA-MATB-IM*20. Any further explanations are therefore omitted.

The following should be noted to summarize the results of the correlation analysis on the ratings. The results are for trial *ACS-VAA-CMLB-OB*14 and trial *ACS-VAA-MATB-IM*20 are consistent with each other. More extensive and versatile sample sets should be used to avoid stimuli-set-based correlations. Apart from several sample-set-induced correlations, perception-based correlations occur between all three tested texture attributes as well as between the both tested gloss attributes. Either, each one single attribute for texture and gloss is sufficient or other

attributes for texture and gloss should be tested.

Nature of Essential Attributes from Principal Component Analysis followed by Orthogonal Rotation The nature of the essential visual appearance attributes is also evaluated by means of a principal component analysis followed by an orthogonal rotation. In the principal component analysis, the dimensionality of the underlying space was determined by means of the cumulated variances (section 7.4.2). For a number of five or six components more than 90 % and 95 % of the total variance is explained. For the maximum number of six essential dimensions, the eigenvectors are set equal to the component coefficients of the principal components.

These component coefficients or component loadings take arbitrary values between zero and minus or plus one. For normally strongly fluctuating values of the component loadings, the principal components are difficult to be interpreted. The interpretation can be simplified by means of an orthogonal rotation of the coordinate axes. In an orthogonal rotation, the coordinate axes are rotated with the following objective (section 4.5.4). All component loadings in the rotated coordinate system should take values close to zero or close to minus and plus one. A component loading near zero indicates a low variation of the considered variable for the corresponding principal component. A high variation of any sampled variable for an arbitrary principal component is indicated by a component loading near minus or plus one.

For the just set number of six principal components, the component loadings were determined. They are used to explain the results about the nature of the essential visual appearance attributes.

All rotated component loadings based on six principal components are shown in figure 7.29, figure 7.30, figure 7.31 and in figure 7.32 as projected three-dimensional plots of colored bars. Figure 7.29 and figure 7.30 show the rotated component loadings for trial *ACS-VAA-CMLB-OB*14.

In figure 7.29, the negative component loadings are shown. The first component corresponds to gloss tested by the gloss attributes lightness difference or contrast gloss ($dLCG$) and distinctness-of-image gloss ($DOIG$). The texture tested by texture contrast (TC), graininess or coarseness (GC) and sparkle or glint (SG) is represented by the second component. The third, fifth and sixth component is for redness (ap), blueness (bn) and yellowness (bp), respectively. Chroma (C) is represented by the fifth and sixth component. In addition to blueness (bn) and chroma (C), the fifth component specifies the hue shift (dH). The fourth component is missing in the list just given above. This list connecting components and attributes is incomplete. It is only based on the negative component loadings. The positive component loadings should be considered as well.

The positive component loadings are shown in figure 7.30. Thus, the fourth component is for greenness (an) and hue shift (dH). Lightness (L) is specified by the seventh component. The tested color attributes redness, yellowness, greenness, blueness, chroma, lightness and hue shift as well as all gloss and texture attributes are included in the first six rotated principal components. The transferability of the presently tested color attributes redness, yellowness, greenness and blueness in the commonly used color attributes hue and chroma results in the following statement. The four color attributes hue, chroma, lightness and hue shift as well as a combined gloss attribute and a combined texture attribute are essential for the perception-based characterization of printed special effect colors. This result about the nature of the essential attributes for trial *ACS-VAA-CMLB-OB*14 is subsequently checked with the data for trial *ACS-VAA-MATB-IM*20. The rotated component loadings for trial *ACS-VAA-MATB-IM*20 are shown in figure 7.31 and figure 7.32.

Figure 7.31 shows the negative component loadings. The second component is for blueness (bn) and chroma (C). Redness (ap) is represented by the fourth component. These are the connections of components and attributes based on the negative component loadings. The corresponding positive component loadings should be considered to complete the list.

The positive component loadings are shown in figure 7.32. The texture appearance tested with texture contrast (TC) and graininess or coarseness (GC) is also represented by the first component. The fifth component is for lightness difference or contrast gloss ($dLCG$) and for distinctness-of-image gloss ($DOIG$) describing the gloss appearance. The lightness (L) and yellowness (bp) are specified by the second and fourth component, respectively. The sixth component represents

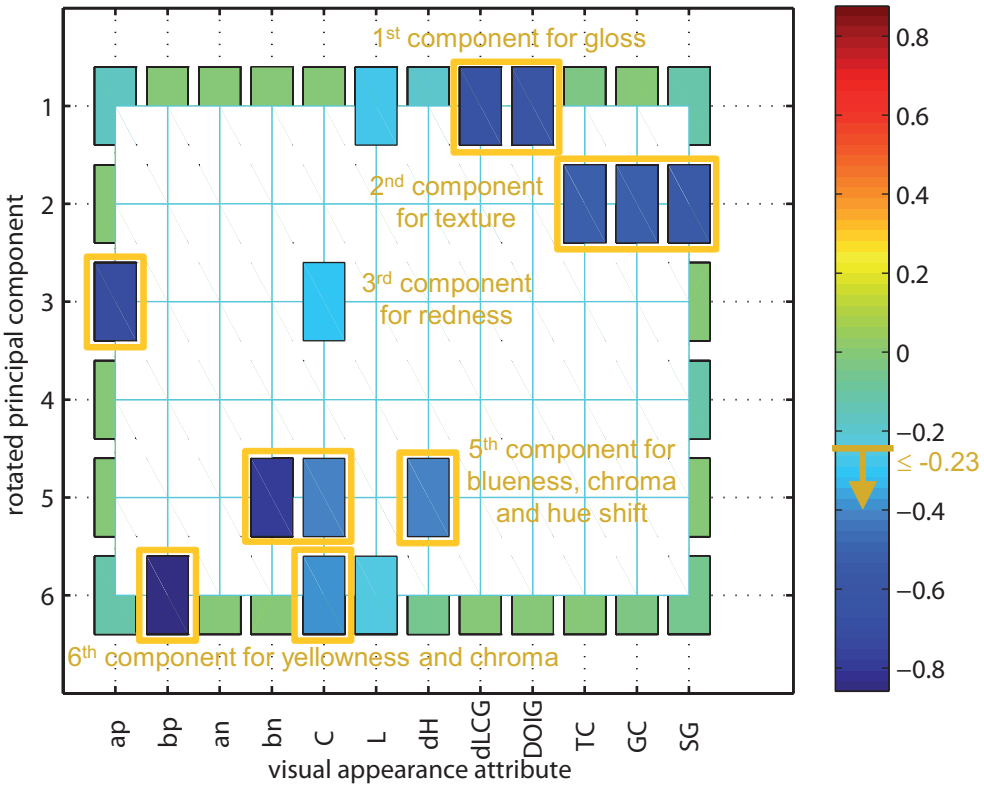

Figure 7.29: Negative composition loadings of rotated principal components for visual appearance attributes (table 7.2) below mean negative composition loading of -0.23 for trial *ACS-VAA-CMLB-OB*14 (table 7.6).

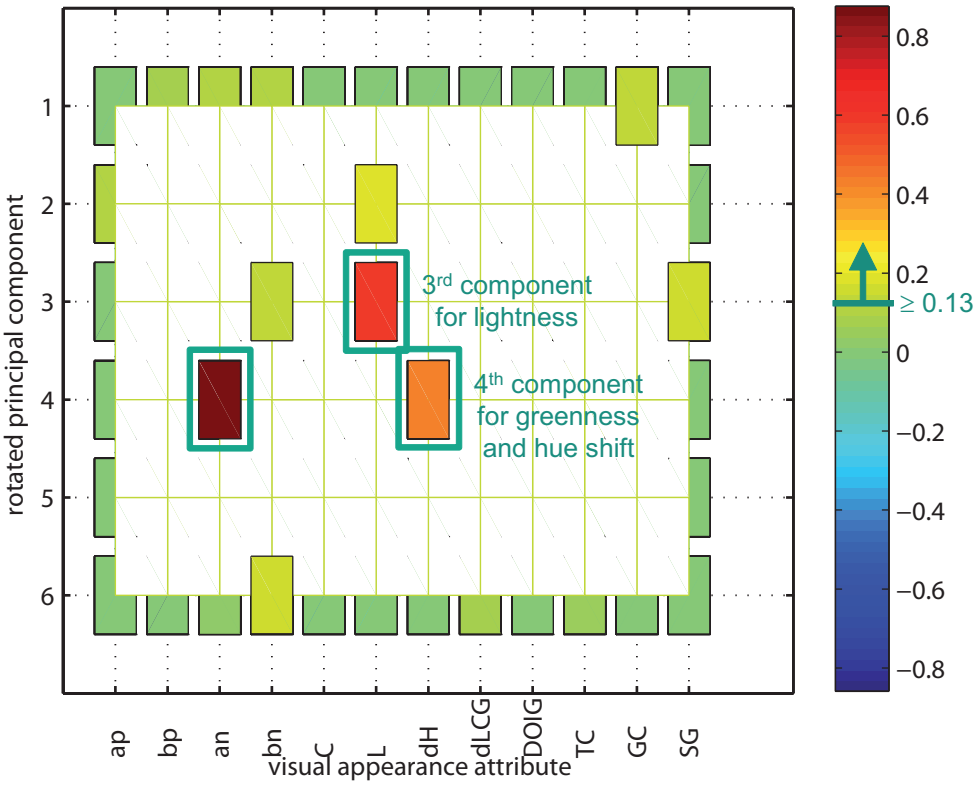

Figure 7.30: Positive composition loadings of rotated principal components for visual appearance attributes (table 7.2) above mean positive composition loading of 0.13 for trial *ACS-VAA-CMLB-OB*14 (table 7.6).

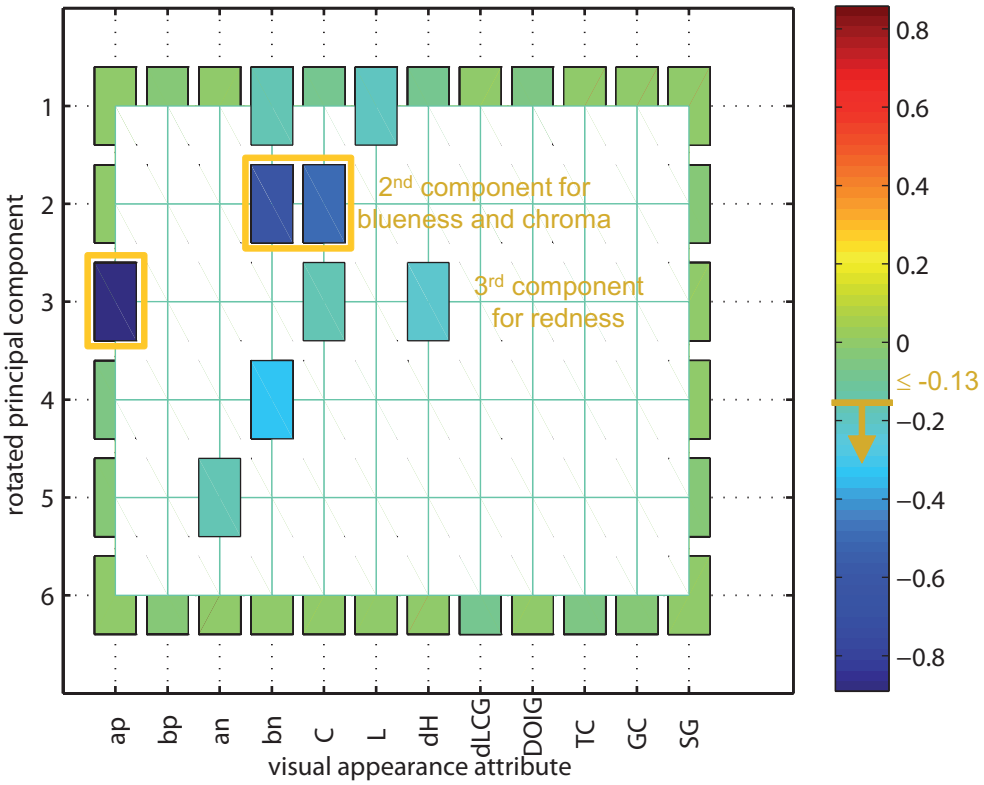

Figure 7.31: Negative composition loadings of rotated principal components for visual appearance attributes (table 7.2) below mean negative composition loading of -0.13 for trial *ACS-VAA-MATB-IM*20 (table 7.6).

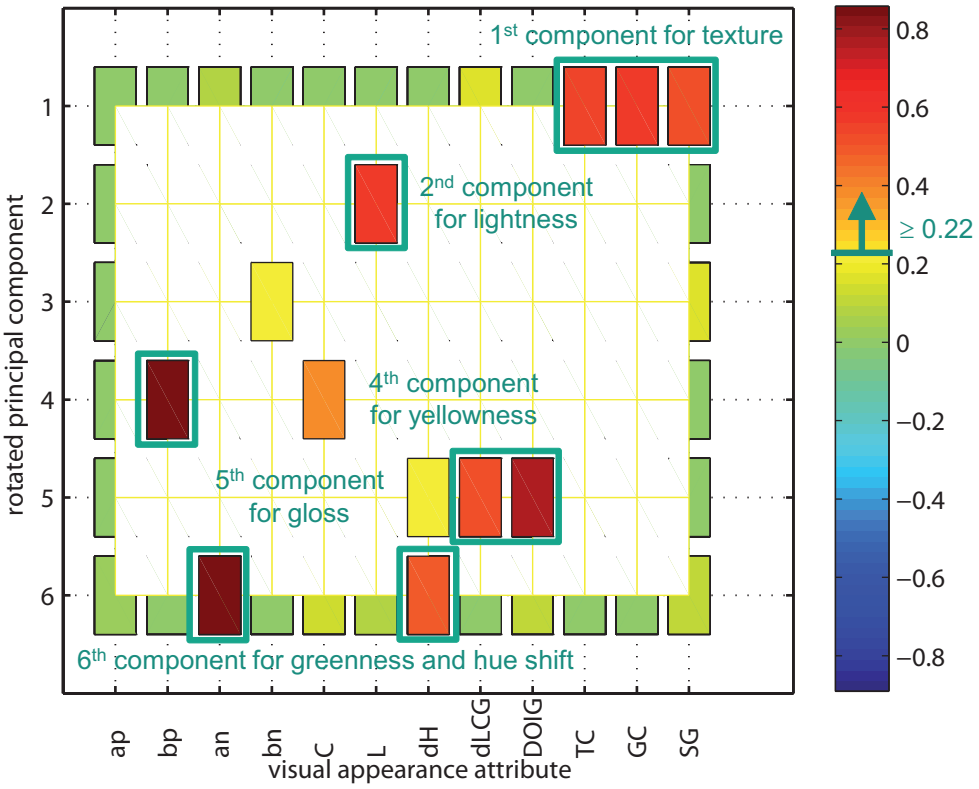

Figure 7.32: Positive composition loadings of rotated principal components for visual appearance attributes (table 7.2) above mean positive composition loading of 0.22 for trial *ACS-VAA-MATB-IM*20 (table 7.6).

greenness (an) and hue shift (dH). In the first six components, the color attributes redness, yellowness, greenness, blueness, chroma, lightness and hue shift as well as all gloss attributes and texture attributes are included. Thus, the four color attributes hue, chroma, lightness and hue shift as well as a combined gloss attribute and a combined texture attribute are essential for the visual description of printed special effect colors. The essentiality of these visual appearance attributes was found for both trials.

Summarizing the results of the principal component analysis followed by an orthogonal rotation yields the following statements. The first six principal components represent the nature of nine presently tested or six commonly used visual appearance attributes. The six or four essential color attributes are redness, yellowness, greenness, blueness and lightness and hue shift or hue, chroma, lightness and hue shift, respectively. The remaining two essential attributes are combined attributes describing the appearance of gloss and of texture. These statements are valid for trial $ACS\text{-}VAA\text{-}CMLB\text{-}OB14$ as well as for trial $ACS\text{-}VAA\text{-}MATB\text{-}IM20$.

The enlisted results about the nature of essential visual appearance attributes for printed special effect colors can be checked by means of an exploratory factor analysis based on a dimension reduction. The results of the exploratory factor analysis based on the dimension reduction are presented in the following.

Nature of Essential Attributes from Exploratory Factor Analysis based on Dimension Reduction As just mentioned, the exploratory factor analysis (EFA) is another method to identify the nature of the essential visual appearance attributes. The EFA is based on the results obtained in the dimension reduction (DR). In a DR, the dimensionality can be determined by means of the eigenvalue of the covariance or correlation matrix plotted against the eigenvalue number. Using the eigenvalue method with the $Jolliffe$ criterion, a number of four or five visual appearance attributes was found to be essential. However, the explained variances determined during the principal component analysis (PCA) exceed the 90 % and 95 % level for five and six composition dimensions, respectively. The maximum number of six dimensions was used as basis for the conducted EFA.

In the present case, the factor analysis uses maximum likelihood estimation to calculate the factor loadings. The interpretation of the factor loadings is simplified by a subsequent orthogonal rotation (OR) of the factors included in the algorithm.

The rotated factor loadings were determined for six dimensions. They are used to explain the results about the nature of the essential visual appearance attributes.

Figure 7.33, figure 7.34, figure 7.35 and figure 7.36 show the rotated factor loadings for six factor dimensions as projections of vertical colored bars on the horizontal plane. The rotated factor loadings for trial $ACS\text{-}VAA\text{-}CMLB\text{-}OB14$ are shown in figure 7.33 and figure 7.34.

Figure 7.33 shows the negative factor loadings. The first and second rotated factor are for lightness (L). Yellowness (bp) and redness (ap) are represented by the fourth and sixth rotated factor, respectively. For the remaining rotated factors and visual appearance attributes, no strongly negative factor loadings occur. The positive factor loading are considered to look for further connections of rotated factors and visual appearance attributes.

The positive factor loadings are shown in figure 7.34. A strongly positive factor loading connects the second rotated factor and the visual appearance attributes redness (ap), chroma (C) and yellowness (bp). Blueness (bn) and greenness (an) are specified by the fourth and fifth rotated factor, respectively. The first rotated factor represents the hue shift (dH) and the texture. The texture appearance was tested by means of texture contrast (TC), graininess or coarseness (GC) and by sparkle or glint (SG). The lightness shift or contrast gloss ($dLCG$) and the distinctness-of-image gloss ($DOIG$) were used to ask for the gloss appearance. The gloss is represented in the third rotated factor. All tested texture and gloss attributes as well as the color attributes redness, yellowness, greenness, blueness, chroma and lightness are all included in the first six rotated factors. Remember that redness, yellowness, greenness and blueness specify hue and chroma. Thus, hue, chroma, lightness and hue shift as well as a combined gloss attribute and a combined texture attribute are essential for the characterization of printed special effect colors. Basing on

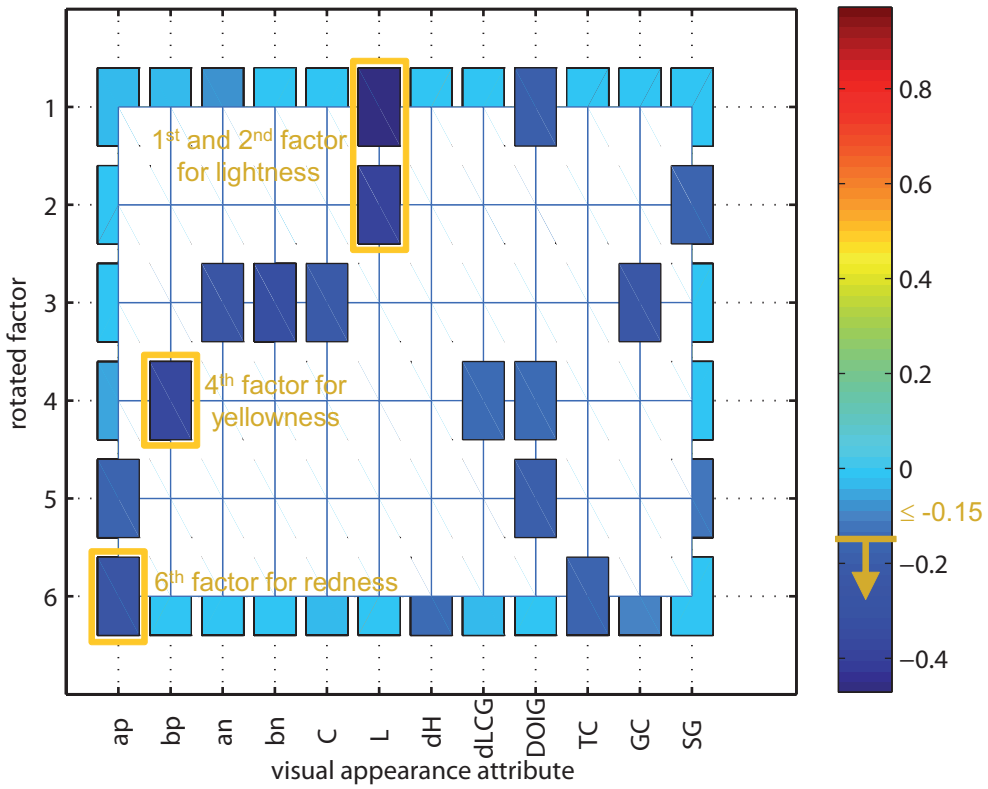

Figure 7.33: Negative factor loadings of rotated factors for visual appearance attributes (table 7.2) below mean negative factor loading of -0.15 for trial $ACS\text{-}VAA\text{-}CMLB\text{-}OB14$ (table 7.6).

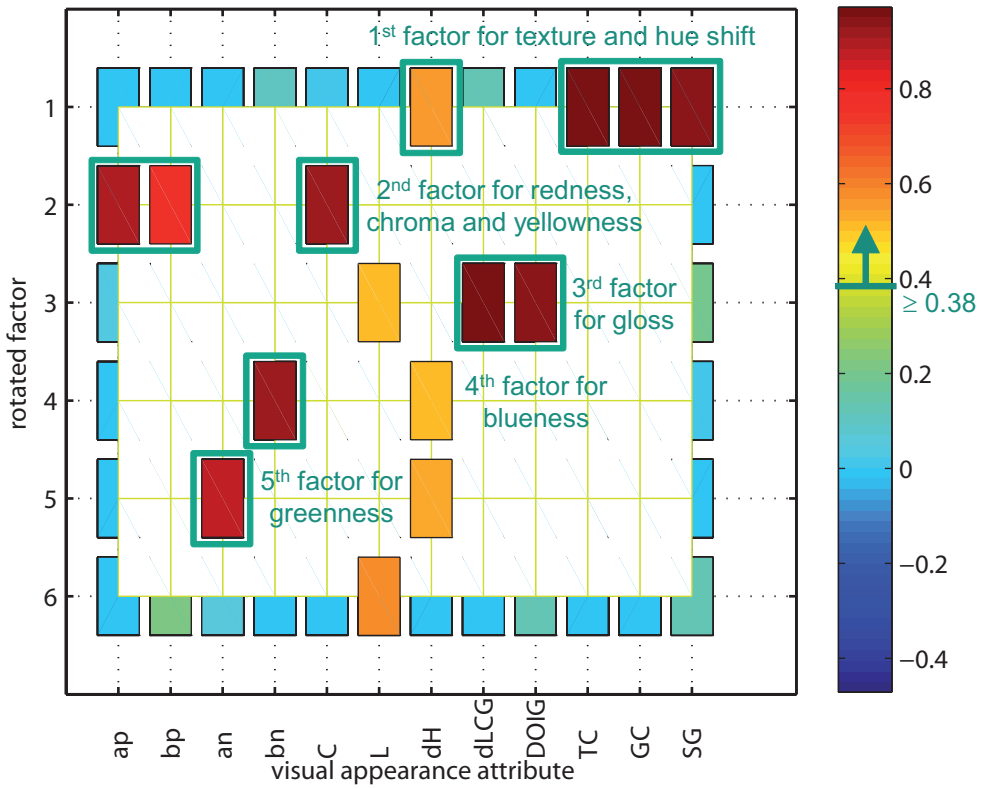

Figure 7.34: Positive factor loadings of rotated factors for visual appearance attributes (table 7.2) above mean positive factor loading of 0.38 for trial *ACS-VAA-CMLB-OB*14 (table 7.6).

these findings for trial *ACS-VAA-CMLB-OB*14, trial *ACS-VAA-MATB-IM*20 is considered. For trial *ACS-VAA-MATB-IM*20, the factor loadings are shown in figure 7.35 and figure 7.36.

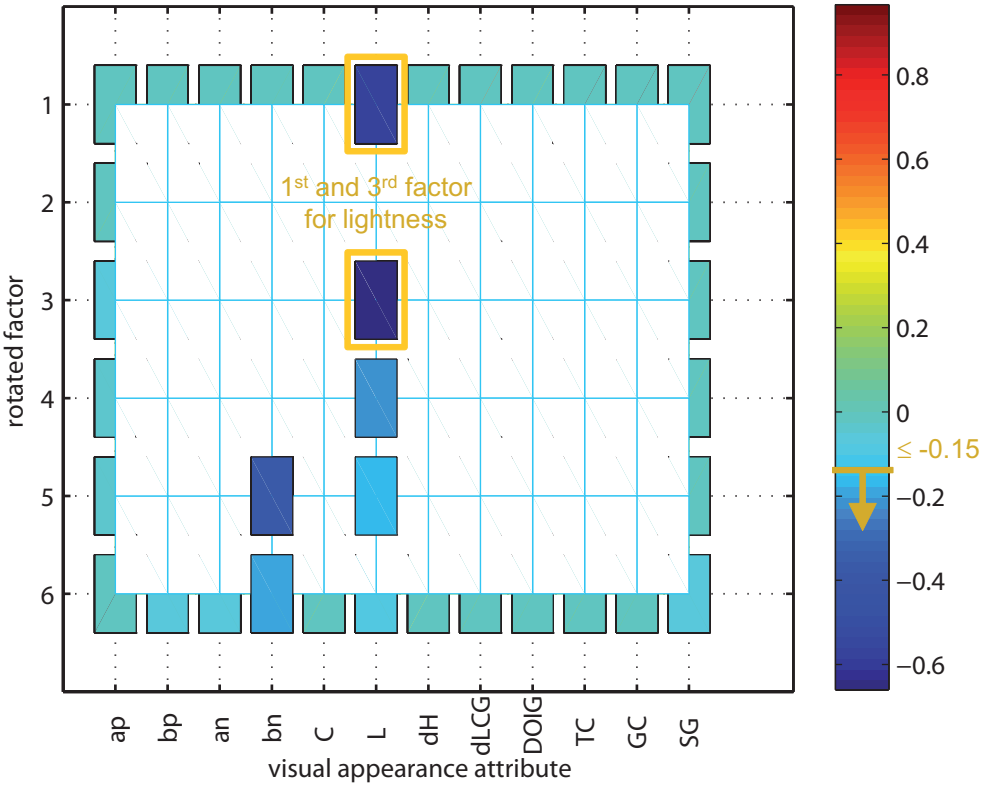

Figure 7.35: Negative factor loadings of rotated factors for visual appearance attributes (table 7.2) below mean negative factor loading of -0.15 for trial *ACS-VAA-MATB-IM*20 (table 7.6).

Figure 7.35 shows the negative factor loadings. The first and third rotated factor are for lightness (L). No further connections between rotated factors and visual appearance attributes are indicated by the negative factor loadings. The positive factor loadings are therefore examined.

The positive factor loadings are shown in figure 7.36. The texture and gloss appearance is described by the first and second rotated factor, respectively. The texture contrast (TC), graininess or coarseness (GC) and by sparkle or glint (SG) were used to scale the appearance of texture. The appearance of gloss was scaled by the use of lightness shift or contrast gloss ($dLCG$) and distinctness-of-image gloss ($DOIG$). In addition to gloss, the second factor represents the hue shift (dH). The third rotated factor specifies chroma (C) and blueness (bn). Greenness (an), yellowness (bp) and redness (ap) are specified by the fourth, fifth and sixth rotated factor, respectively. The first six rotated factors include the tested color attributes redness, yellowness, greenness, blueness, chroma, lightness and hue shift as well as all tested gloss and texture attributes. Thus, the six essential visual appearance attributes are hue, chroma, lightness and hue shift as well as a combined gloss attribute and a combined texture attribute.

The following things should be mentioned to sum up the results of the exploratory factor analysis based on a dimension reduction. The results of trial *ACS-VAA-CMLB-OB*14 are consistent with those of trial *ACS-VAA-MATB-IM*20. In consideration of all methods and criteria applied to determine the number of essential visual appearance attributes, a number of six factors was evaluated. Nine experimentally judged or six commonly used visual appearance attributes are included in the first six factors. Redness, yellowness, greenness, blueness, lightness and hue shift or hue, chroma, lightness and hue shift are the six or four essential color attributes, respectively. A

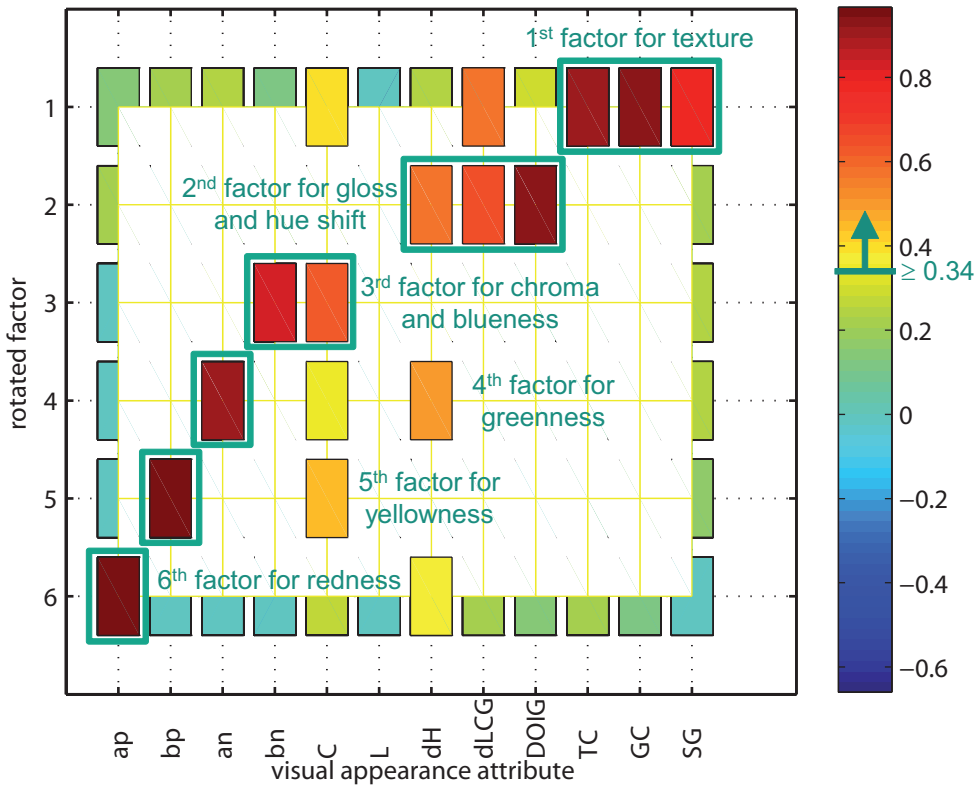

Figure 7.36: Positive factor loadings of rotated factors for visual appearance attributes (table 7.2) above mean positive factor loading of 0.34 for trial $ACS\text{-}VAA\text{-}MATB\text{-}IM20$ (table 7.6).

combined gloss attribute and a combined texture attribute are the remaining two essential visual appearance attributes.

These results concerning the nature of the essential visual appearance attributes for printed special effect colors correspond to the results of the principal component analysis followed by an orthogonal rotation. The principal component analysis followed by an orthogonal rotation is presented above.

7.5 Comparison of the Results about Essential Attributes

In this section, the results of the present study are summarized and compared with the results of other studies having comparable objectives. Remember, the objective of this study is to determine the number and nature of the essential visual appearance attributes.

A number of 14 rolled screen and 20 planar flexo printing samples (chapter 5) were presented in a color matching light booth and a multi-angle test bench, respectively. In relative and absolute category scaling experiments, visual appearance differences and twelve visual appearance attributes were rated, respectively. The collected sets of visual dissimilarity and rating data were evaluated by means of different statistical methods. These include classical multidimensional scaling, two correlation analyses, a principal component analysis followed by an orthogonal rotation and an exploratory factor analysis based on a dimension reduction.

The *number* of essential visual appearance attribute was found on the basis of the $STRESS$, cumulated variances, eigenvalues and correlation coefficients. In spite of the obvious differences in the statistical measures and methods applied on different sets of visual data, the $STRESS$, cumulated variances and eigenvalues indicate that between *four* and *six* visual appearance attributes are essential for printed special effect colors. For the different sets of visual rating data, significantly positive correlation coefficients between the tested gloss and texture attributes suggest their combination. The two gloss and three texture attributes expected to be essential can be combined in an over gloss and texture attribute. The correlation coefficients as well as the composition and factor loadings give information about the *nature* of the at most six essential visual appearance attributes. The four color attributes *hue*, *chroma*, *lightness* and *hue shift* as well as the two combined attributes for *gloss* and *texture* were found to be essential although different sets of visual data were evaluated by the use of different statistical measures and methods.

These findings about the number and nature of essential visual appearance attributes are just valid for the present conditions. Mainly, these include the estimated attributes (section 7.2.1), the assessed samples (section 7.2.2), the experimental equipment (section 7.2.3), the participating subjects (section 7.3.2) as well as the applied experimental procedures and statistical evaluations.

Upon other conditions, the results about the number and nature of the essential visual appearance attributes might be different. A comparison with the results of other studies is given by means of table 7.11.

In contrast to gloss and texture, color research began a long time ago. At first, the number of essential color attributes was found to be three. Much later, the nature of the essential color attributes was described by names. Therefore, the number and nature of essential color attributes is not treated in the same study.

Basing on the knowledge that three color attributes are essential, *Maxwell* [179] is one of the first color scientists who assigned names. These are the brightness, the tint or hue and the purity.

In the context of introducing the standard observer and the chromaticity diagram, *Judd* [135] names three related color attributes. They are called brightness, dominant wavelength and colorimetric purity.

In several further publications, *Judd* [136, 137, 138, 139, 140] vividly describes the novel experience of a stranded islander with the ordering of colored pebbles according to their color appearance. In this so-called desert island experiment, the color attributes lightness, hue and saturation are found to be essential.

The results found in this study are consistent with those early findings. As for ordinary light absorbing colors, the three color attributes hue, chroma and lightness are essential for printed special effect colors. In addition, the hue shift is required to describe the geometry-dependent color. It is not possible to give any statement about the existence of other essential shift attributes such as the chroma shift not estimated in this study (section 7.2.1).

Compared to color, visual appearance research in the domain of gloss and texture began much later. The number and nature of the essential gloss attributes were determined in the same study.

The appearance of gloss was investigated in the studies of *Pellacini et al.* [200] and *Ferwerda et al.* [80]. Glossy objects in rendered images were visually assessed in relative and absolute

Table 7.11: Results of other studies about the number (*num.*) and nature (*nat.*) of essential visual appearance attributes (*VAA*) or perception-related parameters (*PRP*).

study		*VAA* or *PRP*	
domain	researcher	*num.*	*nat.*
color	*Maxwell* [179]	three	brightness
			tint, hue
			purity
	Judd [135]	three	brightness
			dominant wavelength
			colorimetric purity
	Judd [136, 137, 138, 139, 140]	three	lightness
			hue
			saturation
gloss	*Pellacini et al.* [200], *Ferwerda et al.* [80]	two	contrast gloss
			distinctness-of-image gloss
	Wills et al. [245]	two	specular gloss, sheen, distinctness-of-image gloss, bloom, haze, diffuseness, contrast gloss
texture	*Rao* and *Lohse* [212]	three	repetitiveness, randomness, directionality, orientation, regularity, uniformity
			texture contrast, directionality
			graininess, coarseness, complexity
	Long and *Leow* [167]	four	texture features
	Gurnsey and *Fleet* [92]	three	texture filters

magnitude estimation experiments. On the basis of the collected dissimilarity and rating data, two gloss attributes named contrast gloss and distinctness-of-image gloss were found to be essential.

The same number of gloss attributes was found to be essential in the study of *Wills et al.* [245]. This result is based on dissimilarity data collected in a paired comparison experiment on rendered images of glossy objects. Instead of visual data, the nature of the essential texture attributes was determined by the use of different perception-related parameters for specular gloss, sheen, distinctness-of-image gloss, bloom, haze, diffuseness and contrast gloss.

In contrast to the mentioned studies on the appearance of gloss, this study shows that the two tested gloss attributes can be combined. Thus, the combined gloss attribute includes the lightness shift or contrast gloss (*dLCG*) and the distinctness-of-image gloss (*DOIG*). Note that no statement is possible about the existence of essential gloss attributes being not estimated during the visual experiments (section 7.2.1). For example, metal and pearl gloss were assumed to be essential. Due to the necessary limitations, metal gloss and pearl gloss were omitted in favor of contrast gloss and distinctness-of-image gloss. Apart from the selected attributes, this low number of essential gloss attributes might be caused not sufficiently high gloss variations among the assessed samples (section 7.2.2).

As in case of gloss, the visual appearance of texture started to be a research much later than the visual appearance of color. The same study often investigates the number as well as the nature of the essential texture attributes.

In their study on the appearance of texture, *Rao* and *Lohse* [212] investigated twelve texture attributes in sorting and rating experiments. Three texture dimensions were found to be sufficient to represent a wide range of natural textures included in the *Brodatz* album. The repetitiveness, randomness, directionality, regularity, orientation and uniformity are represented by the first dimension. The second dimension represents the texture contrast and directionality. The granularity, complexity and coarseness are described by the third dimension.

On the basis of a similar sorting experiment using *Brodatz* textures, *Long* and *Leow* [167] found that a number of four texture dimensions is required. The nature of the essential texture attributes was specified by different computational texture features being a kind of perception related parameters.

In contrast to the natural *Brodatz* textures, *Gurnsey* and *Fleet* [92] conducted visual experiments with artificial textures based on filtered noise. A number of three texture dimensions was found to be essential. The texture filters were used to specify the nature of the essential texture attributes.

In comparison to the enlisted studies on the appearance of texture, the presented study shows some deviations. The three tested texture attributes named texture contrast (TC), graininess and coarseness (GC) as well as sparkle and glint (SG) are joined to a combined texture attribute. As mentioned above, other texture attributes not estimated in this study might be essential (section 7.2.1). The not sufficiently high texture variations of the assessed samples are a further source for the low number of essential texture attributes (section 7.2.2).

Apart from the absent testing and the insufficient variations, the illumination conditions during the experiment might be not suitable (section 7.2.3). By definition [154, 150, 152, 57], graininess and coarseness are perceived under diffuse illumination while sparkle and glint are perceived under directional illumination. In the color matching light booth, the illumination is rather diffuse so that sparkle and glint can not be perceived. In contrast, graininess and coarseness can not be perceived in the multi-angle test bench. Both illumination conditions should be realized in the same experimental equipment.

Chapter 8

Summary and Outlook

This final chapter summarizes the thesis and presents challenges for further research on printed special effect colors. The *summary* and *outlook* are given in section 8.1 and section 8.2, respectively.

8.1 Summary

In the style of the trisection in partial problems, the summary is given in three parts. These focus on the *produced screen and flexo printing samples* (section 8.1.1), the *collected bidirectional reflectance and texture data* (section 8.1.2) and the *determined number and nature of essential visual appearance attributes* (section 8.1.3).

8.1.1 Produced Screen and Flexo Printing Samples

The first partial problem is the lack of knowledge on the field of printing with special effect inks (section 1.1.1, chapter 2). The first approach intended to produce samples of printed special effect colors for the most representative application cases (section 1.2.1, chapter 5).

In two *printing technologies* with varying *printing parameters*, printing inks with *special effect pigments* of two different pigment producers were processed. Furthermore, the *paper quality*, the *background color* and the *varnishing state* (section 5.1, section 5.2, section 5.3) were varied.

In more detail, 22 special effect pigments of *BASF SE* were processed in screen printing. A white glossy coated and black uncoated paper were used. With 22 special effect pigments and two paper qualities or background colors, 44 application cases were realized (section 5.1.1, section 5.2.1, section 5.3.1).

The flexo printing technology was applied in case of 28 special effect pigments of *MERCK KGaA*. A white glossy and matt coated paper was partially primed with a black light-absorbing ink and partly finished with a clear gloss varnish. In total, 28 special effect pigments, two paper qualities, two background colors and two varnishing states result in 224 application cases (section 5.1.2, section 5.2.2, section 5.3.2).

8.1.2 Collected Bidirectional Reflectance and Texture Data

The availability of measured or modeled bidirectional reflectance and texture distributions for systems with special effect pigments is the second partial problem (section 1.1.2, chapter 3). In connection with the approach of this problem, a freely available bidirectional reflectance and texture database was generated (section 1.2.2, chapter 6).

The printed samples were optically measured in multiple geometric configurations (section 6.1). The determined *reflectance spectra*, *color coordinates* and *texture parameters* were filed in a hierarchical structure (section 6.2). The *freely available bidirectional reflectance and texture data* (*www.idd.tu-darmstadt.de*, *office@idd.tu-darmstadt.de*) were used to investigate the influence of the printing parameters on perception-related parameters (section 6.3).

In particular, the multi-angle spectrophotometer *MA98* was used for spectral measurements in 19 geometric configurations on the screen printing samples (section 6.1.1). All flexo printing samples were measured with the multi-angle spectrophotometer *BYK-mac* equipped with spectral detectors in six bidirectional geometries and an imaging detector for spatial measurement in three bidirectional and a diffuse geometry. With the robot-based gonioreflectometer *ARGon*^{3} high-precision spectral measurements were realized in 270 geometric configurations on ten representative flexo printing samples (section 6.1.2).

For further research, all detected reflectance spectra, calculated color coordinates and determined texture parameters are filed in a tree structure. This hierarchic structure consists of seven structure levels with one or two structuring criteria and several structuring cases. The first (section 6.2.1) and second (section 6.2.2) structure level is used for the printing technology and pigment producer and for the pigment series and product number, respectively. The paper quality, varnishing state, background color and the optical instrument are distinguished on the third (section 6.2.3), fourth (section 6.2.4), fifth (section 6.2.5) and sixth (section 6.2.6) structure level. The seventh (section 6.2.7) structure level enlists the instrument specifications and determined data.

The multi-angle color coordinates were used to calculate perception-related parameters for the hue shift, lightness shift, contrast gloss and distinctness-of-image gloss. The hue difference

sum, lightness difference sum and relative luminance difference together with the sparkle area, sparkle intensity, sparkle grade and graininess were used to evaluate the influence of the special effect pigment, paper quality, varnishing state and the background color. The *hue difference sum* (section 6.3.1) is medium high and very high for the interference effect and multi-color pigments, respectively. For the sparkle pigments, the *sparkle parameters* (section 6.3.3) are high. The *graininess* (section 6.3.3) is not particularly high for the comparably large sparkle pigments. The paper quality has a negligible influence on all perception-related parameters. The *lightness difference sum* (section 6.3.1) and the *relative luminance difference* (section 6.3.2) are not suited to represent the perceived lightness shift and contrast gloss or distinctness-of-image gloss. Compared to the white paper background, all considered parameters are significantly higher for the black printed background.

8.1.3 Determined Number and Nature of Essential Attributes

The third partial problem is the incomplete characterization of printed special effect colors with visual appearance attributes (section 1.1.3, chapter 4). The identification of the essential appearance attributes is focused in the third approach (section 1.2.3, chapter 7).

To find the *number* and *nature* of the *essential visual appearance attributes*, a *methodical concept* was designed (section 7.1) and the *experimental conditions* were specified (section 7.2). Three series of *visual experiments* were conducted (section 7.3) and analyzed in several *statistical evaluations* (section 7.4).

The methodical concept intended different visual experiments and statistical methods. In the two visual experiments differing in the estimated appearance dimensions, the required data are collected (section 7.1.1). Dissimilarity data are obtained in a relative category scaling experiment of visual appearance differences between two samples. In an absolute category scaling experiment of twelve visual appearance attributes, ratings are the resulting data. By means of statistical evaluations of the collected data, the interim and final results are obtained (section 7.1.2). The interim results are the configuration from classical multidimensional scaling and the composition from principal component analysis. A correlation analysis on the configuration and rating data, the principal component analysis followed by an orthogonal rotation and an exploratory factor analysis based on a dimension reduction give information about the number and nature of essential visual appearance attributes.

To specify the experimental conditions, twelve visual appearance attributes were selected and adapted, several printing samples were selected and prepared and two experimental setups were adapted and designed. The twelve selected and adapted visual appearance attributes are the redness, yellowness, greenness, blueness, chroma, lightness, hue shift, lightness shift and contrast gloss, distinctness-of-image gloss, texture contrast, graininess and coarseness and the sparkle and glint (section 7.2.1). With respect to the sample set, 14 screen printing samples and 20 flexo printing samples were selected and prepared as rolled and planar samples (section 7.2.2). To simulate multiple geometric configurations simultaneously or successively, the rolled and planar samples were assessed in an adapted commercial color matching light booth or a custom-made multi-angle test bench (section 7.2.3).

Three trials differing in the experimental procedure, appearance dimension, technical equipment and in the sample set were conducted with qualified subjects of both genders and varying age (section 7.3.1, section 7.3.2). The total visual appearance difference and twelve visual appearance attributes were assessed in relative and absolute category scaling experiments, respectively. In the color matching light booth and the multi-angle test bench, 14 rolled screen and 20 planar flexo printing samples were presented to the subjects.

The configuration obtained in classical multidimensional scaling of the dissimilarities and of the composition obtained in the principal component analysis of the ratings have comparable geometric structures. In these geometric structures, perceptually similar samples are located next to each other in local groups (section 7.4.1). Beyond these interim results, final results about the number and nature of the essential visual appearance attributes are received (section 7.4.2). The stress values obtained in the classical multidimensional scaling, the cumulated variances obtained in the

principal component analysis and the eigenvalues obtained in the dimension reduction indicate the existence of at most *six essential visual appearance attributes*. The two gloss and three texture attributes assumed to be essential and tested in the visual experiments can be each subsumed to a combined gloss attribute and a combined texture attribute as found in a correlation analysis of the ratings. In the correlation analysis between the ratings and the configuration, the principal component analysis followed by an orthogonal rotation and in the exploratory factor analysis based on the dimension reduction, the six essential visual appearance attributes were found to be the *four color attributes* called *hue*, *chroma*, *lightness* and *hue shift*, *a combined gloss attribute* and *a combined texture attribute*.

8.2 Outlook

At the beginning, the underlying problem of this research purpose is presented (section 1.1). On the basis of the three partial problems, the corresponding approaches are formulated (section 1.2).

The achieved results are concluded in the summary (section 8.1). Based on this, the present limitations are enlisted and the corresponding challenges are worked out in the following.

Section 1.2.1 gives an outlook on the *printing of predefined special effects*. An outlook on the *modeling of bidirectional optical properties* is provided in section 8.2.2. Section 8.2.3 presents an outlook on the *control of visual appearance attributes*.

8.2.1 Printing Predefined Special Effects

The incomplete knowledge about the influences in printing with special effect inks is the first partial problem (section 1.1.1). The first approach (section 1.2.1) purposes a series of printing trials to process special effect samples. Multiple application cases varying in the printing technology, the special effect pigment, the paper quality, the varnishing state and in the background color were realized (section 8.1.1). The necessary limitations in the number of printing parameters and variation levels provide challenges for further research.

Other pigment producers can be asked for their visually unique and best-selling special effect pigments. For more detailed evaluations about the influences of the particle size and material composition, special effect pigments of different narrow particle size ranges and purposely varied material compositions should be used.

Further representative paper grades or other materials such as plastic films might be selected. Substrates with predefined or previously determined roughness and porosity can be used to evaluate the influence of these substrate properties in more detail.

Apart from the unvarnished and glossy varnished surface, further varnishing states can be realized. Instead of applying a glossy varnish in solid area, a matt varnish can be used, the varnish supply can be varied or halftone areas can be designed.

In addition to the white and black background, other background colors are possible. Different background colors can be realized by using colored papers or by priming with a light-absorbing ink.

Furthermore, the influence of other printing parameters can be investigated. For example, the pigment occupancy can be varied by means of the ink supply, the pigment concentration or the tonal value. Moreover, the pigment orientation can be varied by chemical additives influencing the drying time of the printing ink and by the machine speed influencing the application behavior and the ink leveling. The final objective of further research should be the *printing* of *special effect colors* with *predefined optical properties* and *visual appearance attributes*.

8.2.2 Modeling Bidirectional Optical Properties

The second partial problem (section 1.1.2) is the availability of measured and modeled data describing the bidirectional reflectance and texture distribution of systems with special effect pigments. The generation of a bidirectional reflectance and texture database is the corresponding second approach (section 1.2.2). A bidirectional reflectance and texture database was built up on the basis of multi-angle measurements on the printed special effect samples (section 8.1.2). The database was used to evaluate the influence of the varied printing parameters on perception-related parameters. The technical limitations of the optical instruments, the effort-caused limitations in the data volume and the knowledge limitations concerning representative perception-related parameters leave much space for challenges.

The geometric configurations providing the most meaningful data should be known and realized in commercial multi-angle spectrophotometers. In addition to the usual near-at-gloss and far-from-gloss detection, the important geometric configurations may include geometries with a detection system in specular direction for the determination of gloss attributes. Apart from spectral detectors, imaging detectors should be installed to determine texture parameters.

The parameters used to investigate the influences of the printing parameters are based on existing definitions of more or less perception-based parameters. The suitability of these perception-related parameters must be questioned. Other parameters should be tested on their suitability to represent visual appearance attributes. At best, the psychophysical functions connecting optically measured data with visual appearance attributes are known from psychophysical experiments.

To model the bidirectional reflectance and texture distribution, the model parameters of a model equation can be spectrally fitted to the measured data. The fitted model parameters can be used to describe the optical properties. The derived model equation allows to simulate the visual appearance in computer graphics rendering. The *modeling* of the *bidirectional reflectance and texture distribution* should be pursued further.

8.2.3 Control Visual Appearance Attributes

The incomplete perception-based characterization of printed special effect colors is introduced as the third partial problem (section 1.1.3). The associated third approach (section 1.2.3) intends to identify the essential visual appearance attributes. By means of visual experiments under specified conditions and statistical evaluations, the number and nature of the essential visual appearance attributes was identified (section 8.1.3). The necessary limitations concerning the visual appearance attributes, the printed special effect samples, the experimental equipment, the participating subjects, the experimental trials and the statistical evaluations bring along multiple challenges.

Among all visual appearance attributes mentioned in literature, the ones expected to be most representative were selected and adapted for the visual experiments. Further visual appearance attributes such as the chroma or color shift and the metal or pearl gloss should be included in the visual experiments.

Apart from the small number of selected samples, a greater variety of samples each in fine appearance gradations should be provided. The application of liquid adhesive in the preparation of the rolled and planar samples caused small ripples what should be avoided.

In contrast to the adapted commercial color matching light booth, the custom-made multi-angle test bench calls for some improvements such as the more uniform illumination of the test field or the more ergonomic mounting of the chin rest. The more exact fixation of the planar samples on the sample holder as well as the more reliable and user-friendly setting of the reference geometry are further examples for improvements.

Furthermore, the number of subjects can be increased and their induction can be extended. Other experimental procedures and evaluation methods can be applied to derive the desired psychophysical function for the essential visual appearance attributes. With further visual experiments and statistical evaluations, the following objective can be achieved. As in case of light-absorbing inks, the *process control* and *quality assurance* in printing with special effect inks should be based on the *essential visual appearance attributes*.

Bibliography

[1] American Society for Testing and Materials (ASTM). Standard Test Method for Specular Gloss, ASTM D 523-89, 1989.

[2] American Society for Testing and Materials (ASTM). Standard Test Method for Evaluation of Visual Difference with a Gray Scale, ASTM D 2616-96, 1996.

[3] American Society for Testing and Materials (ASTM). Standard Test Method for Specular Gloss, ASTM D 523-89 (Reapproved 1999), 1999.

[4] American Society for Testing and Materials (ASTM). Standard Test Method for Visual Evaluation of Gloss Difference Between Surfaces of Similar Appearance, ASTM D 4449-90 (Reapproved 1999), 1999.

[5] American Society for Testing and Materials (ASTM). Standard Test Methods for Instrumental Measurement of Distinctness-of-Image Gloss of Coating Surfaces, ASTM D 5767-95 (Reapproved1999), 1999.

[6] American Society for Testing and Materials (ASTM). Standard Practice for Specifying the Geometry of Multiangle Spectrophotometers, ASTM D 2175-01, 2001.

[7] American Society for Testing and Materials (ASTM). Standard Practice for Multiangle Measurements of Metal Flake Pigmented Materials, ASTM E 2194-03, 2003.

[8] American Society for Testing and Materials (ASTM). Standard Terminology of Appearance, ASTM E 284-03a, 2003.

[9] American Society for Testing and Materials (ASTM). Standard Test Methods for Measurement of Gloss and High-Gloss Surfaces by Goiniophotometry, ASTM E 430-97 (Reapproved 2003), 2003.

[10] American Society for Testing and Materials (ASTM). Standard Practice for Specifying and Verifying the Performance of Color-Measuring Instruments, ASTM E 2214-08, 2008.

[11] J. C. Ashbaugh, R. S. Berns, B. A. Darling, and L. A. Taplin. Artist material BRDF Database for Computer Graphics Rendering. In *Final Program and Proceedings of 17th Color Imaging Conference, Albuquerque, New Mexico*, volume 17, pages 62–68, 2009.

[12] T. Atamas, K.-O. Hauer, and A. Höpe. Appearance Measurements of Goniochromatic Colours. In *Conference Proceedings Publication, Predicting Perceptions: The 3rd International Conference on Appearance*, pages 17–19, Edinburgh, UK, April 2012.

[13] G. Baba. Gonio-Spectrophotometric Analysis of Pearl-Mica Paint (2). *Die Farbe*, 37:99–100, 1990.

[14] F.-W. Bach, K. Möhwald, A. Laarmann, and T. Wenz. *Moderne Beschichtungsverfahren*. Wiley-VCH, Weinheim, 2005.

[15] W. Bäumer. Perlglanz und Perlglanzpigmente (1). *Farbe und Lack*, 79(6):530–536, 1973.

[16] W. Bäumer. Perlglanz und Perlglanzpigmente (2). *Farbe und Lack*, 79(7):638–645, 1973.

[17] W. Bäumer. Perlglanz und Perlglanzpigmente (3). *Farbe und Lack*, 79(8):747–755, 1973.

[18] T. Bäurle. The determination of the color tolerances for metallic and pearlescent colors. *Die Farbe*, 42:145–150, 1996.

[19] M. Becher, S. Hornig, T. Roos, and C. Wildner. Evaluierung eines Mehrwinkelprüfstands für gedruckte Spezialeffektfarben (Evaluation of a Multi-Angle Test Bench for Printed Special Effect Colors). Advanced Design Project (ADP), Technische Universität Darmstadt, Fachbereich Maschinenbau, Fachgebiet Druckmaschinen und Druckverfahren, Darmstadt, 2012.

[20] G. Benzing, R. Besold, H Endriß, B. Lembeck, E. Quellmalz, V. Radtke, H. Schäfer, R. Schwindt, and J. Schröder. *Pigmente und Farbstoffe für die Lackindustrie - Eigenschaften und praktische Anwendungen*. Expert, Ehningen bei Böblingen, 2nd edition, 1992.

[21] R. S. Berns. *Principles of Color Technology*. John Wiley and Sons Inc., New York, 3rd edition, 2000.

[22] R. S. Berns. Improving Artwork Reproduction Through 3D-Spectral Capture and Computer Graphics Rendering. Projet overview, Rochester Institute of Technology, College of Science, Center for Imaging Science,Munsell Color Science Laboratory, Rochester, New York, United States, May 2006.

[23] R. S. Berns. Artist Material Database. Technical report, Rochester Institute of Technology, College of Science, Center for Imaging Science,Munsell Color Science Laboratory, Rochester, New York, United States, April 2012.

[24] R. Besold. Metallic Effect - Characterization, Parameter and Methods for Instrumentally Determination. *Die Farbe*, 37:79–85, 1990.

[25] C. Bettner. Aufbau eines Prüfstandes zur visuellen Abmusterung von Interferenzeffektfarben (Construction of a Colour Matching Test Rig for Interference Colours). Studienarbeit (seminar thesis), Technische Universität Darmstadt, Fachbereich Maschinenbau, Fachgebiet Druckmaschinen und Druckverfahren, Darmstadt, 2008.

[26] F. W. Billmeyer and M. Saltzman. *Grundlagen der Farbtechnologie*. Muster-Schmidt, Göttingen, Zürich, 2nd edition, 1993.

[27] D. Bimler, J. Kirkland, and R. Jacobs. Color-Vision Tests Considered as a Special Case of Multidimensional Scaling. *Color Research and Application*, 25(3):160–169, 2000.

[28] K. Böhm, G. Paff, and J. Weitzel. Ein effektvolles Farbenspiel - Wie Perlglanzpigmente in Druckfarben für verschiedene Druckverfahren eingesetzt werden können. *Farbe und Lack*, 105(10):30–42, 1999.

[29] D. H. Brainard, W. A. Brunt, and J. M. Speigle. Color constancy in the nearly natural image. 1. Asymmetric matches. *Journal of the Optical Society of America*, 14(9):2091–2110, 1997.

[30] D. H. Brainard and B. A. Wandell. Asymmetric color matching: how color appearance depends on the illuminant. *Journal of the Optical Society of America*, 9(9):1433–1448, 1992.

[31] E. Brenner, J. J. M. Granzier, and J. B. J. Smeets. Combining local and global contributions to perceived colour: An analysis of the variability in symmetric and asymmetric colour matching. *Vision Research*, 47:114–125, 2007.

[32] S. Bühne, A. Wooker, and A. Linzmaier. Orientierung von Effektpigmenten - Einfluss der Rheologie in wässrigen Lacksystemen. *Farbe und Lack*, 114(11):34–39, 2008.

[33] G. J. Chamberlin and D. G. Chamberlin. *Colour - Its Measurement, Computation and Application*. Heyden, London, Philadelphia, Rheine, 1980.

[34] J. Chamorro-Martínez, E. Galán-Perales, B. Parados-Suárez, and J. M. Soto-Hidalgo. Perceptually-Based Functions for Coarseness Textural Feature Representation. In *Proceedings of the 3rd Iberian conference on Pattern Recognition and Image Analysis (IbPRIA)*, pages 579–586, 2007.

[35] C. Charrier, L. T. Maloney, H. Cherifi, and K. Knoblauch. Maximum likelihood difference scaling of image quality in compression-degraded images. *Journal of the Optical Society of America*, 24(11):3418–3426, 2007.

[36] Y. Chen. Model Evaluation and Measurement Optimization for the Reproduction of Artist Paint Surfaces through Computer Graphics Renderings. Master thesis, Rochester Institute of Technology, , Center for Imaging Science, Rochester, New York, United States, February 2008.

[37] E. Chorro, e. Perales, V. Navarro, N. Alcòn, and A. Rabal. Reproducibility comparison between two multi-gonio-spectrophotometers. In *Proceedings of the 11th Congress of the International Color Association (AIC)*, Sydney, 2009.

[38] J. M. Coggins and A. K. Jain. A spatial filtering approach to texture analysis. *Pattern Recognition Letters*, 3(3):195–203, 1985.

[39] R. M. Cornell and U. Schwertmann. *The Iron Oxides: Structure, Properties, Reactions, Occurrences and Uses*. Wiley-VCH, Weinheim, 2nd edition, 2006.

[40] W. R. Cramer. Farbmessung an Glimmerpigmenten. *Technisches Messen*, 59(5):229–232, 1992.

[41] W. R. Cramer. Magical Mixtures. *Paint and Coatings Industry*, (9):72–75, 1999.

[42] W. R. Cramer. Effekte sichten und beziffern - cis- und trans-Geometrien bei farbmetrischer Beurteilung von Effektpigmenten. *Farbe und Lack*, 108(3):48–55, 2002.

[43] W. R. Cramer. Examples of Interference and the Color Pigment Mixtures Green with Red and Red with Green. *Color Research and Application*, 27(1):276–281, 2002.

[44] W. R. Cramer. Ohne Glimmer, aber mit Glitzer - Neue Effekte auf synthetischer Basis. *Farbe und Lack*, 109(4):132–136, 2003.

[45] W. R. Cramer. Der richtige Blickwinkel - Visuelle und instrumentelle Abmusterung von Interferenzeffektpigmenten im Vergleich. *Farbe und Lack*, 112(9):26–30, 2006.

[46] W. R. Cramer and P. W. Gabel. Effektvolles messen. *Farbe und Lack*, 107(1):42–49, 2001.

[47] W. R. Cramer and P. W. Gabel. Measuring Special Effects - A Comparison of Various Spectrophotometers. *Paint and Coatings Industry*, (9):36–46, 2001.

[48] W. R. Cramer and P. W. Gabel. Das gewisse Etwas - Dreiecksbeziehungen aus Bunt-, Aluminium- und Interferenzpigmenten. *Farbe und Lack*, 109(10):78–84, 2003.

[49] Z. P. Czornij. Hochwertige Eisenoxide als Pigmente in Fahrzeuglacken. *Farbe und Lack*, 106(8):38–43, 2000.

[50] K. Dana. BRDF/BTF Measurement Device. In *Proceedings of International Conference on Computer Vision ICCV*, pages 460–466, 2001.

[51] K. Dana and S. Nayar. 3D textured surface modelling. In *Workshop on the Integration of Appearance and Geometric Methods in Object Recognition*, pages 46–56, 1999.

[52] K. J. Dana, S. K. Nayar, B. van Ginneken, and J. J. Koederink. Reflectance and Texture of Real-World Surfaces. Technical Report CUCS-048-96, Columbia University , 1996.

[53] K. J. Dana, S. K. Nayar, and J. J. van Ginneken, B. Koederink. Reflectance and Texture of Real-World Surfaces. In *Prooceeding of the IEEE Conference on Computer Vision and Pattern Recognition, San Juan*, pages 151–157, 1997.

[54] K. J. Dana, S. K. Nayar, and J. J. van Ginneken, B. Koederink. Reflectance and Texture of Real-World Surfaces. *ACM Transaction on Graphics*, 18(1):1–34, 1999.

[55] S. Daultrey. *Concepts and Techniques in Modern Geography No. 8: Principal Components Analysis*. Geo Abstracts Limited, Norwich, 1976.

[56] M. D. de Fez, P. Capilla, M. J. Luque, J. Pérez-Carpinell, and J. C. del Pozo. Asymmetric Colour Matching: Memory Matching Versus Simultaneous Matching. *Color Research and Application*, 26(6):458–468, 2001.

[57] N. Dekker, E. J. J. Kirchner, R. Supèr, G. J. van den Kieboom, and R. Gottenbos. Total Appearance Differences for Metallic and Pearlescent Materials: Contributions From Color and Texture. *Color Research and Application*, 36(1):4–14, 2010.

[58] Deutschen Gesellschaft für Psychologie (DGPs) and Berufsverband Deutscher Psychologinnen und Psychologen e. V. (BDP). *Ethische Richtlinien der Deutschen Gesellschaft für Psychologie e. V. und des Berufsverbandes Deutscher Psychologinnen und Psychologen e. V. zugleich Berufsordnung des Berufsverbandes Deutscher Psychologinnen und Psychologen e. V.* Deutschen Gesellschaft für Psychologie (DGPs) and Berufsverband Deutscher Psychologinnen und Psychologen e. V. (BDP), Berlin, 2005.

[59] Deutsches Institut für Normung (DIN). Statistische Auswertungen - Messbare (kontinuierliche) Merkmale, DIN 53804 Teil 1:1981-09, September 1981.

[60] Deutsches Institut für Normung (DIN). Statistische Auswertung von Daten - Testverfahren und Vertrauensbereiche für Erwartungswerte und Varianzen, DIN 55303 Teil 2:1984-05, Mai 1984.

[61] Deutsches Institut für Normung (DIN). Grundbegriffe der Messtechnik - Behandlung von Unsicherheiten bei der Auswertung von Messungen, DIN 1318 Teil 4:1985-12, Dezember 1985.

[62] Deutsches Institut für Normung (DIN). Statistische Auswertung von Daten - Bestimmung eines statistischen Anteilsbereichs, DIN 55303 Teil 5:1987-02, Februar 1987.

[63] Deutsches Institut für Normung (DIN). Papier und Pappe - Bestimmung des Wasserabsorptionsvermögens - Cobb-Verfahren, DIN EN 20535:1994-09, September 1994.

[64] Deutsches Institut für Normung (DIN). Farbtoleranzen für Automobillackierungen - Teil 2: Effektlackierungen, DIN 6175-2:2001-03, März 2001.

[65] Deutsches Institut für Normung (DIN). Papier und Pappe - Bestimmung des Glanzes - Messung mit einem parallelen Strahl bei 45°, DIN-Verfahren, DIN EN 14086:2003-04, April 2003.

[66] Deutsches Institut für Normung (DIN). Papier und Pappe - Bestimmung des Glanzes - Teil 2: Messung mit einem parallelen Strahl bei 75°, DIN-Verfahren, DIN EN ISO 8254-2:2003-04 , April 2003.

[67] Deutsches Institut für Normung (DIN). Prüfung von Papier und Pappe - Bestimmung der Glätte nach Bekk, DIN 53107:2003-12, Dezember 2003.

[68] Deutsches Institut für Normung (DIN). Prüfung von Papier und Pappe - Bestimmung der Rauheit nach Bendtsen, DIN 53108:2011-01, Januar 2011.

[69] D. Edwards, S. Boulos, J. Johnson, P. Shirley, M. Ashikhmin, M. Stark, and C. Wyman. The Halfway Vector Disk for BRDF Modeling. *ACM Transaction on Graphics*, 25(1):1–18, 2006.

[70] W. H. Ehrenstein and A. Ehrenstein. *Modern Techniques in Neuroscience Research*, chapter Psychophysical Methods, pages 1211–1241. Springer, Berlin, New York, 1999.

[71] K. Emrith, M. J. Chantler, P. R. Green, M. L. Smith, and L. N. Smith. Human Subjectivity to Apparent Randomness of Surface Textures. In *Book of Abstracts of 2nd CIE Expert Symposium on Appearance: When appearance meets lighting*, pages 79–80, Ghent, Belgium, 2010.

[72] P. G. Engeldrum. *Psychometric scaling: a toolkit for imaging systems.* Imcotek Press, Winchester, 2000.

[73] S. Ershov, K. Kolchin, and K. Myszkowski. Rendering Pearlescent Appearance Based on Paint-Composition Modelling. *Eurographics*, 20(2):1–12, 2001.

[74] S. Ershov, R. Ďurikovič, K. Kolchin, and K. Myszkowski. Reverse engineering approach to appearance-based design of metallic and pearlescent paints. *The Visual Computer*, 8–9(20):586–599, 2004.

[75] C. Eugène. Measurement of "total visual appearance": A CIE challenge of soft metrology. 12th imeko tc1 and tc7 joint symposium on man science and measurement, CIE, 2008.

[76] M. D. Fairchild. *Color Appearance Models.* John Wiley and Sons Ltd., Chichester, 2nd edition, 2005.

[77] D. Farnsworth. The Farnsworth-Munsell 100-Hue and Dichotomous Tests for Color Vision. *Journal of the Optical Society of America*, 33(10):568–578, 1943.

[78] D. Farnsworth. *The Farnsworth-Munsell 100-Hue Test for the Examination of Color Discrimination - Manual by Dean Farnsworth*, 1957.

[79] M. Fedutina. Durchführung und Auswertung von Farbdiskriminierungsexperimenten auf einem Flüssigkristallbildschirm. Master thesis, Technische Universität Darmstadt, Fachbereich Maschinenbau, Fachgebiet Druckmaschinen und Druckverfahren, Darmstadt, 2010.

[80] J. A. Ferwerda, F. Pellacini, and P. P. Greenberg. A physically-based model for surface gloss perception. In *Proceedings of SPIE Human Vision and Electronic Imaging*, pages 291–301, 2001.

[81] R. W. Fleming, R. O. Dror, and E. H. Adelson. Real-world illumination and the perception of surface reflectance properties. *Jounal of Vision*, 3(5):347–368, 2003.

[82] W. Franz. Color Formulation and Quality Assurance for Special-Effect Paints - Challenges and Solutions. *European Coatings*, 19(10):19–24, 2004.

[83] P. W. Gabel, A. Eberle, and H. Pieper. Goniochromatic Quality Control of Pearl Pigments. *Die Farbe*, 42(4–6):159–168, 1996.

[84] P. W. Gabel and H. Pieper. Farbmessung von Interferenzpigmenten - Colour measurement of interference pigments. *Technisches Messen*, 59(5):226–228, 1992.

[85] N. Gebhardt. Einige BRDF Modelle. Technical report, Technische Universität Wien, 2003.

[86] R. Glausch, M. Kieser, R. Maisch, G. Pfaff, and J. Weitzel. *Perlglanzpigmente.* Vincentz, Hannover, 1996.

[87] J. J. M. Granzier, J. B. J. Smeets, and E. Brenner. A Direct Test Of The "Grey World Hypothesis" - A Comparison Of Different Matching Methods. In *Proceedings of the Third European Conference on Color in Graphics, Imaging, and Vision*, pages 131–136, 2006.

[88] J. Gu, C.-I. Tu, R. Ramamoorthi, P. Belhumeur, W. Matusik, and S. Nayar. Time-Varying Surface Appearance: Acquisition, Modeling and Rendering. In *ACM Transactions on Graphics (TOG) - Proceedings of ACM SIGGRAPH 2006*, volume 25, pages 762–771, 2006.

[89] S.-S. Guan and M. R. Luo. A Colour-Difference Formula for Assessing Large Colour Differences. *Color Research and Application*, 24(5):344–355, 1999.

[90] S.-S. Guan and M. R. Luo. Investigation of Parametric Effects Using Small Colour Differences. *Color Research and Application*, 24(5):331–343, 1999.

[91] J. Guild. The Colorimetric Properties of the Spectrum. *Philosophical Transactions of the Royal Society of London*, 230:149–187, 1932.

[92] R. Gurnsey and D. J. Fleet. Texture space. *Vision Research*, 41:745–757, 2001.

[93] M. Haas. Impacts on the Impression of Printed Effect Pigments. In *Proceedings of the 38th International Research Conference of IARIGAI*, 2011.

[94] Martin Haas. *Untersuchungen zum Verdrucken von Interferenzeffektfarben im Flexodruckverfahren.* Phd thesis, Technische Universität Darmstadt, Fachbereich Maschinenbau, Fachgebiet Druckmaschinen und Druckverfahren, Darmstadt, 2012.

[95] V. Hall-Goulle, G. Fern, R. Schmid, and M. McGarvey. Für den gewissen Aha-Effekt - Mit neuen Effektpigmenten für Druckfarben Aufmerksamkeit gewinnen. *Farbe und Lack*, 116(5):28–32, 2010.

[96] A. Handl. *Theorie und Praxis multivariater Verfahren unter besonderer Berücksichtigung von S-PLUS (Statistik und ihre Anwendungen).* Springer Verlag, Berlin, Heidelberg, 2nd edition, 2010.

[97] J. Y. Hardeberg. *Aquisition and reproduction of color images: colorimetric and multispectral approaches.* Phd thesis, Ecole Nationale Supérieure des Télécommunications, 1999.

[98] W. Heidrich. *High-Quality Shading and Lighting for Hardware-Accelerated Rendering.* Phd thesis, Universität Erlangen-Nürnberg, Technische Fakultät, Erlangen, Nürnberg, 1999.

[99] E. Hering. *Outlines of a Theory of the Light Sense.* Harvard University Press, Cambridge, 1920.

[100] Y.-X. Ho, M. Landy, and L. T. Maloney. Conjoint Measurement of Gloss and Surface Texture. *Psychological Science*, 19(2):196–204, 2008.

[101] F. Hofmeister. Koloristische Bewertung von Perlglanzpigmenten. *Farbe und Lack*, 93(10):799–802, 1987.

[102] F. Hofmeister, R. Maisch, and H. G. Gabel. Farbmetrische Charakterisierung und Identifizierung von Mica-Lackierungen. *Farbe und Lack*, 98(8):593–596, 1992.

[103] F. Hofmeister and H. Pieper. Remissionsmessungen von Interferenz-, Aluminium- und Körperfarbenpigmenten. *Farbe und Lack*, 95(8):557–560, 1989.

[104] F. Hofmeister and H. Pieper. Einfluss einer variablen Messgeometrie auf die Farborte von Interferenzpigmenten. *Farbe und Lack*, 96(10):773–775, 1990.

[105] A. Höpe and K.-O. Hauer. Three-dimensional appearance characterization of diffuse standard reflection materials. *Metrologia*, 47(3):295–304, 2010.

[106] A. Höpe, K.-O. Hauer, T. Atamas, and K. Kehren. Appearance of Printed Special Effect Ink in Commercially used Multi-Geometry Configurations. In *Book of Abstracts of 2nd CIE Expert Symposium on Appearance: When appearance meets lighting*, pages 60–62, Ghent, Belgium, 2010.

[107] A. Höpe, D. Hünerhoff, and K.-O. Hauer. *Industrial Robotics - Programming, Simulation and Applications*, chapter Robot-based Gonioreflectometer, pages 623–632. Industrial Robotics: Programming, Simulation and Applications. InTech, 2006.

[108] A. Höpe, S. Teichert, and K.-O. Hauer. Appearance characterisation of reference materials for reflectometry: Measurement of the reflection indicatrix. In *Poster at the 10th International Conference on New Developments and Applications in Optical Radimetry, Daejeon, Republic of Korea*, volume 10, 2008.

[109] D. Hünerhoff, U. Grusemann, and A. Höpe. New robot-based gonioreflectometer for measuring spectral diffuse reflection. *Metrologia*, 43(2):11–16, 2006.

[110] R. W. G. Hunt. *Measuring Colour*. Fountain Press, Chichester, 3rd edition, 1998.

[111] R. S. Hunter and R. W. Harold. *The Measurement of Appearance*. John Wiley and Sons Inc., New York, 3rd edition, 1987.

[112] H. Hupp. *Qualitäts- und Prozesskontrolle gedruckter Interferenzeffektfarben erster Generation*. Phd thesis, Technische Universität Darmstadt, Fachbereich Maschinenbau, Fachgebiet Druckmaschinen und Druckverfahren, Darmstadt, 2008.

[113] H. Hupp. *Qualitäts- und Prozesskontrolle gedruckter Interferenzeffektfarben erster Generation*. Sierke, Göttingen, 2008.

[114] H. Hupp and E. Dörsam. Measuring printed special-effect colours - First Experiences with the Multi FX10 spectrophotometer. In *Proceedings of the 33rd International Research Conference of IARIGAI*, pages 121–138, 2006.

[115] H. Hupp and E. Dörsam. Quality control for printed interference colours - investigation for a basic measuring geometry. In *Proceedings of the 34th International Research Conference of IARIGAI*, pages 257–266, 2007.

[116] H. Hupp and E. Dörsam. Verfahren und Vorrichtung für die messtechnische Erfassung von einer auf einen Bedruckstoff aufgebrachten Farbschicht. Patent, August 2007.

[117] H. Hupp and E. Dörsam. Verfahren zur messtechnischen Erfassung von einer auf einen Bedruckstoff aufgetragenen Farbschicht. Patent, December 2007.

[118] International Commission on Illumination (CIE). CIE Publication No. 46: A review of publications on properties and reflection values of material reflection standards. Technical report, Central bureau of the International Commission on Illumination (CIE), Vienna, 1979.

[119] International Commission on Illumination (CIE). CIE Publication No. 116: Survey of reference materials for testing the performance of spectrophotometers and colorimeters. Technical report, Central Bureau of the International Commission on Illumination (CIE), Vienna, 1994.

[120] International Commission on Illumination (CIE). CIE TC1-65 - A Framework for the Measurement of Visual Appearance - Technical Report 2005. Technical report, Technical Committee TC1-65, 2005.

[121] International Organization for Standardization (ISO). Paper and board - Determination of CIE whiteness, $D65/10^\circ$ (outdoor daylight), ISO 11475:2004, 2004.

[122] International Organization for Standardization (ISO). Paper and board - Determination of roughness/smoothness (air leak methods) - Part 4: Print-surf method, ISO 8791-4:2007, 2007.

[123] International Organization for Standardization (ISO). Paper and board - Determination of opacity (paper backing) - Diffuse reflectance method, ISO 2471:2008, 2008.

[124] International Organization for Standardization (ISO). Paper, board and pulps - Measurement of diffuse blue reflectance factor - Part 2: Outdoor daylight conditions (D65 brightness), ISO 2470-2:2008, 2008.

[125] International Organization for Standardization (ISO). Paper and board - Measurement of specular gloss - Part 1: 75° gloss with a converging beam, TAPPI method, ISO 8254-1:2009, 2009.

[126] International Organization for Standardization (ISO). Paper and board - Determination of thickness, density and specific volume, ISO 534:2011, 2011.

[127] International Organization for Standardization (ISO). Paper and board - Determination of grammage, ISO 536:2012, 2012.

[128] S. Ishihara. *Ishihara's Test for Colour Deficiency - The Series of Plates Desigend as a Test for Colour Deficiency*. Kanehara Trading Inc., Tokyo, 2003.

[129] J. D. Jackson. *Classical Electrodynamics*. John Wiley and Sons Inc., New York, London, Sydney, 1962.

[130] R. N. Jagtap, C. K. Nere, and K. G. Patel. Coloration of Polypropylene with Interference Pigment and the Effect of Wetting Agents on Its Optical Properties. *Journal of Coatings Technology and Research*, 2(8):599–606, 2005.

[131] N. Jaworska and A. Chupetlovska-Anastasova. A review of multidimentional scaling (MDS) and its utility in various psychological domains. *Tutorials in Quantitative Methods for Psychology*, 5(1):1–10, 2009.

[132] P. Ji, J. Dong, L. Qi, and M. Chantler. Perceived Directionality of Random-phase Fractal Surfaces Based on Mojette Transform. In *Conference Proceedings of 3rd International Conference on Appearance - Predicting Perceptions*, Edinburgh, UK, 2012.

[133] W. Ji, M. R. Pointer, R. M. Luo, and J. Dakin. Gloss as an aspect of the measurement of appearance. *Journal of Optical Society of America*, 23(1):22–33, 2006.

[134] I.T. Jolliffe. *Principal Component Analysis*. Springer, New York, Berlin, Heidelberg, 2nd edition, 2002.

[135] D. B. Judd. The 1931 I. C. I. Standard Observer and Coordinate System for Colorimetry. *Journal of the Optical Society of America*, 23(10):359–373, 1933.

[136] D. B. Judd. Introduction to Color. In *Symposium on Color, American Society for Testing and Material*, pages 1–13, 1941.

[137] D. B. Judd. Colorimetry of Pulp and Paper with Special Reference to "Brightness" and "Whiteness". *Pulp and Paper Magazine of Canada*, 43:1–7, 1942.

[138] D. B. Judd. Description of Color. In *Proceedings of the Optical Society of America*, pages 51–56, 1956.

[139] D. B. Judd. Some Color Demonstrations I Have Shown. *Jounal of the Optical Society of America*, 49(4):322–328, 1959.

[140] D. B. Judd. Physiological Optics at the National Bureau of Standards. *Applied Optics*, 6(1):13–26, 1967.

[141] M. Kasch. Frischer Wind - Effektpigmente für innovative Designs. *mo - Magazin für Oberflächentechnik*, 57(1–2):36–37, 2003.

[142] K. Kehren. Einfluss optischer Aufheller auf die Druckbildwiedergabe. Diplomarbeit (Master thesis), Technische Universität Darmstadt, Fachbereich Maschinenbau, Institut für Papierfabrikation und Mechanische Verfahrenstechnik, Darmstadt, 2008.

[143] K. Kehren. Einfluss optischer Aufheller auf die Druckbildwiedergabe. In Schabel, editor, *Fortschritt-Berichte Papiertechnik*, volume 3. Shaker, Aachen, 1st edition, 2008.

[144] K. Kehren, E. Dörsam, and H. Hupp. Printed interference effect colours - Process control and quality assurance. In *Proceedings of the 36th International Research Conference of IARIGAI*, volume 36, pages 329–336, 2009.

[145] K. Kehren, P. Urban, and E. Dörsam. Bidirectional Reflectance and Texture Database of Printed Special Effect Colors. In *Proceedings of 19th Color and Imaging Conference (CIC)*, volume 19, November 2011.

[146] K. Kehren, P. Urban, and E. Dörsam. Visual Appearance of Printed Special Effect Colors. In *Proceedings of 20th Color and Imaging Conference (CIC)*, pages 200–205, 2012.

[147] K. Kehren, P. Urban, E. Dörsam, A. Höpe, and D. R. Wyble. Performance of multi-angle spectrophotometers. In *Proceedings of AIC Midterm Meeting*, pages 473–476, 2011.

[148] H. Kipphan. *Handbook of Print Media - Technologies and Production Methods*. Springer, Berlin, Heidelberg, New York, 2000.

[149] H. Kipphan. *Handbuch der Printmedien - Technologien und Produktionsverfahren*. Springer, Berlin, Heidelberg, New York, 2000.

[150] E. Kirchner, K. de Haas, and L. Njo. Objektiv glitzern und funkeln - Effektlacke mit Textur instrumentell charakterisieren. *Farbe und Lack*, 114(2):32–36, 2008.

[151] E. Kirchner and N. Dekker. Performance measures of color-difference equations: correlation coefficient versus standardized residual sum of squares. *Jounal of the Optical Society of America*, 28(9):1841–1848, September 2011.

[152] E. Kirchner, N. Dekker, R. Supèr, G.-J. van den Kieboom, and R. Gottenbos. Quantifying the influence of texture on perceived color differences for effect coatings. In *Proceedings of the 11th Congress of the International Color Association (AIC)*, Sydney, 2009.

[153] E. Kirchner and J. Ravi. Predicting and Measuring the Perceived Texture of Car Paints. In *Conference Proceedings of 3rd International Conference on Appearance - Predicting Perceptions*, Edinburgh, UK, 2012.

[154] E. Kirchner, G.-J. van den Kieboom, L. Njo, R. Supèr, and R. Gottenbos. Observation of Visual Texture of Metallic and Pearlescent Materials. *Color Research and Application*, 32(4):256–266, 2007.

[155] S. Kitamura. Measurement of Surface Features and the Evaluation of Gloss. In *Book of Abstracts of 2nd CIE Expert Symposium on Appearance: When appearance meets lighting*, pages 179–182, Ghent, Belgium, 2010.

[156] W. Kohn. *Statistik: Datenanalyse und Wahrscheinlichkeitsrechnung (Statistik und ihre Anwendungen)*. Springer Verlag, Heidelberg, Berlin, 2004.

[157] G. Kortüm. *Reflexionsspektroskopie. Grundlagen, Methodik, Anwendungen*. Springer-Verlag, Berlin, Heidelberg, New York, 1969.

[158] J. B. Kruskal. Multidimensional Scaling by Optimizing Goodness of Fit to a Nonmetric Hypothesis. *Psychometrica*, 9(1):1–27, 1964.

[159] R. G. Kuehni. *Color space and its divisions: color order from antiquity to the present*. John Wiley and Sons Inc., Hoboken, 2003.

[160] Y Kwak and C. You. Visually Perceived Roughness and Bumpiness. In *Book of Abstracts of 2nd CIE Expert Symposium on Appearance: When appearance meets lighting*, pages 189–190, Ghent, Belgium, 2010.

[161] M. A. Lavin. The Gloss of Glossy Things. *MIT Artificial Intelligence Laboratory Working Papers*, (41):1–7, 1973.

[162] F. B. Leloup, P. Hanselaer, M. R. Pointer, and P. Dutré. Integration of Multiple Cues for Visual Gloss Evaluation. In *Conference Proceedings of 3rd International Conference on Appearance*, Edinburgh, UK, 2012.

[163] F. B. Leloup, M. R. Pointer, P. Dutre, and P. Hanselaer. Geometry of illumination, luminance contrast and gloss perception. *Jounal of the Optical Society of America*, 27(9):2046–2054, 2010.

[164] F. B. Leloup, M. R. Pointer, P. Dutre, and P. Hanselaer. Luminance-based specular gloss characterization. *Jounal of the Optical Society of America*, 28(9):1322–1330, 2011.

[165] F. B. Leloup, Pointer M. R., J. De Brabanter, P. Dutré, and P. Hanselaer. The Influence of the Illumination Geometry and Luminance Contrast on Gloss Perception. In *Book of Abstracts of 2nd CIE Expert Symposium on Appearance*, pages 90–92, Ghent, Belgium, 2010.

[166] S.-S. Liu and M. E. Jernigan. Texture Analysis and Discrimination in Additive Noise. *Computer Vision, Graphics, and Image Processing*, 49:52–67, 1990.

[167] H. Long and W. K. Leow. Perceptual texture space improves perceptual consistency of computational features. In *Proceedings of International Joint Conference on Artificial Intelligence (IJCAI)*, pages 1391–1396, 2001.

[168] H.-W. Loy. Iriodin - Perlglanz für den kreativen Drucker. *Deutscher Drucker*, 37(8):1–4, 2001.

[169] R. D. Lozano. Appearance in paints: Gloss, spatial filtering and definition of image (DOI). In *Proceedings of Interim Meeting of the International Color Association (AIC)*, pages 83–96, 2004.

[170] D. L. MacAdam. Visual Sensitivities to Color Differences in Daylight. *Journal of the Optical Society of America*, 32(5):247–274, 1942.

[171] F. J. Maile, G. Pfaff, and P. Reynders. Effect Pigments - Past, Present and Future. *Progress in Organic Coatings*, 54:150–163, 2005.

[172] R. Maisch and M. Weigand. *Perlglanzpigmente - Physikalische Grundlagen, Eigenschaften, Anforderungen*. Moderne Indusrie, Landsberg am Lech, 1991.

[173] J. V. Martonchik, C. J. Bruegge, and A. H. Strahler. A Review of Reflectance Nomenclature Used in Remote Sensing. *Remote Sensing Reviews*, 19:9–20, 2000.

[174] A. Materka and M. Strzelecki. Texture Analysis Methods – A Review. Technical report, Technical University of Lodz, Institute of Electronics, 2003.

[175] W. Matusik. *A Data-Driven Reflectance Model*. Phd thesis, Massechusetts Institute of Technology, Electrical Engineering and Computer Science, Massechusetts, 2003.

[176] W Matusik, B Ajdin, J. Gu, J. Lawrence, H. P. A. Lensch, F. Pellacini, and S. Rusinkiewicz. Printing Spatially-Varying Reflectance. *ACM Transactions on Graphics (TOG)*, 28(5):128:1–128:9, 2009.

[177] W. Matusik, G. Pfaff, M. Brand, and L. McMillan. Efficient Isotropic BRDF Measurement. In *Proceedings of Eurographics Symposium on Rendering*, pages 241–249, 2003.

[178] W. Matusik, H. Pfister, M. Brand, and L. McMillan. A Data-Driven Reflectance Model. In *Proceedings of 30th Siggraph Conference*, pages 759–769, 2003.

[179] J. Maxwell. On the Theory of Compound Colours, and the Relations of the Colours of the Spectrum. *Philosophical Transactions of the Royal Society of London*, 150:57–84, 1860.

[180] C. S. McCamy. Observation and Measurement of the Appearance of Metallic Materials. Part I. Macro Appearance. *Color Research and Application*, 21(4):292–304, 1996.

[181] C. S. McCamy. Observation and Measurement of the Appearance of Metallic Materials. Part II. Micro Appearance. *Color Research and Application*, 23(6):362–373, 1998.

[182] Merck KGaA. *Effect Pigments - Farbkarte für den Flexodruck - Colorcard Flexo Printing*. Merck KGaA, Pigments Division, Printing Industries, Darmstadt, Januar 2004.

[183] Merck KGaA. *Effect Pigments - Farbkarte für den Siebdruck - Colorcard Screen Printing*. Merck KGaA, Pigments Division, Printing Industries, Darmstadt, Januar 2004.

[184] Merck KGaA. *Effect Pigments - Farbkarte für den Tiefdruck - Colorcard Gravure Printing*. Merck KGaA, Pigments Division, Printing Industries, Darmstadt, Januar 2004.

[185] Merck KGaA. *Effect Pigments - Farbkarte für den Offsetdruck - Colorcard Offset Printing*. Merck KGaA, Pigments Division, Printing Industries, Darmstadt, August 2005.

[186] E. D. Montag and R. S. Berns. Visual Determination of Hue Suprathreshold Tolerances Using CRT-Generated Stimuli. *Color Research and Application*, 24(3):164–176, 1999.

[187] E. D. Montag and R. S. Berns. Lightness Dependencies and the Effect of Texture on Suprathreshold Lightness Tolerances. *Color Research and Application*, 25(4):241–249, 2000.

[188] E. D. Montag and Wilber D. C. A Comparison of Constant Stimuli and Gray-Scale Methods of Color Difference Scaling. *Color Research and Application*, 29(1):36–44, 2003.

[189] A. E. O. Munsell, L. L. Sloan, and H. Godlove. Neutral Value Scales. I. Munsel Neutral Value Scale. *Journal of the Optical Society of America*, 23:394–411, 1933.

[190] S. M. Newhall, R. W. Burnham, and J. R. Clark. Comparison of Successive with Simultaneous Color Matching. *Journal of the Optical Society of America*, 47(1):43–56, 1957.

[191] F. E. Nicodemus, J. C. Richmond, J. J. Hsia, I. W. Ginsberg, and T. Limperis. Geometrical Considerations and Nomenclatuere for Reflectance. Technical report, National Bureau of Standards, Washington DC, 1977.

[192] G. Obein, K. Knoblauch, and F. Viénot. Difference scaling of gloss: Nonlinearity, binocularity, and constancy. *Journal of Vision*, 4(4):711–720, 2004.

[193] T. Ojala, Pietikäinen M., and D. Harwood. A Comparative Study of Texture Measures with Classification Based on Feature Distributions. *Pattern Recognition*, 29(1):51–59, 1996.

[194] T. Ojala, M. Pietikäinen, and T. Mäenpää. Gray Scale and Rotation Invariant Texture Classification with Local Binary Patterns. In *Proceedings of the 6th European Conference on Computer Vision*, volume 1, pages 404–420, 2000.

[195] T. Ojala, K. Valkealahti, E. Oja, and M. Pietikäinen. Texture Discrimination with Multidimensional Distributuions of Signed Gray Level Differences. In *Proceedings of the 4th Asian Conference on Computer Vision*, volume 2, pages 1082–1088, 2000.

[196] Y. Okumura. Developing a Spectral and Colorimetric Database of Artist Paint Materials. Master thesis, Rochester Institute of Technology, College of Science, Center for Imaging Science, Rochester, New York, United States, September 2005.

[197] K. Pawlowski. *Untersuchung zur Bestimmung der Farbdichte druckfrischer Offsetfarben mit einem Druckinspektionssystem.* Phd thesis, Technische Universität Darmstadt, Fachbereich Maschinenbau, Fachgebiet Druckmaschinen und Druckverfahren, Darmstadt, 2010.

[198] K. Pawlowski. *Untersuchungen zur Bestimmung der Farbdichte druckfrischer Offsetfarben mit einem Druckinspektionssystem.* Sierke Verkag, Göttingen, Juni 2011.

[199] F. Pedrotti, L. Pedrotti, W. Bausch, and H. Schmidt. *Optik für Ingenieure: Grundlagen.* Springer, Berlin, 2nd edition, 2002.

[200] F. Pellacini, J. A. Ferwerda, and D. P. Greenberg. Toward a Physically-Based Light Refection Model for Image Synthesis. In *ACM Transaction on Graphics, Proceedings of Siggraph 2000*, pages 55–64, 2000.

[201] G. Pfaff. Perlglanzpigmente. *Spektrum der Wissenschaft*, (10):99–101, 1997.

[202] G. Pfaff. Perlglanzpigmente: Der Chemiker als Designer von Farbe und Glanz. *Chemie in unserer Zeit*, 31(1):6–16, 1997.

[203] G. Pfaff. Special Effect Pigments Based on Silica Flakes. *Inorganic Materials*, 39(2):123–126, 2003.

[204] G. Pfaff, P. Gabel, M. Kieser, F. Maile, and J. Weitzel. *Spezielle Effektpigmente - Grundlagen und Anwendungen.* Vincentz Network, Hannover, 2nd edition, 2007.

[205] G. Pfaff, P. Gabel, M. Kieser, F. Maile, and J. Weitzel. *Special Effect Pigments - Technical Basics and Applications.* Vincentz Network, Hannover, 2nd edition, 2008.

[206] R. Pfaff, G. ; Maisch. Perlglanzpigmente für Lacke und andere Anwendungen. *Farbe und Lack*, 101(2):89–93, 1995.

[207] M. Pharr and G.. Humphreys. *Physically Based Rendering: From Theory to Implementation.* Elsevier, Amsterdam, Boston, Heidelberg, London, New York, Oxford, Paris, San Diego, San Francisco, Singapore, Sydney, Tokyo, 2nd edition, 2010.

[208] J. B. Phillips, J. A. Ferwerda, and A. Nunziata. Gloss discrimination and eye movements. In *Proceedings of SPIE*, volume 7527, 2010.

[209] K. Pianoforte. Metallic and Special Effect Inks. *Ink Wold*, (12):32–34, 2005.

[210] R. W. Picard, T. Kabir, and F. Liu. Real-time Recognition with the entire Brodatz Texture Database. In *Proceedings of the IEEE Conference on Computer Vision and Pattern Recognition*, pages 638–639, 1993.

[211] M. Pointer. Appearance: Measurement and Instrumentation. In *Book of Abstracts of 2nd CIE Expert Symposium on Appearance*, pages 58–59, Ghent, Belgium, 2010.

[212] A. R. Rao and G. L. Lohse. Toward a Texture Naming System: Identifying Relevant Dimensions of Texture. *Vision Research*, 36(11):1649–1669, 1996.

[213] T. Rentschler. Ausflug ins Blaue - Mit Effektpigmenten funkelnd stylen und das Glitzern messen. *Farbe und Lack*, 118(1):29–32, 2012.

[214] M. Richter. *Einführung in die Farbmetrik*. de Gruyter, Berlin, New York, 2nd edition, 1981.

[215] A. B. J. Rodrigues. Measurement of Metallic and Pearlescent Colors. *Die Farbe*, 37:65–78, 1990.

[216] A. B. J. Rodrigues and L. E. Steenhoek. ASTM E-12.12: Measurement of Metallic and Pearlescent Colors. *Die Farbe*, 42(4–6):151–158, 1996.

[217] G. Rösler. Multigeometry Color Measurement of Effect Surfaces: Results, Possibilities and Limitations. *Die Farbe*, 37:111–121, 1990.

[218] J. Sajdowski. Papier zum Leben erweckt. *Paperazzo*, (3):10–12, 2009.

[219] K. Schläpfer. *Farbmetrik in der grafischen Industrie*. UGRA, St. Gallen, 3rd edition, 2002.

[220] P. Schlichting and T. Leuschner. Glänzende Ideen für die Veredelung im Bogenoffset. *Deutscher Drucker*, 39(15):22–25, 2003.

[221] R. Schmid, N. Mronga, V. Radtke, and O. Seeger. Optisch variable Glanzpigmente. *Farbe und Lack*, 104(5):44–48, 1998.

[222] M. Schnös. Massively Parallel SVBRDF Fitting of BTF Data. Bachelor thesis, Technische Universität Darmstadt, Department of Computational Engineering, Darmstadt, 2009.

[223] P. Shah, M. Chantler, and P. Green. Analysis of Human Perception of Surface Directionality. In *Conference Proceedings of 3rd International Conference on Appearance - Predicting Perceptions*, Edinburgh, UK, 2012.

[224] P. J. Shah, M. J. Chantler, and P. R Green. Human Perception of Surface Directionality. In *Book of Abstracts of 2nd CIE Expert Symposium on Appearance: When appearance meets lighting*, pages 81–82, Ghent, Belgium, 2010.

[225] J. R. Smith and S.-F. Chang. Transform features for texture classification and discrimination in large image databases. In *Proceedings of IEEE International Conference on Image Processing*, pages 1–5, 1994.

[226] J. M. Speigle and D. H. Brainard. Predicting color from gray: the relationship between achromatic adjustment and asymmetric matching. *Journal of the Optical Society of America*, 16(10):2370–2376, 1999.

[227] F. Sperber. Konstruktion einer Abmusterungskabine zur visuellen Beurteilung von Interferenzeffektfarben (Design of a Colour Matching Booth for Interference Effect Colours). Studienarbeit (seminar thesis), Technische Universität Darmstadt, Fachbereich Maschinenbau, Fachgebiet Druckmaschinen und Druckverfahren, Darmstadt, 2009.

[228] W. S. Stiles and J. M. Burch. N. P. L. colour-matching investigation: Final report (1958). *Optica Acta*, 6(1):1–26, 1959.

[229] Stora Enso AG. *LumiArt - Paper for Image Printing*. Stora Enso AG, May 2007.

[230] Stora Enso AG. *LumiSilk - Paper for Images and Text*. Stora Enso AG, May 2007.

[231] B. G. Tabachnick and L. S. Fidell. *Using Multivariate Statistics*. Allyn and Bacon, Boston, London, Toronto, Sydney, Tokyo, Singapore, 4th edition, 2001.

[232] X. Tang. Texture Information in Run-Length Matrices. *IEEE Transactions on Image Processing*, 7(11):1602–1609, 1998.

[233] K.-C. Ullmann. Perlglanz-Effektpigmente im Tiefdruck. *Flexo- und Tiefdruck*, 14(6):4–8, 2003.

[234] P. Urban, R. S. Berns, and M. R. Rosen. Constructing Euclidean Color Spaces based on Color Difference Formulas. In *Final Program and Proceedings of 15th Color Imaging Conference*, pages 77–82, Albuquerque, New Mexico, 2007.

[235] P. Urban, D. Schleicher, M. R. Rosen, and R. S. Berns. Embedding non-euclidean color spaces into Euclidean color spaces with minimal isometric disagreement. *Journal of the Optical Society of America*, 24(6):1516–1528, 2007.

[236] P. Vangorp and P. Dutré. Shape-Dependent Gloss Correction. In *Proceedings of the 5th Symposium on Applied Perception in Graphics and Visualization (APGV)*, pages 123–130, 2008.

[237] R. Ďuricovič, S. Ershov, K. Kolchin, and K. Myszkowski. Solution of an Inverse Problem in Rendering Metallic and Pearlescent Appearance. *3D Forum Society*, 18(4):54–60, 2004.

[238] R. Ďuricovič and W. L. Martens. Simulation of Sparkling and Depth Effects in Paints. *Association for Computing Machinery*, 19:193–198, 2003.

[239] K. Velhagen and D. Broschmann. *Tafeln zur Prüfung des Farbensinns*. Thieme, Stuttgart, New York, 33th edition, 2003.

[240] J. Venna and S. Kaski. Local Multidimensional Scaling. *Neural Networks*, 19:889–899, 2006.

[241] A. J. Vingrys and P. E. King-Smith. A quantitative Scoring Technique for Panel Tests of Color Vision. *Investigative Ophthalmology and Visual Science*, 29(1):50–63, 1988.

[242] T. Vladusich, M. P. Lucassen, and F. W. Cornelissen. Brightness and Darkness as Perceptual Dimensions. *Public Library of Science (PLoS), Computational Biology*, 3(10):1849–1858, 2007.

[243] M. Vogt. Konzept einer Abmusterungskabine zur visuellen Beurteilung von Interferenzeffektfarben (Design Concept of a Colour Matching Booth for Interference Colours). Studienarbeit (seminar thesis), Technische Universität Darmstadt, Fachbereich Maschinenbau, Fachgebiet Druckmaschinen und Druckverfahren, Darmstadt, 2007.

[244] G. Ward Larson and R. Shakespeare. *Rendering with Radiance: The Art of Science of Lighting Visualization*. Morgan Kaufmann Publishers Incorporation, Massachusetts, 1998.

[245] J. Wills, S. Garwal, D. Kriegman, and S. Belongie. Toward a Perceptual Space for Gloss. *ACM Transaction on Graphics*, 28(4):103:1–103:15, 2009.

[246] S. Wold, K. Esbensen, and P. Geladi. Principal Component Analysis. *Chemometrics and Intelligent Laboratory Systems*, 2:37–52, 1987.

[247] W. D. Wright. A Re-Determination of the Mixture Curves of the Spectrum. *Transactions on the Optical Society*, 31:201–218, 1930.

[248] P. Wu, B. S. Manjunath, S. Newsam, and H. D. Shin. A texture descriptor for browsing and similarity retrieval. *Signal Processing: Image Communication*, 16:33–43, 2000.

[249] D. R. Wyble and D. C. Rich. Evaluation of Methods for Verifying the Performance of Color-Measuring Instruments, Part I: Repeatability. *Color Research and Application*, 32:166–175, 2007.

[250] D. R. Wyble and D. C. Rich. Evaluation of Methods for Verifying the Performance of Color-Measuring Instruments, Part II: Inter-Instrument Reproducibility. *Color Research and Application*, 32:176–194, 2007.

[251] G. Wyszecki and G. H. Fielder. New Color-Matching Ellipses. *Journal of the Optical Society of America*, 61(9):1135–1152, 1971.

[252] G. Wyszecki and W. S. Stiles. *Color Science - Concepts and Methods, Quantitative Data and Farmulae*. John Wiley and Sons Incorporation, New York, 2nd edition, 2000.

[253] G-.S. Xia, J. Delon, and Y. Gousseau. Locally Invariant Texture Analysis from the Topographic Map. In *Proceedings of the International Conference on Pattern Recognition*, pages 1–4, 2008.

[254] G-.S. Xia, J. Delon, and Y. Gousseau. Shape-based Invariant Texture Indexing. *International Journal of Computer Vision*, 88(3):382–403, 2010.

[255] T. Young. The Bakerian Lecture: On the Theory of Light and Colours. *Philosophical Transactions of the Royal Society of London*, 92:12–49, 1802.

Appendix A

Special Effect Pigments of Printing Trials

Further information about the pigments used in the screen and flexo printing trials are given in section A.1 and section A.2.

A.1 Special Effect Pigments of Screen Printing Trials

Section A.1.1, section A.1.2, section A.1.3 and section A.1.4 specify the *BASF* pigments used in screen printing.

A.1.1 Pigment Class of Special Effect Pigments used in Screen Printing Trials

The pigment class is assigned in table A.1.

Table A.1: Pigment class of *BASF* pigments used in screen printing.

pigment name	pigment class
Black Olive 90*C*0*Z*	silver white pigment
Firemist 9*G*630*L Blue*	sparkle pigment
Firemist 9*G*680*D Colormotion Blue Topaz*	multi-color pigment
Firemist 9*G*480*D Colormotion Ruby*	multi-color pigment
Firemist 9*G*230*L Gold*	sparkle pigment
Firemist 9*G*830*L Green*	sparkle pigment
Firemist 9*G*130*L Pearl*	sparkle pigment
Firemist 9*G*430*L Red*	sparkle pigment
Firemist 9*G*730*L Turquoise*	sparkle pigment
Firemist 9*G*530*L Violet*	sparkle pigment
Glacier 9*S*130*D Frost White*	silver white pigment
Lumina 9*A*30*D Aqua Blue*	interference effect pigment
Lumina 9232*D Brass*	gold pigment
Lumina 9359*D Copper*	iron oxide pigment
Lumina 9*Y*30*D Gold*	interference effect pigment
Lumina 9*G*30*D Green*	interference effect pigment
Lumina 9*R*30*D Red*	interference effect pigment
Lumina 9680*H Royal Blue*	interference effect pigment
Lumina 9450*D Russet*	iron oxide pigment
Lumina 9*T*30*D Turquoise*	interference effect pigment
Santa Fe 9332*D Desert Blush*	gold pigment
Santa Fe 9832*D Kiwi*	gold pigment

A.1.2 Particle Size of Special Effect Pigments used in Screen Printing Trials

Table A.2 enlists the particle size.

Table A.2: Particle size of *BASF* pigments used in screen printing.

pigment name	particle size
Black Olive 90*C*0*Z*	6 μm - 48 μm
Firemist 9*G*630*L Blue*	5 μm - 300 μm
Firemist 9*G*680*D Colormotion Blue Topaz*	13 μm - 180 μm
Firemist 9*G*480*D Colormotion Ruby*	13 μm - 180 μm
Firemist 9*G*230*L Gold*	5 μm - 300 μm
Firemist 9*G*830*L Green*	5 μm - 300 μm
Firemist 9*G*130*L Pearl*	5 μm - 300 μm
Firemist 9*G*430*L Red*	5 μm - 300 μm
Firemist 9*G*730*L Turquoise*	5 μm - 300 μm
Firemist 9*G*530*L Violet*	5 μm - 300 μm
Glacier 9*S*130*D Frost White*	8 μm - 45 μm
Lumina 9*A*30*D Aqua Blue*	8 μm - 48 μm
Lumina 9232*D Brass*	8 μm - 48 μm
Lumina 9359*D Copper*	8 μm - 48 μm
Lumina 9*Y*30*D Gold*	8 μm - 48 μm
Lumina 9*G*30*D Green*	8 μm - 48 μm
Lumina 9*R*30*D Red*	8 μm - 48 μm
Lumina 9680*H Royal Blue*	6 μm - 48 μm
Lumina 9450*D Russet*	8 μm - 48 μm
Lumina 9*T*30*D Turquoise*	8 μm - 48 μm
Santa Fe 9332*D Desert Blush*	8 μm - 48 μm
Santa Fe 9832*D Kiwi*	8 μm - 48 μm

A.1.3 Substrate Material of Special Effect Pigments used in Screen Printing Trials

The substrate material is named in table A.3.

Table A.3: Substrate material of *BASF* pigments used in screen printing.

pigment name	substrate material
Black Olive 90*C*0*Z*	natural mica
Firemist 9*G*630*L Blue*	synthetic borosilicate
Firemist 9*G*680*D Colormotion Blue Topaz*	synthetic borosilicate
Firemist 9*G*480*D Colormotion Ruby*	synthetic borosilicate
Firemist 9*G*230*L Gold*	synthetic borosilicate
Firemist 9*G*830*L Green*	synthetic borosilicate
Firemist 9*G*130*L Pearl*	synthetic borosilicate
Firemist 9*G*430*L Red*	synthetic borosilicate
Firemist 9*G*730*L Turquoise*	synthetic borosilicate
Firemist 9*G*530*L Violet*	synthetic borosilicate
Glacier 9*S*130*D Frost White*	synthetic mica
Lumina 9*A*30*D Aqua Blue*	natural mica
Lumina 9232*D Brass*	natural mica
Lumina 9359*D Copper*	natural mica
Lumina 9*Y*30*D Gold*	natural mica
Lumina 9*G*30*D Green*	natural mica
Lumina 9*R*30*D Red*	natural mica
Lumina 9680*H Royal Blue*	natural mica
Lumina 9450*D Russet*	natural mica
Lumina 9*T*30*D Turquoise*	natural mica
Santa Fe 9332*D Desert Blush*	natural mica
Santa Fe 9832*D Kiwi*	natural mica

A.1.4 Coating Material of Special Effect Pigments used in Screen Printing Trials

Table A.4 designates the coating material.

Table A.4: Coating material of *BASF* pigments used in screen printing.

pigment name	coating material
Black Olive 90*C*0*Z*	cobalt oxide
Firemist 9*G*630*L Blue*	titanium dioxide
Firemist 9*G*680*D Colormotion Blue Topaz*	silicon dioxide, tin dioxide, titanium dioxide
Firemist 9*G*480*D Colormotion Ruby*	silicon dioxide, tin dioxide, titanium dioxide
Firemist 9*G*230*L Gold*	titanium dioxide
Firemist 9*G*830*L Green*	titanium dioxide
Firemist 9*G*130*L Pearl*	titanium dioxide
Firemist 9*G*430*L Red*	titanium dioxide
Firemist 9*G*730*L Turquoise*	titanium dioxide
Firemist 9*G*530*L Violet*	titanium dioxide
Glacier 9*S*130*D Frost White*	titanium dioxide
Lumina 9*A*30*D Aqua Blue*	titanium dioxide
Lumina 9232*D Brass*	iron(III) oxide, titanium dioxide
Lumina 9359*D Copper*	iron(III) oxide
Lumina 9*Y*30*D Gold*	titanium dioxide
Lumina 9*G*30*D Green*	titanium dioxide
Lumina 9*R*30*D Red*	titanium dioxide
Lumina 9680*H Royal Blue*	titanium dioxide
Lumina 9450*D Russet*	iron(III) oxide
Lumina 9*T*30*D Turquoise*	titanium dioxide
Santa Fe 9332*D Desert Blush*	iron(III) oxide, titanium dioxide
Santa Fe 9832*D Kiwi*	iron(III) oxide, titanium dioxide

A.2 Special Effect Pigments of Flexo Printing Trials

The *MERCK* pigments used in flexo printing are specified in section A.2.1, section A.2.2, section A.2.3 and section A.8.

A.2.1 Pigment Class of Special Effect Pigments used in Flexo Printing Trials

Table A.5 assigns pigment classes.

Table A.5: Pigment class of *MERCK* pigments used in flexo printing.

pigment name	pigment class
Iriodin 123 *Bright Lustre Satin*	silver white pigment
Iriodin 103 *Rutile Sterling Silver*	silver white pigment
Iriodin 153 *Flash Pearl*	silver white pigment
Iriodin 323 *Royal Gold Satin*	gold pigment
Iriodin 305 *Solar Gold*	gold pigment
Iriodin 300 *Gold Pearl*	gold pigment
Iriodin 520 *Bronze Satin*	iron oxide pigment
Iriodin 4504 *Lava Red*	iron oxide pigment
Iriodin 500 *Bronze*	iron oxide pigment
Iriodin 201 *Rutil Fine Gold*	interference effect pigment
Iriodin 211 *Rutil Fine Red*	interference effect pigment
Iriodin 221 *Rutil Fine Blue*	interference effect pigment
Iriodin 231 *Rutil Fine Green*	interference effect pigment
Iriodin 205 *Rutil Platinum Gold*	interference effect pigment
Iriodin 215 *Rutil Red Pearl*	interference effect pigment
Iriodin 225 *Rutil Blue Pearl*	interference effect pigment
Iriodin 235 *Rutil Green Pearl*	interference effect pigment
*Colorstream F*1000 *Autumn Mystery*	multi-color pigment
*Colorstream T*1001 *Viola Fantasy*	multi-color pigment
*Colorstream T*1002 *Arctic Fire*	multi-color pigment
*Colorstream T*1003 *Tropic Sunrise*	multi-color pigment
*Colorstream T*1004 *Lapis Sunlight*	multi-color pigment
*Colorstream T*1005 *Pacific Lagoon*	multi-color pigment
*Colorstream T*1006 *Royal Damask*	multi-color pigment
Miraval 5311 *Scenic White*	sparkle pigment
Miraval 5320 *Scenic Gold*	sparkle pigment
Miraval 5321 *Scenic Copper*	sparkle pigment
Miraval 5325 *Scenic Turquoise*	sparkle pigment

A.2.2 Particle Size of Special Effect Pigments used in Flexo Printing Trials

The particle sizes are enlisted in table A.6.

Table A.6: Particle size of *MERCK* pigments used in flexo printing.

pigment name	particle size
Iriodin 123 *Bright Lustre Satin*	5 μm - 25 μm
Iriodin 103 *Rutile Sterling Silver*	10 μm - 60 μm
Iriodin 153 *Flash Pearl*	20 μm - 100 μm
Iriodin 323 *Royal Gold Satin*	5 μm - 25 μm
Iriodin 305 *Solar Gold*	10 μm - 60 μm
Iriodin 300 *Gold Pearl*	10 μm - 60 μm
Iriodin 520 *Bronze Satin*	5 μm - 25 μm
Iriodin 4504 *Lava Red*	5 μm - 50 μm
Iriodin 500 *Bronze*	10 μm - 60 μm
Iriodin 201 *Rutil Fine Gold*	5 μm - 25 μm
Iriodin 211 *Rutil Fine Red*	5 μm - 25 μm
Iriodin 221 *Rutil Fine Blue*	5 μm - 25 μm
Iriodin 231 *Rutil Fine Green*	5 μm - 25 μm
Iriodin 205 *Rutil Platinum Gold*	10 μm - 60 μm
Iriodin 215 *Rutil Red Pearl*	10 μm - 60 μm
Iriodin 225 *Rutil Blue Pearl*	10 μm - 60 μm
Iriodin 235 *Rutil Green Pearl*	10 μm - 60 μm
*Colorstream F*1000 *Autumn Mystery*	5 μm - 50 μm
*Colorstream T*1001 *Viola Fantasy*	5 μm - 50 μm
*Colorstream T*1002 *Arctic Fire*	5 μm - 50 μm
*Colorstream T*1003 *Tropic Sunrise*	5 μm - 50 μm
*Colorstream T*1004 *Lapis Sunlight*	5 μm - 50 μm
*Colorstream T*1005 *Pacific Lagoon*	10 μm - 60 μm
*Colorstream T*1006 *Royal Damask*	10 μm - 60 μm
Miraval 5311 *Scenic White*	10 μm - 100 μm
Miraval 5320 *Scenic Gold*	10 μm - 100 μm
Miraval 5321 *Scenic Copper*	10 μm - 100 μm
Miraval 5325 *Scenic Turquoise*	10 μm - 100 μm

A.2.3 Substrate Material of Special Effect Pigments used in Flexo Printing Trials

Table A.7 names the substrate material.

Table A.7: Substrate material of *MERCK* pigments used in flexo printing.

pigment name	substrate material
Iriodin 123 *Bright Lustre Satin*	natural mica
Iriodin 103 *Rutile Sterling Silver*	natural mica
Iriodin 153 *Flash Pearl*	natural mica
Iriodin 323 *Royal Gold Satin*	natural mica
Iriodin 305 *Solar Gold*	natural mica
Iriodin 300 *Gold Pearl*	natural mica
Iriodin 520 *Bronze Satin*	natural mica
Iriodin 4504 *Lava Red*	natural mica
Iriodin 500 *Bronze*	natural mica
Iriodin 201 *Rutil Fine Gold*	natural mica
Iriodin 211 *Rutil Fine Red*	natural mica
Iriodin 221 *Rutil Fine Blue*	natural mica
Iriodin 231 *Rutil Fine Green*	natural mica
Iriodin 205 *Rutil Platinum Gold*	natural mica
Iriodin 215 *Rutil Red Pearl*	natural mica
Iriodin 225 *Rutil Blue Pearl*	natural mica
Iriodin 235 *Rutil Green Pearl*	natural mica
*Colorstream F*1000 *Autumn Mystery*	synthetic silicon dioxide
*Colorstream T*1001 *Viola Fantasy*	synthetic silicon dioxide
*Colorstream T*1002 *Arctic Fire*	synthetic silicon dioxide
*Colorstream T*1003 *Tropic Sunrise*	synthetic silicon dioxide
*Colorstream T*1004 *Lapis Sunlight*	synthetic silicon dioxide
*Colorstream T*1005 *Pacific Lagoon*	synthetic silicon dioxide
*Colorstream T*1006 *Royal Damask*	synthetic silicon dioxide
Miraval 5311 *Scenic White*	synthetic borosilicate
Miraval 5320 *Scenic Gold*	synthetic borosilicate
Miraval 5321 *Scenic Copper*	synthetic borosilicate
Miraval 5325 *Scenic Turquoise*	synthetic borosilicate

A.2.4 Coating Material of Special Effect Pigments used in Flexo Printing Trials

The coating material is designated in table A.8.

Table A.8: Coating material of *MERCK* pigments used in flexo printing.

pigment name	coating material
Iriodin 123 *Bright Lustre Satin*	tin dioxide, titanium dioxide
Iriodin 103 *Rutile Sterling Silver*	tin dioxide, titanium dioxide
Iriodin 153 *Flash Pearl*	tin dioxide, titanium dioxide
Iriodin 323 *Royal Gold Satin*	iron(III) oxide, tin dioxide, titanium dioxide
Iriodin 305 *Solar Gold*	iron(III) oxide, tin dioxide, titanium dioxide
Iriodin 300 *Gold Pearl*	iron(III) oxide, titanium dioxide
Iriodin 520 *Bronze Satin*	iron(III) oxide
Iriodin 4504 *Lava Red*	iron(III) oxide
Iriodin 500 *Bronze*	iron(III) oxide
Iriodin 201 *Rutil Fine Gold*	tin dioxide, titanium dioxide
Iriodin 211 *Rutil Fine Red*	tin dioxide, titanium dioxide
Iriodin 221 *Rutil Fine Blue*	tin dioxide, titanium dioxide
Iriodin 231 *Rutil Fine Green*	tin dioxide, titanium dioxide
Iriodin 205 *Rutil Platinum Gold*	tin dioxide, titanium dioxide
Iriodin 215 *Rutil Red Pearl*	tin dioxide, titanium dioxide
Iriodin 225 *Rutil Blue Pearl*	tin dioxide, titanium dioxide
Iriodin 235 *Rutil Green Pearl*	tin dioxide, titanium dioxide
*Colorstream F*1000 *Autumn Mystery*	iron(III) oxide
*Colorstream T*1001 *Viola Fantasy*	tin dioxide, titanium dioxide
*Colorstream T*1002 *Arctic Fire*	tin dioxide, titanium dioxide
*Colorstream T*1003 *Tropic Sunrise*	tin dioxide, titanium dioxide
*Colorstream T*1004 *Lapis Sunlight*	tin dioxide, titanium dioxide
*Colorstream T*1005 *Pacific Lagoon*	silicon dioxide, tin dioxide, titanium dioxide
*Colorstream T*1006 *Royal Damask*	silicon dioxide, tin dioxide, titanium dioxide
Miraval 5311 *Scenic White*	silicon dioxide, tin dioxide, titanium dioxide
Miraval 5320 *Scenic Gold*	silicon dioxide, tin dioxide, titanium dioxide
Miraval 5321 *Scenic Copper*	silicon dioxide, tin dioxide, titanium dioxide
Miraval 5325 *Scenic Turquoise*	silicon dioxide, tin dioxide, titanium dioxide

Appendix B

Papers of Printing Trials

Section B.1 and section B.1 give further information about the papers used in the screen and flexo printing trials, respectively.

B.1 Papers of Screen Printing Trials

The papers used in screen printing are specified in table B.1.

Table B.1: Papers used in screen printing.

paper	*LuxoMagic*	*PopSet*
producer	*Sappi Ltd.*	*Arjo Wiggins Fine Papers Ltd.*
class	art paper	fine paper
color	white	black
pulp	wood-free	wood-free
bleaching	elementary chlorine free	elementary chlorine free
coating	simple glossy coated	uncoated
resistance	aging-resistant	aging-resistant
fastness	not specified	light-fast
safety	food-safe	food-safe
grammage [127]	150 g/m^2	120 g/m^2
DIN gloss (45°) [65]	46.45 % ± 1.41 %	0.37 % ± 0.04 %
DIN gloss (75°) [66]	11.71 % ± 1.53 %	0.19 % ± 0.05 %
TAPPI gloss (75°) [125]	70.44 % ± 1.54 %	2.98 % ± 1.25 %
PPS roughness [122]	0.70 μm ± 0.02 μm	7.37 μm ± 0.26 μm
Bendtsen roughness [68]	0 ml/min ± 0 ml/min	356 ml/min ± 54 ml/min
Bekk smoothness [67]	1182.67 s ± 30.38 s	11.28 s ± 0.74 s
Cobb water absorption [63]	0.36 g/m^2 ± 0.02 g/m^2	0.26 g/m^2 ± 0.03 g/m^2

B.2 Papers of Flexo Printing Trials

Table B.2 specifies the papers used in flexo printing.

Table B.2: Papers used in flexo printing [229, 230].

paper	*LumiArt*	*LumiSilk*
producer	*Stora Enso AG*	*Stora Enso AG*
class	art paper	art paper
color	white	white
pulp	wood-free	wood-free
bleaching	elementary chlorine free	elementary chlorine free
coating	double glossy coated	double matt coated
grammage [127]	120 g/m^2	120 g/m^2
bulk [126]	0.78 cm^3/g [229]	0.87 cm^3/g [229]
CIE whiteness ($D65$, 10°) [121]	122 [229]	122 [229]
ISO brightness ($D65$, 10°) [124]	99 % [229]	99 % [229]
opacity ($D65$, 10°) [123]	94 % [229]	95 % [229]
TAPPI gloss (75°) [125]	70 % [229]	30 % [229]
PPS roughness [122]	0.8 μm [229]	1.4 μm [229]
DIN gloss (45°) [65]	44.11 % ± 2.52 %	6.15 % ± 0.44 %
DIN gloss (75°) [66]	11.64 % ± 0.92 %	1.46 % ± 0.04 %
TAPPI gloss (75°) [125]	70.57 % ± 2.21 %	27.01 % ± 1.82 %
PPS roughness [122]	0.71 μm ± 0.03 μm	2.06 μm ± 0.08 μm
Bendtsen roughness [68]	0 ml/min ± 0 ml/min	11 ml/min ± 4 ml/min
Bekk smoothness [67]	875.25 s ± 22.11 s	336.15 s ± 28.59 s
Cobb water absorption [63]	60.86 g/m^2 ± 4.99 g/m^2	57.68 g/m^2 ± 2.28 g/m^2

Appendix C

Geometric Configurations of Optical Measurements

The geometric configurations (section 3.2) realized in the optical measurements (section 6.1) are specified in section C.1, section C.2 and section C.3.

C.1 Geometric Configurations of Multi-Angle Spectrophotometer $MA98$

Table C.1 itemizes the geometric configurations (section 3.2.2) of the multi-angle spectrophotometer $MA98$ (section 3.2.3).

Table C.1: Geometric configurations of multi-angle spectrophotometer $MA98$.

ω_i		ω_r			
θ_i	ϕ_i	θ_r	ϕ_r	θ_{as}	ϕ_{az}
45°	0°	60°	180°	−15°	0°
45°	0°	30°	180°	15°	0°
45°	0°	20°	180°	25°	0°
45°	0°	0°	90°	45°	0°
45°	0°	30°	0°	75°	0°
45°	0°	65°	0°	110°	0°
15°	0°	30°	180°	−15°	0°
15°	0°	0°	90°	15°	0°
15°	0°	60°	180°	−45°	0°
15°	0°	30°	0°	45°	0°
15°	0°	65°	0°	80°	0°
45°	0°	50.1443°	−213.4032°	25°	90°
45°	0°	50.1443°	213.4032°	25°	−90°
45°	0°	90.0178°	−224.9748°	60°	125.3°
45°	0°	90.0178°	224.9748°	60°	−125.3°
15°	0°	28.9133°	60.9567°	38.3°	43°
15°	0°	28.9133°	−60.9567°	38.3°	−43°
15°	0°	52.2168°	−243.4362°	46.9°	104.5°
15°	0°	52.2168°	243.4362°	46.9°	−104.5°

C.2 Geometric Configurations of Multi-Angle Spectrophotometer *BYK-mac*

The geometric configurations (section 3.2.2) realized in multi-angle spectrophotometer *BYK-mac* (section 3.2.3) are itemized in table C.2.

Table C.2: Geometric configurations of multi-angle spectrophotometer *BYK-mac*.

ω_i		ω_r			
θ_i	ϕ_i	θ_r	ϕ_r	θ_{as}	ϕ_{az}
45°	0°	60°	180°	−15°	0°
45°	0°	30°	180°	15°	0°
45°	0°	20°	180°	25°	0°
45°	0°	0°	90°	45°	0°
45°	0°	30°	0°	75°	0°
45°	0°	65°	0°	110°	0°

C.3 Geometric Configurations of Robot-Based Gonioreflectometer *ARGon*^{3}

Table C.3 enlists the geometric configurations (section 3.2.2) realized with the robot-based gonioreflectometer *ARGon*^{3} (section 3.2.3).

Table C.3: Geometric configurations of multi-angle spectrophotometer *ARGon*^{3}.

ω_i		ω_r	
θ_i	ϕ_i	θ_r	ϕ_r
45°	0°	0°	0°
45°	0°	7.5°	0°
45°	0°	7.5°	45°
45°	0°	7.5°	90°
45°	0°	7.5°	135°
45°	0°	7.5°	180°
45°	0°	15°	0°
45°	0°	15°	22.5°
45°	0°	15°	45°
45°	0°	15°	67.5°
45°	0°	15°	90°
45°	0°	15°	112.5°
45°	0°	15°	135°
45°	0°	15°	157.5°
45°	0°	15°	180°
45°	0°	22.5°	0°
45°	0°	22.5°	15°
45°	0°	22.5°	30°
45°	0°	22.5°	45°
45°	0°	22.5°	60°
45°	0°	22.5°	75°
45°	0°	22.5°	90°
45°	0°	22.5°	105°
45°	0°	22.5°	120°
45°	0°	22.5°	135°
45°	0°	22.5°	150°
45°	0°	22.5°	165°
45°	0°	22.5°	180°

ω_i		ω_r	
θ_i	ϕ_i	θ_r	ϕ_r
45°	0°	30°	0°
45°	0°	30°	11.25°
45°	0°	30°	22.5°
45°	0°	30°	33.75°
45°	0°	30°	45°
45°	0°	30°	56.25°
45°	0°	30°	67.5°
45°	0°	30°	78.75°
45°	0°	30°	90°
45°	0°	30°	101.25°
45°	0°	30°	112.5°
45°	0°	30°	123.75°
45°	0°	30°	135°
45°	0°	30°	146.25°
45°	0°	30°	157.5°
45°	0°	30°	168.75°
45°	0°	30°	180°
45°	0°	37.5°	0°
45°	0°	37.5°	9°
45°	0°	37.5°	18°
45°	0°	37.5°	27°
45°	0°	37.5°	36°
45°	0°	37.5°	45°
45°	0°	37.5°	54°
45°	0°	37.5°	63°
45°	0°	37.5°	72°
45°	0°	37.5°	81°
45°	0°	37.5°	90°
45°	0°	37.5°	99°
45°	0°	37.5°	108°
45°	0°	37.5°	117°
45°	0°	37.5°	126°
45°	0°	37.5°	135°
45°	0°	37.5°	144°
45°	0°	37.5°	153°
45°	0°	37.5°	162°
45°	0°	37.5°	171°
45°	0°	37.5°	180°

ω_i		ω_r	
θ_i	ϕ_i	θ_r	ϕ_r
45°	0°	45°	15°
45°	0°	45°	22.5°
45°	0°	45°	30°
45°	0°	45°	37.5°
45°	0°	45°	45°
45°	0°	45°	52.5°
45°	0°	45°	60°
45°	0°	45°	67.5°
45°	0°	45°	75°
45°	0°	45°	82.5°
45°	0°	45°	90°
45°	0°	45°	97.5°
45°	0°	45°	105°
45°	0°	45°	112.5°
45°	0°	45°	120°
45°	0°	45°	127.5°
45°	0°	45°	135°
45°	0°	45°	142.5°
45°	0°	45°	150°
45°	0°	45°	157.5°
45°	0°	45°	165°
45°	0°	45°	172.5°
45°	0°	45°	180°
45°	0°	52.5°	0°
45°	0°	52.5°	7.5°
45°	0°	52.5°	15°
45°	0°	52.5°	22.5°
45°	0°	52.5°	30°
45°	0°	52.5°	37.5°
45°	0°	52.5°	45°
45°	0°	52.5°	52.5°
45°	0°	52.5°	60°
45°	0°	52.5°	67.5°
45°	0°	52.5°	75°
45°	0°	52.5°	82.5°
45°	0°	52.5°	90°
45°	0°	52.5°	97.5°
45°	0°	52.5°	105°
45°	0°	52.5°	112.5°
45°	0°	52.5°	120°
45°	0°	52.5°	127.5°
45°	0°	52.5°	135°
45°	0°	52.5°	142.5°
45°	0°	52.5°	150°
45°	0°	52.5°	157.5°
45°	0°	52.5°	165°
45°	0°	52.5°	172.5°
45°	0°	52.5°	180°

ω_i		ω_r	
θ_i	ϕ_i	θ_r	ϕ_r
45°	0°	60°	0°
45°	0°	60°	5°
45°	0°	60°	10°
45°	0°	60°	15°
45°	0°	60°	20°
45°	0°	60°	25°
45°	0°	60°	30°
45°	0°	60°	35°
45°	0°	60°	40°
45°	0°	60°	45°
45°	0°	60°	50°
45°	0°	60°	55°
45°	0°	60°	60°
45°	0°	60°	65°
45°	0°	60°	70°
45°	0°	60°	75°
45°	0°	60°	80°
45°	0°	60°	85°
45°	0°	60°	90°
45°	0°	60°	95°
45°	0°	60°	100°
45°	0°	60°	105°
45°	0°	60°	110°
45°	0°	60°	115°
45°	0°	60°	120°
45°	0°	60°	125°
45°	0°	60°	130°
45°	0°	60°	135°
45°	0°	60°	140°
45°	0°	60°	145°
45°	0°	60°	150°
45°	0°	60°	155°
45°	0°	60°	160°
45°	0°	60°	165°
45°	0°	60°	170°
45°	0°	60°	175°
45°	0°	60°	180°

ω_i		ω_r	
θ_i	ϕ_i	θ_r	ϕ_r
45°	0°	67.5°	0°
45°	0°	67.5°	5°
45°	0°	67.5°	10°
45°	0°	67.5°	15°
45°	0°	67.5°	20°
45°	0°	67.5°	25°
45°	0°	67.5°	30°
45°	0°	67.5°	35°
45°	0°	67.5°	40°
45°	0°	67.5°	45°
45°	0°	67.5°	50°
45°	0°	67.5°	55°
45°	0°	67.5°	60°
45°	0°	67.5°	65°
45°	0°	67.5°	70°
45°	0°	67.5°	75°
45°	0°	67.5°	80°
45°	0°	67.5°	85°
45°	0°	67.5°	90°
45°	0°	67.5°	95°
45°	0°	67.5°	100°
45°	0°	67.5°	105°
45°	0°	67.5°	110°
45°	0°	67.5°	115°
45°	0°	67.5°	120°
45°	0°	67.5°	125°
45°	0°	67.5°	130°
45°	0°	67.5°	135°
45°	0°	67.5°	140°
45°	0°	67.5°	145°
45°	0°	67.5°	150°
45°	0°	67.5°	155°
45°	0°	67.5°	160°
45°	0°	67.5°	165°
45°	0°	67.5°	170°
45°	0°	67.5°	175°
45°	0°	67.5°	180°

ω_i		ω_r	
θ_i	ϕ_i	θ_r	ϕ_r
45°	0°	75°	0°
45°	0°	75°	4.5°
45°	0°	75°	9°
45°	0°	75°	13.5°
45°	0°	75°	18°
45°	0°	75°	22.5°
45°	0°	75°	27°
45°	0°	75°	31.5°
45°	0°	75°	36°
45°	0°	75°	40.5°
45°	0°	75°	45°
45°	0°	75°	49.5°
45°	0°	75°	54°
45°	0°	75°	58.5°
45°	0°	75°	63°
45°	0°	75°	67.5°
45°	0°	75°	72°
45°	0°	75°	76.5°
45°	0°	75°	81°
45°	0°	75°	85.5°
45°	0°	75°	90°
45°	0°	75°	94.5°
45°	0°	75°	99°
45°	0°	75°	103.5°
45°	0°	75°	108°
45°	0°	75°	112.5°
45°	0°	75°	117°
45°	0°	75°	121.5°
45°	0°	75°	126°
45°	0°	75°	130.5°
45°	0°	75°	135°
45°	0°	75°	139.5°
45°	0°	75°	144°
45°	0°	75°	148.5°
45°	0°	75°	153°
45°	0°	75°	157.5°
45°	0°	75°	162°
45°	0°	75°	166.5°
45°	0°	75°	171°
45°	0°	75°	175.5°
45°	0°	75°	180°

ω_i		ω_r	
θ_i	ϕ_i	θ_r	ϕ_r
45°	0°	82.5°	0°
45°	0°	82.5°	4.5°
45°	0°	82.5°	9°
45°	0°	82.5°	13.5°
45°	0°	82.5°	18°
45°	0°	82.5°	22.5°
45°	0°	82.5°	27°
45°	0°	82.5°	31.5°
45°	0°	82.5°	36°
45°	0°	82.5°	40.5°
45°	0°	82.5°	45°
45°	0°	82.5°	49.5°
45°	0°	82.5°	54°
45°	0°	82.5°	58.5°
45°	0°	82.5°	63°
45°	0°	82.5°	67.5°
45°	0°	82.5°	72°
45°	0°	82.5°	76.5°
45°	0°	82.5°	81°
45°	0°	82.5°	85.5°
45°	0°	82.5°	90°
45°	0°	82.5°	94.5°
45°	0°	82.5°	99°
45°	0°	82.5°	103.5°
45°	0°	82.5°	108°
45°	0°	82.5°	112.5°
45°	0°	82.5°	117°
45°	0°	82.5°	121.5°
45°	0°	82.5°	126°
45°	0°	82.5°	130.5°
45°	0°	82.5°	135°
45°	0°	82.5°	139.5°
45°	0°	82.5°	144°
45°	0°	82.5°	148.5°
45°	0°	82.5°	153°
45°	0°	82.5°	157.5°
45°	0°	82.5°	162°
45°	0°	82.5°	166.5°
45°	0°	82.5°	171°
45°	0°	82.5°	175.5°
45°	0°	82.5°	180°